UNIVERSITY OF CALIFORNIA,
IRVINE

Vehicle-Bridge Interaction and Vibration Suppression Using Magnetorheological Nanocomposites

DISSERTATION

submitted in partial satisfaction of the requirements

for the degree of

DOCTOR OF PHILOSOPHY

in Civil Engineering

by

Yongxue Li

Dissertation Committee:

Professor Lizhi Sun, Chair

Associate Professor Farzin Zareian

Assistant Professor Anne Lemnitzer

2015

DEDICATION

To

my grandma and my parents,

Dezhen Sun, Kaichao Li and Hongchun Xiong

TABLE OF CONTENTS

LIST OF FIGURES

LIST OF TABLES

ACKNOWLEDGEMENTS

I would like to express my sincere gratitude to Professor Lizhi Sun, my Ph.D. advisor and my Ph.D. committee chair, for his continuous guidance and supports during my graduate studies at UCI. His knowledge and insightfulness played an enormous role in my research and his great erudition, integrity, and graciousness will always be my pursuit. Without his encouragement and patience, this work would never be possible.

I am also grateful to the other members of my dissertation committee, Professor Anne Lemnitzer and Professor Farzin Zareian at the University of California, Irvine, for their valuable time to read and comment on this dissertation.

Many thanks go to Professor Guiwei Liu at Harbin Institute of Technology, who is the first person to instruct me on how to do academic research and encourage me to continue my research life at United States. I also want to thank Professor Honglin Wu and Professor Hang Sun at Harbin Institute of Technology, who gave me many advices on my research works.

I would also like to thank my colleagues, Drs. Hua Liu, Rui Li and Yu Wang, Ph.D. candidate Ping Zhang, Ph.D. student Dongxu Liu for their contributions to my graduate study at UCI and their kind help from the first day I came to the United States.

And, thank you, my dear grandma and parents, for your endless love and support throughout my life. My grandma passed away fifteen years ago, and I wish she would be proud of me. She was my first teacher to teach me reading, writing and how to be a good man, and she always encouraged me to be a scholar in my life. I miss her and dedicate this dissertation to her memory.

CURRICULUM VITAE

Yongxue Li

September 28, 1985	Born, Chengdu, P.R.China
2005-2009	Bachelor of Engineering in Road and Bridge Engineering Harbin Institute of Technology, Harbin, China
2009-2011	Master of Engineering in Bridge and Tunnel Engineering Harbin Institute of Technology, Harbin, China
2011-2015	Doctor of Philosophy in Civil Engineering University of California, Irvine Irvine, California

Publications

1. Li, Y.X., and Sun, L.Z. (2015). "Transverse vibration of undamped elastically connected double-beam system with arbitrary conditions." Journal of Engineering Mechanics, vol. 141, 04015070-1-18.

2. Kuo, C.C., Li, Y.X., Nguyen, D., Buchsbaum, S., Innes, L., Esser-Kahn, A.P., Valdevit, L., Sun, L.Z., Siwy, Z., and Dennin, M. (2015). "Macroscopic strain controlled ion current in an elastomeric microchannel." Journal of Applied Physics, vol. 117, 174904-1-6.

3. Li, Y.X. and Sun, L.Z., (2015), "Semi-Active Vibration Control of Double-Beam System by Using Magneto-Rheological Elastomers." ASCE Engineering Mechanics Institute Conference, June 16-19, 2015.

4. Li, Y.X., Hu, Z.J., and Sun, L.Z., " Dynamical Behaviors of a Double-Beam System Interconnected by Viscoelastic Layer." International Journal of Mechanical Sciences, (Accepted).

5. Hussain, H.K., Zhang, L., Liu, G.W., Li, Y., (2011), " Evaluation Behavior of Qing Shan

Concrete Bridge under Static Load Test." Research Journal of Applied Sciences, Engineering and Technology, 3(7), 677-688.

6. Hussain, H.K., Wei, L.G., Zhen, Z.L., Li, Y., (2011), " Site Inspection and Evaluation Behavior of Qing Shang Concrete Bridge." World Academy of Science, Engineering and Technology, 78, 322-328.

7. Li, Y.X. and Liu, G.W., (2011), “Numerical simulation on seismic behavior of PUFA retrofitted RC column”, Highway, June 15, pp.95-99.

8. Li, Y.X. and Liu, G.W., (2010), “Anti-Seismic Analysis of Ductility of Reinforced Concrete Bridge Piers with Rectangle Section”, Highway, October 15, pp.20-27.

ABSTRACT OF THE DISSERTATION

Vehicle-Bridge Interaction and Vibration Suppression Using Magnetorheological Nanocomposites

by

Yongxue Li

Doctor of Philosophy in Civil Engineering

University of California, Irvine, 2015

Professor Lizhi Sun, Chair

The objective of the research in this dissertation is to use novel adaptive materials called magnetorheological nanocomposites (MRNs) to build semi-active structures, and further apply such smart structures into the vehicle-bridge coupling system of high-speed rail so that the dynamic responses of the bridge can be controlled and suppressed significantly.

First, the dynamic behavior of a simplified double-beam system interconnected by an elastic layer is investigated. A semi-analytical method is developed to analyze the natural frequencies and corresponding mode shapes. The dynamic responses of forced system vibration are determined by the modal-expansion method using the natural frequencies and mode shapes obtained from the free vibration analysis.

Second, considering the damping effect of the viscoelastic layer, a double-beam system with a viscoelastic layer between two beams is observed. An iteration algorithm with modal-expansion method is used to analyze the dynamic responses of forced system vibration.

Third, an active control structure, a semi-active control structure and corresponding control algorithms are developed to suppress the vibration of the double-beam system with elastic layer or viscoelastic layer. In the active control structure, the independent modal space control and linear quadratic regulator are adopted to determine the active control force. With the mode shape filter and dynamic mechanical model, the determinations of stiffness increase and damping increase are obtained.

Fourth, a co-simulation method is proposed to complete the dynamic simulation of vehicle-bridge coupling system. The Matlab/Simulink is used to build a platform to ensure MSC/NASTRAN for bridge model and MSC/ADAMS for vehicle model working together. The vehicle-bridge coupling relationships are coded as a program block and inputted into that platform.

Finally, the semi-active control structure based on MRNs is inputted into the vehicle-bridge coupling system of high-speed railway to control and suppress the vibration of the bridge. MRNs are applied as the viscoelastic layer between floating slab track and bridge main beam to build the

semi-active control structure for bridges. The semi-active control algorithm for MRNs is developed and inputted into that co-simulation platform. Numerical experiments have been made to illustrate and verify the efficiency of the proposed semi-active control structure in the end.

Chapter 1 Introduction

1.1 Introduction

With the fast developing economy, more and more high-speed rails have been built in the world. First, the trains passing the bridge induce dynamic impact to bridge structures, reducing their safety and service life. Second, the vibration of bridges in turn affects the running stability and safety of the trains. And thus, the dynamic responses of bridges in railway engineering under the high-speed train loads become one of the fundamental problems needed to be solved in the research and design works.

In order to reduce the vibration of the structures, several methods have been studied deeply, and among of them, structural vibration control has been observed more than 40 years. Yao (1972) firstly introduced the modern control theory into civil engineering in 1972, from when the research about structural vibration control started. Until now, the main structural vibration control could be classified as three parts: active control, passive control and semi-active control. Many theoretical and experimental works about different types of the structures have been made to show the efficiency of those vibration control methods.

In those structural vibration control methods, many smart materials are applied to realize the control effects. Magnetorheological (MR) materials are just a group of those smart materials whose

mechanical and rheological properties can be controlled rapidly and reversibly by applied external magnetic fields. The main MR materials include MR fluid (MRF), MR foam, MR gel, and MR elastomers (MREs). The mechanism of the field-dependent controllability of MR materials is the magnetic interaction among the ferromagnetic particles contained in these materials, which can be adjusted by the applied magnetic fields.

In those three research topics introduced above, researchers have been facing two challenges. First, there are very few works about applying the vibration control structure into vehicle-bridge coupling system, especially into the high-speed rail bridge structures. The abundant existed structural vibration control works are for buildings. Several researches that are about bridge structures are observed for earthquake effects. The vibration control on bridges for vehicle-bridge coupling system is still a new research area. Second, the adjustable ability of the MR materials is still weak and it is hard to apply it to make best control effects in structural vibration control. Due to the limit of the matrix, the adjustable range of the MR materials, especially the MREs, is still small and it is not enough to apply it to do the structural vibration control effectively.

The two posted challenges lead to this research on applying novel adaptive materials magnetorheological nanocomposites (MRNs) to build semi-active control structures which can be applied into vehicle-bridge coupling system of high-speed rail to control and reduce the vibration of bridges. MRNs are improved MREs by adding carbon nanotubes (CNTs) to reinforce

conventional MREs, and their initial and adjustable stiffness and damping are better than MREs. The advantages of MRNs make it possible to use them in structural vibration control. Considering the ballastless track structure, which chooses floating slab track as the main constituent part, is widely existed in modern bridges of high-speed rail, the MRNs are able to be installed as the viscoelastic layer between floating slab track and bridge main beam to build a semi-active control structure. With a corresponding control algorithm, the vibration control based on MRNs for high-speed rail bridges can be completed successfully.

It is expected that when the MRNs are applied as the viscoelastic layer between floating slab track and bridge main beam, the semi-active control can work effectively to suppress the vibration of bridge structures when the high-speed trains are passing.

1.2 Scope

The research in this dissertation is the first attempt to use novel adaptive materials magnetorheological nanocomposites (MRNs) to build semi-active control structures, and further apply such smart structures into vehicle-bridge coupling system of high-speed rail so that the vibration of the whole system could be controlled effectively and the dynamic responses of bridge can be reduced significantly. The dynamic behavior of a simplified double-beam system with elastic layer or viscoelastic layer is studied firstly, which is the theoretical basis for the control

structure research on the same mechanic models. In next step, the active control and semi-active control are developed for those double-beam systems and the specific control algorithms are derived. A co-simulation method is proposed to simulate the vehicle-bridge coupling system, and it is built successfully in Matlab/Simulink platform. Last but not least, the semi-active control based on MRNs is inputted into the co-simulation platform, and the its application in vehicle-bridge coupling system of high-speed rail is completed successfully to control and reduce the bridge dynamic responses and protect the whole system safety.

This dissertation is organized as follows.

Chapter 2 investigate the dynamic behavior of a double-beam system interconnected by elastic layer. First, a semi-analytical method is developed to analyze the natural frequencies and corresponding mode shapes of that double-beam system. Second, the dynamic responses of forced system vibration are determined by the modal-expansion method using the natural frequencies and mode shapes obtained from the free vibration analysis. Finally, various double-beam system models are studied to verify the semi-analytical method and conduct the systematic parametric analysis of the structural resonance condition and dynamic responses.

Chapter 3 observes a double-beam system interconnected by a viscoelastic layer, in which the damping effect cannot be ignored. First, the natural frequencies and corresponding mode shapes

are analyzed by a similar semi-analytical method. Second, an iteration algorithm with modal-expansion method is used to analyze the dynamic responses of forced system vibration. Finally, the semi-analytical method and iteration algorithm are verified by the calculations of various double-beam system models and the systematic parametric analysis is conducted .

Chapter 4 and Chapter 5 develop an active control structure, a semi-active control structure and corresponding control algorithms to suppress the vibration of the double-beam system with elastic layer and viscoelastic layer, respectively. First, in the active control structure, independent modal space control and linear quadratic regulator are adopted to decouple equations of motion with active control and determine the active control force in physical space. Second, a linear model is assumed as the dynamic mechanical model of the adjustable viscoelastic layer and the relationship between stiffness, damping coefficient with inputted currents is also defined as a linear model. Third, in the semi-active control structure, based on that semi-active control force is assumed to be close to active force and with the mode shape filter, the determination methods of stiffness increase and damping increase are derived. Fourth, the calculation methods for double-beam system with that active control and that semi-active control are developed. Finally, several double-beam system with active control structure or semi-active control structure models are calculated to illustrate the efficiency of the proposed active control and semi-active control.

Chapter 6 proposes a co-simulation method to complete the dynamic simulation of vehicle-bridge

coupling system. First, bridge structures are modelled by finite element method software MSC/NASTRAN, and dynamics of multibody system software MSC/ADAMS is used to simulate the vibration of vehicle system. Second, the vehicle-bridge coupling relationships are introduced and the classical theories about them are adopted, including wheel-rail contact geometric parameters, wheel-rail contact forces and track irregularity. Third, the Matlab/Simulink is used to build a platform to ensure MSC/NASTRAN and MSC/ADAMS working together, and the vehicle-bridge coupling relationships are coded as a program block and inputted into that platform. Finally, numerical examples of vehicle-bridge coupling system are calculated to illustrate the practicability of the proposed co-simulation method.

Chapter 7 inputs the semi-active control structure based on MRNs into the vehicle-bridge coupling system of high-speed rail to control vibration of the whole system and reduce the dynamic responses of bridge. First, MRNs are applied as the viscoelastic layer between floating slab track and bridge main beam to build the semi-active control structure for high-speed rail bridges. Second, the dynamic mechanical model of MRNs is derived based on their properties. Third, the semi-active control algorithm developed for double-beam system with viscoelastic layer is used to derive the semi-active control algorithm for MRNs. Fourth, that semi-active control is inputted into the co-simulation platform of vehicle-bridge coupling system, and the simulation of the whole system with semi-active control is completed. Finally, numerical examples are demonstrated to prove the efficiency of the semi-active control structure proposed in this research by MRNs for the

vehicle-bridge coupling system of high-speed rail.

Chapter 8 concludes the dissertation by summarizing the major contributions. In addition, some suggestions for the future work are also discussed.

Chapter 2 Dynamic Behavior of Undamped Double-Beam Systems Interconnected with Elastic Layers

2.1 Introduction

The main research objective in this dissertation is to apply novel adaptive materials as a semi-active control in high-speed rail bridge, and the vibration of bridge can be controlled and reduced when the trains are passing. In order to realize that objective, the novel adaptive materials will be used as the viscoelastic layer between floating slab track and bridge main beam, which will be introduced specifically in Chapter 6 and Chapter 7. In that case, the floating slab track and bridge main beam with the viscoelastic layer between them will form a kind of double-beam system, consisting of two one-dimensional continuous beams connected by a uniformly distributed elastic or viscoelastic layer. To that structure, it should aim to find what exactly the characteristics of structural vibration is, and then, indicate a means to reduce or control vibration into an accepted level. Therefore, in this chapter, the dynamic behavior of an undamped double-beam system interconnected by elastic layer is investigated firstly, which will be the theoretical basis for the control structure research works studied in Chapter 4 and Chapter 5.

In fact, the double-beam system is an ideal model for special structures discussed and applied in engineering, such as sandwich or composite beam, continuous dynamic vibration absorber, active constrained layer damping, and so on. Due to its potentially wide applications in many engineering

areas, the free and forced vibrations of the double-beam system have been studied by many investigators in the past decades. A theory for the free vibration of elastically connected parallel beams has been developed by Seelig and Hoppmann (1964a), who studied the natural frequencies and mode shapes for a double-beam system. They further extended the research into the forced vibration (Seelig and Hoppmann 1964b) under impact load condition. Dublin and Friedrich (1956) presented a method of obtaining the forced vibration response for two elastic beams interconnected by spring-damper, and the exciting force is a sinusoidal load. Resonance conditions of a double-beam system under a moving load oscillating longitudinally along the beam about a fixed point is derived by Kessel (1966), who also considered the damping effect in the same system later (Kessel and Raske 1967). Rao (1974) added the rotary inertia and shear deformation effects into the elastically connected parallel system flexural vibration, the double-beam system results are compared with some experimental values. Chonan (1976) moved his attention to the mass of the spring which is the connection between two beams, by the method of the Laplace transformations, dynamic behaviors of the double-beam system related to spring mass are investigated. Irie et al. (1982) discussed the steady-state responses of a double-beam system with internal damping under sinusoidal force, and a transfer matrix technique is adopted for solving the differential equations. Free and forced vibrations of a double-beam system with unequal masses and unequal flexural rigidities are investigated by Hamada et al. (1983) who applied finite integral transformation and Laplace transformation. Cottle (1990) analyzed the layered beam with mixed boundary conditions, and a general solution assumption and a semi-analytical method are applied to solve the equations.

Chen and Sheu (1995) studied the free vibration, dynamic response and static buckling of two identical parallel beams with a viscoelastic material layer in between, the boundary conditions of those two beams can be different, and a dynamic stiffness matrix, which is based on their another work (Chen and Sheu 1993), is established to solve the problem. A same layered beam without axial forces is also discussed by Chen and Sheu (1994) by using same method. Kukla and Skalmierski (1994) considered the transverse free vibration of an axially loaded double-beam system too, but one beam is compressed under the axial force and another beam is under a tensile force. Oniszczuk (2000c, 2003c) presented the analytical solutions for free and forced vibrations of an undamped elastically connected complex double-beam system with simply supported boundary condition, based on his similar research for the double-string system (Oniszczuk 2000a, 2000b, 2003b). Oniszczuk also conducted similar vibration studies for other structures (Oniszczuk 1999, 2000d, 2002a, 2002b, 2003a, 2004), but the basic method to solve the equations is same as in the double-beam system. Vu et al. (2000) presented an exact method to analyze a two identical beams system subject to harmonic excitation, and boundary conditions on the same side of the system must be same. Li and Hua (2007) introduce a spectral finite element method for a more general double-beam system, which could have unequal masses, unequal flexural rigidities and arbitrary boundary conditions. Zhang et al. (2008) discussed the effects of compressive axial load on the forced vibrations of the double-beam system under two particular excitation loadings. Xin and Gao (2011) applied the double-beam system into a specific engineering structure, a bridge with a slab track on it, and use finite element method and multibody dynamics theory to solve the

problem. Some other structures, which are similar to double-beam system, are also analyzed by many researchers, such as sandwich beam (Lu and Douglas 1974; Douglas and Yang 1978; Frostig and Baruch 1993 and 1994; Macé 1994), continuous dynamic vibration absorber (Yamaguchi 1985; Vu 1987; Aida et al. 1992; Chen and Lin 1998; Kawazoe et al. 1998), and composite layered foundation (Yankelevsky 1991), the methods solving equations among all of them are also useful and helpful for double-beam system.

Although there have been research efforts investigating the dynamic responses of double-beam systems as shown above, they are limited to simplified cases that the two beams must be either the same, have same transverse deformation, and/or have the simply supported boundary conditions. Due to unequal masses, unequal flexural rigidities of the beams, and variety of possible combinations of the boundary conditions for the system, the vibration analysis for those general double-beam systems is indeed complicated. On the other hand, in real engineering practices, such as the floating slab track on bridge which is the main structure studied in this research, the double-beam system cannot always have two same beams or same boundary conditions. Therefore, a general double-beam system must be considered. This chapter presents a semi-analytical method to obtain the natural frequencies and corresponding mode shapes for the general double-beam system, which may have unequal masses, unequal flexural rigidities, and arbitrary boundary conditions. In addition, for the same double-beam model, the forced vibration excited by arbitrary loading is analyzed by the classical modal expansion method, based on the natural frequencies and

mode shapes obtained from the free vibration analysis, and a specific orthogonality condition for that double-beam system is derived and applied to decouple differential equations. The natural frequencies and mode shapes are calculated by the semi-analytical method for three cases of arbitrary masses, arbitrary flexural rigidities and arbitrary boundary conditions models. Furthermore, various double-beam system models are studied with a concentrated harmonic force in the midspan of upper beam to conduct the systematic parametric analysis of the structural resonance condition and dynamic responses.

2.2 Formulation of the Problem

As shown in Fig. 2-1, the physical model of a double-beam system with elastic layer is composed of an upper beam and a lower beam joined by a uniformly distributed-connecting elastic layer. In this chapter, both beams are homogeneous, prismatic and have the same length L, however, they can have different mass, flexural rigidity and boundary conditions, which makes the model to be more real in engineering projects.

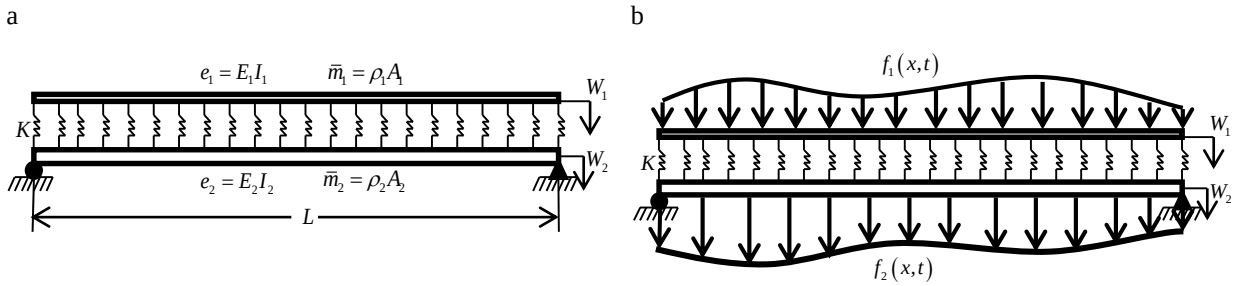

Fig. 2-1. The physical model of a double-beam system: (a) free vibration model; (b) forced vibration model.

Applying the Bernoulli-Euler beam theory, the free and forced transverse vibrations of a double-beam system with an elastic layer, as shown in Fig. 2-1, are described by the governing equations of motion as follows:

$$\frac{\partial^2}{\partial x^2}\left(E_1 I_1 \frac{\partial^2 W_1}{\partial x^2} \right) + K\left(W_1 - W_2\right) + \rho_1 A_1 \frac{\partial^2 W_1}{\partial t^2} = f_1\left(x,t\right) \tag{2-1a}$$

$$\frac{\partial^2}{\partial x^2}\left(E_2 I_2 \frac{\partial^2 W_2}{\partial x^2} \right) - K\left(W_1 - W_2\right) + \rho_2 A_2 \frac{\partial^2 W_2}{\partial t^2} = f_2\left(x,t\right) \tag{2-1b}$$

where $W_1 = W_1\left(x,t\right)$ and $W_2 = W_2\left(x,t\right)$ are transverse beam deflections of the upper and lower beams, respectively; x and t are the spatial co-ordinate and the time; E_1 and E_2 are the Young moduli of elasticity of the upper beam and lower beam; I_1 and I_2 are the moment of inertia of the beam cross section for upper beam and lower beam; ρ_1 and ρ_2 are the mass density of the upper beam and lower beam; A_1 and A_2 are the cross-sectional area of the upper beam and lower beam; K is the stiffness of the elastic layer; and $f_1\left(x,t\right)$ and $f_2\left(x,t\right)$ are the exciting force acting on the upper and lower beams, respectively.

If $f_1\left(x,t\right) = f_2\left(x,t\right) = 0$, Eq. (2-1) is the governing equation of motion for free vibration of a double-beam system; otherwise, it is the governing equation for forced vibration.

Considering the two beams are uniform and homogeneous, let us assume:

$$E_1 I_1 = e_1, \quad E_2 I_2 = e_2, \quad \rho_1 A_1 = \bar{m}_1, \quad \rho_2 A_2 = \bar{m}_2 \tag{2-2}$$

where e_1 and e_2 are the flexural rigidity of the upper beam and lower beam, and $\bar{m}_1$ and $\bar{m}_2$

are the mass per unit length of the upper beam and lower beam.

With the assumption of Eq. (2-2), Eq. (2-1) become

$$e_1 \frac{\partial^4 W_1}{\partial x^4} + K\left(W_1 - W_2\right) + \bar{m}_1 \frac{\partial^2 W_1}{\partial t^2} = f_1\left(x,t\right) \tag{2-3a}$$

$$e_2 \frac{\partial^4 W_2}{\partial x^4} - K\left(W_1 - W_2\right) + \bar{m}_2 \frac{\partial^2 W_2}{\partial t^2} = f_2\left(x,t\right) \tag{2-3b}$$

The initial conditions in general form are as follows:

$$W_1\left(x,0\right) = W_{10}\left(x\right),\ \ W_2\left(x,0\right) = W_{20}\left(x\right),\ \ \dot{W}_1\left(x,0\right) = V_{10}\left(x\right),\ \ \dot{W}_2\left(x,0\right) = V_{20}\left(x\right) \tag{2-4}$$

As to the boundary conditions at the ends ($x = 0$, L) of the two beams, since it can analyze different kinds of them in this chapter, so some common ones are listed as follows:

Simply supported: $W_i\left(0,t\right) = W_i\left(L,t\right) = W_i''\left(0,t\right) = W_i''\left(L,t\right) = 0$ (2-5a)

Clamped: $W_i\left(0,t\right) = W_i\left(L,t\right) = W_i'\left(0,t\right) = W_i'\left(L,t\right) = 0$ (2-5b)

Free: $W_i''\left(0,t\right) = W_i''\left(L,t\right) = W_i'''\left(0,t\right) = W_i'''\left(L,t\right) = 0$ (2-5c)

Spring supported: $W_i''\left(0,t\right) = W_i''\left(L,t\right) = 0$, $E_i I_i W_i'''\left(0,t\right) = -KW_i\left(0,t\right)$,

$$E_i I_i W_i'''\left(L,t\right) = KW_i\left(L,t\right) \tag{2-5d}$$

where i =1 or 2 represents upper beam or lower beam.

2.3 Solution of the Problem for Free Vibration

Based on the previous research results, it can be easily understood that the solutions for Eq. (2-3) are separable in time and space. The solutions can be assumed in the form as follows

$$W_1(x,t) = T(t)X_1(x) = De^{i\omega t}Ae^{px}, \quad W_2(x,t) = T(t)X_2(x) = De^{i\omega t}Be^{px} \tag{2-6}$$

where $T(t) = De^{i\omega t}$ is time function; $X_1(x) = Ae^{px}$ and $X_2(x) = Be^{px}$ is the mode shape function of the upper beam and lower beam, respectively; ω is the natural frequency of the double-beam system; A, B, D, P are unknown constants; and $i = \sqrt{-1}$ is imaginary unit.

With Eq. (2-6), the differential Eq. (2-3) become a set of algebraic ones and can be written in matrix form as follows

$$\begin{bmatrix} e_1P^4 + K - \bar{m}_1\omega^2 & -K \\ -K & e_2P^4 + K - \bar{m}_2\omega^2 \end{bmatrix} \begin{Bmatrix} A \\ B \end{Bmatrix} = \begin{Bmatrix} 0 \\ 0 \end{Bmatrix} \tag{2-7}$$

It is understandable that finding the solutions to Eq. (2-7) is an eigenvalue problem. The nontrivial solution for Eq. (2-7) requires the determinant of the coefficient matrix equal to 0, which derives out an eighth order polynomial equation in terms of P:

$$e_1e_2P^8 + \left(e_1K + e_2K - \bar{m}_1\omega^2e_2 - \bar{m}_2\omega^2e_1\right)P^4 + \left(\bar{m}_1\bar{m}_2\omega^4 - \bar{m}_1\omega^2K - \bar{m}_2\omega^2K\right) = 0 \tag{2-8}$$

Defining $Q = P^4$, Eq. (2-8) can be changed into a second order polynomial equation

$$e_1 e_2 Q^2 + \left(e_1 K + e_2 K - \bar{m}_1 \omega^2 e_2 - \bar{m}_2 \omega^2 e_1\right) Q + \left(\bar{m}_1 \bar{m}_2 \omega^4 - \bar{m}_1 \omega^2 K - \bar{m}_2 \omega^2 K\right) = 0 \tag{2-9}$$

Since the discriminant of this algebraic equation is positive

$$\Delta = \left[\left(\bar{m}_1 e_2 - \bar{m}_2 e_1\right)\omega^2 + K\left(e_1 - e_2\right)\right]^2 + 4 e_1 e_2 K^2 > 0 \tag{2-10}$$

Therefore the two roots of Eq. (2-9) are

$$Q_{1,2} = \frac{-\left(e_1 K + e_2 K - \bar{m}_1 \omega^2 e_2 - \bar{m}_2 \omega^2 e_1\right) \pm \sqrt{\Delta}}{2 e_1 e_2} \tag{2-11}$$

The eight roots of Eq. (2-8), that are also the values of constant *P*, can be written as

$$P_1 = \sqrt[4]{Q_1}\ , \quad P_2 = -\sqrt[4]{Q_1}\ , \quad P_3 = \sqrt[4]{Q_1} i\ , \quad P_4 = -\sqrt[4]{Q_1} i\ , \quad P_5 = \sqrt[4]{Q_2}\ , \quad P_6 = -\sqrt[4]{Q_2}\ , \quad P_7 = \sqrt[4]{Q_2} i\ ,$$

$$P_8 = -\sqrt[4]{Q_2} i \tag{2-12}$$

Using Eq. (2-7), the relationship among the constants *A* and *B* is given by

$$B = \frac{K}{e_2 P^4 + K - \bar{m}_2 \omega^2} \times A = \frac{e_1 P^4 + K - \bar{m}_1 \omega^2}{K} \times A \tag{2-13}$$

Considering there are eight roots P_j ($j = 1, 2 \ldots 8$) for Eq. (2-8), so there should be eight values in constants *A* and *B*, which makes Eq. (2-13) to be written specifically as

$$B_j = \frac{K}{e_2 P_j^4 + K - \bar{m}_2 \omega^2} \times A_j = \frac{e_1 P_j^4 + K - \bar{m}_1 \omega^2}{K} \times A_j = \beta_j A_j \tag{2-14}$$

Finally, the solution of Eq. (2-3) can be obtained in the form as follows

$$W_1(x,t)=\sum_{n=1}^{\infty}D_n e^{i\omega_n t}\left[\sum_{j=1}^{8}\left(A_{nj}e^{P_{nj}x}\right)\right] \tag{2-15a}$$

$$W_2(x,t)=\sum_{n=1}^{\infty}D_n e^{i\omega_n t}\left[\sum_{j=1}^{8}\left(B_{nj}e^{P_{nj}x}\right)\right]=\sum_{n=1}^{\infty}D_n e^{i\omega_n t}\left[\sum_{j=1}^{8}\left(\beta_{nj}A_{nj}e^{P_{nj}x}\right)\right] \tag{2-15b}$$

where ω_n is the *n*th natural frequency; and A_{nj}, B_{nj}, D_n, P_{nj}, β_{nj} are the unknown constants corresponding to *n*th natural frequency.

Substituting Eq. (2-15) into the real boundary conditions defined in Eq. (2-5) results in a set of eight algebraic equations with eight unknown constants A_{nj} ($j=1,2...8$) under each natural frequency. In matrix form, it can be represented as

$$[E]_{8\times8}\{A\}_{8\times1}=\{0\}_{8\times1} \tag{2-16}$$

where $\{A\}_{8\times1}=\{A_{n1}\quad A_{n2}\quad A_{n3}\quad A_{n4}\quad A_{n5}\quad A_{n6}\quad A_{n7}\quad A_{n8}\}^T$ is unknown constants vector; $\{0\}_{8\times1}=\{0\quad 0\quad 0\quad 0\quad 0\quad 0\quad 0\quad 0\}^T$ is zero vector; $[E]_{8\times8}$ is boundary conditions coefficient matrix.

As to $[E]_{8\times8}$ matrix, it depends on specific boundary conditions of upper and lower beams, and will be different when considering different boundary conditions. Meanwhile, in this chapter, the method adopting $[E]_{8\times8}$ matrix makes it is possible to discuss all kinds of boundary conditions and calculate the model that upper beam boundary conditions are different from lower beam, which

is an obvious advantage from previous research. The specific $[E]_{8\times8}$ matrix for several typical boundary conditions of double-beam system is demonstrated in Appendix 1.

The theory is same as in Eq. (2-7), nontrivial solutions for Eq. (2-16) will exist only when the determinant of the boundary conditions coefficient matrix $[E]_{8\times8}$ is equal to 0, so it makes $[E]_{8\times8}$ to be the frequency characteristic matrix.

$$|E| = 0 \tag{2-17}$$

Based on the Equations derived above, a semi-analytical method is developed to determine the natural frequencies and mode shapes of the whole double-beam system. The semi-analytical method can be generally expressed in a flowchart form as shown in Fig. 2-2. Once the frequency range is determined, all the natural frequencies and corresponding mode shapes in that range can be obtained by the semi-analytical method.

Due to the possible error of natural frequency by the finite step $\Delta\omega$, it is impossible to obtain the precise ω satisfying $|E| = 0$ directly. A searching process is needed, in which a classical numerical analysis method called Secant Method is adopted in this chapter and it is demonstrated specifically in Appendix 2.

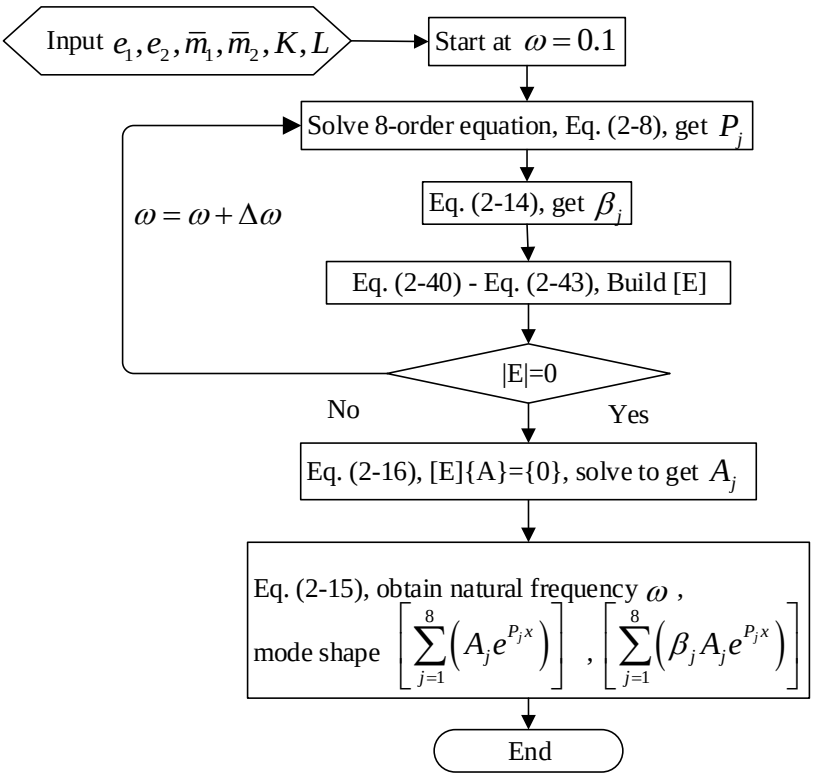

Fig. 2-2. Flowchart of the semi-analytical method to determine natural frequencies and mode shapes of double-beam with elastic layer system.

Although the natural frequencies and mode shapes have been obtained by the semi-analytical method introduced above, it is still needed to find the final form of the free vibration, which requires determining the value of constant D_n from the initial conditions defined in Eq. (2-4).

If the unknown variable is ω, the solution of the Eq. (2-13) will be

$$\omega = \pm\sqrt{\frac{\left(e_2 P^4 + K\right)B - AK}{\bar{m}_2 B}} = \pm\sqrt{\frac{\left(e_1 P^4 + K\right)A - BK}{\bar{m}_1 A}} \tag{2-18}$$

It is easy to find out that there are actually two roots value for each ω. Although the negative value is meaningless for real structure, it is meaningful for solving the equations of motion and obtaining the final form of free vibration. Based on Eq. (2-18), the two roots for each ω_n can be in the form

$$\omega_{n1} = \omega_n, \quad \omega_{n2} = -\omega_n \tag{2-19}$$

The assuming final solutions for free vibration can be written as

$$W_1(x,t) = \sum_{n=1}^{\infty}\left(D_{n1}e^{i\omega_n t} + D_{n2}e^{-i\omega_n t}\right)\left[\sum_{j=1}^{8}\left(A_{nj}e^{P_{nj}x}\right)\right] = \sum_{n=1}^{\infty}\left(D_{n1}e^{i\omega_n t} + D_{n2}e^{-i\omega_n t}\right)\phi_{n1}(x) = \sum_{n=1}^{\infty}T_n(t)\phi_{n1}(x) \tag{2-20a}$$

$$W_2(x,t) = \sum_{n=1}^{\infty}\left(D_{n1}e^{i\omega_n t} + D_{n2}e^{-i\omega_n t}\right)\left[\sum_{j=1}^{8}\left(\beta_{nj}A_{nj}e^{P_{nj}x}\right)\right] = \sum_{n=1}^{\infty}\left(D_{n1}e^{i\omega_n t} + D_{n2}e^{-i\omega_n t}\right)\phi_{n2}(x) = \sum_{n=1}^{\infty}T_n(t)\phi_{n2}(x) \tag{2-20b}$$

where $\phi_{n1}(x)$ and $\phi_{n2}(x)$ are the mode shape functions under *n*th natural frequency for the upper and lower beams, respectively, and $T_n(t)$ is time function corresponding to *n*th natural frequency.

Substituting Eq. (2-20) into Eq. (2-4), the initial conditions could be denoted as

$$\sum_{n=1}^{\infty}(D_{n1} + D_{n2})\phi_{n1}(x) = W_{10}(x) \tag{2-21a}$$

$$\sum_{n=1}^{\infty}(D_{n1} + D_{n2})\phi_{n2}(x) = W_{20}(x) \tag{2-21b}$$

$$\sum_{n=1}^{\infty}\left(i\omega_n D_{n1}-i\omega_n D_{n2}\right)\phi_{n1}\left(x\right)=V_{10}\left(x\right) \tag{2-21c}$$

$$\sum_{n=1}^{\infty}\left(i\omega_n D_{n1}-i\omega_n D_{n2}\right)\phi_{n2}\left(x\right)=V_{20}\left(x\right) \tag{2-21d}$$

In order to apply modal expansion method to solve Eq. (2-21), it is necessary to derive the orthogonality condition for different mode shapes of the double-beam system with elastic layer. The governing equations Eq. (2-3) for free vibration ($f_1\left(x,t\right)=f_2\left(x,t\right)=0$) can be written as

$$-\bar{m}_1\frac{\partial^2 W_1}{\partial t^2}=e_1\frac{\partial^4 W_1}{\partial x^4}+K\left(W_1-W_2\right) \tag{2-22a}$$

$$-\bar{m}_2\frac{\partial^2 W_2}{\partial t^2}=e_2\frac{\partial^2 W_2}{\partial x^2}-K\left(W_1-W_2\right) \tag{2-22b}$$

The left terms $-\bar{m}_1\frac{\partial^2 W_1}{\partial t^2}$ and $-\bar{m}_2\frac{\partial^2 W_2}{\partial t^2}$ are due to acceleration, so they are a kind of inertial force $f_{I1}\left(x,t\right)$ and $f_{I2}\left(x,t\right)$. The right terms are related to displacement, so they can be treated as a sort of elastic force. When considering the whole double-beam system, which consists of upper beam and lower beam, an energy equilibrium equation will be obtained as

$$\int_0^L\left[W_{1m}\left(x,t\right)f_{I1n}\left(x,t\right)+W_{2m}\left(x,t\right)f_{I2n}\left(x,t\right)\right]dx=\int_0^L\left[W_{1n}\left(x,t\right)f_{I1m}\left(x,t\right)+W_{2n}\left(x,t\right)f_{I2m}\left(x,t\right)\right]dx \tag{2-23}$$

Substituting Eq. (2-20) into Eq. (2-23), and applying the definitions of $f_{I1}\left(x,t\right)$ and $f_{I2}\left(x,t\right)$, Eq. (2-23) reads

$$\int_0^L \left[T_m(t)\phi_{m1}(x)(-\bar{m}_1)\omega_n^2 T_n(t)\phi_{n1}(x) \right] dx + \int_0^L \left[T_m(t)\phi_{m2}(x)(-\bar{m}_2)\omega_n^2 T_n(t)\phi_{n2}(x) \right] dx$$
$$= \int_0^L \left[T_n(t)\phi_{n1}(x)(-\bar{m}_1)\omega_m^2 T_m(t)\phi_{m1}(x) \right] dx + \int_0^L \left[T_n(t)\phi_{n2}(x)(-\bar{m}_2)\omega_m^2 T_m(t)\phi_{m2}(x) \right] dx \quad (2\text{-}24)$$

Merging the similar items, the Eq. (2-24) will be simplified as

$$\left\{ \bar{m}_1 \int_0^L \left[\phi_{n1}(x)\phi_{m1}(x) \right] dx + \bar{m}_2 \int_0^L \left[\phi_{n2}(x)\phi_{m2}(x) \right] dx \right\} \times T_m(t) T_n(t) \left(\omega_m^2 - \omega_n^2 \right) = 0 \quad (2\text{-}25)$$

Since for different natural frequencies, $\omega_m^2 \neq \omega_n^2$, so the orthogonality condition for different mode shapes of the double-beam system with elastic layer is

$$\int_0^L \left[\phi_{n1}(x)\bar{m}_1\phi_{m1}(x) + \phi_{n2}(x)\bar{m}_2\phi_{m2}(x) \right] dx = \bar{M}_n \delta_{mn} \quad (2\text{-}26)$$

where $\bar{M}_n$ is the generalized mass in the *n*th mode, δ_{mn} is the Kronecker delta function.

Once the orthogonality condition is derived, go back to the initial condition Eq. (2-21). $Eq.(2-21a) \times \phi_{m1}(x)\bar{m}_1 + Eq.(2-21b) \times \phi_{m2}(x)\bar{m}_2$, and integrate it respect to *x* from 0 to *L*

$$\int_0^L \phi_{m1}(x)\bar{m}_1 \sum_{n=1}^{\infty} (D_{n1} + D_{n2})\phi_{n1}(x)\,dx + \int_0^L \phi_{m2}(x)\bar{m}_2 \sum_{n=1}^{\infty} (D_{n1} + D_{n2})\phi_{n2}(x)\,dx$$
$$= \int_0^L \phi_{m1}(x)\bar{m}_1 W_{10}(x)\,dx + \int_0^L \phi_{m2}(x)\bar{m}_2 W_{20}(x)\,dx \quad (2\text{-}27)$$

The orthogonality condition is applied into Eq. (2-27), and it will be transferred as

$$D_{n1} + D_{n2} = \frac{\int_0^L \left[\phi_{n1}(x)\bar{m}_1 W_{10}(x) + \phi_{n2}(x)\bar{m}_2 W_{20}(x) \right] dx}{\int_0^L \left[\phi_{n1}(x)\bar{m}_1\phi_{n1}(x) + \phi_{n2}(x)\bar{m}_2\phi_{n2}(x) \right] dx} \quad (2\text{-}28)$$

$Eq.(2-21c)\times\phi_{m1}(x)\bar{m}_1 + Eq.(2-21d)\times\phi_{m2}(x)\bar{m}_2$, and integrate it respect to *x* from 0 to *L*; apply orthogonality condition like in Eq. (2-27), it will be

$$D_{n1} - D_{n2} = \frac{1}{i\omega_n}\frac{\int_0^L\left[\phi_{n1}(x)\bar{m}_1V_{10}(x)+\phi_{n2}(x)\bar{m}_2V_{20}(x)\right]dx}{\int_0^L\left[\phi_{n1}(x)\bar{m}_1\phi_{n1}(x)+\phi_{n2}(x)\bar{m}_2\phi_{n2}(x)\right]dx} \tag{2-29}$$

Solving Eq. (2-28) and Eq. (2-29), the solution of D_{n1} and D_{n2} can be

$$D_{n1} = \frac{1}{2}\times\left\{\frac{\bar{W}_n}{\bar{M}_n}+\frac{1}{i\omega_n}\times\frac{\bar{V}_n}{\bar{M}_n}\right\} \tag{2-30a}$$

$$D_{n2} = \frac{1}{2}\times\left\{\frac{\bar{W}_n}{\bar{M}_n}-\frac{1}{i\omega_n}\times\frac{\bar{V}_n}{\bar{M}_n}\right\} \tag{2-30b}$$

$$\bar{M}_n = \int_0^L\left[\phi_{n1}(x)\bar{m}_1\phi_{n1}(x)+\phi_{n2}(x)\bar{m}_2\phi_{n2}(x)\right]dx \tag{2-30c}$$

$$\bar{W}_n = \int_0^L\left[\phi_{n1}(x)\bar{m}_1W_{10}(x)+\phi_{n2}(x)\bar{m}_2W_{20}(x)\right]dx \tag{2-30d}$$

$$\bar{V}_n = \int_0^L\left[\phi_{n1}(x)\bar{m}_1V_{10}(x)+\phi_{n2}(x)\bar{m}_2V_{20}(x)\right]dx \tag{2-30e}$$

where $\bar{M}_n$, $\bar{W}_n$, $\bar{V}_n$ is the generalized mass, displacement and velocity in the *n*th mode.

Until here, all constants in the assumed solutions in Eq. (2-6) or Eq. (2-20) have been determined. Therefore the free vibration of a double-beam system with elastic layer is solved successfully.

2.4 Solution of the Problem for Forced Vibration

Once the natural frequencies and mode shapes of a double-beam system are obtained by the

analysis of free vibration, it is possible to determine the response of the forced vibration in the same model. It is similar to the solutions of free vibration, particular solutions of forced vibration in the same model could be assumed in the following form

$$W_1(x,t)=\sum_{n=1}^{\infty}T_n(t)\left[\sum_{j=1}^{8}\left(A_{nj}e^{P_{nj}x}\right)\right]=\sum_{n=1}^{\infty}T_n(t)\phi_{n1}(x) \tag{2-31a}$$

$$W_2(x,t)=\sum_{n=1}^{\infty}T_n(t)\left[\sum_{j=1}^{8}\left(\beta_{nj}A_{nj}e^{P_{nj}x}\right)\right]=\sum_{n=1}^{\infty}T_n(t)\phi_{n2}(x) \tag{2-31b}$$

where $\phi_{n1}(x)=\sum_{j=1}^{8}\left(A_{nj}e^{P_{nj}x}\right)$ is mode shape function of upper beam corresponding to *n*th natural frequency; $\phi_{n2}(x)=\sum_{j=1}^{8}\left(\beta_{nj}A_{nj}e^{P_{nj}x}\right)$ is mode shape function of lower beam corresponding to *n*th natural frequency; $T_n(t)$ is time function corresponding to *n*th natural frequency; $\phi_{n1}(x)$ and $\phi_{n2}(x)$ are known from the free vibration analysis, but $T_n(t)$ is unknown function which need to be solved.

Substituting the assumed solutions Eq. (2-31) into motion equations of the whole system Eq. (2-3), so they become

$$e_1\sum_{n=1}^{\infty}T_n(t)\frac{d^4\phi_{n1}(x)}{dx^4}+K\sum_{n=1}^{\infty}T_n(t)\left[\phi_{n1}(x)-\phi_{n2}(x)\right]+\bar{m}_1\sum_{n=1}^{\infty}\frac{d^2T_n(t)}{dt^2}\phi_{n1}(x)=f_1(x,t) \tag{2-32a}$$

$$e_2\sum_{n=1}^{\infty}T_n(t)\frac{d^4\phi_{n2}(x)}{dx^4}-K\sum_{n=1}^{\infty}T_n(t)\left[\phi_{n1}(x)-\phi_{n2}(x)\right]+\bar{m}_2\sum_{n=1}^{\infty}\frac{d^2T_n(t)}{dt^2}\phi_{n2}(x)=f_2(x,t) \tag{2-32b}$$

Introducing free vibration equations in here can simplify the motion equations of forced vibration.

Substituting Eq. (2-20) into Eq. (2-22), eliminating the same term $\left(D_{n1}e^{i\omega_n t}+D_{n2}e^{-i\omega_n t}\right)$ and multiplying the $T_n(t)$ in each term, the Eq. (2-22) will be in form of:

$$e_1\sum_{n=1}^{\infty}T_n(t)\frac{d^4\phi_{n1}(x)}{dx^4}+K\sum_{n=1}^{\infty}T_n(t)\left[\phi_{n1}(x)-\phi_{n2}(x)\right]=\bar{m}_1\sum_{n=1}^{\infty}\omega_n^2T_n(t)\phi_{n1}(x) \tag{2-33a}$$

$$e_2\sum_{n=1}^{\infty}T_n(t)\frac{d^4\phi_{n2}(x)}{dx^4}-K\sum_{n=1}^{\infty}T_n(t)\left[\phi_{n1}(x)-\phi_{n2}(x)\right]=\bar{m}_2\sum_{n=1}^{\infty}\omega_n^2T_n(t)\phi_{n2}(x) \tag{2-33b}$$

Introducing Eq. (2-33) into Eq. (2-32) yields:

$$\sum_{n=1}^{\infty}\left[\bar{m}_1\phi_{n1}(x)\frac{d^2T_n(t)}{dt^2}+\bar{m}_1\omega_n^2\phi_{n1}(x)T_n(t)\right]=f_1(x,t) \tag{2-34a}$$

$$\sum_{n=1}^{\infty}\left[\bar{m}_2\phi_{n2}(x)\frac{d^2T_n(t)}{dt^2}+\bar{m}_2\omega_n^2\phi_{n2}(x)T_n(t)\right]=f_2(x,t) \tag{2-34b}$$

$Eq.(2-34a)\times\phi_{m1}(x)+Eq.(2-34b)\times\phi_{m2}(x)$, integrate it respect to x from 0 to L, and apply orthogonality condition Eq. (2-26), so it will be

$$\frac{d^2T_n(t)}{dt^2}+\omega_n^2T_n(t)=F_n(t) \tag{2-35a}$$

$$F_n(t)=\frac{\int_0^L\left[\phi_{n1}(x)\,f_1(x,t)+\phi_{n2}(x)\,f_2(x,t)\right]dx}{\int_0^L\left[\phi_{n1}(x)\bar{m}_1\phi_{n1}(x)+\phi_{n2}(x)\bar{m}_2\phi_{n2}(x)\right]dx} \tag{2-35b}$$

Using Duhamel's integral, particular solution of Eq. (2-35) can be obtained as

$$T_n(t)=\frac{1}{\omega_n}\int_0^t F_n(\tau)\cdot\sin\left[\omega_n(t-\tau)\right]d\tau \tag{2-36}$$

Until here, $T_n(t)$ is solved, $\phi_{n1}(x)$ and $\phi_{n2}(x)$ are known functions from free vibration analysis, by assuming solutions Eq. (2-31), so the forced vibration of a double-beam system with elastic layer is solved successfully.

2.5 Numerical Examples

In order to illustrate the semi-analytical method presented in this chapter, some numerical examples are discussed in detail. In this section, free vibration and forced vibration numerical examples are demonstrated, respectively. Since the method proposed in this chapter is able to calculate the natural frequencies and mode shapes of a double-beam system with arbitrary boundary conditions, several typical boundary conditions of double-beam system are analyzed in free vibration part. The model with upper beam simply supported-simply supported and lower beam simply supported-simply supported (Fig. 2-3(a)), is applied to verify the correctness and accuracy of the proposed method. In the forced vibration part, upper beam spring supported-spring supported and lower beam simply supported-simply supported (Fig. 2-3(b)) is the main boundary condition simulated because it is realistic in engineering projects.

a

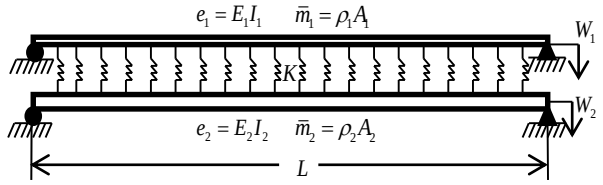

b

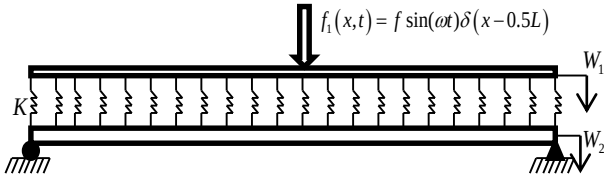

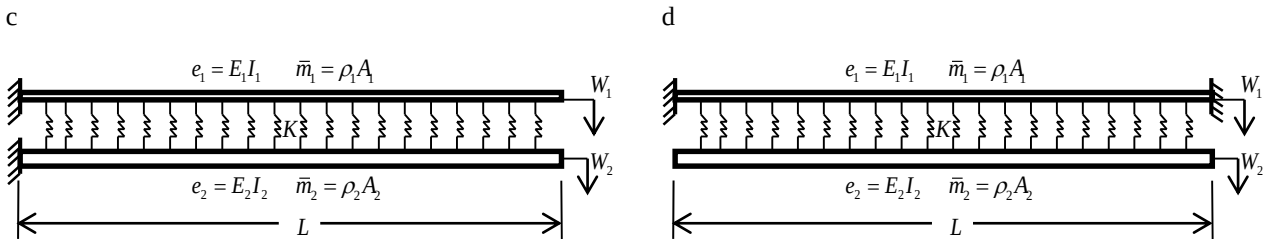

Fig. 2-3. The model of a double-beam system: (a) free vibration model with same boundary condition for upper and lower beam: simply supported-simply supported; (b) forced vibration model with a concentrated harmonic force in midspan of upper beam; (c) free vibration model with boundary condition: upper beam clamped-free and lower beam clamped-free; and (d) free vibration model with boundary condition: upper beam clamped-clamped and lower beam free-free.

2.5.1 Free Vibration

The values for the basic parameters of the double-beam system from reference (Oniszczuk 2000c) are used in the numerical calculations.

$E = 1\times10^{10}\,Nm^{-2}$, $I = 4\times10^{-4}\,m^4$, $\rho = 2\times10^{3}\,kgm^{-3}$, $A = 5\times10^{-2}\,m^2$, $L = 10m$,

$e = EI = 4\times10^{6}\,Nm^2$, $m = \rho A = 1\times10^{2}\,kgm^{-1}$, $K = (1\sim5)\times10^{5}\,Nm^{-2}$.

Five cases are investigated in here for verification and discussion:

Case 1: upper beam simply supported-simply supported and lower beam simply supported-simply supported (Fig. 2-3(a)), $e_1 = e_2 = e$, $m_1 = m_2 = m$;

Case 2: upper beam spring supported-spring supported and lower beam simply supported-simply supported (Fig. 2-1(a)), $e_1 = e_2 = e$, $m_1 = m_2 = m$;

Case 3: upper beam spring supported-spring supported and lower beam simply supported-simply supported (Fig. 2-1(a)), $e_1 = 0.8e$, $e_2 = e$, $m_1 = 0.2m$, $m_2 = m$;

Case 4: upper beam clamped-free and lower beam clamped-free (Fig. 2-3(c)), $e_1 = e_2 = e$, $m_1 = m_2 = m$;

Case 5: upper beam clamped-clamped and lower beam free-free (Fig. 2-3(d)), $e_1 = e$, $e_2 = 0.8e$, $m_1 = m$, $m_2 = 0.2m$.

The natural frequencies and mode shapes of the five cases are calculated by the semi-analytical method presented in this chapter, the first six natural frequencies and normal mode shapes of each case are summarized in Tables 2-1 to 2-5, Fig. 2-4 and Fig. 2-13 to Fig. 2-16, respectively. The comparative results available in reference (Oniszczuk 2000c) are also summarized in Table 2-1. Some of the specific results are shown in Appendix 3.

Table 2-1. Natural Frequencies of double-beam system ω_n (s^{-1}); Case 1

$K\times10^{-5}$	$n=1$		$n=2$		$n=3$		$n=4$		$n=5$		$n=6$	
$\left(Nm^{-2}\right)$	Present	Ref.	Present	Ref.	Present	Ref.	Present	Ref.	Present	Ref.	Present	Ref.
1	19.74	19.7	48.88	48.9	78.96	79	90.74	90.7	177.65	177.7	183.20	183.2
2	19.74	19.7	66.25	66.3	78.96	79	101.16	101.2	177.65	177.7	188.58	188.6
3	19.74	19.7	78.94	79	79.96	79.9	110.61	110.6	177.65	177.7	193.81	193.8
4	19.74	19.7	78.96	79	91.59	91.6	119.31	119.3	177.65	177.7	198.90	198.9
5	19.74	19.7	78.96	79	101.93	101.9	127.41	127.4	177.65	177.7	203.86	203.9

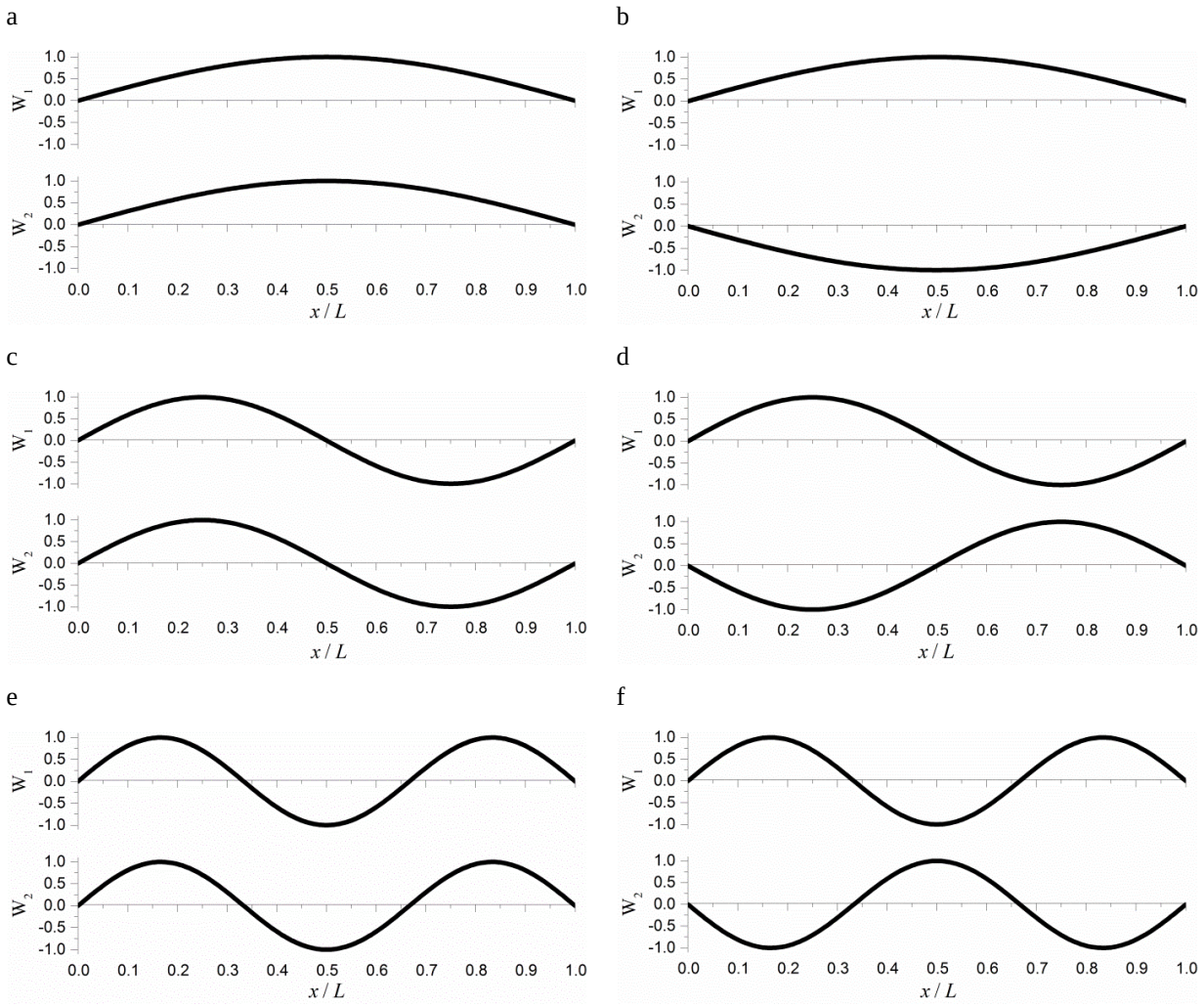

Fig. 2-4. The first six normal mode shapes of the double-beam system for Case 1, $K = 1\times10^{5}$: (a) mode 1; (b) mode 2; (c) mode 3; (d) mode 4; (e) mode 5; (f) mode 6.

In Table 2-1, it can be seen that the natural frequencies calculated by the semi-analytical method presented in this chapter, are in excellent agreement with the analytical solutions from previous research in reference (Oniszczuk 2000c). Therefore, the correctness and accuracy of the semi-analytical method are proved and demonstrated by the comparison above in Table 2-1.

The data in Table 2-2 to Table 2-5 are also plotted in Fig. 2-5, which indicate the effects of elastic

layer stiffness *K* on the natural frequency ω_n of whole double-beam system. In general, as shown in Fig. 2-5, there is a tendency to increase the natural frequency ω_n in case of increasing the elastic layer stiffness *K*. However, some natural frequencies are not so sensitive to the elastic layer stiffness, such as ω_1 in each case and ω_2, ω_5 in Case 4. It can be explained by their corresponding mode shapes: for ω_1 in each case and ω_2, ω_5 in Case 4, the corresponding mode shapes are symmetric mode shapes which vibrate as a single beam. The elastic layer does not deform much and it cannot produce significant force to affect two-beam vibrations. Therefore, the change of elastic layer stiffness cannot change their natural frequencies apparently. For the mode shapes of other natural frequencies are of antisymmetric mode shape, large deformation will be produced in elastic layer and its internal force is significant to affect two-beam vibrations. Therefore those natural frequencies are sensitive to the stiffness of elastic layer. In addition, in Case 2 and Case 3, the increase of higher natural frequencies is greater than the lower ones. On the other hand, in Case 1, Case 4, and Case 5, the increase of higher natural frequencies is smaller although ω_n is increasing with the increase of *K*. The primary reason for that difference is due to the boundary conditions of the two-beam system, as shown in Case 2 and Case 3 which are better for adjusting the higher frequencies than those in Case 1, Case 4 and Case 5. When $K = 4\times10^5\, Nm^{-2}$ in Case 3, the values of ω_4 and ω_5 are very close, and it also can be seen for ω_4 and ω_5 in Case 5 when $K = 2\times10^5\, Nm^{-2}$. It means that the two different natural frequencies may have same values when *K* reaches some special values, and this phenomenon is also illustrated in previous research work (Chen and Sheu 1994). To avoid the resonance and protect the safety of

the whole system, those *K* values cannot be choosen when design it.

From Case 1 and Case 2, when the boundary condition of upper beam is spring supported-spring supported, the natural frequencies of whole double-beam system are smaller than it is simply supported-simply supported (see Table 2-1 and Table 2-2), so the higher natural frequencies could be avoided effectively by the boundary condition presented in this chapter. From Case 2 and Case 3, when the upper beam is smaller than lower beam, the natural frequencies become higher (see Table 2-2 and Table 2-3), that could help to solve some low frequency domain vibration problems in engineering projects. The models in Case 3 and Case 5 are two typical beam-type vibration suppression structures, which can be recognized as floating slab and beam-type dynamic vibration absorber, respectively, and it can be found that changing the stiffness of the elastic layer can alter the natural frequencies of whole double-beam system apparently (see Table 2-3 and Table 2-5), demonstrating that those two structures are able to avoid the resonance situation occurred in normal structures and potentially to reduce the original structural vibrations.

a

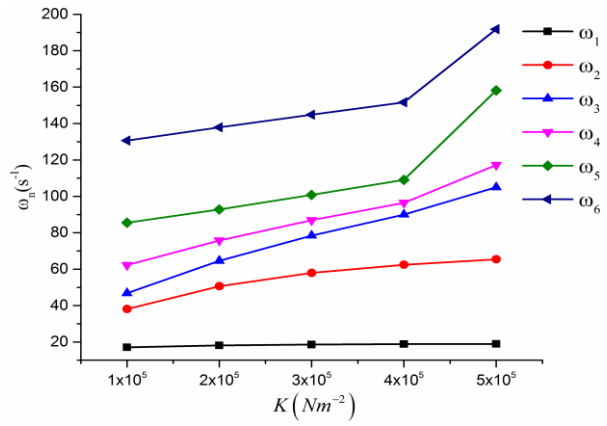

b

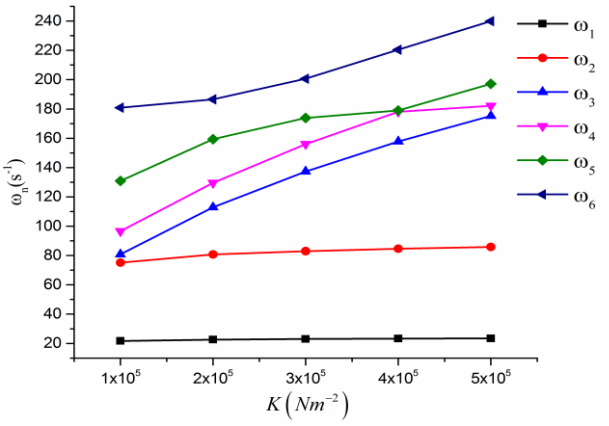

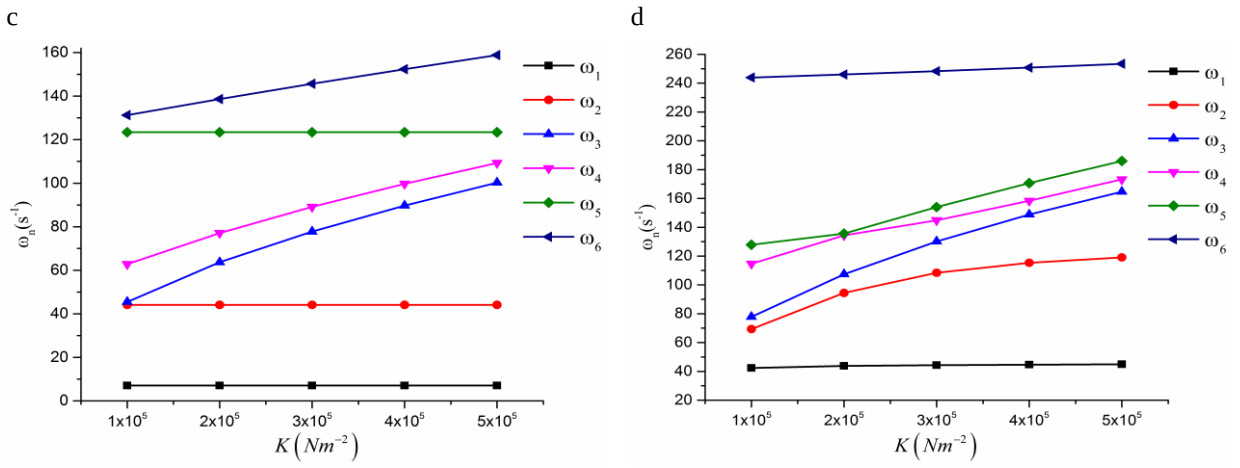

Fig. 2-5. Natural frequencies of double-beam system ω_n versus elastic layer stiffness K: (a) Case 2; (b) Case 3; (c) Case 4; (d) Case 5.

2.5.2 Forced Vibration

The values for the basic parameters of the double-beam system are the same from reference (Oniszczuk 2000c) as in free vibration.

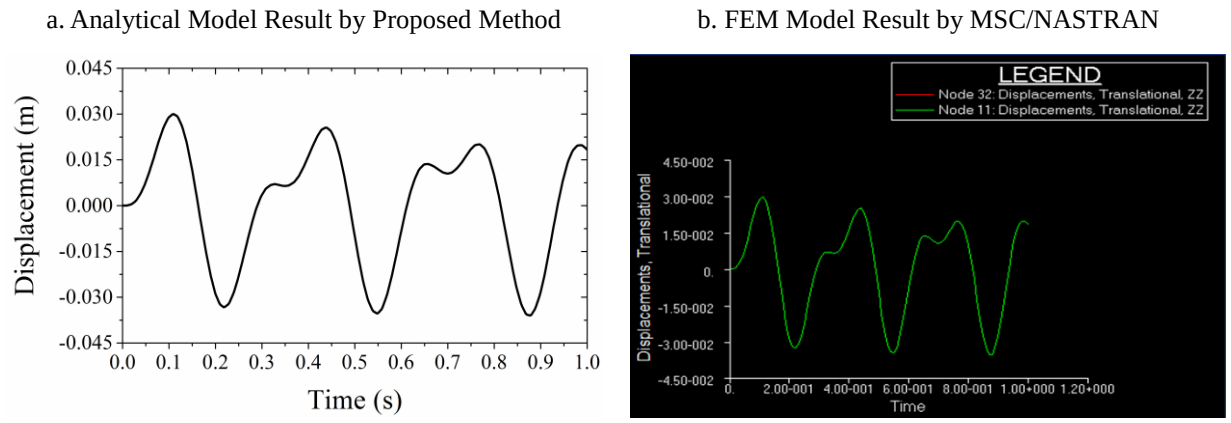

Fig. 2-6. Displacement at midspan point of two beams.

A forced vibration of a double-beam system model is calculated and compared with the same

model analyzed by the finite element method software MSC/NASTRAN. The boundary conditions of the double-beam system are simply supported-simply supported for the upper beam and simply supported-simply supported for the lower beam, and the exciting forces are $f_1(x,t)=10000\sin(37.68t)$, $f_2(x,t)=0$. As shown in Fig. 2-6, it can be seen that the dynamic responses calculated by the method presented in this chapter, are in excellent agreement with the finite element method solutions. Therefore, the correctness and accuracy of the proposed method are proved and demonstrated by the comparison.

Then, several cases are calculated and analyzed in here, all of them are with the same boundary condition: upper beam spring supported-spring supported and lower beam simply supported-simply supported (Fig. 2-3(b)), which is more realistic in engineering projects. Among all of those cases; the exciting force of the double-beam system is $f_1(x,t)=f\sin(\omega t)\delta(x-0.5L)$, $f_2(x,t)=0$, (Fig. 2-3(b)), where f is amplitude and ω is frequency of a concentrated harmonic force acted on the midspan of the upper beam; $\delta(x)$ is Dirac delta function.

2.5.2.1 Resonance Condition

The solution for double-beam system forced vibration is derived as Eq. (2-31), Eq. (2-35) and Eq. (2-36), considering the exciting force is $f_1(x,t)=f\sin(\omega t)\delta(x-0.5L)$, $f_2(x,t)=0$, so the specific solution becomes

$$W_1(x,t)=\sum_{n=1}^{\infty}T_n(t)\phi_{n1}(x)=\sum_{n=1}^{\infty}\frac{f\overline{H}}{\omega_n}\cdot\frac{\left[\omega\sin(\omega_n t)-\omega_n\sin(\omega t)\right]}{\omega^2-\omega_n^2}\phi_{n1}(x) \tag{2-37a}$$

$$W_2(x,t)=\sum_{n=1}^{\infty}T_n(t)\phi_{n2}(x)=\sum_{n=1}^{\infty}\frac{f\overline{H}}{\omega_n}\cdot\frac{\left[\omega\sin(\omega_n t)-\omega_n\sin(\omega t)\right]}{\omega^2-\omega_n^2}\phi_{n2}(x) \tag{2-37b}$$

where $\overline{H}=\dfrac{\int_0^L\phi_{n1}(x)\delta(x-0.5L)dx}{\int_0^L\left[\phi_{n1}(x)m_1\phi_{n1}(x)+\phi_{n2}(x)m_2\phi_{n2}(x)\right]dx}$ (2-38)

In Eq. (2-37), the denominator is $\left(\omega_n^2-\omega^2\right)$, so when the harmonic force frequency ω is close to the natural frequency of double-beam system ω_n, the dynamic responses of the two beams, W_1 and W_2, both of them will be unlimited, which is called resonance phenomenon. Therefore, the resonance condition for double-beam system is

$$\omega=\omega_n,\quad n=1,2,3,... \tag{2-39}$$

Two cases are calculated in here for verifying the resonance condition:

Case 1: two identical beams, $e_1=e_2=e$, $m_1=m_2=m$, $K=1\times10^5\,Nm^{-2}$;

Case 2: smaller upper beam, $e_1=0.8e$, $e_2=e$, $m_1=0.2m$, $m_2=m$, $K=1\times10^5\,Nm^{-2}$.

The frequency responses at the midspan of the two beams are calculated by the equations presented in this chapter, and the absolute amplitude of the frequency responses at the two beams midspan points are shown in Fig. 2-7.

a

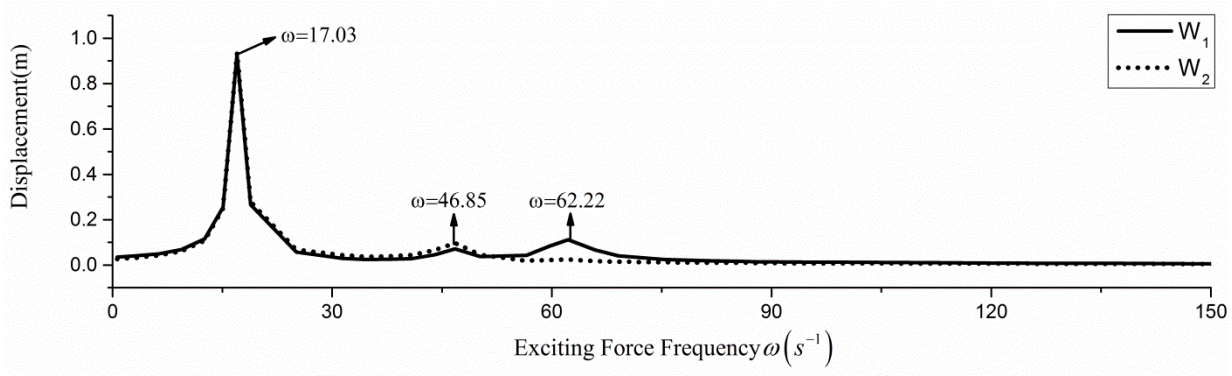

b

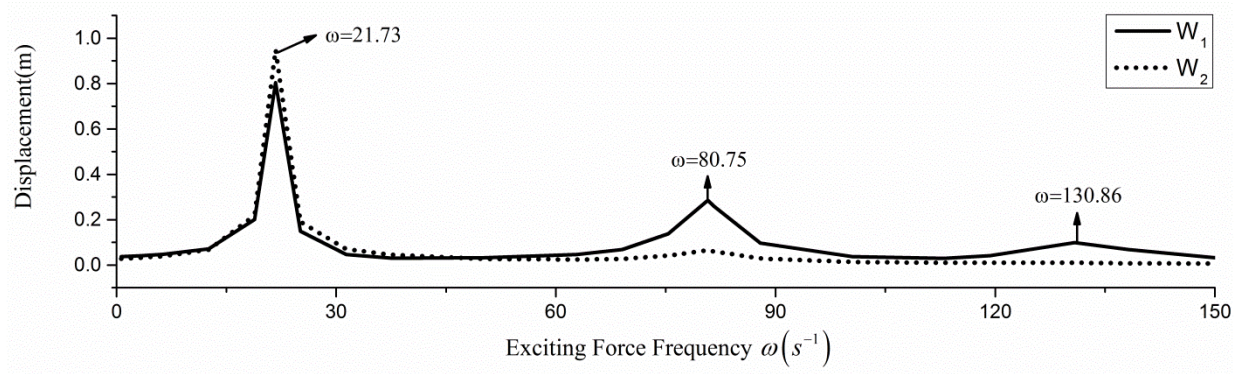

Fig. 2-7. Frequency response at midspan point of two beams: (a)Two identical beams; (b) Smaller upper beam.

From Fig. 2-7, Table 2-2 and Table 2-3, it can be easily seen that the dynamic response of two beams reach some peak values when the exciting force frequencies ω is close to the natural frequencies of double-beam system ω_n, which is just the resonance phenomenon and verifies the resonance condition derived above. When designing the double-beam system, it is supposed to make the natural frequencies of system being far away from the frequency of exciting force, and avoid the resonance phenomenon happened.

Also in Fig. 2-7, when the resonance frequency $\omega = 62.22$ in Case 1, and $\omega = 80.75, 130.86$ in

Case 2, only the upper beam has the peak values, and in contrast, lower beam doesn't have. The main reason for that is the corresponding mode shapes. Checking the mode shapes in Fig. 2-13(d), Fig. 2-14(c) and Fig. 2-14(e), it is found that the deformation amplitude of lower beam is very small comparing with the upper beam, so in those resonance frequencies, the lower beam dynamic response is not as great as upper beam, although there is still resonance happened to lower beam.

2.5.2.2 Effect of Elastic Layer Stiffness

An important parameter in the double-beam system is the stiffness of elastic layer, *K*, which is the connection between upper beam and lower beam, so it is necessary to make some discussions about the effect of elastic layer stiffness *K* on two beams dynamic responses.

Three cases are investigated in here for discussion:

$e_1 = e_2 = e$, $m_1 = m_2 = m$; Case 1: $K = 1\times10^4\, Nm^{-2}$; Case 2: $K = 2\times10^4\, Nm^{-2}$; Case 3: $K = 3\times10^4\, Nm^{-2}$.

The absolute amplitude of frequency responses at the midspan of the two beams are shown in a form of semi-log plots in Fig. 2-8.

As to the upper beam, from Fig. 2-8(a), with the increase of layer stiffness *K*, the dynamic response is generally reduced. Although the resonance frequencies is increase with *K*, the peak values at

resonance frequencies are also decreased. Upper beam in here is a kind of a beam on elastic foundation, when the elastic layer becomes stiffer, the restrict to the upper beam gets stronger, so the upper beam vibrates smaller under same exciting force.

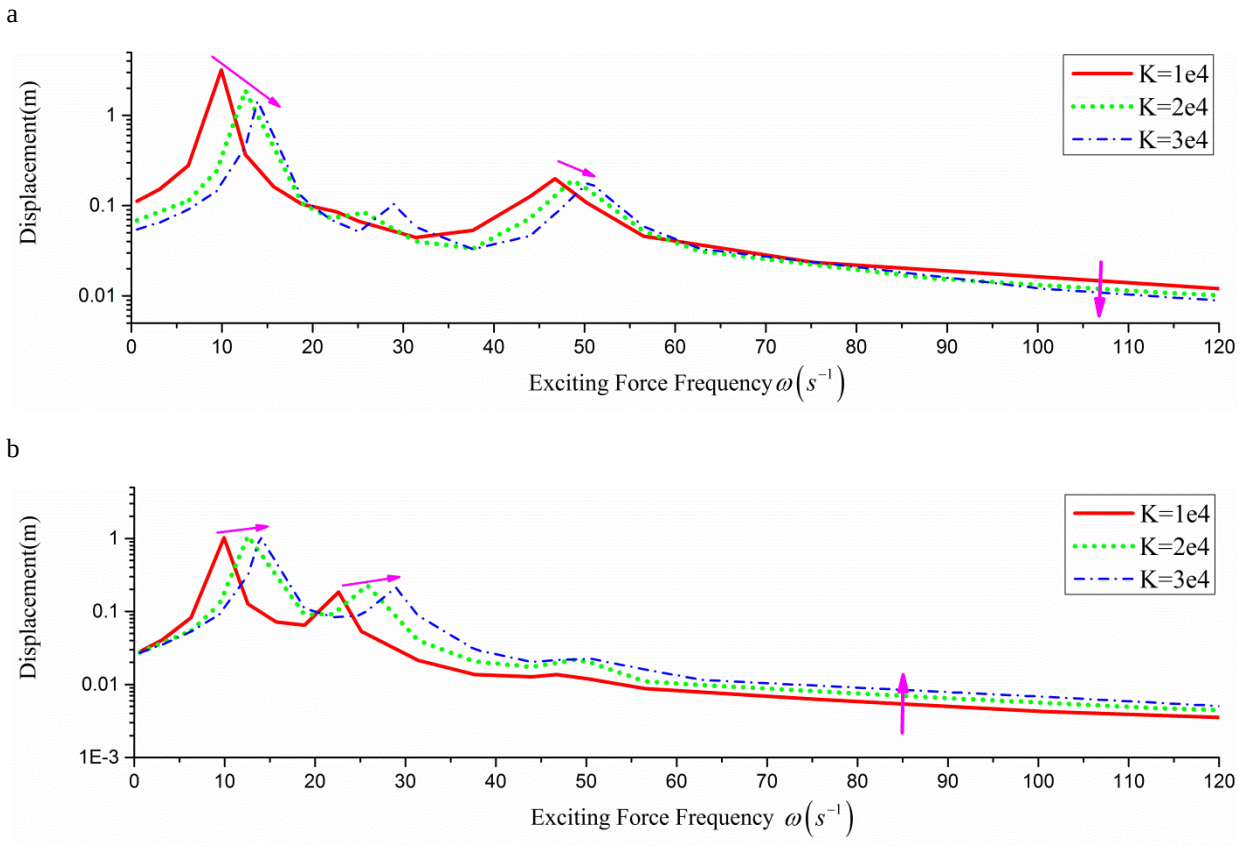

Fig. 2-8. Frequency response at midspan point of two beams: (a) upper beam; (b) lower beam.

From Fig. 2-8(b), the lower beam has an opposite changes comparing with upper beam. The dynamic response is generally increased with the increase of layer stiffness *K*, and the peak values at resonance frequencies are also increased. Elastic layer is the connection between upper beam and lower beam, and it transfers the vibration energy from upper beam to lower beam. When elastic

layer is softer, it deforms larger and upper beam can absorb more exciting energy, so the energy transferred to lower beam is less; when the elastic layer gets stiffer, its deformation is smaller and less energy absorbed by upper beam itself, so more and more energy is transferred to lower beam and makes the vibration of it increased.

2.5.2.3 Effect of Upper Beam Mass

In many real engineering projects, the upper beam and lower beam are not identical in a double-beam system. Considering reducing the dynamic vibration of lower beam, the upper beam is often designed as a kind of vibration absorber, so the physical property of the upper beam has significant effects in dynamic vibration reduction. Among those physical properties, the mass of the upper beam is discussed in here.

Three cases are investigated in here for discussion:

$e_1 = 0.8e$, $e_2 = e$, $m_2 = m$, $K = 1\times10^5\, Nm^{-2}$; Case 1: $m_1 = 0.1m$; Case 2: $m_1 = 0.5m$; Case 3: $m_1 = m$.

The frequency response at the midspan of the lower beam is shown in semi-log plots in Fig. 2-9.

The general tendency for the dynamic response of lower beam is decreased in the case of increasing upper beam mass, which can be found from Fig. 2-9. In the whole double-beam system, upper beam accept the exciting energy firstly, absorbs some of them and then transfer the others to lower

beam by elastic layer. If the mass of upper beam becomes larger, when upper beam vibrates, it will absorb more exciting energy to complete its own vibration, so the energy left for lower beam is reduced and the vibration of lower beam gets smaller. However, the mass of upper beam cannot grow to very large, since when it exceeds a limit value, the vibration energy of upper beam itself will be too huge and it will be transferred to lower beam by elastic layer too, so the lower beam vibration is not reduced anymore in that case.

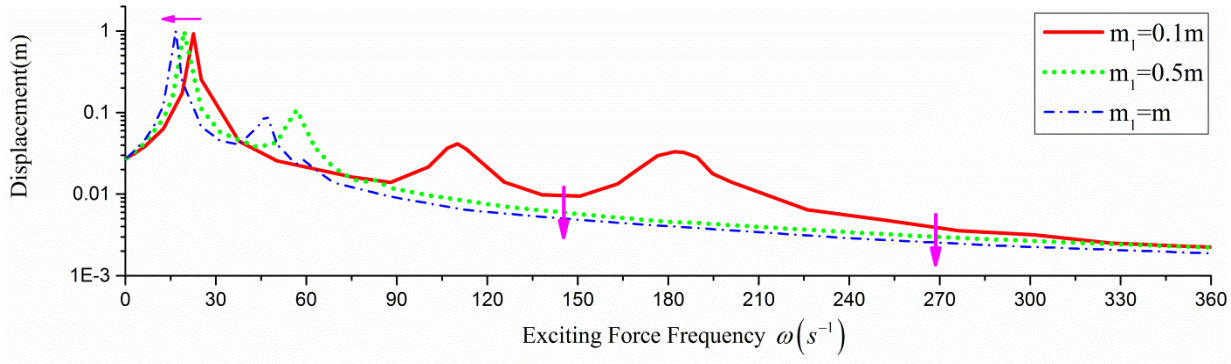

Fig. 2-9. Frequency response at midspan point of lower beam.

2.5.2.4 Effect of Upper Beam Flexural Rigidity

The mass and flexural rigidity are two main physical properties for a beam structure neglecting the shear effect. The effect of upper beam mass on double-beam system dynamic responses is discussed and shown in the section above, so this section is used to explain how the upper beam flexural rigidity affects the vibration responses in both beams and how it works to reduce the dynamic response.

Also, three cases are investigated in here for discussion:

$e_2 = e$, $m_1 = 0.2m$, $m_2 = m$, $K = 1\times10^5\, Nm^{-2}$; Case 1: $e_1 = 0.1e$; Case 2: $e_1 = 0.5e$; Case 3: $e_1 = e$.

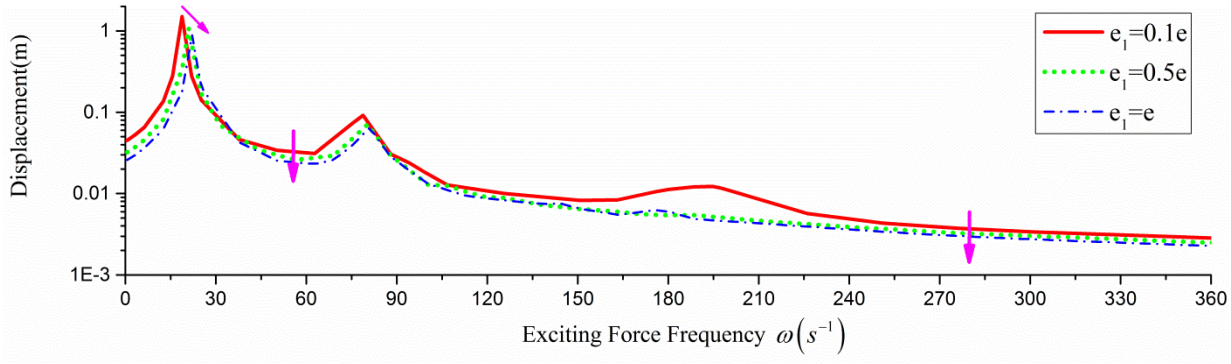

Fig. 2-10. Frequency response at midspan point of lower beam.

The frequency response at the midspan of the lower beam is shown in semi-log plots in Fig. 2-10. According to the simulation results shown in Fig. 2-10, the dynamic response of lower beam is generally decreased with the increase of upper beam flexural rigidity. The principle for that phenomenon is similar to the one in upper beam mass effect discussion: when upper beam is soft, less energy could let it deform and vibrate, so more energy is transferred to lower beam; when upper beam gets stiffer and flexural rigidity gets larger, more exciting energy is needed to complete upper beam deformation and vibration, so less energy could be obtained by lower beam and its dynamic response gets smaller. But if the flexural rigidity of upper beam exceeds a limit value, upper beam will be treated as a rigid body and it will not absorb any energy, all the exciting energy will be accepted by lower beam and its dynamic response will be very large.

2.5.2.5 Double-Beam System Dynamic Parameter

After completing a larger number of simulation works on double-beam system, four parameters $\frac{E_1 I_1}{L_1^4 \bar{m}_1}$, $\frac{E_2 I_2}{L_2^4 \bar{m}_2}$, $\frac{K}{\bar{m}_1}$ and $\frac{K}{\bar{m}_2}$, which could determine the system dynamic responses, are summarized and figured out. If the values of those four parameters are the same in two different double-beam systems with same boundary conditions, the natural frequencies and corresponding mode shapes will be same, and the Dynamic Factor $\frac{W_{n,MAX}(x,t)}{W_{n,0}(x)}$ ($W_{n,MAX}(x,t)$ is maximum dynamic displacement at location *n* of upper beam<$n=1$> or lower beam<$n=2$>; $W_{n,0}(x)$ is static displacement at location *x* of the same beam under a static force whose amplitude is equal to maximum value of the exciting force) of each beam under an exciting force will have same values. Therefore, those four parameters have a key role in determining the dynamic response of double-beam system, and it is necessary to show some simulation results on them.

In order to illustrate the dynamic factor $\frac{W_{n,MAX}(x,t)}{W_{n,0}(x)}$ under those four dynamic parameters, four cases are investigated in here:

Two identical beams: $m_1 = m_2 = m$, $K = 1\times10^3 \sim 1\times10^6\, Nm^{-2}$; Case 1: $e_1 = e_2 = e$; Case 2: $e_1 = e_2 = 10e$;

Smaller upper beam: $m_1 = 0.2m$, $m_2 = m$, $K = 1\times10^3 \sim 1\times10^6\, Nm^{-2}$; Case 3: $e_1 = 0.8e$, $e_2 = e$;

Case 4: $e_1 = 8e$, $e_2 = 10e$.

In each case itself, all basic parameters are constant except *K*, so the dynamic parameters $\frac{E_1 I_1}{L_1^4 \bar{m}_1}$ and $\frac{E_2 I_2}{L_2^4 \bar{m}_2}$ are consistent but $\frac{K}{\bar{m}_1}$ and $\frac{K}{\bar{m}_2}$ are variables; combining the exciting force with different frequencies, it is better to plot the dynamic factor in a form of plane in 3-D coordinate. The frequency responses of dynamic factor $\frac{W_{n,MAX}(x,t)}{W_{n,0}(x)}$ at the midspan ($x = 0.5L$) of the two beams are plotted in a 3-D coordinate system, which are shown in a form of semi-log planes plots in Fig. 2-11 and Fig. 2-12.

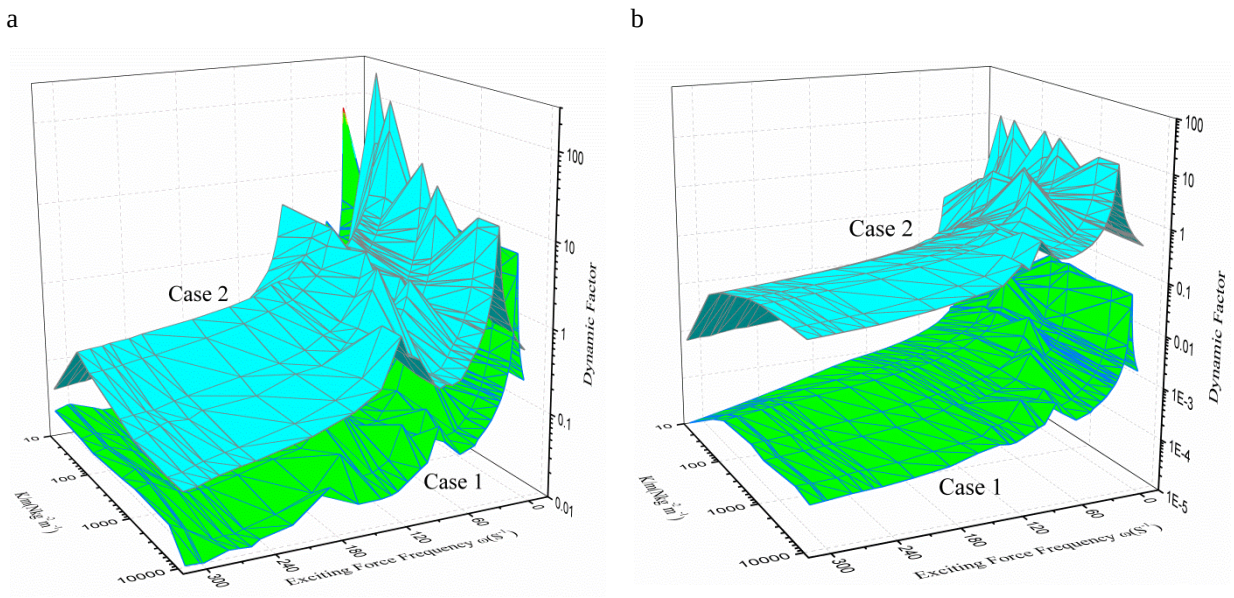

Fig. 2-11. Frequency response at midspan point of two beams for Case 1 and Case 2: (a) upper beam; (b) lower beam.

From Fig. 2-11 and Fig. 2-12, it can be seen that the dynamic factor of each beam indeed forms a

plane in the 3-D coordinate. It is useful to engineers when they design a double-beam system: once they get the four dynamic parameters values of a double-beam system, they can check the standard figures and find out the right plane, then they can read out the Dynamic Factor of each beam under the specific exciting force frequency directly instead of doing difficult calculation works.

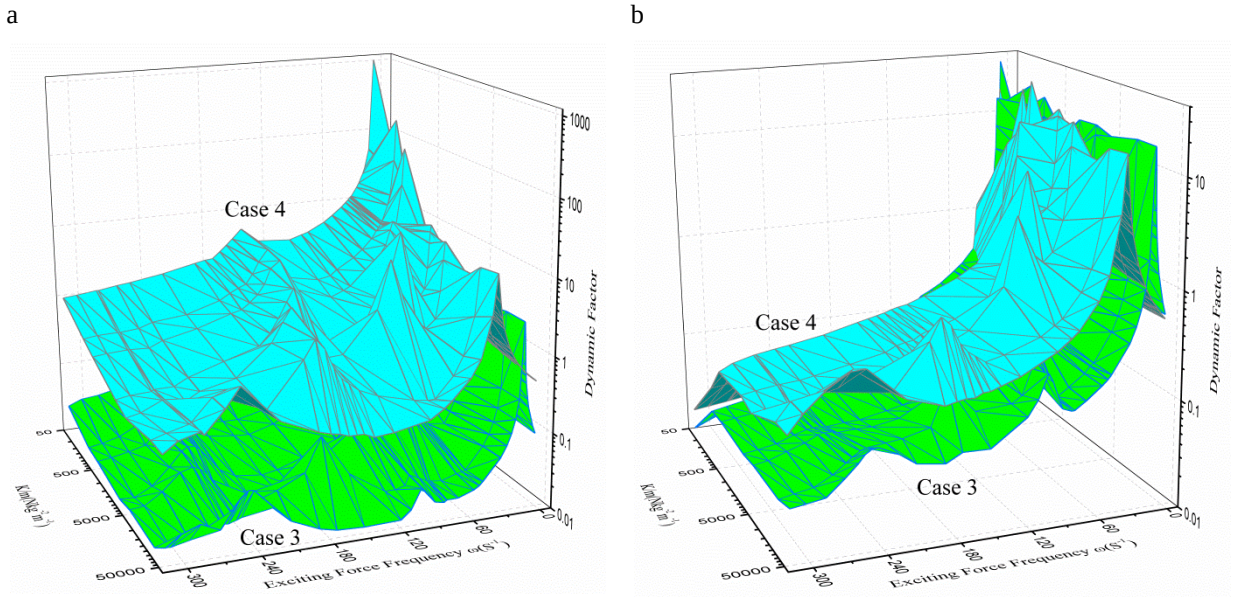

Fig. 2-12. Frequency response at midspan point of two beams for Case 3 and Case 4: (a) upper beam; (b) lower beam.

2.6 Conclusions

A semi-analytical method is developed in this chapter to analyzing the natural frequencies and corresponding mode shapes of an undamped double-beam system, which may have arbitrary beam mass, beam flexural rigidity and/or boundary condition. The initial conditions are considered to find the free vibration final form, which are the exact solutions of the motion differential equations formulated by the classical Bernoulli-Fourier method. The correctness and accuracy of the semi-

analytical method presented in this chapter has been demonstrated by comparing the results with analytical solutions from previous research in the literature; and the models, which have different beam mass, beam flexural rigidity and different boundary condition, are also calculated to show their natural frequencies and corresponding mode shapes. A discussion about the effect of elastic layer stiffness on double-beam system natural frequencies is further accomplished.

The dynamic response of forced vibration in the same undamped double-beam system is determined by the modal-expansion method using the natural frequencies and mode shapes obtained from the free vibration analysis. The specific orthogonality condition for a double-beam system is derived, and then applied to decouple the motion differential equations. Various double-beam system models with a concentrated harmonic force in the midspan of upper beam have been calculated with systematic parametric studies showing the following conclusions:

1. Effect of elastic layer stiffness: Increase elastic layer stiffness in a range, dynamic responses of upper beam are reduced, but dynamic responses of lower beam are increased.

2. Effect of upper beam mass: Dynamic responses of lower beam are significantly decreased when increase the mass of upper beam in a range.

3. Effect of upper beam flexural rigidity: Dynamic responses of lower beam are reduced if increase the flexural rigidity of upper beam in a range.

All of those parametric study conclusions, including the four dynamic parameters defined in this

chapter for double-beam system, can be helpful to engineers to design the complex double-beam systems in engineering practice.

Appendix 1. Matrix $[E]_{8\times8}$ for Several Typical Boundary Conditions of Double-Beam System

The matrix $[E]_{8\times8}$ is the frequency characteristic matrix for calculating the natural frequencies of a double beam system, so it is very important and it should be demonstrated precisely for each boundary conditions. The specific matrix $[E]_{8\times8}$ for several typical boundary conditions of double-beam system is denoted as follows.

(1) If the boundary conditions of lower beam and upper beam are both simply supported - simply supported, the $[E]_{8\times8}$ matrix will be denoted as

$$[E]=\begin{bmatrix} \beta_{n1} & \beta_{n2} & \beta_{n3} & \beta_{n4} & \beta_{n5} & \beta_{n6} & \beta_{n7} & \beta_{n8} \\ \beta_{n1}e^{P_{n1}L} & \beta_{n2}e^{P_{n2}L} & \beta_{n3}e^{P_{n3}L} & \beta_{n4}e^{P_{n4}L} & \beta_{n5}e^{P_{n5}L} & \beta_{n6}e^{P_{n6}L} & \beta_{n7}e^{P_{n7}L} & \beta_{n8}e^{P_{n8}L} \\ \beta_{n1}P_{n1}^2 & \beta_{n2}P_{n2}^2 & \beta_{n3}P_{n3}^2 & \beta_{n4}P_{n4}^2 & \beta_{n5}P_{n5}^2 & \beta_{n6}P_{n6}^2 & \beta_{n7}P_{n7}^2 & \beta_{n8}P_{n8}^2 \\ \beta_{n1}P_{n1}^2e^{P_{n1}L} & \beta_{n2}P_{n2}^2e^{P_{n2}L} & \beta_{n3}P_{n3}^2e^{P_{n3}L} & \beta_{n4}P_{n4}^2e^{P_{n4}L} & \beta_{n5}P_{n5}^2e^{P_{n5}L} & \beta_{n6}P_{n6}^2e^{P_{n6}L} & \beta_{n7}P_{n7}^2e^{P_{n7}L} & \beta_{n8}P_{n8}^2e^{P_{n8}L} \\ 1 & 1 & 1 & 1 & 1 & 1 & 1 & 1 \\ e^{P_{n1}L} & e^{P_{n2}L} & e^{P_{n3}L} & e^{P_{n4}L} & e^{P_{n5}L} & e^{P_{n6}L} & e^{P_{n7}L} & e^{P_{n8}L} \\ P_{n1}^2 & P_{n2}^2 & P_{n3}^2 & P_{n4}^2 & P_{n5}^2 & P_{n6}^2 & P_{n7}^2 & P_{n8}^2 \\ P_{n1}^2e^{P_{n1}L} & P_{n2}^2e^{P_{n2}L} & P_{n3}^2e^{P_{n3}L} & P_{n4}^2e^{P_{n4}L} & P_{n5}^2e^{P_{n5}L} & P_{n6}^2e^{P_{n6}L} & P_{n7}^2e^{P_{n7}L} & P_{n8}^2e^{P_{n8}L} \end{bmatrix} \tag{2-40}$$

(2) If the boundary conditions of lower beam are simply supported - simply supported, and upper

beam are spring supported - spring supported, the $[E]_{8\times 8}$ matrix will be denoted as

$$[E]=\begin{bmatrix} \beta_{n1} & \beta_{n2} & \beta_{n3} & \beta_{n4} & \beta_{n5} & \beta_{n6} & \beta_{n7} & \beta_{n8} \\ \beta_{n1}e^{P_{n1}L} & \beta_{n2}e^{P_{n2}L} & \beta_{n3}e^{P_{n3}L} & \beta_{n4}e^{P_{n4}L} & \beta_{n5}e^{P_{n5}L} & \beta_{n6}e^{P_{n6}L} & \beta_{n7}e^{P_{n7}L} & \beta_{n8}e^{P_{n8}L} \\ \beta_{n1}P_{n1}^2 & \beta_{n2}P_{n2}^2 & \beta_{n3}P_{n3}^2 & \beta_{n4}P_{n4}^2 & \beta_{n5}P_{n5}^2 & \beta_{n6}P_{n6}^2 & \beta_{n7}P_{n7}^2 & \beta_{n8}P_{n8}^2 \\ \beta_{n1}P_{n1}^2e^{P_{n1}L} & \beta_{n2}P_{n2}^2e^{P_{n2}L} & \beta_{n3}P_{n3}^2e^{P_{n3}L} & \beta_{n4}P_{n4}^2e^{P_{n4}L} & \beta_{n5}P_{n5}^2e^{P_{n5}L} & \beta_{n6}P_{n6}^2e^{P_{n6}L} & \beta_{n7}P_{n7}^2e^{P_{n7}L} & \beta_{n8}P_{n8}^2e^{P_{n8}L} \\ P_{n1}^2 & P_{n2}^2 & P_{n3}^2 & P_{n4}^2 & P_{n5}^2 & P_{n6}^2 & P_{n7}^2 & P_{n8}^2 \\ P_{n1}^2e^{P_{n1}L} & P_{n2}^2e^{P_{n2}L} & P_{n3}^2e^{P_{n3}L} & P_{n4}^2e^{P_{n4}L} & P_{n5}^2e^{P_{n5}L} & P_{n6}^2e^{P_{n6}L} & P_{n7}^2e^{P_{n7}L} & P_{n8}^2e^{P_{n8}L} \\ e_1P_{n1}^{\ 3}+K & e_1P_{n2}^{\ 3}+K & e_1P_{n3}^{\ 3}+K & e_1P_{n4}^{\ 3}+K & e_1P_{n5}^{\ 3}+K & e_1P_{n6}^{\ 3}+K & e_1P_{n7}^{\ 3}+K & e_1P_{n8}^{\ 3}+K \\ \left(e_1P_{n1}^{\ 3}-K\right)e^{P_{n1}L} & \left(e_1P_{n2}^{\ 3}-K\right)e^{P_{n2}L} & \left(e_1P_{n3}^{\ 3}-K\right)e^{P_{n3}L} & \left(e_1P_{n4}^{\ 3}-K\right)e^{P_{n4}L} & \left(e_1P_{n5}^{\ 3}-K\right)e^{P_{n5}L} & \left(e_1P_{n6}^{\ 3}-K\right)e^{P_{n6}L} & \left(e_1P_{n7}^{\ 3}-K\right)e^{P_{n7}L} & \left(e_1P_{n8}^{\ 3}-K\right)e^{P_{n8}L} \end{bmatrix} \quad (2\text{-}41)$$

(3) If the boundary conditions of lower beam are clamped - free, and upper beam are clamped - free, the $[E]_{8\times 8}$ matrix will be denoted as

$$[E]=\begin{bmatrix} \beta_{n1} & \beta_{n2} & \beta_{n3} & \beta_{n4} & \beta_{n5} & \beta_{n6} & \beta_{n7} & \beta_{n8} \\ \beta_{n1}P_{n1} & \beta_{n2}P_{n2} & \beta_{n3}P_{n3} & \beta_{n4}P_{n4} & \beta_{n5}P_{n5} & \beta_{n6}P_{n6} & \beta_{n7}P_{n7} & \beta_{n8}P_{n8} \\ \beta_{n1}P_{n1}^2e^{P_{n1}L} & \beta_{n2}P_{n2}^2e^{P_{n2}L} & \beta_{n3}P_{n3}^2e^{P_{n3}L} & \beta_{n4}P_{n4}^2e^{P_{n4}L} & \beta_{n5}P_{n5}^2e^{P_{n5}L} & \beta_{n6}P_{n6}^2e^{P_{n6}L} & \beta_{n7}P_{n7}^2e^{P_{n7}L} & \beta_{n8}P_{n8}^2e^{P_{n8}L} \\ \beta_{n1}P_{n1}^3e^{P_{n1}L} & \beta_{n2}P_{n2}^3e^{P_{n2}L} & \beta_{n3}P_{n3}^3e^{P_{n3}L} & \beta_{n4}P_{n4}^3e^{P_{n4}L} & \beta_{n5}P_{n5}^3e^{P_{n5}L} & \beta_{n6}P_{n6}^3e^{P_{n6}L} & \beta_{n7}P_{n7}^3e^{P_{n7}L} & \beta_{n8}P_{n8}^3e^{P_{n8}L} \\ 1 & 1 & 1 & 1 & 1 & 1 & 1 & 1 \\ P_{n1} & P_{n2} & P_{n3} & P_{n4} & P_{n5} & P_{n6} & P_{n7} & P_{n8} \\ P_{n1}^2e^{P_{n1}L} & P_{n2}^2e^{P_{n2}L} & P_{n3}^2e^{P_{n3}L} & P_{n4}^2e^{P_{n4}L} & P_{n5}^2e^{P_{n5}L} & P_{n6}^2e^{P_{n6}L} & P_{n7}^2e^{P_{n7}L} & P_{n8}^2e^{P_{n8}L} \\ P_{n1}^3e^{P_{n1}L} & P_{n2}^3e^{P_{n2}L} & P_{n3}^3e^{P_{n3}L} & P_{n4}^3e^{P_{n4}L} & P_{n5}^3e^{P_{n5}L} & P_{n6}^3e^{P_{n6}L} & P_{n7}^3e^{P_{n7}L} & P_{n8}^3e^{P_{n8}L} \end{bmatrix} \quad (2\text{-}42)$$

(4) If the boundary conditions of lower beam are free - free, and upper beam are clamped - clamped, the $[E]_{8\times 8}$ matrix will be denoted as

$$[E]=\begin{bmatrix} \beta_{n1}P_{n1}^2 & \beta_{n2}P_{n2}^2 & \beta_{n3}P_{n3}^2 & \beta_{n4}P_{n4}^2 & \beta_{n5}P_{n5}^2 & \beta_{n6}P_{n6}^2 & \beta_{n7}P_{n7}^2 & \beta_{n8}P_{n8}^2 \\ \beta_{n1}P_{n1}^2e^{P_{n1}L} & \beta_{n2}P_{n2}^2e^{P_{n2}L} & \beta_{n3}P_{n3}^2e^{P_{n3}L} & \beta_{n4}P_{n4}^2e^{P_{n4}L} & \beta_{n5}P_{n5}^2e^{P_{n5}L} & \beta_{n6}P_{n6}^2e^{P_{n6}L} & \beta_{n7}P_{n7}^2e^{P_{n7}L} & \beta_{n8}P_{n8}^2e^{P_{n8}L} \\ \beta_{n1}P_{n1}^3 & \beta_{n2}P_{n2}^3 & \beta_{n3}P_{n3}^3 & \beta_{n4}P_{n4}^3 & \beta_{n5}P_{n5}^3 & \beta_{n6}P_{n6}^3 & \beta_{n7}P_{n7}^3 & \beta_{n8}P_{n8}^3 \\ \beta_{n1}P_{n1}^3e^{P_{n1}L} & \beta_{n2}P_{n2}^3e^{P_{n2}L} & \beta_{n3}P_{n3}^3e^{P_{n3}L} & \beta_{n4}P_{n4}^3e^{P_{n4}L} & \beta_{n5}P_{n5}^3e^{P_{n5}L} & \beta_{n6}P_{n6}^3e^{P_{n6}L} & \beta_{n7}P_{n7}^3e^{P_{n7}L} & \beta_{n8}P_{n8}^3e^{P_{n8}L} \\ 1 & 1 & 1 & 1 & 1 & 1 & 1 & 1 \\ e^{P_{n1}L} & e^{P_{n2}L} & e^{P_{n3}L} & e^{P_{n4}L} & e^{P_{n5}L} & e^{P_{n6}L} & e^{P_{n7}L} & e^{P_{n8}L} \\ P_{n1} & P_{n2} & P_{n3} & P_{n4} & P_{n5} & P_{n6} & P_{n7} & P_{n8} \\ P_{n1}e^{P_{n1}L} & P_{n2}e^{P_{n2}L} & P_{n3}e^{P_{n3}L} & P_{n4}e^{P_{n4}L} & P_{n5}e^{P_{n5}L} & P_{n6}e^{P_{n6}L} & P_{n7}e^{P_{n7}L} & P_{n8}e^{P_{n8}L} \end{bmatrix} \tag{2-43}$$

Appendix 2. Natural Frequency Roots Search Method - Secant Method

If the determinant of frequency characteristic matrix $[E]_{8\times8}$ is denoted as a function of ω, $f(\omega)$, so the real natural frequency ω is the root of $f(\omega)=0$. Based on the semi-analytical method introduced in this chapter, an approximation root $\omega_{n,1}$ is determined, and the specific algorithm based on secant method can be applied as follows:

(1) Calculate distinct values of $\omega_{n,0}$, and function values of $f(\omega_{n,0})$, $f(\omega_{n,1})$:

$$\omega_{n,0}=\omega_{n,1}-\Delta\omega, \tag{2-44}$$

$$f(\omega_{n,0})=|E|_{\omega=\omega_{n,0}},\quad f(\omega_{n,1})=|E|_{\omega=\omega_{n,1}} \tag{2-45}$$

(2) Calculate:

$$\omega_{n,i+1}=\omega_{n,i}-\frac{f(\omega_{n,i})}{f(\omega_{n,i})-f(\omega_{n,i-1})}(\omega_{n,i}-\omega_{n,i-1}) \tag{2-46}$$

$$f(\omega_{n,i})=|E|_{\omega=\omega_{n,i}},\ f(\omega_{n,i-1})=|E|_{\omega=\omega_{n,i-1}},\quad i=1,2,3,... \tag{2-47}$$

(3) If $|\omega_{n,i+1}-\omega_{n,i}|\le\xi$, then the final root $\omega_n=\omega_{n,i+1}$; else continue iteration process in step (2).

where ω_n is *n*th natural frequency; $\omega_{n,i}$ is the *i*th distinct value of ω_n, $i=1,2,3,...$; ξ is the

allowable error defined by user.

Appendix 3. Numerical Examples Results Data - Natural Frequency and Mode Shape

The first six natural frequencies and normal mode shapes of Case 2 to Case 5, are summarized as follows:

Table 2-2. Natural Frequencies of double-beam system ω_n (s^{-1}); Case 2

$K\times10^{-5}\left(Nm^{-2}\right)$	$n=1$	$n=2$	$n=3$	$n=4$	$n=5$	$n=6$
1	17.03	38.09	46.85	62.22	85.51	130.65
2	18.11	50.65	64.63	75.75	92.80	137.87
3	18.56	57.93	78.44	86.90	100.77	144.89
4	18.82	62.44	90.02	96.46	109.04	151.67
5	18.97	65.41	104.99	117.23	158.18	191.80

Table 2-3. Natural Frequencies of double-beam system ω_n (s^{-1}); Case 3

$K\times10^{-5}\left(Nm^{-2}\right)$	$n=1$	$n=2$	$n=3$	$n=4$	$n=5$	$n=6$
1	21.73	75.18	80.75	96.60	130.86	180.87
2	22.62	80.70	112.89	129.53	159.37	186.58
3	23.02	82.99	137.32	156.03	173.88	200.61
4	23.26	84.58	157.80	178.09	178.97	220.37
5	23.41	85.81	175.28	182.17	197.21	239.86

Table 2-4. Natural Frequencies of double-beam system ω_n (s^{-1}); Case 4

$K\times10^{-5}\left(Nm^{-2}\right)$	$n=1$	$n=2$	$n=3$	$n=4$	$n=5$	$n=6$
1	7.03	44.07	45.45	62.79	123.39	131.25
2	7.03	44.07	63.68	77.08	123.39	138.66
3	7.03	44.07	77.79	89.11	123.39	145.69
4	7.03	44.07	89.72	99.71	123.39	152.40
5	7.03	44.07	100.25	109.28	123.39	158.83

Table 2-5. Natural Frequencies of double-beam system ω_n (s^{-1}); Case 5

$K\times10^{-5}\left(Nm^{-2}\right)$	$n=1$	$n=2$	$n=3$	$n=4$	$n=5$	$n=6$
1	42.31	69.30	77.85	114.64	127.86	243.89
2	43.76	94.38	107.44	134.43	135.64	246.05
3	44.34	108.35	130.17	144.84	154.03	248.31
4	44.68	115.34	148.87	158.34	170.65	250.74
5	44.92	119.06	164.73	173.20	186.02	253.41

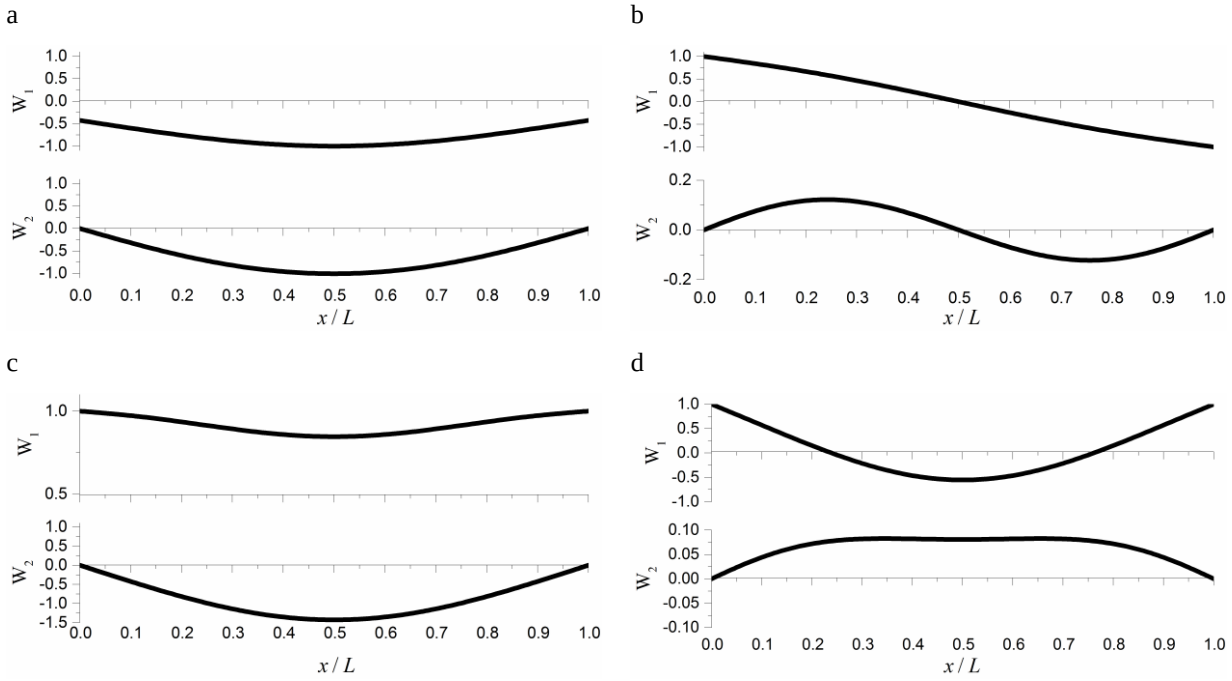

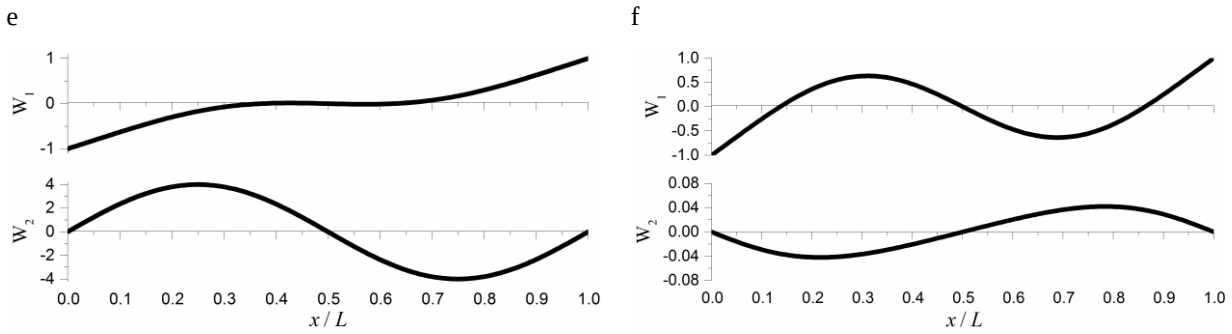

Fig. 2-13. The first six normal mode shapes of the double-beam system for Case 2, $K = 1\times10^{5}$: (a) mode 1; (b) mode 2; (c) mode 3; (d) mode 4; (e) mode 5; (f) mode 6.

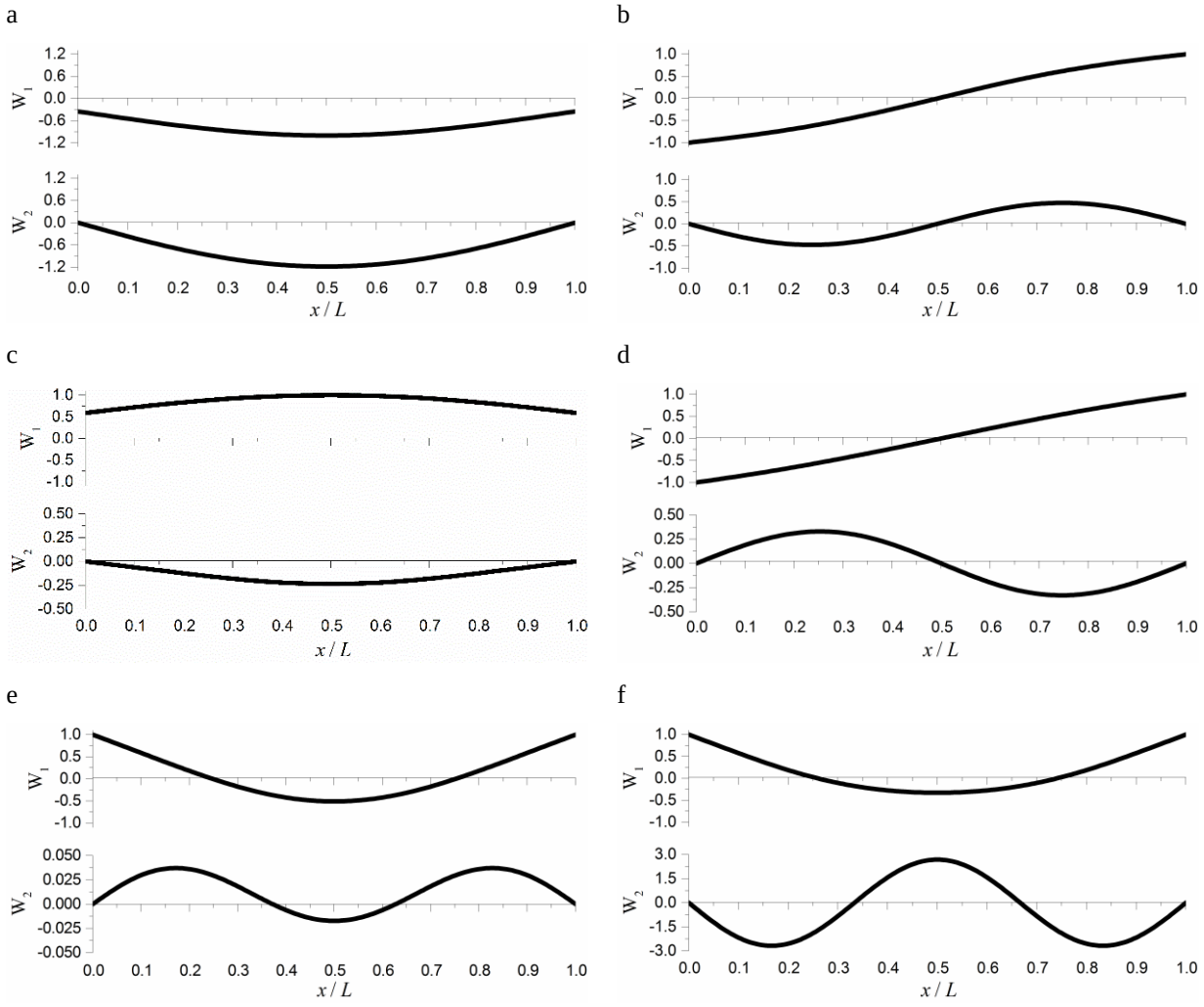

Fig. 2-14. The first six normal mode shapes of the double-beam system for Case 3, $K = 1\times10^{5}$: (a) mode 1; (b) mode 2; (c) mode 3; (d) mode 4; (e) mode 5; (f) mode 6.

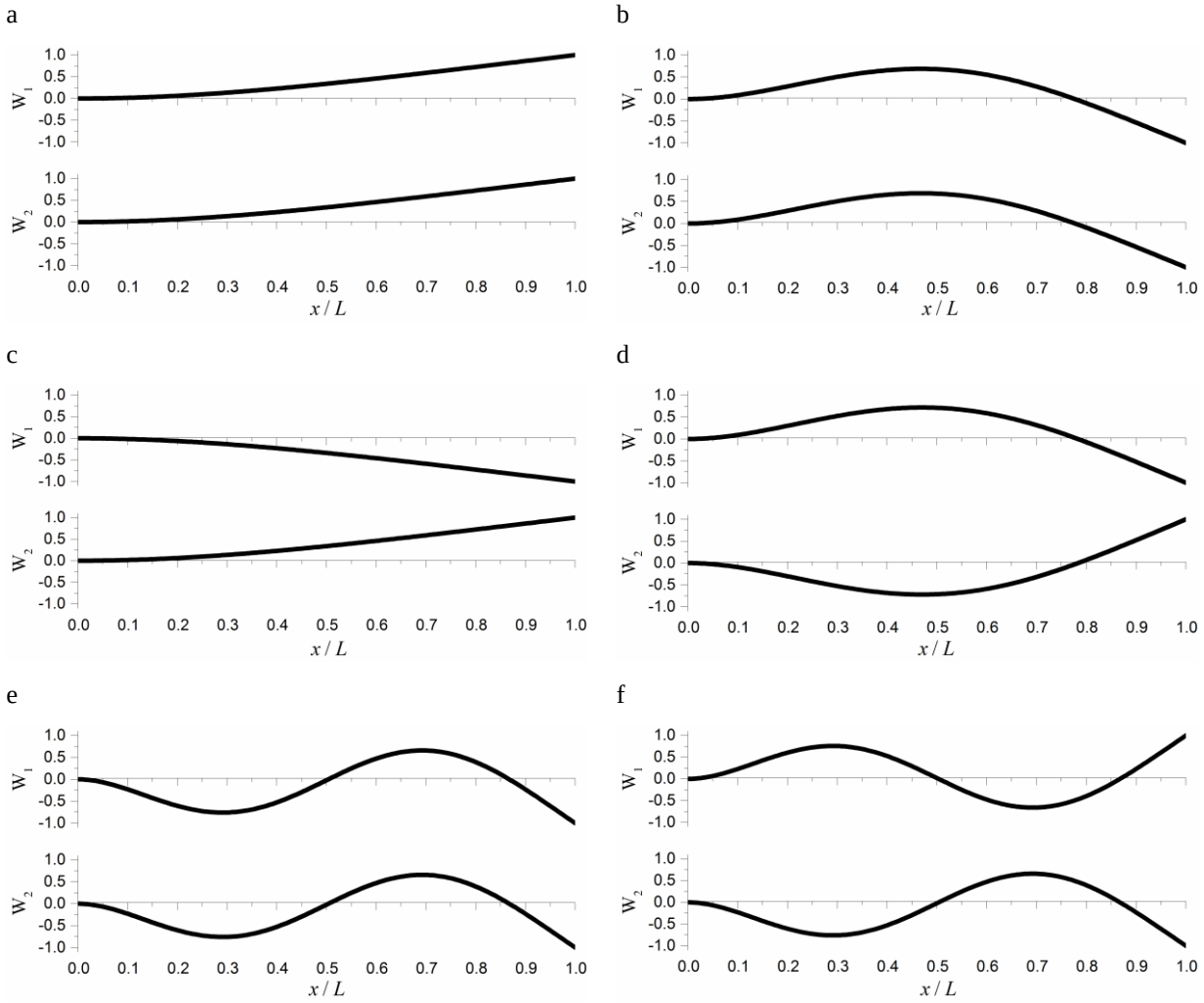

Fig. 2-15. The first six normal mode shapes of the double-beam system for Case 4, $K = 1\times10^{5}$: (a) mode 1; (b) mode 2; (c) mode 3; (d) mode 4; (e) mode 5; (f) mode 6.

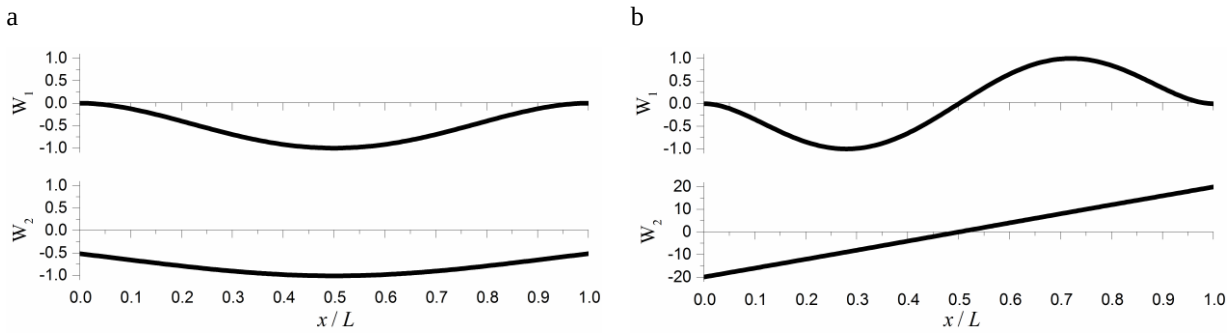

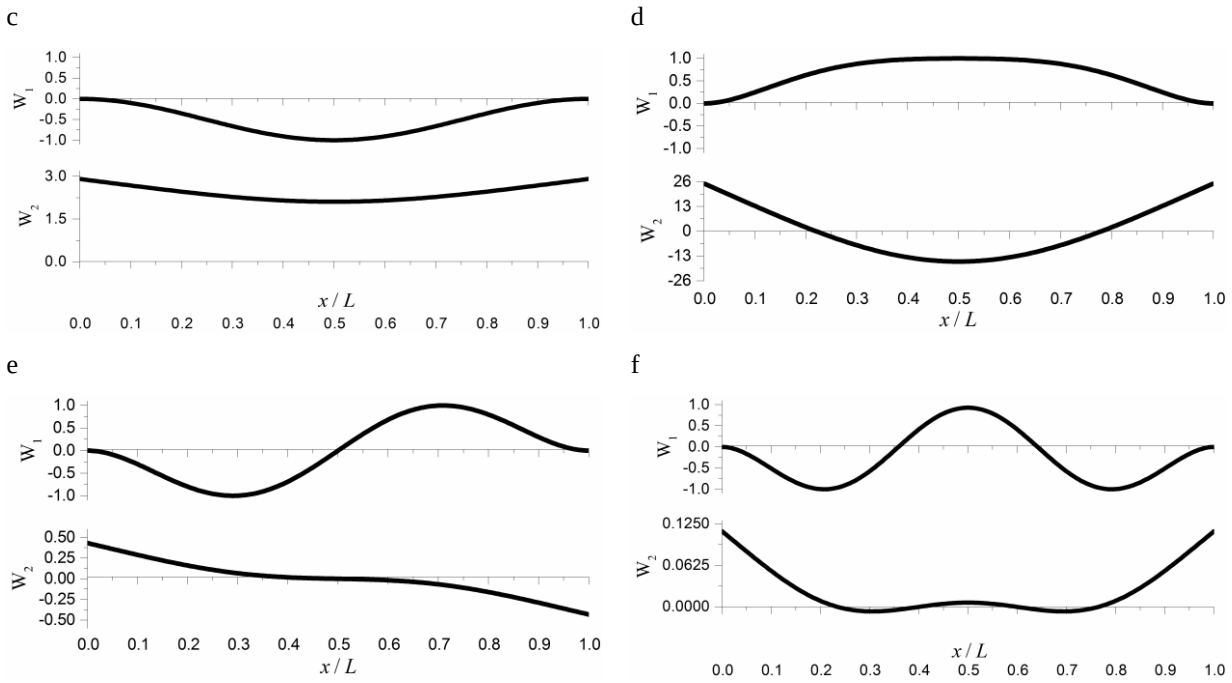

Fig. 2-16. The first six normal mode shapes of the double-beam system for Case 5, $K = 1\times10^{5}$: (a) mode 1; (b) mode 2; (c) mode 3; (d) mode 4; (e) mode 5; (f) mode 6.

Chapter 3 Dynamic Behavior of Double-Beam Systems Interconnected with Viscoelastic Layers

3.1 Introduction

In Chapter 2, the undamped double-beam system interconnected by elastic layers has been studied carefully, and the free vibration and forced vibration of it has been calculated and analyzed specifically. In fact, in real engineering practices, the materials applied to connect the floating slab track and bridge main beam are usually rubbers or other viscoelastic materials whose damping cannot be ignored. In addition, one advantage of the novel adaptive materials applied in this research to build the semi-active control structure is that its damping is controllable, so it means the damping effects of the material must be considered and used. Based on the works in Chapter 2, in this chapter, the double-beam system interconnected by viscoelastic layers is analyzed and the damping effects of the viscoelastic layers on the dynamic behavior of whole double-beam system is studied. The research works in this chapter will be the theoretical basis for the control structure studies in Chapter 5 and Chapter 7.

It is similar to the introduction in Chapter 2, most research efforts in the literature have simplified the double-beam systems as two identical beams, and/or with simply supported boundary conditions for both beams, and/or same transverse deformations in two beams. Among those, the viscoelastic damping characteristics of the connecting layer between the two beams is often

ignored (Seelig and Hoppmann 1964a, 1964b; Kessel 1966; Rao 1974; Chonan 1976; Hamada, Nakayama and Hayashi 1983; Kukla and Skalmierski 1994; Oniszczuk 2000, 2003; Zhang, Lu and Ma 2008; Stojanovic and Kozic 2012; Zhang, Huang, Zhang and Hua 2014; Mao and Wattanasakulpong 2015; Li and Sun 2015). To take into account the damping effect, researchers frequently make some assumptions to reduce the difficulty of solving. For example, based on their early work on the axially-loaded damped Timoshenko beam on a viscoelastic foundation (Chen and Sheu 1993), Chen and Sheu (1994, 1995) studied the free vibration, dynamic response and static buckling of two identical beams with a viscoelastic material layer in between. Li and Hua (2007) introduced a finite element numerical method for a double-beam system which could have unequal masses, unequal flexural rigidities and arbitrary boundary conditions; but for damping issue, they also assumed the two beams must be identical. Kessel and Raske (1967) solved a double-beam system under the cyclic moving load with both individual damping and relative damping. Although the two beams can be different, they must have same simply supported boundary conditions. Abu-Hilal (2006) investigated the dynamic response of a double-beam system with viscoelastic layer damping traversed by a constant moving load and obtained the dynamic deflections of both beams in analytical closed forms. By using the direct Lyapunov method and simplifying the damping as viscous damping of each beam itself, the stability and instability of a double-beam system subjected to compressive axial loading is investigated by Pavlovic et al. (2012). In those two papers, the two beams are identical with same simply supported boundary condition. Vu et al. (2000) presented an exact method to analyze a two-beam system

with a viscoelastic layer, with boundary conditions on the same side of the system being same and the two identical beams. Irie et al. (1982) discussed the steady-state responses of a double-beam system under the sinusoidal force and a transfer matrix technique is adopted for solving the differential equations, but the damping considered in it is beam internal damping instead of the viscoelastic layer damping. Cottle (1990) explored the layered beam with mixed boundary conditions and a semi-analytical method was applied to solve the equations with the assumption of same lateral displacements in beams. Xin and Gao (2011) applied the double-beam system into a specific engineering structure, a bridge with a viscoelastic layer and a slab track on it, and used the finite element method and multibody dynamics theory to solve the problem. Dublin and Friedrich (1956) obtained the forced vibration responses for two elastic beams interconnected by spring-damper system, with two spring-damper systems between two beams instead of uniformly distributed spring-damper systems. Other similar structures have also been analyzed, such as sandwich beams (Lu and Douglas 1974; Douglas and Yang 1978; Frostig and Baruch 1993, 1994; Mace 1994), continuous dynamic vibration absorbers (Yamaguchi 1985; Vu 1987; Aida, Toda, Ogawa and Imada 1992; Chen and Lin 1998; Kawazoe, Kono, Aida, Aso and Ebisuda 1998), and composite layered foundations (Yankelevsky 1991).

While there have been plenty of research efforts investigating the double-beam systems as shown above, most of them treat the viscoelastic layer damping as zero. Some limited efforts consider the damping effect with simplified double-beam systems. In real engineering practices, such as

floating slab track on bridge which is mainly studied in this research, the damping is an inherent properties of the materials for viscoelastic layer and its value cannot be ignored and the structure cannot be always simplified as above. Therefore, a general double-beam system with arbitrary viscoelastic layer damping must be considered. This chapter presents a semi-analytical method to obtain the natural frequencies and corresponding mode shapes for a general double-beam system, in which the viscoelastic layer damping is nonzero and two beams may have unequal masses, unequal flexural rigidities and arbitrary boundary conditions. In addition, to the double-beam system with viscoelastic layer, the forced vibration excited by arbitrary loading is analyzed using the classical modal expansion method and a proposed iteration algorithm, based on the natural frequencies and mode shapes obtained from the free vibration analysis. A specific orthogonality condition for that double-beam system is derived and applied to decouple differential equations. The natural frequencies and mode shapes are calculated by the semi-analytical method for four cases of arbitrary masses, arbitrary flexural rigidities and arbitrary boundary conditions models. Furthermore, various double-beam system models are studied with a concentrated harmonic force in the midspan of upper beam to conduct the systematic parametric analysis of the structural resonance condition and dynamic responses.

3.2 Formulation of the Problem

As shown in Fig. 3-1, the physical model of a double-beam system discussed in this chapter

includes an upper beam and a lower beam joined by a uniformly distributed-connecting viscoelastic layer. Both beams are homogeneous, prismatic and have the same length *L*, but they could have different mass, flexural rigidity, and boundary conditions. The governing equations of motion for transverse vibrations of the double-beam system with viscoelastic layer, are derived by Bernoulli-Euler beam theory as follows:

$$e_1 \frac{\partial^4 W_1}{\partial x^4} + K\left(W_1 - W_2\right) + C\left(\frac{\partial W_1}{\partial t} - \frac{\partial W_2}{\partial t}\right) + \bar{m}_1 \frac{\partial^2 W_1}{\partial t^2} = f_1\left(x,t\right) \tag{3-1a}$$

$$e_2 \frac{\partial^4 W_2}{\partial x^4} - K\left(W_1 - W_2\right) - C\left(\frac{\partial W_1}{\partial t} - \frac{\partial W_2}{\partial t}\right) + \bar{m}_2 \frac{\partial^2 W_2}{\partial t^2} = f_2\left(x,t\right) \tag{3-1b}$$

where $W_i = W_i\left(x,t\right)$ is transverse beam deflections, *x*, *t* are the spatial co-ordinate and the time, e_i and $\bar{m}_i$ are the beam flexural rigidity and beam mass per unit length, *i*=1 or 2 represents upper beam or lower beam, K and C are the stiffness and damping coefficients of the viscoelastic layer, and $f_1\left(x,t\right)$, $f_2\left(x,t\right)$ are the exciting force acting on the upper and lower beams.

If $f_1\left(x,t\right) = f_2\left(x,t\right) = 0$, Eq. (3-1) is the governing equation of motion for free vibration of a double-beam system; otherwise, it is the governing equation for forced vibration.

The initial conditions in general form are as follows:

$$W_1\left(x,0\right) = W_{10}\left(x\right),\ W_2\left(x,0\right) = W_{20}\left(x\right),\ \dot{W}_1\left(x,0\right) = V_{10}\left(x\right),\ \dot{W}_2\left(x,0\right) = V_{20}\left(x\right) \tag{3-2}$$

As to the boundary conditions at the ends ($x = 0$, *L*) of the two beams, since it can analyze

different kinds of them in this chapter, so some common ones are listed as follows:

Simply supported: $W_i(0,t)=W_i(L,t)=W_i''(0,t)=W_i''(L,t)=0$ (3-3a)

Clamped: $W_i(0,t)=W_i(L,t)=W_i'(0,t)=W_i'(L,t)=0$ (3-3b)

Free: $W_i''(0,t)=W_i''(L,t)=W_i'''(0,t)=W_i'''(L,t)=0$ (3-3c)

Spring supported: $W_i''(0,t)=W_i''(L,t)=0$, $E_iI_iW_i'''(0,t)=-KW_i(0,t)$,

$E_iI_iW_i'''(L,t)=KW_i(L,t)$ (3-3d)

where i=1 or 2 represents upper beam or lower beam.

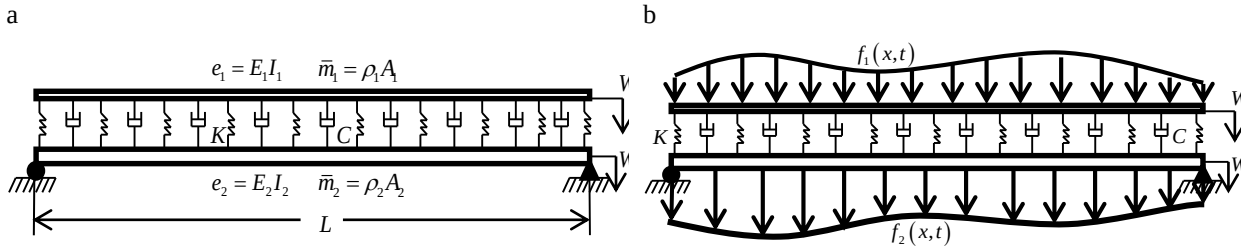

Fig. 3-1. The physical model of a double-beam system: (a) free vibration model; (b) forced vibration model.

3.3 Solution of the Problem for Free Vibration

Based on the previous research results and experiences, the solutions for Eq. (3-1) is supposed to be separable in time and space, and therefore, they can be assumed in the form as follows

$W_1(x,t)=T(t)X_1(x)=De^{i\omega t}Ae^{px}$, $W_2(x,t)=T(t)X_2(x)=De^{i\omega t}Be^{px}$ (3-4)

where $T(t)=De^{i\omega t}$ is time function, $X_1(x)=Ae^{px}$ and $X_2(x)=Be^{px}$ is the mode shape function of the upper beam and lower beam, respectively, ω is the natural frequency of the double-beam system, *A*, *B*, *D*, *P* are unknown constants, and $i=\sqrt{-1}$ is imaginary unit.

Introducing the general solutions Eq. (3-4) into Eq. (3-1) and $f_1(x,t) = f_2(x,t) = 0$ for free vibration, the differential Eq. (3-1) becomes a set of algebraic equations and they can be written in matrix form as follows

$$\begin{bmatrix} e_1P^4 + K + Ci\omega - \bar{m}_1\omega^2 & -K - Ci\omega \\ -K - Ci\omega & e_2P^4 + K + Ci\omega - \bar{m}_2\omega^2 \end{bmatrix} \begin{Bmatrix} A \\ B \end{Bmatrix} = \begin{Bmatrix} 0 \\ 0 \end{Bmatrix} \tag{3-5}$$

It can be easily understood that finding the solutions to Eq. (3-5) is an eigenvalue problem, the nontrivial solutions for Eq. (3-5) require the determinant of the coefficient matrix is equal to 0, which derives out an eighth order polynomial equation in *P*.

$$e_1e_2P^8 + \left[\left(e_1 + e_2\right)\left(K + Ci\omega\right) - \bar{m}_1\omega^2e_2 - \bar{m}_2\omega^2e_1\right]P^4 + \left[\bar{m}_1\bar{m}_2\omega^4 - \omega^2\left(K + Ci\omega\right)\left(\bar{m}_1 + \bar{m}_2\right)\right] = 0 \tag{3-6}$$

The eight roots of Eq. (3-6), that are also the values of constant *P*, can be solved as

$$P_1 = \sqrt[4]{Q_1},\ P_2 = -\sqrt[4]{Q_1},\ P_3 = \sqrt[4]{Q_1}i,\ P_4 = -\sqrt[4]{Q_1}i,\ P_5 = \sqrt[4]{Q_2},\ P_6 = -\sqrt[4]{Q_2},\ P_7 = \sqrt[4]{Q_2}i,$$

$$P_8 = -\sqrt[4]{Q_2}i \tag{3-7}$$

$$Q_{1,2} = \frac{-\left[\left(e_1 + e_2\right)\left(K + Ci\omega\right) - \bar{m}_1\omega^2e_2 - \bar{m}_2\omega^2e_1\right] \pm \sqrt{\Delta}}{2e_1e_2} \tag{3-8}$$

$$\Delta = \left[e_1\left(K + Ci\omega - \bar{m}_2\omega^2\right) - e_2\left(K + Ci\omega - \bar{m}_1\omega^2\right)\right]^2 + 4e_1e_2\left(K + Ci\omega\right)^2 \tag{3-9}$$

Using Eq. (3-5), considering there are eight roots P_j ($j = 1, 2...8$), the relationship among the constants *A* and *B* is given by

$$B_j = \frac{K + Ci\omega}{e_2 P_j^4 + K + Ci\omega - \bar{m}_2\omega^2} \times A_j = \frac{e_1 P_j^4 + K + Ci\omega - \bar{m}_1\omega^2}{K + Ci\omega} \times A_j = \beta_j A_j \text{ , } (j = 1, 2...8) \quad (3\text{-}10)$$

Finally, the solution of Eq. (3-1) can be obtained in the form as follows

$$W_1(x,t) = \sum_{n=1}^{\infty} D_n e^{i\omega_n t} \left[\sum_{j=1}^{8} \left(A_{nj} e^{P_{nj} x} \right) \right] \quad (3\text{-}11a)$$

$$W_2(x,t) = \sum_{n=1}^{\infty} D_n e^{i\omega_n t} \left[\sum_{j=1}^{8} \left(B_{nj} e^{P_{nj} x} \right) \right] = \sum_{n=1}^{\infty} D_n e^{i\omega_n t} \left[\sum_{j=1}^{8} \left(\beta_{nj} A_{nj} e^{P_{nj} x} \right) \right] \quad (3\text{-}11b)$$

where ω_n is *n*th natural frequency, and A_{nj}, B_{nj}, D_n, P_{nj}, β_{nj} are the unknown constants corresponding to *n*th natural frequency.

Substituting Eq. (3-11) into the real boundary conditions defined in Eq. (3-3) results in a set of eight algebraic equations with eight unknown constants A_{nj} ($j = 1, 2...8$) under each natural frequency. In matrix form, it can be represented as

$$[E]_{8\times8} \{A\}_{8\times1} = \{0\}_{8\times1} \quad (3\text{-}12)$$

where $\{A\}_{8\times1} = \{A_{n1} \quad A_{n2} \quad A_{n3} \quad A_{n4} \quad A_{n5} \quad A_{n6} \quad A_{n7} \quad A_{n8}\}^T$ is unknown constants vector, $\{0\}_{8\times1} = \{0 \quad 0 \quad 0 \quad 0 \quad 0 \quad 0 \quad 0 \quad 0\}^T$ is zero vector, and $[E]_{8\times8}$ is boundary conditions coefficient matrix.

Due to the method adopting $[E]_{8\times8}$ matrix which depends on specific boundary conditions, this chapter can analyze arbitrary boundary conditions and upper beam boundary conditions can be

different from lower beam, which is an obvious advantage from previous researches. If lower beam is simply supported - simply supported and upper beam is spring supported - spring supported, the $[E]_{8\times 8}$ matrix can be denoted as Eq. (3-13).

$$[E]=\begin{bmatrix}
\beta_{n1} & \beta_{n2} & \beta_{n3} & \beta_{n4} & \beta_{n5} & \beta_{n6} & \beta_{n7} & \beta_{n8} \\
\beta_{n1}e^{P_{n1}L} & \beta_{n2}e^{P_{n2}L} & \beta_{n3}e^{P_{n3}L} & \beta_{n4}e^{P_{n4}L} & \beta_{n5}e^{P_{n5}L} & \beta_{n6}e^{P_{n6}L} & \beta_{n7}e^{P_{n7}L} & \beta_{n8}e^{P_{n8}L} \\
\beta_{n1}P_{n1}^2 & \beta_{n2}P_{n2}^2 & \beta_{n3}P_{n3}^2 & \beta_{n4}P_{n4}^2 & \beta_{n5}P_{n5}^2 & \beta_{n6}P_{n6}^2 & \beta_{n7}P_{n7}^2 & \beta_{n8}P_{n8}^2 \\
\beta_{n1}P_{n1}^2e^{P_{n1}L} & \beta_{n2}P_{n2}^2e^{P_{n2}L} & \beta_{n3}P_{n3}^2e^{P_{n3}L} & \beta_{n4}P_{n4}^2e^{P_{n4}L} & \beta_{n5}P_{n5}^2e^{P_{n5}L} & \beta_{n6}P_{n6}^2e^{P_{n6}L} & \beta_{n7}P_{n7}^2e^{P_{n7}L} & \beta_{n8}P_{n8}^2e^{P_{n8}L} \\
P_{n1}^2 & P_{n2}^2 & P_{n3}^2 & P_{n4}^2 & P_{n5}^2 & P_{n6}^2 & P_{n7}^2 & P_{n8}^2 \\
P_{n1}^2e^{P_{n1}L} & P_{n2}^2e^{P_{n2}L} & P_{n3}^2e^{P_{n3}L} & P_{n4}^2e^{P_{n4}L} & P_{n5}^2e^{P_{n5}L} & P_{n6}^2e^{P_{n6}L} & P_{n7}^2e^{P_{n7}L} & P_{n8}^2e^{P_{n8}L} \\
e_1P_{n1}^3+K+Ci\omega_n & e_1P_{n2}^3+K+Ci\omega_n & e_1P_{n3}^3+K+Ci\omega_n & e_1P_{n4}^3+K+Ci\omega_n & e_1P_{n5}^3+K+Ci\omega_n & e_1P_{n6}^3+K+Ci\omega_n & e_1P_{n7}^3+K+Ci\omega_n & e_1P_{n8}^3+K+Ci\omega_n \\
\left(e_1P_{n1}^3-K-Ci\omega_n\right)e^{P_{n1}L} & \left(e_1P_{n2}^3-K-Ci\omega_n\right)e^{P_{n2}L} & \left(e_1P_{n3}^3-K-Ci\omega_n\right)e^{P_{n3}L} & \left(e_1P_{n4}^3-K-Ci\omega_n\right)e^{P_{n4}L} & \left(e_1P_{n5}^3-K-Ci\omega_n\right)e^{P_{n5}L} & \left(e_1P_{n6}^3-K-Ci\omega_n\right)e^{P_{n6}L} & \left(e_1P_{n7}^3-K-Ci\omega_n\right)e^{P_{n7}L} & \left(e_1P_{n8}^3-K-Ci\omega_n\right)e^{P_{n8}L}
\end{bmatrix} \quad (3\text{-}13)$$

From Eq. (3-12), boundary conditions coefficient matrix $[E]_{8\times 8}$ is frequency characteristic matrix, and the nontrivial solutions for Eq. (3-12) will exist only when $|E|=0$.

Based on the equations derived above, a semi-analytical method is developed to determine the natural frequencies and mode shapes of the whole double-beam system: (1) start from $\omega=0.1$, solve eighth order polynomial equation Eq. (3-6) and obtain P_j. (2) based on Eq. (3-10), obtain the relationship parameter β_j. (3) according to real boundary conditions, build frequency characteristic matrix $[E]_{8\times 8}$. (4) calculate the determinant of matrix $[E]_{8\times 8}$. (5) if $|E|=0$, the ω is outputted as the natural frequency, solve Eq. (3-12) to obtain A_j, and determine the corresponding mode shape by Eq. (3-11). (6) if $|E|\neq 0$, modify the value of ω by $\omega=\omega+\Delta\omega$ and start doing the calculation from step (1) again until the right value of ω is founded. Due to the error of natural frequency increase step $\Delta\omega$, it is impossible to obtain the precise ω, which can satisfy $|E|=0$, directly. Therefore, a searching process is needed in here. If the determinant

of frequency characteristic matrix $[E]_{8\times 8}$ is denoted as a function of ω, $f(\omega)$, the real natural frequency ω value should be the root of $f(\omega)=0$. Therefore, in the searching process, a numerical analysis method, Secant Method, can be adopted to solve that problem after an approximation roots $\omega_{n,1}$ are determined by the semi-analytical method.

In order to find the final form of the double-beam system free vibration, initial conditions defined in Eq. (3-2) are applied to determine the values of constants D_n. Before that, a specific discussion on natural frequency ω in double-beam system is shown here. In this chapter, the double-beam system with zero viscoelastic layer damping is called undamped double-beam system, and the one with nonzero viscoelastic layer damping is called damped double-beam system. Considering the undamped double-beam system ($C=0$), the equations about natural frequency, which are from Eq. (3-5), will be written as follows

$$-\bar{m}_1 A\omega_{Undamped}^2 + K(A-B) + e_1 P^4 A = 0 \tag{3-14a}$$

$$-\bar{m}_2 B\omega_{Undamped}^2 - K(A-B) + e_2 P^4 B = 0 \tag{3-14b}$$

Substituting Eq. (3-14), $K(A-B)+e_1P^4A=\bar{m}_1A\omega_{Undamped}^2$ and $-K(A-B)+e_2P^4B=\bar{m}_2B\omega_{Undamped}^2$, into Eq. (3-5) with $C\neq 0$, and defining $\xi=\dfrac{-C(B-A)}{(\bar{m}_2B-\bar{m}_1A)\omega_{Undamped}}$, the Eq. (3-5) will be

$$\omega^2 - 2\xi\omega_{Undamped} i\omega - \omega_{Undamped}^2 = 0 \tag{3-15}$$

The solution for Eq. (3-15) can be written as

$$\omega = \pm\sqrt{1-\xi^2}\,\omega_{Undamped} + \xi\omega_{Undamped}\,i = \pm\omega_{Damped} + \xi\omega_{Undamped}\,i \tag{3-16}$$

where ω is natural frequency of damped double-beam system, $\omega_{Damped} = \sqrt{1-\xi^2}\,\omega_{Undamped}$ is real natural frequency of damped double-beam system, $\omega_{Undamped}$ is natural frequency of undamped double-beam system, and $\xi = \dfrac{-C(B-A)}{(\bar{m}_2 B - \bar{m}_1 A)\,\omega_{Undamped}}$ is damping ratio of damped double-beam system.

Based on Eq. (3-16), the assuming final solutions for double-beam system free vibration can be written as

$$W_1(x,t) = \sum_{n=1}^{\infty}\left(D_{n1}e^{i\omega_{n,Damped}t} + D_{n2}e^{-i\omega_{n,Damped}t}\right)e^{-\xi\omega_{n,Undamped}t}\left[\sum_{j=1}^{8}\left(A_{nj}e^{P_{nj}x}\right)\right] = \sum_{n=1}^{\infty}\left(D_{n1}e^{i\omega_{n1}t} + D_{n2}e^{i\omega_{n2}t}\right)\phi_{n1}(x) \tag{3-17a}$$

$$W_2(x,t) = \sum_{n=1}^{\infty}\left(D_{n1}e^{i\omega_{n,Damped}t} + D_{n2}e^{-i\omega_{n,Damped}t}\right)e^{-\xi\omega_{n,Undamped}t}\left[\sum_{j=1}^{8}\left(\beta_{nj}A_{nj}e^{P_{nj}x}\right)\right] = \sum_{n=1}^{\infty}\left(D_{n1}e^{i\omega_{n1}t} + D_{n2}e^{i\omega_{n2}t}\right)\phi_{n2}(x) \tag{3-17b}$$

$$\omega_{n1} = \omega_{n,Damped} + \xi\omega_{n,Undamped}\,i \tag{3-17c}$$

$$\omega_{n2} = -\omega_{n,Damped} + \xi\omega_{n,Undamped}\,i \tag{3-17d}$$

where $\phi_{n1}(x)$ and $\phi_{n2}(x)$ are the mode shape functions under *n*th natural frequency for the upper and lower beams, respectively, $\omega_{n,Undamped}$ and $\omega_{n,Damped}$ are *n*th natural frequency for undamped double beam system and *n*th real natural frequency for damped double-beam system,

defined in Eq. (3-16), and ω_{n1}, ω_{n2} are two roots of *n*th natural frequency for damped double-beam system.

Substituting Eq. (3-17) into Eq. (3-2), the initial conditions could be denoted as

$$\sum_{n=1}^{\infty}\left(D_{n1}+D_{n2}\right)\phi_{n1}\left(x\right)=W_{10}\left(x\right) \tag{3-18a}$$

$$\sum_{n=1}^{\infty}\left(D_{n1}+D_{n2}\right)\phi_{n2}\left(x\right)=W_{20}\left(x\right) \tag{3-18b}$$

$$\sum_{n=1}^{\infty}\left(i\omega_{n1}D_{n1}+i\omega_{n2}D_{n2}\right)\phi_{n1}\left(x\right)=V_{10}\left(x\right) \tag{3-18c}$$

$$\sum_{n=1}^{\infty}\left(i\omega_{n1}D_{n1}+i\omega_{n2}D_{n2}\right)\phi_{n2}\left(x\right)=V_{20}\left(x\right) \tag{3-18d}$$

In order to apply modal expansion method to solve Eq. (3-18), it is necessary to derive the orthogonality condition for different mode shapes of double-beam system with viscoelastic layer. The governing equations Eq. (3-1) with $f_1\left(x,t\right)=f_2\left(x,t\right)=0$ can be written in the form of:

$$-\bar{m}_1\frac{\partial^2 W_1}{\partial t^2}=e_1\frac{\partial^4 W_1}{\partial x^4}+K\left(W_1-W_2\right)+C\left(\frac{\partial W_1}{\partial t}-\frac{\partial W_2}{\partial t}\right) \tag{3-19a}$$

$$-\bar{m}_2\frac{\partial^2 W_2}{\partial t^2}=e_2\frac{\partial^2 W_2}{\partial x^2}-K\left(W_1-W_2\right)-C\left(\frac{\partial W_1}{\partial t}-\frac{\partial W_2}{\partial t}\right) \tag{3-19b}$$

The left terms $-\bar{m}_1\frac{\partial^2 W_1}{\partial t^2}$ and $-\bar{m}_2\frac{\partial^2 W_2}{\partial t^2}$ are due to acceleration, so they are a kind of inertial

force $f_{I1}(x,t)$ and $f_{I2}(x,t)$. The right terms $e_1\frac{\partial^4 W_1}{\partial x^4}$, $e_2\frac{\partial^2 W_2}{\partial x^2}$ and $K(W_1-W_2)$ are related to displacement, so they can be treated as a sort of elastic force. Although the right term $C\left(\frac{\partial W_1}{\partial t}-\frac{\partial W_2}{\partial t}\right)$ is damping force which is related to two beams velocities, it also can be treated as an outer force which produces two beams displacements, therefore, it can be treated as a special sort of elastic force. According to Bitti Theory, when considering the whole double-beam system, which consists of upper beam and lower beam, an energy equilibrium equation will be obtained as

$$\int_0^L\left[W_{1m}(x,t)\,f_{I1n}(x,t)+W_{2m}(x,t)\,f_{I2n}(x,t)\right]dx=\int_0^L\left[W_{1n}(x,t)\,f_{I1m}(x,t)+W_{2n}(x,t)\,f_{I2m}(x,t)\right]dx \tag{3-20}$$

Substituting Eq. (3-19) into Eq. (3-20), applying the definitions of $f_{I1}(x,t)$ $f_{I2}(x,t)$ and merging the similar items, the Eq. (3-20) will be

$$\left\{\bar{m}_1\int_0^L\left[\phi_{n1}(x)\phi_{m1}(x)\right]dx+\bar{m}_2\int_0^L\left[\phi_{n2}(x)\phi_{m2}(x)\right]dx\right\}\times T_m(t)T_n(t)\left(\omega_m^2-\omega_n^2\right)=0 \tag{3-21}$$

Since for different natural frequencies, $\omega_m^2\neq\omega_n^2$, so the orthogonality condition for different mode shapes of the double-beam system with viscoelastic layer is

$$\int_0^L\left[\phi_{n1}(x)\bar{m}_1\phi_{m1}(x)+\phi_{n2}(x)\bar{m}_2\phi_{m2}(x)\right]dx=\bar{M}_n\delta_{mn} \tag{3-22}$$

where $\bar{M}_n$ is the generalized mass in the *n*th mode, and δ_{mn} is the Kronecker delta function.

Go back to the initial conditions Eq. (3-18), $Eq.(3-18a)\times\phi_{m1}(x)\bar{m}_1+Eq.(3-18b)\times\phi_{m2}(x)\bar{m}_2$,

and integrate it respect to x from 0 to L

$$\int_0^L \phi_{m1}(x)\bar{m}_1 \sum_{n=1}^{\infty}(D_{n1}+D_{n2})\phi_{n1}(x)\,dx + \int_0^L \phi_{m2}(x)\bar{m}_2 \sum_{n=1}^{\infty}(D_{n1}+D_{n2})\phi_{n2}(x)\,dx$$
$$= \int_0^L \phi_{m1}(x)\bar{m}_1 W_{10}(x)\,dx + \int_0^L \phi_{m2}(x)\bar{m}_2 W_{20}(x)\,dx \tag{3-23}$$

The orthogonality condition is applied into Eq. (3-23), and it will be transferred as

$$D_{n1}+D_{n2} = \frac{\int_0^L \left[\phi_{n1}(x)\bar{m}_1 W_{10}(x) + \phi_{n2}(x)\bar{m}_2 W_{20}(x)\right]dx}{\int_0^L \left[\phi_{n1}(x)\bar{m}_1 \phi_{n1}(x) + \phi_{n2}(x)\bar{m}_2 \phi_{n2}(x)\right]dx} \tag{3-24}$$

$Eq.(3-18c)\times\phi_{m1}(x)\bar{m}_1 + Eq.(3-18d)\times\phi_{m2}(x)\bar{m}_2$, and integrate it respect to x from 0 to L; apply orthogonality condition like in Eq. (3-23), it will be

$$\omega_{n1}D_{n1} + \omega_{n2}D_{n2} = \frac{1}{i}\frac{\int_0^L \left[\phi_{n1}(x)\bar{m}_1 V_{10}(x) + \phi_{n2}(x)\bar{m}_2 V_{20}(x)\right]dx}{\int_0^L \left[\phi_{n1}(x)\bar{m}_1 \phi_{n1}(x) + \phi_{n2}(x)\bar{m}_2 \phi_{n2}(x)\right]dx} \tag{3-25}$$

Solving Eq. (3-24) and Eq. (3-25), the solution of D_{n1} and D_{n2} can be

$$D_{n1} = \frac{1}{(\omega_{n2}-\omega_{n1})}\times\left\{\omega_{n2}\frac{\bar{W}_n}{\bar{M}_n} - \frac{1}{i}\times\frac{\bar{V}_n}{\bar{M}_n}\right\} \tag{3-26a}$$

$$D_{n2} = \frac{1}{(\omega_{n1}-\omega_{n2})}\times\left\{\omega_{n1}\frac{\bar{W}_n}{\bar{M}_n} - \frac{1}{i}\times\frac{\bar{V}_n}{\bar{M}_n}\right\} \tag{3-26b}$$

$$\bar{M}_n = \int_0^L \left[\phi_{n1}(x)\bar{m}_1\phi_{n1}(x) + \phi_{n2}(x)\bar{m}_2\phi_{n2}(x)\right]dx \tag{3-26c}$$

$$\bar{W}_n = \int_0^L \left[\phi_{n1}(x)\bar{m}_1 W_{10}(x) + \phi_{n2}(x)\bar{m}_2 W_{20}(x)\right]dx \tag{3-26d}$$

$$\bar{V}_n = \int_0^L \left[\phi_{n1}(x)\bar{m}_1 V_{10}(x) + \phi_{n2}(x)\bar{m}_2 V_{20}(x)\right]dx \tag{3-26e}$$

where $\bar{M}_n$, $\bar{W}_n$, $\bar{V}_n$ is the generalized mass, displacement and velocity in the nth mode.

Until here, all constants in the assumed solutions Eq. (3-17) have been determined. Therefore, the free vibration of a double-beam system with viscoelastic layer is solved successfully.

3.4 Solution of the Problem for Forced Vibration

It is similar to the solutions of free vibration, particular solutions of forced vibration in the double-beam system could be assumed in the following form

$$W_1(x,t)=\sum_{n=1}^{\infty}T_n(t)\left[\sum_{j=1}^{8}\left(A_{nj}e^{P_{nj}x}\right)\right]=\sum_{n=1}^{\infty}T_n(t)\phi_{n1}(x) \tag{3-27a}$$

$$W_2(x,t)=\sum_{n=1}^{\infty}T_n(t)\left[\sum_{j=1}^{8}\left(\beta_{nj}A_{nj}e^{P_{nj}x}\right)\right]=\sum_{n=1}^{\infty}T_n(t)\phi_{n2}(x) \tag{3-27b}$$

where $\phi_{n1}(x)=\sum_{j=1}^{8}\left(A_{nj}e^{P_{nj}x}\right)$, $\phi_{n2}(x)=\sum_{j=1}^{8}\left(\beta_{nj}A_{nj}e^{P_{nj}x}\right)$ are mode shape functions of upper beam and lower beam corresponding to *n*th natural frequency, and $T_n(t)$ is time function corresponding to *n*th natural frequency. $\phi_{n1}(x)$ and $\phi_{n2}(x)$ are known from the free vibration analysis, and $T_n(t)$ is unknown function which need to be solved.

Substituting the assumed solutions Eq. (3-27) into Eq. (3-1), so they become

$$\begin{aligned}&e_1\sum_{n=1}^{\infty}T_n(t)\frac{d^4\phi_{n1}(x)}{dx^4}+K\sum_{n=1}^{\infty}T_n(t)\left[\phi_{n1}(x)-\phi_{n2}(x)\right]+C\sum_{n=1}^{\infty}\frac{dT_n(t)}{dt}\left[\phi_{n1}(x)-\phi_{n2}(x)\right]\\&+\bar{m}_1\sum_{n=1}^{\infty}\frac{d^2T_n(t)}{dt^2}\phi_{n1}(x)=f_1(x,t)\end{aligned} \tag{3-28a}$$

$$e_2\sum_{n=1}^{\infty}T_n(t)\frac{d^4\phi_{n2}(x)}{dx^4}-K\sum_{n=1}^{\infty}T_n(t)\left[\phi_{n1}(x)-\phi_{n2}(x)\right]-C\sum_{n=1}^{\infty}\frac{dT_n(t)}{dt}\left[\phi_{n1}(x)-\phi_{n2}(x)\right]$$
$$+\bar{m}_2\sum_{n=1}^{\infty}\frac{d^2T_n(t)}{dt^2}\phi_{n2}(x)=f_2(x,t) \quad \text{(3-28b)}$$

Introducing free vibration equations of undamped double-beam system in here can simplify the motion equations of forced vibration. In undamped double-beam system, damping ratio $\xi=\frac{-C(B-A)}{(\bar{m}_2B-\bar{m}_1A)\omega_{Undamped}}=0$, from Eq. (3-16), $\omega=\pm\omega_{Undamped}$, the solutions for free vibration can be obtained from Eq. (3-17) and written as

$$W_1(x,t)=\sum_{n=1}^{\infty}\left(D_{n1}e^{i\omega_{n,Undamped}t}+D_{n2}e^{-i\omega_{n,Undamped}t}\right)\phi_{n1}(x) \quad \text{(3-29a)}$$

$$W_2(x,t)=\sum_{n=1}^{\infty}\left(D_{n1}e^{i\omega_{n,Undamped}t}+D_{n2}e^{-i\omega_{n,Undamped}t}\right)\phi_{n2}(x) \quad \text{(3-29b)}$$

where $\phi_{n1}(x)$ and $\phi_{n2}(x)$ are undamped double-beam system ($C=0$) mode shapes, and $\omega_{n,Undamped}$ is *n*th natural frequency for undamped double beam system.

Substituting Eq. (3-29) and $C=0$ into Eq. (3-1) with $f_1(x,t)=f_2(x,t)=0$, eliminating the same term $\left(D_{n1}e^{i\omega_{n,Undamped}t}+D_{n2}e^{-i\omega_{n,Undamped}t}\right)$ and multiplying the $T_n(t)$ in each term, the Eq. (3-1) will be in form

$$e_1\sum_{n=1}^{\infty}T_n(t)\frac{d^4\phi_{n1}(x)}{dx^4}+K\sum_{n=1}^{\infty}T_n(t)\left[\phi_{n1}(x)-\phi_{n2}(x)\right]=\bar{m}_1\sum_{n=1}^{\infty}\omega_{n,Undamped}^2T_n(t)\phi_{n1}(x) \quad \text{(3-30a)}$$

$$e_2\sum_{n=1}^{\infty}T_n(t)\frac{d^4\phi_{n2}(x)}{dx^4}-K\sum_{n=1}^{\infty}T_n(t)\left[\phi_{n1}(x)-\phi_{n2}(x)\right]=\bar{m}_2\sum_{n=1}^{\infty}\omega_{n,Undamped}^2T_n(t)\phi_{n2}(x) \quad \text{(3-30b)}$$

Introducing Eq. (3-30) into Eq. (3-28) produces

$$\sum_{n=1}^{\infty}\left[\bar{m}_1\phi_{n1}(x)\frac{d^2T_n(t)}{dt^2}+\bar{m}_1\omega_{n,Undamped}^2\phi_{n1}(x)T_n(t)\right]=f_1(x,t)-C\left(\frac{\partial W_1}{\partial t}-\frac{\partial W_2}{\partial t}\right) \tag{3-31a}$$

$$\sum_{n=1}^{\infty}\left[\bar{m}_2\phi_{n2}(x)\frac{d^2T_n(t)}{dt^2}+\bar{m}_2\omega_{n,Undamped}^2\phi_{n2}(x)T_n(t)\right]=f_2(x,t)+C\left(\frac{\partial W_1}{\partial t}-\frac{\partial W_2}{\partial t}\right) \tag{3-31b}$$

$Eq.(3-31a)\times\phi_{m1}(x)+Eq.(3-31b)\times\phi_{m2}(x)$, integrate it respect to x from 0 to L, and apply orthogonality condition Eq. (3-22), so it will be

$$\frac{d^2T_n(t)}{dt^2}+\omega_{n,Undamped}^2T_n(t)=F_n(t)+F_{Dn}(t) \tag{3-32a}$$

$$F_n(t)=\frac{\int_0^L\left[\phi_{n1}(x)\,f_1(x,t)+\phi_{n2}(x)\,f_2(x,t)\right]dx}{\int_0^L\left[\phi_{n1}(x)\bar{m}_1\phi_{n1}(x)+\phi_{n2}(x)\bar{m}_2\phi_{n2}(x)\right]dx} \tag{3-32b}$$

$$F_{Dn}(t)=\frac{\int_0^L\left\{\left[\phi_{n2}(x)-\phi_{n1}(x)\right]\left[C\left(\frac{\partial W_1}{\partial t}-\frac{\partial W_2}{\partial t}\right)\right]\right\}dx}{\int_0^L\left[\phi_{n1}(x)\bar{m}_1\phi_{n1}(x)+\phi_{n2}(x)\bar{m}_2\phi_{n2}(x)\right]dx} \tag{3-32c}$$

Using Duhamel's integral, particular solution of Eq. (3-32a) can be obtained as

$$T_n(t)=\frac{1}{\omega_{n,Undamped}}\int_0^t\left[F_n(\tau)+F_{Dn}(\tau)\right]\cdot\sin\left[\omega_{n,Undamped}(t-\tau)\right]d\tau \tag{3-33}$$

In Eq. (3-32) and Eq. (3-33), the unknown damping force $C\left(\frac{\partial W_1}{\partial t}-\frac{\partial W_2}{\partial t}\right)$ is included, therefore,

they are a kind of implicit equations and it is hard to solve them directly. An iteration method, which could be generally expressed in a flowchart form as in Fig. 3-2, is developed in this chapter to solve that problem. By the iteration method, the forced vibration of a double-beam system with viscoelastic layer is solved successfully.

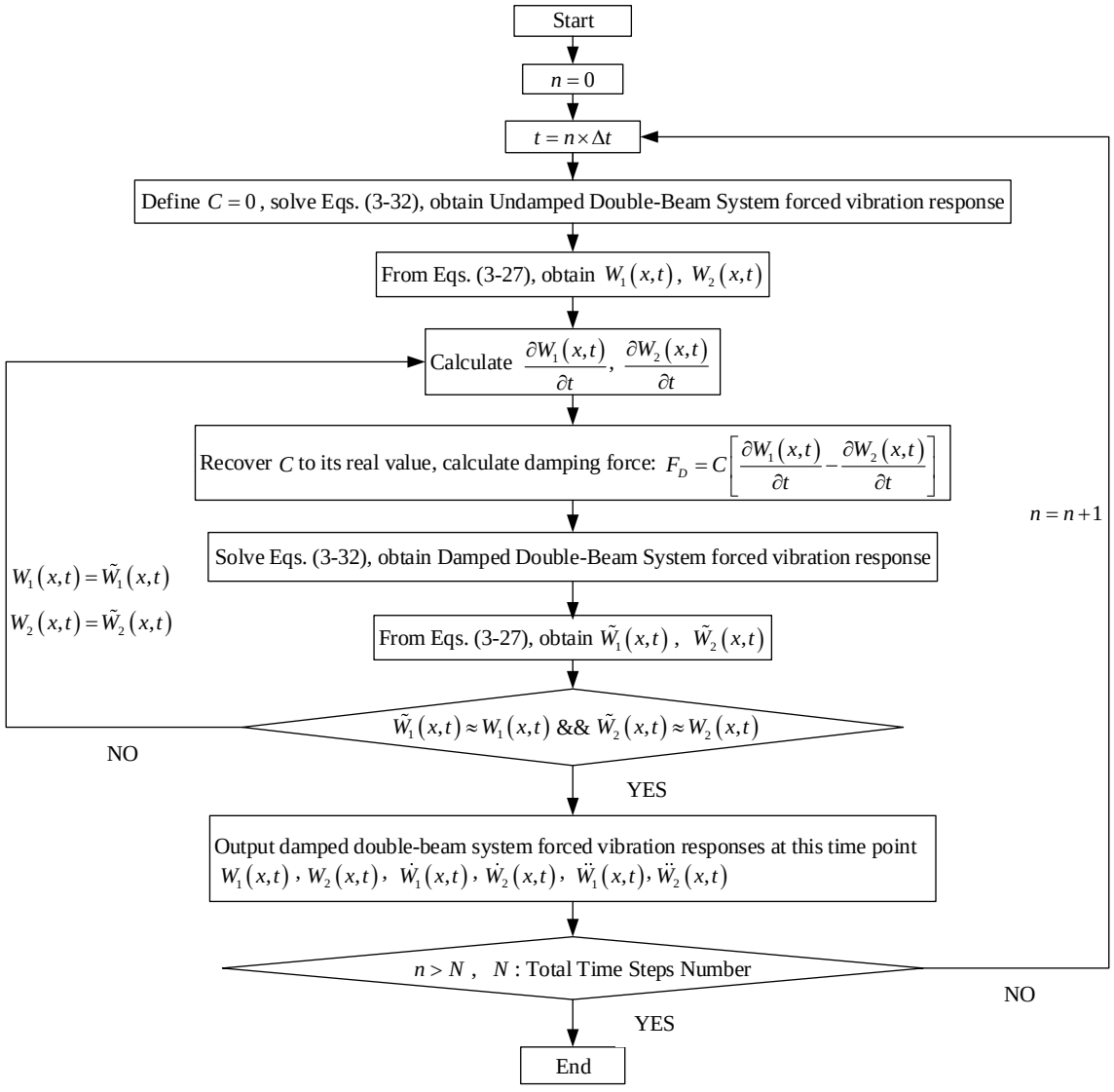

Fig. 3-2. Flowchart of the iteration method to calculate forced vibration responses of a double-beam system with viscoelastic layer.

3.5 Numerical Examples

In order to illustrate the semi-analytical method and the iteration method presented in this chapter, some numerical examples are discussed in detail. Upper beam spring supported-spring supported and lower beam simply supported-simply supported (Fig. 3-1(a)) is the main boundary condition simulated in here. The model with upper beam and lower beam both simply supported-simply supported, is applied to verify the correctness and accuracy of the proposed method.

3.5.1 Free Vibration

The values for the parameters of the double-beam system are from (Oniszczuk 2000c) as follows

$E = 1\times10^{10}\,Nm^{-2}$, $I = 4\times10^{-4}\,m^4$, $\rho = 2\times10^{3}\,kgm^{-3}$, $A = 5\times10^{-2}\,m^2$, $L = 10m$,

$e = EI = 4\times10^{6}\,Nm^2$, $m = \rho A = 1\times10^{2}\,kgm^{-1}$, $K = (1\sim5)\times10^{5}\,Nm^{-2}$, $C = (0\sim1)\times10^{4}\,Nsm^{-1}$

Four cases are investigated in here for verification and discussion. The boundary condition for Case 1 is upper beam simply supported-simply supported and lower beam simply supported-simply supported, and the ones for Case 2 to Case 4 are the same as upper beam spring supported-spring supported and lower beam simply supported-simply supported. The specific parameter values of all cases are as follows

Case 1: $e_1 = e_2 = e$, $m_1 = m_2 = m$, $K = (1\sim5)\times10^{5}\,Nm^{-2}$, $C = 0\,Nsm^{-1}$.

Case 2: $e_1 = e_2 = e$, $m_1 = m_2 = m$, $K = 1\times10^{4}\,Nm^{-2}$, $C = (0\sim1)\times10^{4}\,Nsm^{-1}$.

Case 3: $e_1 = 0.08e$, $e_2 = e$, $m_1 = 0.2m$, $m_2 = m$, $K = 1\times10^4\, Nm^{-2}$, $C = (0 \sim 5)\times10^2\, Nsm^{-1}$.

Case 4: $e_1 = 0.08e$, $e_2 = e$, $m_1 = 0.2m$, $m_2 = m$, $K = (1 \sim 5)\times10^4\, Nm^{-2}$, $C = 100 Nsm^{-1}$.

The natural frequencies and mode shapes of those four cases are calculated by using the semi-analytical method presented in this chapter, the first several natural frequencies and normal mode shapes of each case are summarized in Tables 3-1 to 3-4 and Fig. 3-3 to Fig. 3-9, respectively. The comparative results available in (Oniszczuk 2000c) are also summarized in Table 3-1.

In Table 3-1, the natural frequencies calculated by the semi-analytical method presented in this chapter, are in excellent agreement with the analytical solutions in (Oniszczuk 2000c). Therefore, the correctness and accuracy of the semi-analytical method are apparently proved and demonstrated by the comparison in Table 3-1.

The data in Table 3-2 and Table 3-4 are also plotted in Fig. 3-9, which indicate the effects of viscoelastic layer damping *C* and stiffness *K* on the natural frequency ω_n of whole double-beam system. As shown in Fig. 3-9(a), viscoelastic layer damping *C* doesn't change the natural frequency ω_n significantly in a certain range, but if the damping *C* reach a large value, some natural frequencies will be vanished. When the viscoelastic layer damping *C* reach a certain relative large value, it makes the viscoelastic layer becoming a kind of rigid connection between two beams, the whole system will behave like a single beam instead of two beams. Therefore, some antisymmetric

mode shapes and corresponding natural frequencies will be eliminated, and the symmetric mode shapes and their frequencies, which are similar to the single beam mode shapes, will exist. The Fig. 3-5 and Fig. 3-7, which are the mode shapes under large viscoelastic damping *C* and are similar to the single beam mode shapes, just confirm the conclusion and explanations above. Different from the damping, in general, there is a tendency to increase the natural frequency ω_n in case of increasing the viscoelastic layer stiffness *K* (as shown in Fig. 3-9(b)). Therefore, it is effective to adjust the natural frequencies of whole double-beam system by changing the viscoelastic layer stiffness *K*, that can help people to avoid the resonance phenomenon happened in the double-beam structure during it is under some dynamic loads with specific frequencies.

From Case 2 and Case 3, the data are as shown in Table 3-2 and Table 3-3, if the viscoelastic layer damping and stiffness are the same, when the upper beam is smaller than lower beam, the natural frequencies become a little higher, and that could help to solve some low frequency domain vibration problems in engineering practices.

Table 3-1. Natural Frequencies of double-beam system $\omega_{n,Undamped}$ (s^{-1}); Case 1: $C = 0 Nsm^{-1}$

$K\times10^{-5}$	$n=1$		$n=2$		$n=3$		$n=4$		$n=5$		$n=6$	
$\left(Nm^{-2}\right)$	Present	Ref.	Present	Ref.	Present	Ref.	Present	Ref.	Present	Ref.	Present	Ref.
1	19.74	19.7	48.88	48.9	78.96	79	90.74	90.7	177.65	177.7	183.20	183.2
2	19.74	19.7	66.25	66.3	78.96	79	101.16	101.2	177.65	177.7	188.58	188.6
3	19.74	19.7	78.94	79	79.96	79.9	110.61	110.6	177.65	177.7	193.81	193.8
4	19.74	19.7	78.96	79	91.59	91.6	119.31	119.3	177.65	177.7	198.90	198.9
5	19.74	19.7	78.96	79	101.93	101.9	127.41	127.4	177.65	177.7	203.86	203.9

Table 3-2. Natural Frequencies of double-beam system $\omega_{n,Damped}$ (s^{-1}); Case 2: $K = 1\times10^{4}\,Nm^{-2}$

$C\left(Nsm^{-1}\right)$	ξ	$n=1$	$n=2$	$n=3$	$n=4$	$n=5$	$n=6$
0	0	9.90	12.60	22.58	46.73	79.59	124.08
10^2	0.013	9.90	12.57	22.55	46.72	79.59	124.07
10^3	0.108	9.86	10.18	19.10	45.53	79.20	123.35
10^4	0.537	-	-	19.05	-	78.59	-

Table 3-3. Natural Frequencies of double-beam system $\omega_{n,Damped}$ (s^{-1}); Case 3: $K = 1\times10^{4}\,Nm^{-2}$

$C\left(Nsm^{-1}\right)$	ξ	$n=1$	$n=2$	$n=3$	$n=4$	$n=5$	$n=6$
0	0	17.52	24.49	27.26	41.57	79.47	83.82
50	0.016	17.54	24.45	27.20	-	79.46	-
100	0.032	17.59	24.31	27.02	-	79.43	-
500	0.156	18.33	-	-	-	78.50	-

Table 3-4. Natural Frequencies of double-beam system $\omega_{n,Damped}$ (s^{-1}); Case 4: $C = 100\,Nsm^{-1}$

$K\times10^{-4}\left(Nm^{-2}\right)$	$n=1$	$n=2$	$n=3$	$n=4$	$n=5$	$n=6$
1	17.59	24.31	27.02	79.43	155.77	177.90
2	18.25	34.51	36.54	79.59	158.67	178.21
3	18.43	42.32	44.10	80.13	161.53	178.54
4	18.51	50.51	52.28	81.19	164.35	178.92
5	18.55	56.18	57.30	83.37	167.13	179.33

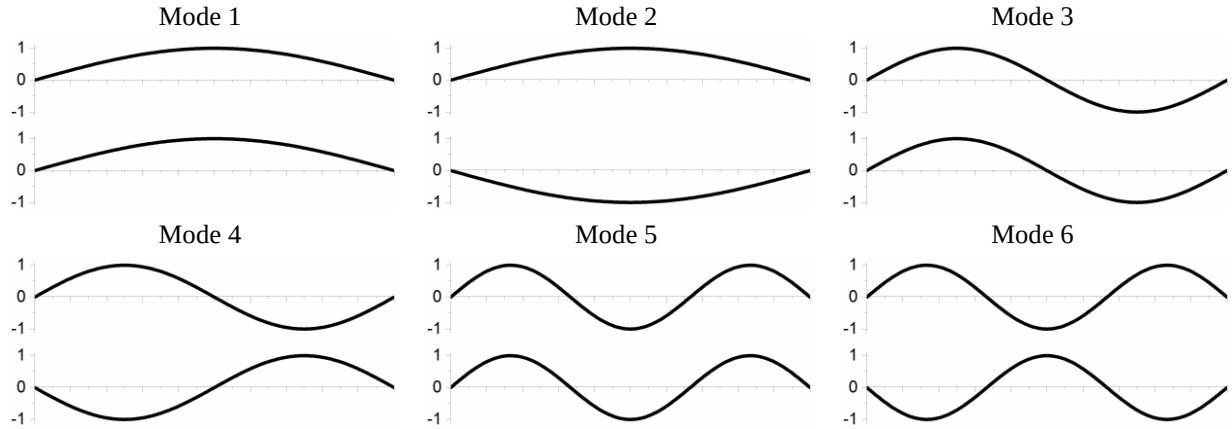

Fig. 3-3. The first six normal mode shapes of the double-beam system for Case 1, $K = 1\times10^{5}, C = 0$.

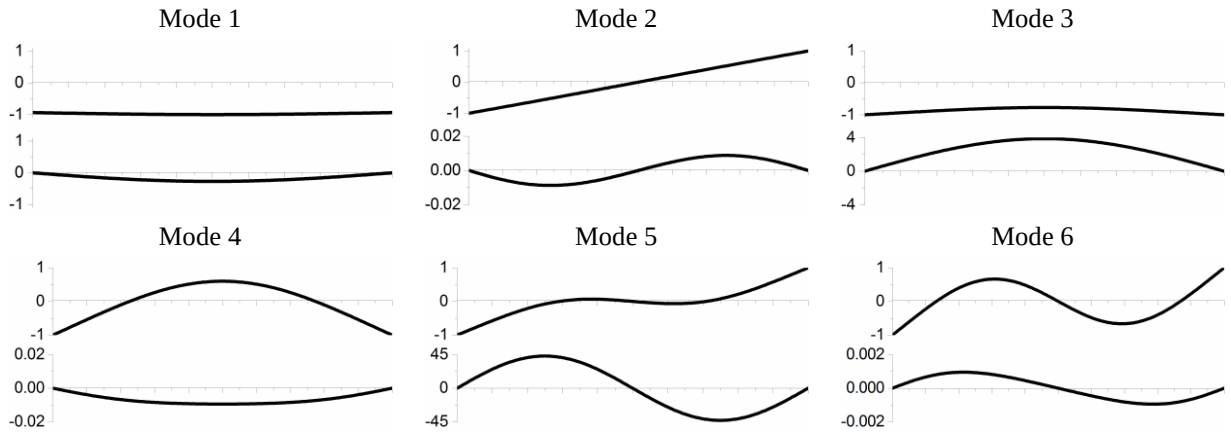

Fig. 3-4. The first six normal mode shapes of the double-beam system for Case 2, $K = 1\times10^4$, $C = 100$.

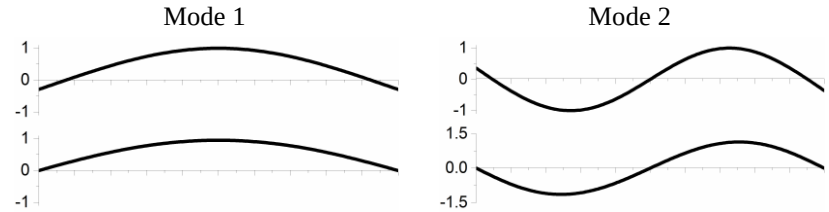

Fig. 3-5. The first two normal mode shapes of the double-beam system for Case 2, $K = 1\times10^4$, $C = 10^4$.

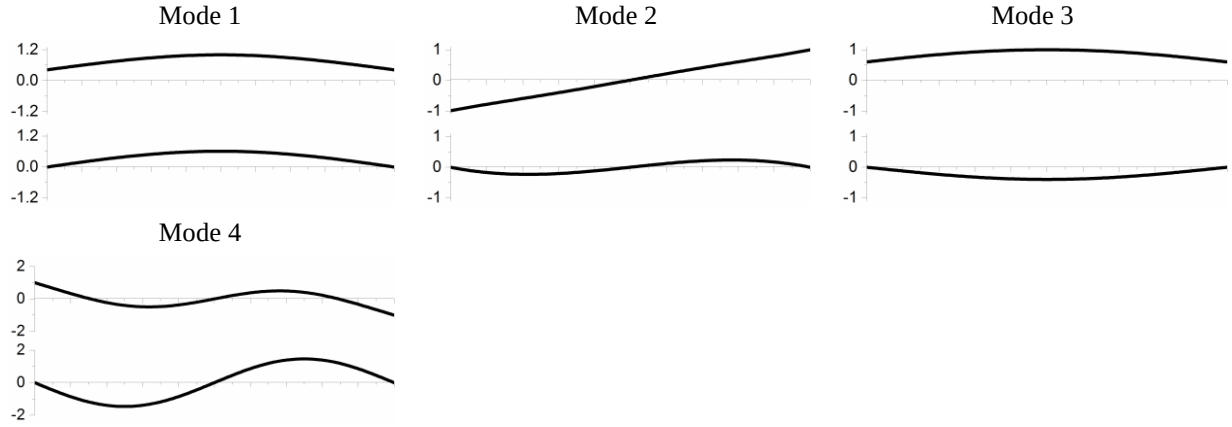

Fig. 3-6. The first four normal mode shapes of the double-beam system for Case 3, $K = 1\times10^4$, $C = 50$.

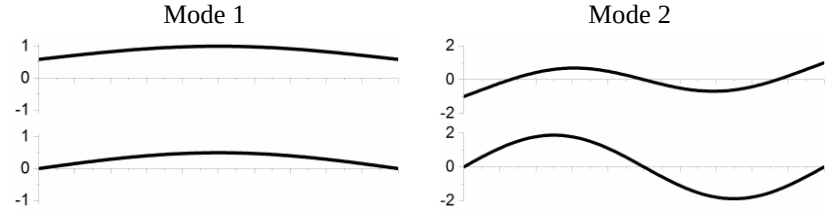

Fig. 3-7. The first two normal mode shapes of the double-beam system for Case 3, $K = 1\times10^4$, $C = 500$.

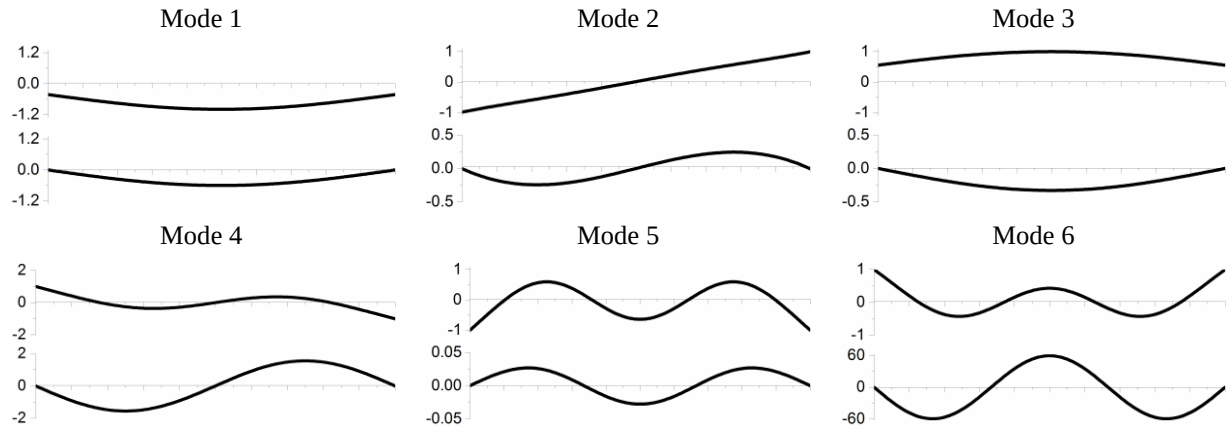

Fig. 3-8. The first six normal mode shapes of the double-beam system for Case 4, $K=1\times10^4$, $C=100$.

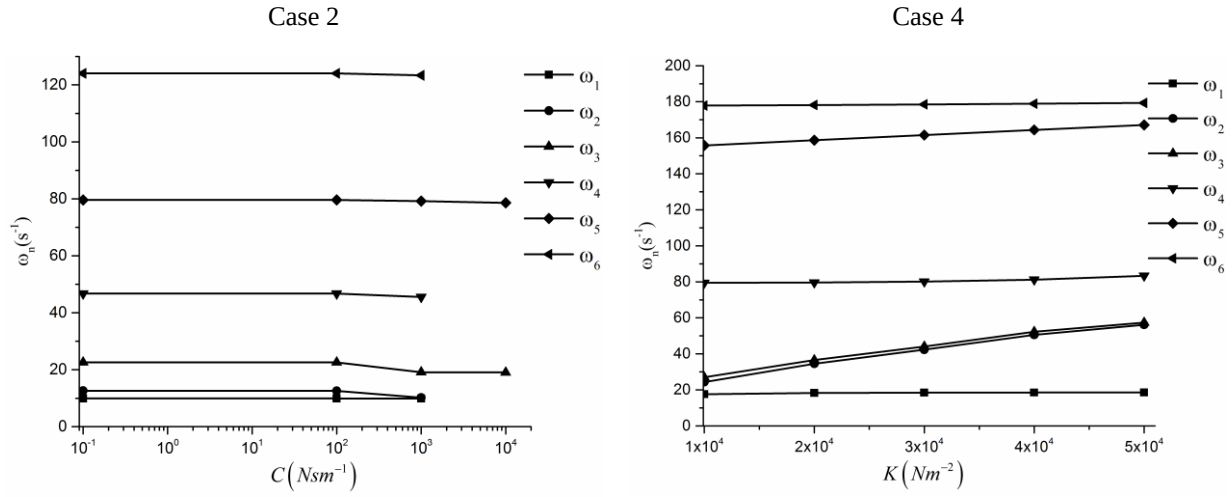

Fig. 3-9. Natural frequency ω_n versus viscoelastic layer damping *C* and stiffness *K*.

3.5.2 Forced Vibration

Various models are calculated and analyzed in here, all of them are with the same boundary condition: upper beam spring supported-spring supported and lower beam simply supported-simply supported, which is more realistic in engineering practices. Among all of those models, the exciting force of the double-beam system is $f_1(x,t)=f\sin(\omega t)\delta(x-0.5L)$, $f_2(x,t)=0$,

where $f = -10000N$ is amplitude and ω is frequency of a concentrated harmonic force acted on the midspan of the upper beam, and $\delta(x)$ is Dirac delta function. The values for the basic parameters of the double-beam system are also the same from (Oniszczuk 2000c).

3.5.2.1 Resonance Condition

Resonance Phenomenon is an important issue in structure vibration problems, and it is so dangerous which must be avoided. According to abundant previous research conclusions, the resonance phenomenon will happen when the frequency of exciting force is close to the structure natural frequency. Due to the complexity of the double-beam system with viscoelastic layer, it is hard to derive the resonance condition in formulation format, but it is still reasonable to conclude as follows: if the frequency of exciting force ω is equal to real natural frequency of damped double-beam system ω_{Damped}, the dynamic responses of the two beams, W_1 and W_2, will be unlimited, which is resonance phenomenon. Therefore, the resonance condition for double-beam system with viscoelastic layer is

$$\omega = \omega_{n,Damped}, \qquad n = 1,2,3,... \tag{3-34}$$

Two cases are calculated in here for verifying the resonance condition: Case 1: two identical beams, $e_1 = e_2 = e$, $m_1 = m_2 = m$, $K = 1\times10^4 Nm^{-2}$, $C = 100Nsm^{-1}$; Case 2: smaller upper beam, $e_1 = 0.08e$, $e_2 = e$, $m_1 = 0.2m$, $m_2 = m$, $K = 1\times10^4 Nm^{-2}$, $C = 100Nsm^{-1}$. The frequency responses at the midspan of the two beams are calculated by the equations presented in this chapter,

and the absolute amplitude of them are shown in Fig. 3-10.

a. Case 1: Two Identical Beams

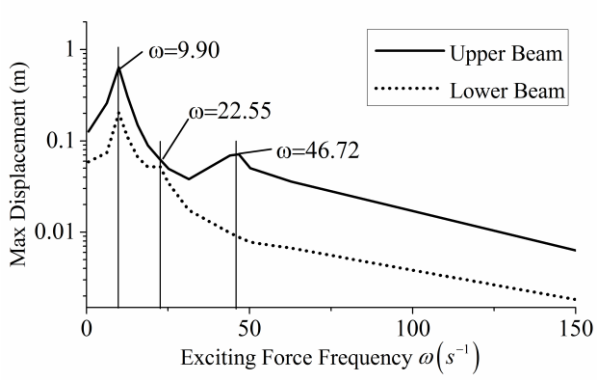

b. Case 2: Smaller Upper Beam

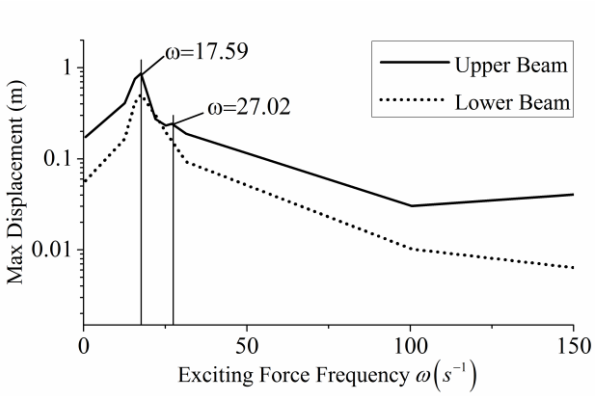

Fig. 3-10. Frequency response at midspan point of two beams.

From Fig. 3-10, Table 3-2 and Table 3-3, it can be easily seen that the dynamic response of two beams reach some peak values when the exciting force frequencies ω is close to the real natural frequencies of the damped double-beam system $\omega_{n,Damped}$, which is just the resonance phenomenon and verifies the resonance condition shown above. When designing the double-beam system, it is supposed to make the natural frequencies of system being far away from the frequency of exciting force, and avoid the resonance phenomenon happened.

Also in Fig. 3-10, when the resonance frequency $\omega = 46.72$ in Case 1, and $\omega = 27.02$ in Case 2, only the upper beam has the peak values, and in contrast, lower beam doesn't have. The main reason for that is the corresponding mode shapes. Checking the mode shapes in Fig. 3-4(d) and Fig. 3-6(c), it is found that the deformation amplitude of lower beam is very small comparing with

the upper beam, therefore in those resonance frequencies, the lower beam dynamic response is not as great as upper beam, although there is still resonance happened to lower beam.

3.5.2.2 Effect of Viscoelastic Layer Stiffness K

Viscoelastic layer is the connection between upper beam and lower beam in double-beam system, therefore, its properties will affect the dynamic responses of two beams apparently. Some discussions about the effect of viscoelastic layer stiffness *K* on two beams dynamic responses are shown in here. Three cases are investigated in here for discussion: $e_1 = e_2 = e$, $m_1 = m_2 = m$, $C = 100 Nsm^{-1}$; Case 1: $K = 1\times10^4 Nm^{-2}$; Case 2: $K = 2\times10^4 Nm^{-2}$; Case 3: $K = 3\times10^4 Nm^{-2}$. The deformation response factor of frequency response at the midspan of the two beams are shown in a form of semi-log plots in Fig. 3-11.

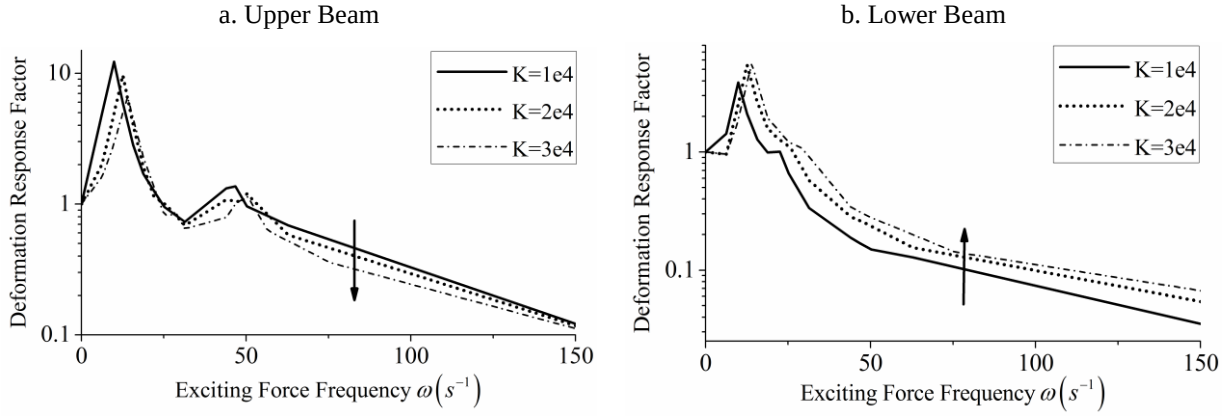

Fig. 3-11. Frequency response at midspan point of two beams.

With the increase of viscoelastic layer stiffness *K*, the dynamic response of upper beam is generally

decreased (as shown in Fig. 3-11(a)). Upper beam in here is a kind of a beam on viscoelastic foundation, when the viscoelastic layer becomes stiffer, the restrict to the upper beam gets stronger, therefore the upper beam vibrates smaller and smaller under same exciting force. From Fig. 3-11(b), the dynamic response of lower beam is generally increased with the increase of layer stiffness *K*, which is opposite to upper beam. Since $f_2(x,t)=0$, therefore the energy which let lower beam vibrate is all from viscoelastic layer. Once the viscoelastic layer gets stiffer, its deformation will be smaller and less energy will be absorbed by upper beam, therefore more exciting energy will be obtained by lower beam and makes its dynamic response increased.

3.5.2.3 Effect of Viscoelastic Layer Damping C

Another parameter of viscoelastic layer in the double-beam system is the damping, *C*, which is an important issue to reduce the vibrations of both beams. Three cases are investigated in here for discussion of damping effects on two beams dynamic responses: $e_1=e_2=e$, $m_1=m_2=m$, $K=1\times10^4\,Nm^{-2}$; Case 1: $C=0Nsm^{-1}$ ($\xi=0$); Case 2: $C=100Nsm^{-1}$ ($\xi=0.0196$); Case 3: $C=500Nsm^{-1}$ ($\xi=0.151$). The deformation response factor of frequency response at the midspan of the two beams are shown in a form of semi-log plots in Fig. 3-12.

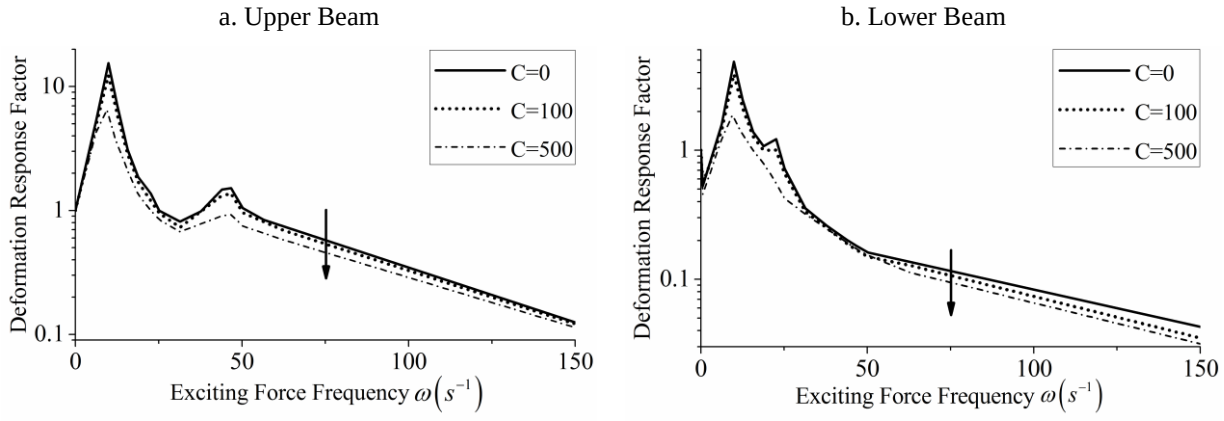

Fig. 3-12. Frequency response at midspan point of two beams.

As shown in Fig. 3-12, for both upper beam and lower beam, the dynamic responses are generally reduced with the increase of damping *C*. Damping is a kind of vibration energy absorber, when increase the damping value, more energy will be absorbed and less energy will be applied to make structure vibration. In double-beam system, the viscoelastic layer is just between upper beam and lower beam, so its damping can effectively absorb the energy when exciting energy is applied to the whole system. Therefore, with the increase of viscoelastic layer damping, more exciting energy could be absorbed and less of them will be applied to upper beam and lower beam, that's why both of them have a reduction on dynamic responses. But the viscoelastic layer damping cannot adopt a very large value, since when it reaches a relative large value, it will become a rigid connection between upper and lower beam, the whole system will vibrate as a single beam system instead of two beams system, which is also proved in the free vibration discussions and shown in Fig. 3-5 and Fig. 3-7, the damping cannot help to absorb energy and reduce the dynamic responses of two beams any more in that case. Therefore, increasing the viscoelastic layer damping value in a

reasonable range could effectively help people to reduce the dynamic responses of both upper beam and lower beam in double-beam system.

3.5.2.4 Effect of Upper Beam Mass

In plenty of engineering projects, the double-beam system usually doesn't have same upper beam and lower beam. To reduce the dynamic responses of the lower beam, the upper beam is designed as vibration absorber. Therefore, the physical property of upper beam has significant effects in dynamic vibration reduction, and the mass of upper beam is discussed firstly in here. Three cases are investigated for discussion: $e_1 = 0.08e_2 = 0.08e$, $m_2 = m$, $K = 1\times10^4\, Nm^{-2}$, $C = 100\, Nsm^{-1}$; Case 1: $m_1 = 0.1m$; Case 2: $m_1 = 0.5m$; Case 3: $m_1 = m$. The deformation response factor of frequency response at the midspan of lower beam is shown as semi-log plots in Fig. 3-13.

From Fig. 3-13, except the resonant frequency domain, when increasing upper beam mass, the dynamic response of lower beam is generally decreased. Since the double-beam system in here is with $f_1(x,t) = f\sin(\omega t)\delta(x-0.5L)$, $f_2(x,t) = 0$, therefore upper beam accepts the exciting energy firstly, absorbs some of them and then transfers the left ones to lower beam by viscoelastic layer. If the upper beam is heavier, more exciting energy are needed to complete its own vibration, the energy left for lower beam is reduced and lower beam vibrates smaller. However, the mass of upper beam cannot grow to very large. If upper beam mass exceeds a limit value, the vibration energy of upper beam itself will be too huge and it will be transferred to lower beam by viscoelastic

layer too, the lower beam vibration will not be reduced anymore in that case.

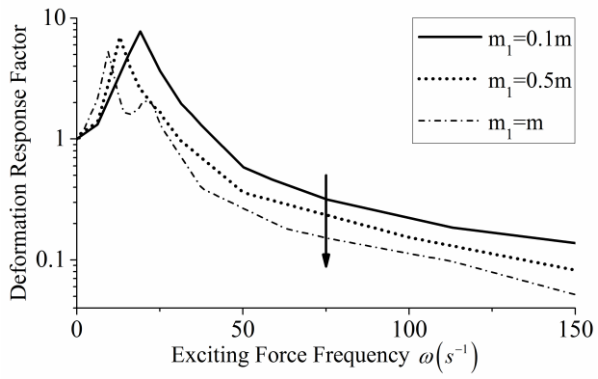

Fig. 3-13. Frequency response at midspan point of lower beam for upper beam mass discussion.

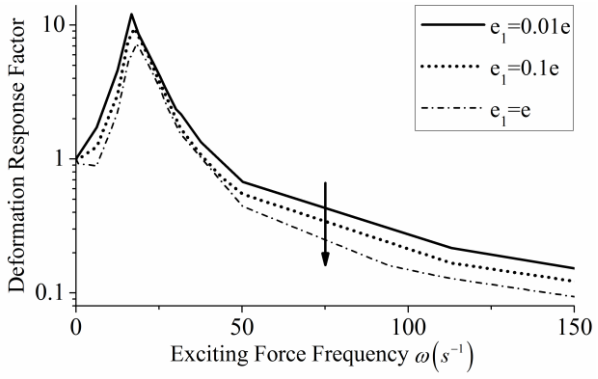

Fig. 3-14. Frequency response at midspan point of lower beam for upper beam flexural rigidity discussion.

However, in resonant frequency domain which is also the small exciting force frequency area in Fig. 3-13, the dynamic response of lower beam is larger when the upper beam mass is larger, which is an opposite tendency comparing with it in non-resonant domain. It is because the change of upper beam mass leads to the apparent difference of natural frequency, and the one with larger upper beam mass has smaller natural frequency. Therefore, the model with larger upper beam mass reaches resonant vibration status at smaller exciting force frequency, and it makes the dynamic response of lower beam has larger value than other cases in that frequency domain. Although the tendency is different due to the resonant vibration, the dynamic response peak value at resonant frequency of the model with smaller upper beam mass is also larger, which is still the same tendency as in non-resonant domain.

3.5.2.5 Effect of Upper Beam Flexural Rigidity

In this section, it will explain how the upper beam flexural rigidity affects the vibration responses in lower beam and how it works to reduce its dynamic response. Also, three cases are investigated in here for discussion: $e_2 = e$, $m_1 = 0.2m_2 = 0.2m$, $K = 1\times10^4\, Nm^{-2}$, $C = 100 Nsm^{-1}$; Case 1: $e_1 = 0.01e$; Case 2: $e_1 = 0.1e$; Case 3: $e_1 = e$. The deformation response factor of frequency response at the midspan of lower beam is shown in Fig. 3-14.

In Fig. 3-14, it is demonstrated that the general tendency for the dynamic response of lower beam is decreased with the increase of upper beam flexural rigidity. When upper beam is soft, less energy can let it deform and vibrate, more energy is obtained by lower beam. When the upper beam flexural rigidity gets larger, more exciting energy is used to complete its deformation and vibration. Thus less energy is transferred to lower beam and its dynamic response gets smaller. If the flexural rigidity exceeds a limit value, the upper beam will become a rigid body and it will not absorb any energy, and all the exciting energy will be transferred to lower beam and make larger dynamic response in lower beam.

3.6 Conclusions

In this chapter, considering the viscoelastic layer damping existed in real engineering practices, a semi-analytical method is developed to analyze the natural frequencies and corresponding mode

shapes of the general double-beam system, which may have arbitrary viscoelastic layer damping, arbitrary beam mass, beam flexural rigidity and/or boundary condition. The free vibration final forms, which are the exact solutions of the motion differential equations formulated by the classical Bernoulli-Fourier method, can be solved based on the initial conditions. Comparing the numerical experiments results with analytical solutions from previous research in the literature, the correctness and accuracy of the semi-analytical method presented in this chapter has been proved. Various models, which have different beam mass, beam flexural rigidity and different boundary condition, are also calculated to show their natural frequencies and corresponding mode shapes. The effects of viscoelastic layer damping and stiffness on double-beam system natural frequencies are further discussed.

The modal-expansion method and an iteration method are applied to find the dynamic response of forced vibration in a double-beam system using the natural frequencies and mode shapes obtained from the free vibration analysis. The specific orthogonality condition for a double-beam system is derived, and then applied to decouple the motion differential equations. Various double-beam system models with a concentrated harmonic force in the midspan of upper beam have been calculated with systematic parametric studies showing the following conclusions:

1. Effect of viscoelastic layer stiffness K: Increase viscoelastic layer stiffness in a range, dynamic responses of upper beam are reduced, but dynamic responses of lower beam are increased.

2. Effect of viscoelastic layer damping C: To both upper beam and lower beam, the dynamic

responses of forced vibration are decreased with the increase tendency of viscoelastic layer damping value in a range.

3. Effect of upper beam mass: Dynamic responses of lower beam are significantly decreased when increase the mass of upper beam in a range.

4. Effect of upper beam flexural rigidity: Dynamic responses of lower beam are decreased if increase the flexural rigidity of upper beam in a range.

Finally, the vibration problem of a double-beam system with viscoelastic layer is solved successfully, and all of those parametric study conclusions can be helpful to engineers to design the double-beam system.

Chapter 4 Active and Semi-Active Vibration Control of Undamped Elastically Connected Double-Beam Systems

4.1 Introduction

In the researches about structural vibration control, the core issue of them is the control algorithm which determines how to apply the control force or how to adjust the parameters of the control structure to reduce the vibration into an accepted level. Due to the complexity of the real structures, it is very hard to derive the control algorithms directly from those real structures. In order to solve that problem, the real structures are usually simplified as some basic mechanical models which can represent their dynamic characteristics. The control algorithms are studied and obtained based on those basic mechanical models, and then, they are inputed into the real structures and verified by some numerical or experimental tests. In this research, the proposed semi-active control is to apply novel adaptive materials as the viscoelastic layer between floating slab track and bridge main beam, and the mechanical model of that whole structure system is just the double-beam system which has been introduced in Chapter 2 and Chapter 3. In this chapter, the active control algorithm and semi-active algorithm are proposed and derived for the double-beam system, which will be theoretical foundation for the studies of the active control and semi-active control in high-speed rail bridges. It is the same as the Chapter 2, in order to start the research from a simple model, the double-beam system interconnect by elastic layers is chosen to be studied firstly in this chapter.

In fact, there have been abundant research efforts in the literature about the dynamic behaviors of the double-beam system in recent years. Those research works include the double-beam system with elastic layer in which the damping is ignored (Seelig and Hoppmann 1964a, 1964b; Kessel 1966; Rao 1974; Chonan 1976; Hamada, Nakayama and Hayashi 1983; Kukla and Skalmierski 1994; Oniszczuk 2000, 2003; Zhang, Lu and Ma 2008; Stojanovic and Kozic 2012; Zhang, Huang, Zhang and Hua 2014; Mao and Wattanasakulpong 2015; Li and Sun 2015), and the one with viscoelastic layer in which the damping characteristics of the connecting layer must be considered (Chen and Sheu 1994, 1995; Li and Hua 2007; Kessel and Raske 1967; Abu 2006; Pavlovic, Kozic and Pavlovic 2012; Vu, Ordonez and Karnopp 2000; Cottle 1990). Although almost all of them have made some simplifications for the structure in order to solve the coupling equations of motion, they are still the fundamental works for the vibration control problem in double-beam system. On the other hand, great progress in the field of structural vibration control has been achieved over the past few decades. Yao (1972) firstly introduced the modern control theory into civil engineering in 1972, from when the research about structural vibration control started. Until now, the main structural vibration control could be classified as three main parts: active control, passive control and semi-active control (Housner et al. 1997; Soong and Spencer 2002). The active control is studied by many scholars for more than 40 years, many achievements have been obtained and there are some real engineering practices applied with it, therefore, it is a more proven control technology (Soong 1990). The essential aspects for the design of an active control structure are reviewed and many topics involved in it are introduced by Alkhatib and Golnaraghi (2003). Yang

et al. (Yang, Akbarpour and Ghaemmaghami 1987; Yang, Long and Wong 1988; Yang, Li and Liu 1991; Yang, Li and Liu 1992) proposed many active control algorithms for the control of structures under seismic load, and some experiments were completed to verify the control efficiency. Li et al. (Li, Liu, Fang and Tam 2000; Li, Liu, Tang, Zhang and Tam 2004) developed some active control algorithms based on genetic algorithm and apply them in the structures under winds, which is another main exciting force to structures. Soong et al. (1991) and Reinhorn et al. (1993) installed full-scale active control structures in actual structures and obtained the control results in an expected level. A type of active control for mechanics and structures, active modal control, is generally reviewed by Inman (2001). Experiments based on the modal control are carried out to verify its feasibility (Meirovitch, Baruh, Montgomery and Williams 1984; Schafer and Holzach 1985). Meirovitch and Silverberg (Meirovitch and Silverberg 1983; Meirovitch 1987) developed the independent modal space control (IMSC), which is an important modal control method, for the distributed systems vibration control. Sadek and Esfandiari (1990) applied an open-closed-loop control for distributed parameter systems to a single Rayleigh beam with damping and it is effective. As to some elastically connected complex systems, Kucuk and Sadek (2005) firstly used optimal control method to actively control the elastically connected rectangular plate-membrane system, and then, they studied the active control for the elastically connected double-string continuous system (Kucuk and Sadek 2007). As shown above, it is easy to find out that there are very few research papers about the active vibration control or semi-active vibration control on double-beam system and very few scholars or engineers consider to apply an efficient active

control structure or semi-active control structure in it. However, in many real engineering practices, such as the floating slab track on bridge which is studied in this paper, the double-beam system has been widely used, therefore, how to use active control structure or semi-active control structure to suppress its vibration for protecting the structure itself is supposed to be a valuable research topic.

This chapter proposes an active control structure installed in the elastic layer location of the double-beam system and a semi-active control structure which adopts the adjustable elastic layer to control the vibration and reduce the dynamic responses of whole structure. The double-beam system with an elastic layer is considered in this chapter, and the active control structure is a distributed control structure with many actuators along the elastic layer which can affect both of beams at same time. By synthesizing IMSC and linear quadratic regulator (LQR), an active control algorithm is developed for the proposed active control structure. IMSC is used to transfer the coupling motion equations of structure in physical space into the decoupled equations in modal space, and the vibration control is also transferred to modal control on each mode. The modal active control force in each mode is determined by LQR, and the final active control force in physical space that can be applied on real structure is finally calculated based on those modal active forces. The semi-active control structure adopts the adjustable elastic layer to take the place of traditional elastic layer between two beams. The active control force produced by the active control structure is set up as the objective and the equivalent semi-active control force is assumed

to be close to that active force. Based on that principle and with the mode shape filter derived in this chapter, the stiffness increase of the adjustable elastic layer which is used to realize the semi-active control is determined. Various models of uncontrolled, active controlled and semi-active controlled double-beam system, which have a concentrated harmonic force in the midspan of upper beam, are calculated and presented to illustrate the efficiency of the proposed active control and semi-active control.

4.2 Formulation of the Vibration Control Problem

In this chapter, the physical model (as shown in Fig. 4-1(a)) of a double-beam system with an active control structure includes an upper beam and a lower beam joined by a uniformly distributed-connecting elastic layer, and is actively controlled by a distributed control structure with many actuators along the elastic layer. And as shown in Fig. 4-1(b), another physical model of a double-beam system with a semi-active control structure consists of the same two beams connected by a uniformly distributed adjustable elastic layer. Both beams are homogeneous, prismatic and have the same length L, but they could have different mass, flexural rigidity, and boundary conditions. The motion governing equations for transverse vibrations of the double-beam system with the active control (Fig. 4-1(a)), can be derived by Bernoulli-Euler beam theory as follows:

$$e_1 \frac{\partial^4 W_1}{\partial x^4} + K\left(W_1 - W_2\right) + \bar{m}_1 \frac{\partial^2 W_1}{\partial t^2} = f_1\left(x,t\right) - f_c\left(x,t\right) \qquad \text{(4-1a)}$$

$$e_2 \frac{\partial^4 W_2}{\partial x^4} - K\left(W_1 - W_2\right) + \bar{m}_2 \frac{\partial^2 W_2}{\partial t^2} = f_2\left(x,t\right) + f_c\left(x,t\right) \tag{4-1b}$$

And the motion governing equations for transverse vibrations of the double-beam system with the semi-active control (Fig. 4-1(b)) are as follows:

$$e_1 \frac{\partial^4 W_1}{\partial x^4} + \left(K + \Delta K\right)\left(W_1 - W_2\right) + \bar{m}_1 \frac{\partial^2 W_1}{\partial t^2} = f_1\left(x,t\right) \tag{4-2a}$$

$$e_2 \frac{\partial^4 W_2}{\partial x^4} - \left(K + \Delta K\right)\left(W_1 - W_2\right) + \bar{m}_2 \frac{\partial^2 W_2}{\partial t^2} = f_2\left(x,t\right) \tag{4-2b}$$

where $W_i = W_i\left(x,t\right)$ is transverse beam deflections, x, t are the spatial co-ordinate and the time, e_i and $\bar{m}_i$ are the beam flexural rigidity and beam mass per unit length, i=1 or 2 represents upper beam or lower beam, K is the stiffness of the elastic layer, ΔK is the stiffness increase of the adjustable elastic layer, $f_c\left(x,t\right)$ is the active control force produced by the distributed control actuators, and $f_1\left(x,t\right)$, $f_2\left(x,t\right)$ are the exciting force acting on the upper and lower beams, respectively.

The initial conditions in general form are as follows:

$$W_1\left(x,0\right) = W_{10}\left(x\right),\ W_2\left(x,0\right) = W_{20}\left(x\right),\ \dot{W}_1\left(x,0\right) = V_{10}\left(x\right),\ \dot{W}_2\left(x,0\right) = V_{20}\left(x\right) \tag{4-3}$$

Based on the research in Chapter 2 and Chapter 3, it could analyze arbitrary boundary conditions at the ends ($x = 0$, L) of the two beams in here, and some common ones can be listed as follows:

Simply supported: $W_i(0,t) = W_i(L,t) = W_i''(0,t) = W_i''(L,t) = 0$ (4-4a)

Clamped: $W_i(0,t) = W_i(L,t) = W_i'(0,t) = W_i'(L,t) = 0$ (4-4b)

Free: $W_i''(0,t) = W_i''(L,t) = W_i'''(0,t) = W_i'''(L,t) = 0$ (4-4c)

Spring supported: $W_i''(0,t) = W_i''(L,t) = 0$, $E_i I_i W_i'''(0,t) = -KW_i(0,t)$,

$E_i I_i W_i'''(L,t) = KW_i(L,t)$ (4-4d)

where i=1 or 2 represents upper beam or lower beam.

a

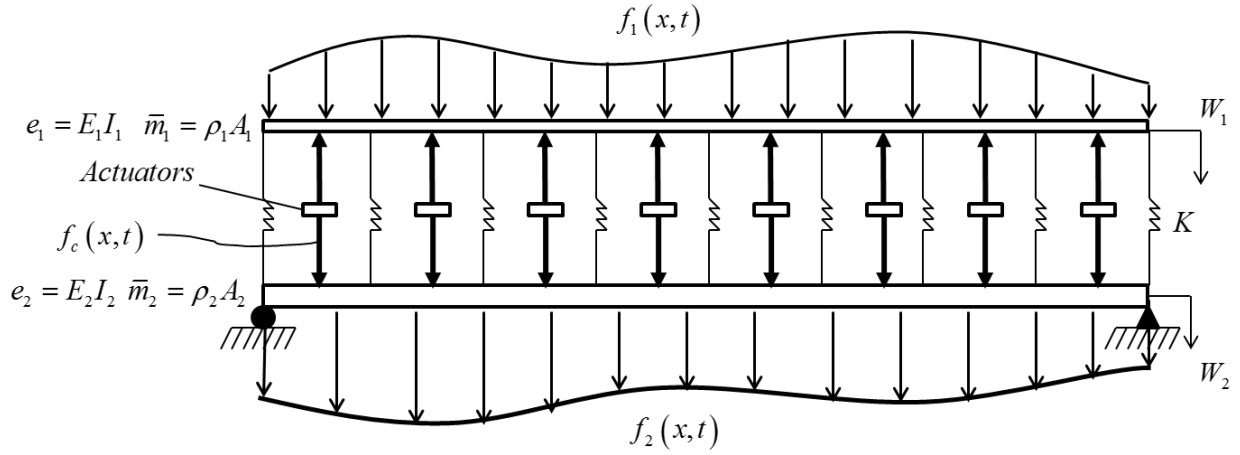

b

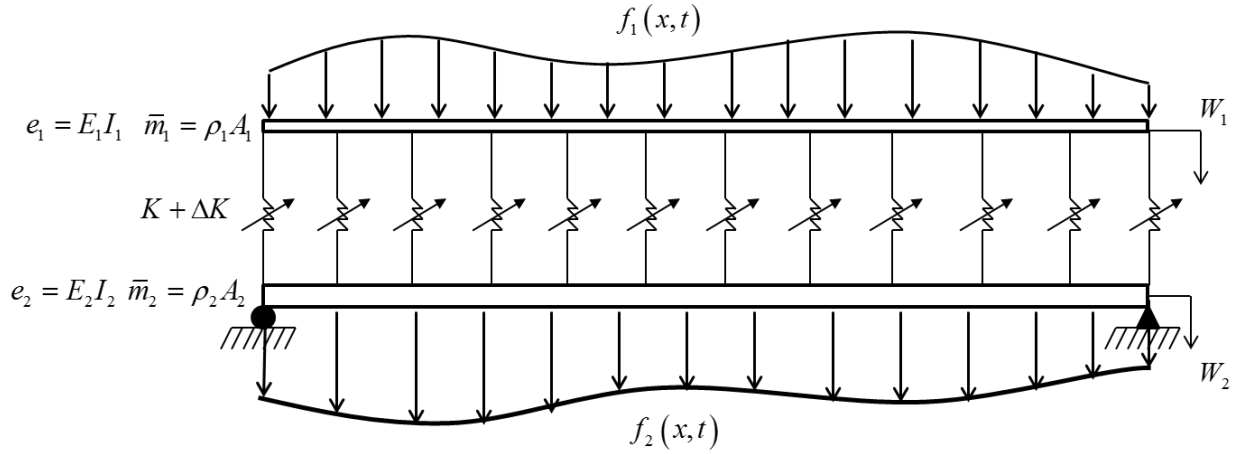

Fig. 4-1. The physical model of a double-beam system: (a) with an active control structure; (b) with a semi-active structure.

4.3 Active Control Algorithm for Actuators in Active Control Structure

In Eq. (4-1), the active control force $f_c(x,t)$ is produced by the actuators in the active control structure, therefore, in order to totally solve and obtain the dynamic responses of the double-beam system with active control structure presented in this chapter, the active control force $f_c(x,t)$ must be determined firstly. As to the active control force, it is the final performance of the active control structure on the whole double-beam system: on one hand, it determines the control effects of the active control structure; on the other hand, it is determined and calculated by the active control algorithm adopted in the active control structure. To the double-beam system with a distributed active control structure discussed in this research, based on abundant advanced control algorithms, a suitable and effective active control algorithm, which synthesizes independent modal space control and linear quadratic regulator, is developed in here.

4.3.1 Independent Modal Space Control Algorithm (IMSC)

Eq. (4-1) are typical linear partial differential equations, in which the method of separation of variables can be applied. Thus, the solutions for Eq. (4-1) could be separable in time and space, and they can be assumed in a form as:

$$W_1(x,t) = \sum_{n=1}^{\infty} T_n(t)\phi_{n1}(x) \tag{4-5a}$$

$$W_2(x,t) = \sum_{n=1}^{\infty} T_n(t)\phi_{n2}(x) \tag{4-5b}$$

where $\phi_{n1}(x)$, $\phi_{n2}(x)$ are mode shape functions of upper beam and lower beam corresponding to *n*th natural frequency, and $T_n(t)$ is time function corresponding to *n*th natural frequency. $\phi_{n1}(x)$ and $\phi_{n2}(x)$ can be determined from a free vibration analysis which is developed in the Chapter 2, and $T_n(t)$ is unknown function which need to be solved.

Substituting the assumed solutions Eq. (4-5) into Eq. (4-1), so they become

$$e_1\sum_{n=1}^{\infty}T_n(t)\frac{d^4\phi_{n1}(x)}{dx^4}+K\sum_{n=1}^{\infty}T_n(t)\left[\phi_{n1}(x)-\phi_{n2}(x)\right]+\bar{m}_1\sum_{n=1}^{\infty}\frac{d^2T_n(t)}{dt^2}\phi_{n1}(x)=f_1(x,t)-f_c(x,t) \tag{4-6a}$$

$$e_2\sum_{n=1}^{\infty}T_n(t)\frac{d^4\phi_{n2}(x)}{dx^4}-K\sum_{n=1}^{\infty}T_n(t)\left[\phi_{n1}(x)-\phi_{n2}(x)\right]+\bar{m}_2\sum_{n=1}^{\infty}\frac{d^2T_n(t)}{dt^2}\phi_{n2}(x)=f_2(x,t)+f_c(x,t) \tag{4-6b}$$

As shown in Chapter 2, if the free vibration of the same double-beam system is considered, the solutions for the free vibration can be written as:

$$W_1^*(x,t)=\sum_{n=1}^{\infty}\left(D_{n1}e^{i\omega_n t}+D_{n2}e^{-i\omega_n t}\right)\phi_{n1}(x) \tag{4-7a}$$

$$W_2^*(x,t)=\sum_{n=1}^{\infty}\left(D_{n1}e^{i\omega_n t}+D_{n2}e^{-i\omega_n t}\right)\phi_{n2}(x) \tag{4-7b}$$

where ω_n is the *n*th natural frequency, $\left(D_{n1}e^{i\omega_n t}+D_{n2}e^{-i\omega_n t}\right)$ is the time function for free vibration corresponding to *n*th natural frequency, and $\phi_{n1}(x)$, $\phi_{n2}(x)$ are the same mode shape functions as the ones in Eq. (4-5).

Substituting Eq. (4-7) into Eq. (4-1) with free vibration conditions $f_1(x,t) = f_2(x,t) = f_c(x,t) = 0$, eliminating the same term $\left(D_{n1}e^{i\omega_n t} + D_{n2}e^{-i\omega_n t}\right)$ and multiplying the $T_n(t)$ in each term, the Eq. (4-1) will be in form of:

$$e_1\sum_{n=1}^{\infty}T_n(t)\frac{d^4\phi_{n1}(x)}{dx^4} + K\sum_{n=1}^{\infty}T_n(t)\left[\phi_{n1}(x)-\phi_{n2}(x)\right] = \bar{m}_1\sum_{n=1}^{\infty}\omega_n^2 T_n(t)\phi_{n1}(x) \tag{4-8a}$$

$$e_2\sum_{n=1}^{\infty}T_n(t)\frac{d^4\phi_{n2}(x)}{dx^4} - K\sum_{n=1}^{\infty}T_n(t)\left[\phi_{n1}(x)-\phi_{n2}(x)\right] = \bar{m}_2\sum_{n=1}^{\infty}\omega_n^2 T_n(t)\phi_{n2}(x) \tag{4-8b}$$

Introducing free vibration equations Eq. (4-8) into them, the motion equations of forced vibration with active control, Eq. (4-6), can be simplified as:

$$\sum_{n=1}^{\infty}\left[\bar{m}_1\phi_{n1}(x)\frac{d^2T_n(t)}{dt^2} + \bar{m}_1\omega_n^2\phi_{n1}(x)T_n(t)\right] = f_1(x,t) - f_c(x,t) \tag{4-9a}$$

$$\sum_{n=1}^{\infty}\left[\bar{m}_2\phi_{n2}(x)\frac{d^2T_n(t)}{dt^2} + \bar{m}_2\omega_n^2\phi_{n2}(x)T_n(t)\right] = f_2(x,t) + f_c(x,t) \tag{4-9b}$$

As derived in Chapter 2, the orthogonality condition for different mode shapes of the double-beam system with elastic layer is:

$$\int_0^L\left[\phi_{n1}(x)\bar{m}_1\phi_{m1}(x) + \phi_{n2}(x)\bar{m}_2\phi_{m2}(x)\right]dx = \bar{M}_n\delta_{mn} \tag{4-10}$$

where $\bar{M}_n$ is the generalized mass in the *n*th mode, and δ_{mn} is the Kronecker delta function.

$Eq.(4-9a)\times\phi_{m1}(x) + Eq.(4-9b)\times\phi_{m2}(x)$, integrate it respect to *x* from 0 to *L*, and apply

orthogonality condition Eq. (4-10), so it will be

$$\frac{d^2T_n(t)}{dt^2}+\omega_n^2T_n(t)=F_n(t)+F_{nc}(t) \tag{4-11a}$$

$$F_n(t)=\frac{\int_0^L\left[\phi_{n1}(x)\,f_1(x,t)+\phi_{n2}(x)\,f_2(x,t)\right]dx}{\int_0^L\left[\phi_{n1}(x)\bar{m}_1\phi_{n1}(x)+\phi_{n2}(x)\bar{m}_2\phi_{n2}(x)\right]dx} \tag{4-11b}$$

$$F_{nc}(t)=\frac{\int_0^L\left\{\left[\phi_{n2}(x)-\phi_{n1}(x)\right]f_c(x,t)\right\}dx}{\int_0^L\left[\phi_{n1}(x)\bar{m}_1\phi_{n1}(x)+\phi_{n2}(x)\bar{m}_2\phi_{n2}(x)\right]dx} \tag{4-11c}$$

Based on the derivations above, the Eq. (4-1), which are the coupling motion equations of double-beam system with an active control structure in the physical space, are transferred as Eq. (4-11), which are the decoupled motion equations of the same structure in modal space. Therefore, the vibration control of the infinite freedom system in physical space is also transferred as the vibration control of several modes in modal space, and this is called Modal Space Control (MSC). Defining the state vector $Z_n(t)=\left[T_n(t)\quad \dot{T}_n(t)\right]^T$, the state-space form of the decoupled equation of motion, Eq. (4-11a), can be written as

$$\dot{Z}_n(t)=J_n\cdot Z_n(t)+K_nF_n(t)+L_nF_{nc}(t) \tag{4-12}$$

where $J_n=\begin{bmatrix}0 & 1\\ -\omega_n^2 & 0\end{bmatrix}$, $K_n=L_n=\begin{Bmatrix}0\\1\end{Bmatrix}$, and $Z_n(t)=\begin{Bmatrix}T_n(t)\\ \dot{T}_n(t)\end{Bmatrix}$.

independent modal space control (IMSC), in which each vibration mode is controlled separately, is just one widely used type of MSC and it is applied in here. According to IMSC and to avoid re-

coupling the double-beam system with an active control structure descried as Eq. (4-12), each *n*th mode shape is controlled by its own control modal force, and the *n*th control modal force which adopts linear state feedback control law can be calculated as

$$F_{nc}(t) = -G_n Z_n(t) = -g_{n1} T_n(t) - g_{n2} \dot{T}_n(t) \tag{4-13}$$

where $G_n = [g_{n1} \quad g_{n2}]$ is feedback gain matrix, g_{n1} is displacement gain, g_{n2} is velocity gain, and all of them are control gains needed to be determined.

By means of the linear quadratic regulator control method, the feedback gain matrix $G_n = [g_{n1} \quad g_{n2}]$ can be determined, therefore, the active control force $F_{nc}(t)$ and $f_c(x,t)$ can be obtained, and the dynamic responses of the double-beam system with an active control structure can be totally calculated eventually.

4.3.2 Linear Quadratic Regulator (LQR)

In fact, the linear quadratic regulator (LQR) control algorithm is an optimal control algorithm: it defines a quadratic performance index $J(t)$, which combines the state vector of the whole system and control command together, as the objective function, and finds the optimal control force by minimizing the objective function $J(t)$ under all specific constrained conditions. According to LQR and the linear differential equations Eq. (4-12) which represent the whole structure system in state-space form, the quadratic performance index $J(t)$ for the active control on double-beam system is as follows

$$J(t)=\int_0^{t_f}\left[Z_n^T(t)QZ_n(t)+F_{nc}^T(t)RF_{nc}(t)\right]=\int_0^{t_f}\left[Z_n^T(t)QZ_n(t)+RF_{nc}^2(t)\right] \quad (4\text{-}14)$$

where $Z_n(t)$ is state vector for the structure model, $F_{nc}(t)$ is active control force, Q is a positive definite or a semi-positive definite weight matrix for state vector, and R is a positive definite weight matrix for control force vector.

The mathematic model for the whole double-beam system optimal control can be denoted as:

Find active control force $F_{nc}(t)$,

to satisfy the objective function $J(t)=\int_0^{t_f}\left[Z_n^T(t)QZ_n(t)+RF_{nc}^2(t)\right]\rightarrow \min$,

with constrained conditions: $\dot{Z}_n(t)=J_n\cdot Z_n(t)+K_nF_n(t)+L_nF_{nc}(t)$ and $Z_n(0)=Z_{n0}$.

The mathematic model is a functional extremum question with constrained conditions. Applying the Lagrange Multiplier Method, Hamiltonian Function and Variation Method, a Riccati matrix equation is finally derived:

$$-PJ_n-J_n^TP+\frac{1}{2}PL_nR^{-1}L_n^TP-Q=0 \quad (4\text{-}15)$$

In this chapter, the weight matrices can be calculated as $Q=\alpha\begin{bmatrix}\omega_n^2 & 0\\ 0 & 1\end{bmatrix}$ and $R=\beta$, in where α and β are positive constants. Due to J_n and L_n are also known, the matrix $P=\begin{bmatrix}P_{11} & P_{12}\\ P_{21} & P_{22}\end{bmatrix}$ can be obtained by solving Riccati matrix equation Eq. (4-15). And then, the active control force $F_{nc}(t)$ is determined as:

$$F_{nc}(t) = -\frac{1}{2}R^{-1}L_n^T P Z_n(t) = -\frac{1}{2}R^{-1}\begin{bmatrix}0 & 1\end{bmatrix}\begin{bmatrix}P_{11} & P_{12}\\ P_{21} & P_{22}\end{bmatrix}\begin{Bmatrix}T_n(t)\\ \dot{T}_n(t)\end{Bmatrix} = -\frac{1}{2}R^{-1}\left[P_{21}T_n(t) + P_{22}\dot{T}_n(t)\right] \quad (4\text{-}16)$$

Comparing Eq. (4-16) with Eq. (4-13), the feedback gain matrix is finally solved by LQR:

$$G_n = \begin{bmatrix}g_{n1} & g_{n2}\end{bmatrix} = \begin{bmatrix}\frac{1}{2}R^{-1}P_{21} & \frac{1}{2}R^{-1}P_{22}\end{bmatrix} \quad (4\text{-}17)$$

By applying an active control algorithm which synthesizes IMSC and LQR, the active control force for each mode shape of the double-beam system, $F_{nc}(t)$, is determined successfully. However, $F_{nc}(t)$ is just a kind of modal control force in the modal space, it cannot be used in the real structure to complete the control work. Therefore, the active control force in physical space, $f_c(x,t)$, should be obtained in next step.

4.3.3 Calculation of Active Control Force in Physical Space

Considering Eq. (4-11c) and Eq. (4-16), the active control force in physical space can be assumed in a form as:

$$f_c(x,t) = \sum_{n=1}^{N}\left\{\bar{G}_{n1}\left[\phi_{n1}(x) - \phi_{n2}(x)\right]T_n(t) + \bar{G}_{n2}\left[\phi_{n1}(x) - \phi_{n2}(x)\right]\dot{T}_n(t)\right\} \quad (4\text{-}18)$$

where $\bar{G}_{n1}$, $\bar{G}_{n2}$ are the control gains for each mode, $\phi_{n1}(x) - \phi_{n2}(x)$ is used to make the $f_c(x,t)$ is related to the responses of both beams , and *N* is total number of modes which are considered to be controlled.

In IMSC, each modal control force can only control that mode and it doesn't affect other modes. Therefore, when substituting Eq. (4-18) into Eq. (4-11c), only $f_{nc}(x,t)=\bar{G}_{n1}\left[\phi_{n1}(x)-\phi_{n2}(x)\right]T_n(t)+\bar{G}_{n2}\left[\phi_{n1}(x)-\phi_{n2}(x)\right]\dot{T}_n(t)$ is used to calculate the *n*th modal control force $F_{nc}(t)$ as:

$$F_{nc}(t)=\frac{\int_0^L\left\{-\left[\phi_{n1}(x)-\phi_{n2}(x)\right]^2\right\}dx}{\int_0^L\left[\phi_{n1}(x)\bar{m}_1\phi_{n1}(x)+\phi_{n2}(x)\bar{m}_2\phi_{n2}(x)\right]dx}\times\left[\bar{G}_{n1}T_n(t)+\bar{G}_{n2}\dot{T}_n(t)\right] \tag{4-19}$$

Comparing Eq. (4-19) with Eq. (4-16), the control gains $\bar{G}_{n1}$ and $\bar{G}_{n2}$ can be calculated by

$$\bar{G}_{n1}=-\frac{1}{2}R^{-1}P_{21}\frac{\int_0^L\left[\phi_{n1}(x)\bar{m}_1\phi_{n1}(x)+\phi_{n2}(x)\bar{m}_2\phi_{n2}(x)\right]dx}{\int_0^L\left\{-\left[\phi_{n1}(x)-\phi_{n2}(x)\right]^2\right\}dx} \tag{4-20a}$$

$$\bar{G}_{n2}=-\frac{1}{2}R^{-1}P_{22}\frac{\int_0^L\left[\phi_{n1}(x)\bar{m}_1\phi_{n1}(x)+\phi_{n2}(x)\bar{m}_2\phi_{n2}(x)\right]dx}{\int_0^L\left\{-\left[\phi_{n1}(x)-\phi_{n2}(x)\right]^2\right\}dx} \tag{4-20b}$$

Until here, control gains $\bar{G}_{n1}$ and $\bar{G}_{n2}$ are solved, and by the assumptions as in Eq. (4-18), the active control force in physical space, $f_c(x,t)$, is determined. Then, it is possible to apply that active control force in the real double-beam system and obtain dynamic responses of it with active control structure which uses that active control algorithm.

4.4 Semi-Active Control Algorithm for Adjustable Elastic Layer in Semi-Active Control Structure

The semi-active vibration control problem of a double-beam system with adjustable elastic layer is described as Eq. (4-2), and the stiffness increase ΔK of the adjustable elastic layer in Eq. (4-2) is controlled and determined by the semi-active control structure and algorithm. Therefore, the semi-active control in here is a kind of active variable stiffness (AVS) system. Based on previous research works, an active control and corresponding active control force is supposed to be set up as an objective, and the semi-active control force is need to be close to that active control force. In this section, the active control and active control force presented in Section 4.3 is chosen as the objective, a semi-active control which makes the semi-active control to be close to that active control and a mode shape filter are developed to calculate ΔK in here.

4.4.1 The Determination of Stiffness Increase in Adjustable Elastic Layer

Based on Eq. (4-2), move the terms, which are related to ΔK, to the right side of the equations, then the Eq. (4-2) can be denoted as

$$e_1 \frac{\partial^4 W_1}{\partial x^4} + K\left(W_1 - W_2\right) + \bar{m}_1 \frac{\partial^2 W_1}{\partial t^2} = f_1\left(x,t\right) - \Delta K\left(W_1 - W_2\right) \tag{4-21a}$$

$$e_2 \frac{\partial^4 W_2}{\partial x^4} - K\left(W_1 - W_2\right) + \bar{m}_2 \frac{\partial^2 W_2}{\partial t^2} = f_2\left(x,t\right) + \Delta K\left(W_1 - W_2\right) \tag{4-21b}$$

As shown in Eq. (4-21), $\Delta K\left(W_1 - W_2\right)$ could be treated as a semi-active control force. Comparing Eq. (4-21) with Eq. (4-1), in order to make the semi-active control being close to the active control, it can assume the semi-active control structure can provide the same control force value as active control structure as follows

$$\Delta K\left(W_1 - W_2\right) = f_c\left(x,t\right) \tag{4-22}$$

Introducing Eq. (4-11c) and substituting Eq. (4-22) into it, it can be transferred as

$$F_{nc}\left(t\right) = \frac{\int_0^L \left\{\left[\phi_{n2}\left(x\right) - \phi_{n1}\left(x\right)\right]\left[W_1\left(x,t\right) - W_2\left(x,t\right)\right]\right\} dx}{\int_0^L \left[\phi_{n1}\left(x\right)\bar{m}_1\phi_{n1}\left(x\right) + \phi_{n2}\left(x\right)\bar{m}_2\phi_{n2}\left(x\right)\right] dx} \times \Delta K \tag{4-23}$$

According to the active control algorithm presented in Section 4.3, the *n*th modal active control force $F_{nc}\left(t\right)$ is determined as Eq. (4-16). Therefore, comparing Eq. (4-23) with Eq. (4-16), the ideal value for the stiffness increase ΔK can be calculated as

$$\Delta K = -\frac{1}{2}R^{-1}\left[P_{21}T_n\left(t\right) + P_{22}\dot{T}_n\left(t\right)\right] \times \frac{\int_0^L \left[\phi_{n1}\left(x\right)\bar{m}_1\phi_{n1}\left(x\right) + \phi_{n2}\left(x\right)\bar{m}_2\phi_{n2}\left(x\right)\right] dx}{\int_0^L \left\{\left[\phi_{n2}\left(x\right) - \phi_{n1}\left(x\right)\right]\left[W_1\left(x,t\right) - W_2\left(x,t\right)\right]\right\} dx} \tag{4-24}$$

Due to the limit of the adjustable elastic layer material, the stiffness increase ΔK cannot reach any value, and there must be a maximum stiffness value $K_{\max}$ and minimum stiffness value $K_{\min}$ for the adjustable elastic layer. Considering about that, the final determination of the stiffness increase ΔK_d can be defined as:

If $\Delta K > K_{\max} - K$, then $\Delta K_d = K_{\max} - K$; (4-25a)

If $\Delta K < K_{\min} - K$, then $\Delta K_d = K_{\min} - K$; (4-25b)

If $K_{\min} - K \le \Delta K \le K_{\max} - K$, then $\Delta K_d = \Delta K$. (4-25c)

where $K_{\max}$ is maximum stiffness value and $K_{\min}$ is minimum stiffness value of the adjustable elastic layer, and ΔK is the calculating stiffness increase value defined as in Eq. (4-24).

Applying Eq. (4-24) and Eq. (4-25), the stiffness increase value ΔK_d is determined and could be adopted by semi-active control structure. But there are two points should be declared in here: First, as shown in Eq. (4-24), ΔK is calculated by one mode of the vibration and it will obtain several different ΔK values based on different modes, therefore, only one main mode will be chosen to be controlled for the semi-active control structure. Second, ΔK_d is supposed to be determined at each time step, therefore, ΔK_d will be changed during the whole vibration process and it should be continually calculated with real time.

4.4.2 The Mode Shape Filter for the Double-Beam System

Checking Eq. (4-24) carefully, in order to calculate the value of ΔK, the parameters R, P_{21}, P_{22}, $\phi_{n1}(x)$, $\phi_{n2}(x)$, $W_1(x,t)$, $W_2(x,t)$, $T_n(t)$ and $\dot{T}_n(t)$ must be known. Among those parameters, R, P_{21} and P_{22} are calculated by Riccati matrix equation Eq. (4-15), $\phi_{n1}(x)$ and $\phi_{n2}(x)$ are obtained by free vibration analysis in Chapter 2, $W_1(x,t)$ and $W_2(x,t)$ are displacement of the two beam detected by the sensors in the structure, therefore, only $T_n(t)$ and

$\dot{T}_n(t)$ should be determined by another method. In this section, a specific mode shape filter for the double-beam system is just introduced to calculate the $T_n(t)$ and $\dot{T}_n(t)$.

As shown in Eq. (4-5), $T_n(t)$ and $\dot{T}_n(t)$ are a kind of generalized coordinates in modal space and they are related to each mode. Therefore, the calculation of them from the detected value of displacement and velocity is just to decompose those from physical space to each mode in modal space and that is why it can be called mode shape filter.

Considering the time is at *t*, the displacement and velocity of both beams are detected by the sensors and are known as $W_1(x,t)$, $W_2(x,t)$, $V_1(x,t)$ and $V_2(x,t)$. According to Eq. (4-5), they can be denoted as

$$W_1(x,t)=\sum_{n=1}^{\infty}T_n(t)\phi_{n1}(x) \tag{4-26a}$$

$$W_2(x,t)=\sum_{n=1}^{\infty}T_n(t)\phi_{n2}(x) \tag{4-26b}$$

$$V_1(x,t)=\sum_{n=1}^{\infty}\dot{T}_n(t)\phi_{n1}(x) \tag{4-26c}$$

$$V_2(x,t)=\sum_{n=1}^{\infty}\dot{T}_n(t)\phi_{n2}(x) \tag{4-26d}$$

$Eq.(4-26a)\times\bar{m}_1\times\phi_{m1}(x)+Eq.(4-26b)\times\bar{m}_2\times\phi_{m2}(x)$, integrate it respect to *x* from 0 to *L*, and apply orthogonality condition Eq. (4-10), the $T_n(t)$ can be derived as

$$T_n(t)=\frac{\int_0^L\left[\phi_{n1}(x)\bar{m}_1W_1(x,t)+\phi_{n2}(x)\bar{m}_2W_2(x,t)\right]dx}{\int_0^L\left[\phi_{n1}(x)\bar{m}_1\phi_{n1}(x)+\phi_{n2}(x)\bar{m}_2\phi_{n2}(x)\right]dx} \tag{4-27}$$

Then, $Eq.(4-26c)\times\bar{m}_1\times\phi_{m1}(x)+Eq.(4-26d)\times\bar{m}_2\times\phi_{m2}(x)$, integrate it respect to *x* from 0 to *L*, and apply orthogonality condition Eq. (4-10), the $\dot{T}_n(t)$ can be derived as

$$\dot{T}_n(t)=\frac{\int_0^L\left[\phi_{n1}(x)\bar{m}_1V_1(x,t)+\phi_{n2}(x)\bar{m}_2V_2(x,t)\right]dx}{\int_0^L\left[\phi_{n1}(x)\bar{m}_1\phi_{n1}(x)+\phi_{n2}(x)\bar{m}_2\phi_{n2}(x)\right]dx} \tag{4-28}$$

Once $\phi_{n1}(x)$ and $\phi_{n2}(x)$ are obtained by free vibration analysis in Chapter 2, and displacement and velocity of the two beam are detected by the sensors in the structure, then, the $T_n(t)$ and $\dot{T}_n(t)$ can be determined by the displacement mode shape filter as Eq. (4-27) and velocity mode shape filter as Eq. (4-28), respectively.

In addition, the mode shape filter for calculating $T_n(t)$ and $\dot{T}_n(t)$ is not only useful in the determination of stiffness increase ΔK as discussing at the beginning of this section, but also is very important for the calculation of the transverse vibration of the whole double-beam system with semi-active control structure, which will be introduced in next section.

4.5 Solution of the Transverse Vibration for Double-Beam System with Vibration Control Structure

Once the active control force or semi-active control parameter is determined by the control algorithm developed in this chapter, the solutions of the transverse vibration for double-beam system with active control structure or semi-active control structure, which is described in Eq. (4-1) or Eq. (4-2), can be solved and the dynamic responses of whole structure system can be obtained.

4.5.1 Solution of the Transverse Vibration for Double-Beam System with Active Control Structure

The active control force is calculated by the active control algorithm as Eq. (4-16), and then, substituting it into Eq. (4-11), the decoupled motion equations of the double-beam system with active control structure will be

$$\frac{d^2T_n(t)}{dt^2}+\frac{1}{2}R^{-1}P_{22}\frac{dT_n(t)}{dt}+\left(\frac{1}{2}R^{-1}P_{21}+\omega_n^2\right)T_n(t)=F_n(t) \tag{4-29a}$$

$$F_n(t)=\frac{\int_0^L\left[\phi_{n1}(x)\,f_1(x,t)+\phi_{n2}(x)\,f_2(x,t)\right]dx}{\int_0^L\left[\phi_{n1}(x)\bar{m}_1\phi_{n1}(x)+\phi_{n2}(x)\bar{m}_2\phi_{n2}(x)\right]dx} \tag{4-29b}$$

Using Duhamel's integral, particular solution of Eq. (4-29a) can be obtained as

$$T_n(t)=\frac{1}{\omega_{nd}}\int_0^t F_n(\tau)e^{-\xi_n\omega_n^*(t-\tau)}\cdot\sin\left[\omega_{nd}(t-\tau)\right]d\tau \tag{4-30}$$

where $\omega_n^* = \sqrt{\omega_n^2 + \frac{1}{2} R^{-1} P_{21}}$, $\xi_n = \frac{1}{4} R^{-1} \frac{P_{22}}{\omega_n^*}$, and $\omega_{nd} = \omega_n^* \sqrt{1-\xi_n^2}$ are the calculation parameters.

$T_n(t)$ is solved by Eq. (4-30), $\phi_{n1}(x)$ and $\phi_{n2}(x)$ are known mode shape functions. By assuming solutions Eq. (4-5), the transverse vibration equations of a double-beam system with active control structure are solved successfully.

4.5.2 Solution of the Transverse Vibration for Double-Beam System with Semi-Active Control Structure

As introduced in Section 4.4, the semi-active control presented in this chapter for the double-beam system is a kind of Active Variable Stiffness (AVS) system, therefore, it requires that the adjustable elastic layer which is under control should be changed with time during the whole vibration process. It leads to three requirements for the vibration calculation of double-beam system with that semi-active control structure:

1. The vibration calculation must be carried out one time step by one time step, because the structure may be different in each time step.

2. In each time step, the analysis of the structure vibration property must be done due to the change of the adjustable elastic layer stiffness.

3. In each time step, the calculation of the forced vibration of double-beam system is generally

same as the method derived in Section 2.4, but the stiffness of the elastic layer must be $K_L + \Delta K$ (K_L is the stiffness value in last time step, and ΔK is calculated by Section 4.4.1 based on the structure and responses from last time step) and the dynamic responses of the two beams in last time step must be applied as the initial condition.

According to the third requirement, the solutions of the forced transverse vibration of double-beam system with semi-active control in time step $T = t_{i-1} \to T = t_i$ can be calculated as follows:

1. Defining the value of elastic layer stiffness as $K_L + \Delta K$ (K_L is the stiffness value in last time step, and ΔK is calculated by Section 4.4.1 based on the structure and responses from last time step) instead of K_L, then, the same derivation works as Eq. (2-31) to Eq. (2-35) are completed.

2. Based on the dynamic responses of two beams in last time step: $W_1(x, t_{i-1})$, $W_2(x, t_{i-1})$, $V_1(x, t_{i-1})$ and $V_2(x, t_{i-1})$, and applying the mode shape filter presented as Eq. (4-27) and Eq. (4-28), the initial condition $T_n(t_{i-1})$ and $\dot{T}_n(t_{i-1})$ can be obtained.

3. Using Duhamel's integral and considering the initial condition $T_n(t_{i-1})$, $\dot{T}_n(t_{i-1})$, particular solution of Eq. (2-35) in time step $T = t_{i-1} \to T = t_i$ ($\Delta t = t_i - t_{i-1}$) can be finally obtained as

$$T_n(t_i) = \frac{\dot{T}_n(t_{i-1})}{\omega_n}\sin(\omega_n \Delta t) + T_n(t_{i-1})\cos(\omega_n \Delta t) + \frac{1}{\omega_n}\int_0^{\Delta t} F_n(\tau)\cdot\sin\left[\omega_n(\Delta t - \tau)\right]d\tau \qquad (4\text{-}31)$$

Based on those three requirements and Eq. (4-31), a calculation method which could be generally expressed in a flowchart form as in Fig. 4-2, is developed in this chapter to solve and obtain the

dynamic responses of the whole double-beam system with semi-active control structure.

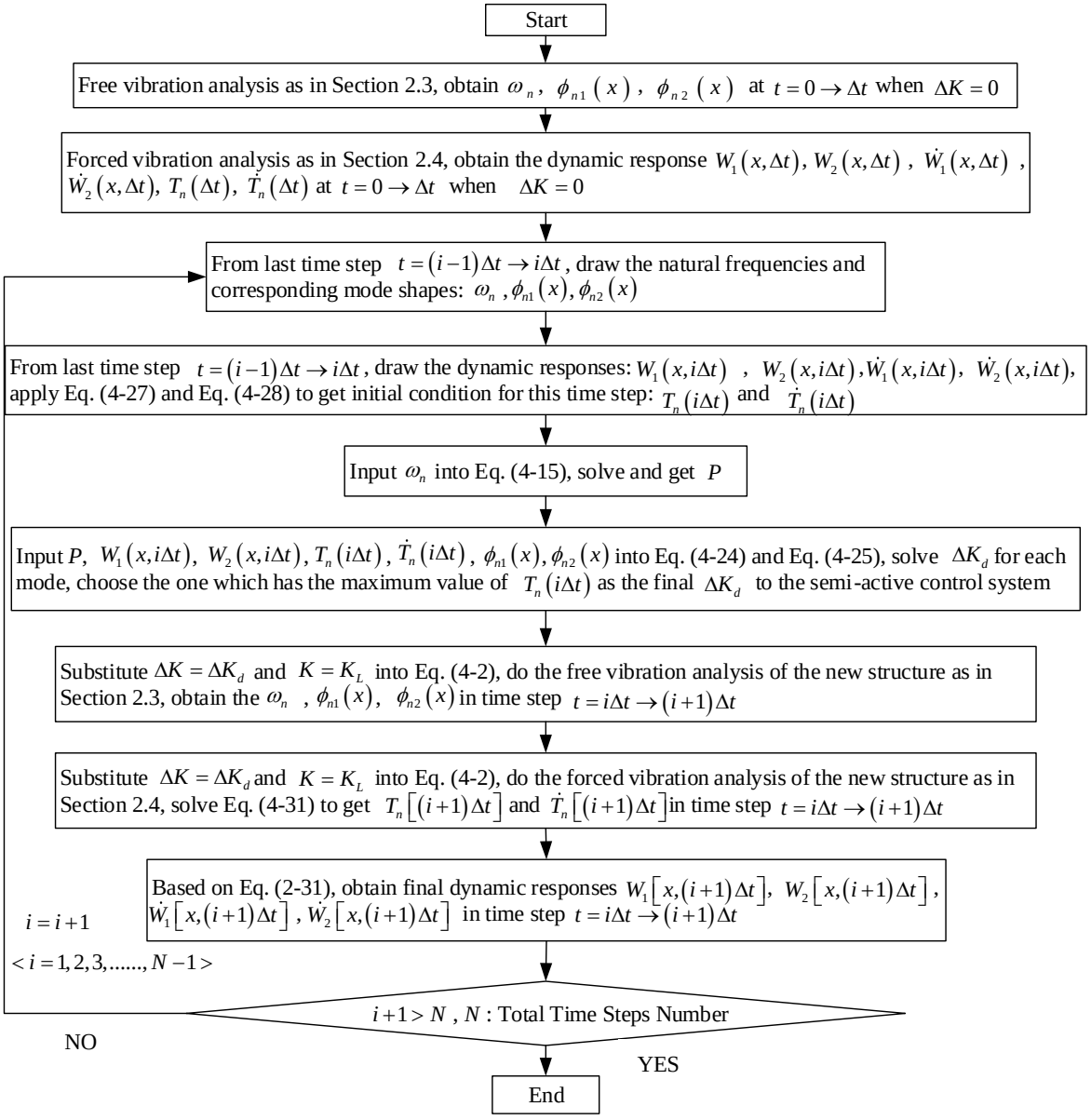

Fig. 4-2. Flowchart of the calculation method to solve and obtain the dynamic responses of double-beam system with semi-active control structure.

Finally, applying the method shown as flowchart in Fig. 4-2 and doing the calculation one time step by one time step until the end, the dynamic responses of whole double-beam system with

semi-active control are solved and obtained successfully.

4.6 Numerical Examples

In order to illustrate the active control structure, semi-active control structure and the corresponding control algorithm presented in this chapter for double-beam system, some numerical examples of uncontrolled, active controlled and semi-active controlled double-beam system are investigated in detail. The values for the parameters of the double-beam system are as follows

$E = 1\times10^{10}\,Nm^{-2}$, $I = 4\times10^{-4}m^4$, $\rho = 2\times10^{3}\,kgm^{-3}$, $A = 5\times10^{-2}m^2$, $e = EI = 4\times10^{6}\,Nm^2$,

$m = \rho A = 1\times10^{2}\,kgm^{-1}$, $L = 10m$, $K = 1\times10^{5}\,Nm^{-2}$, $K_{\max} = 1.4\times10^{5}\,Nm^{-2}$, $K_{\min} = 7\times10^{4}\,Nm^{-2}$

The exciting force of the double-beam system is $f_1(x,t) = f\sin(\omega t)\delta(x-0.5L)$, $f_2(x,t) = 0$, where $f = -10000N$ is amplitude and $\omega = 10Hz$ is frequency of a concentrated harmonic force acted on the midspan of the upper beam, and $\delta(x)$ is Dirac delta function. Three cases are investigated in here for discussion:

Case 1: upper beam spring supported-spring supported and lower beam simply supported-simply supported, $e_1 = e_2 = e$, $m_1 = m_2 = m$;

Case 2: upper beam spring supported-spring supported and lower beam simply supported-simply supported, $e_1 = 0.8e$, $e_2 = e$, $m_1 = 0.2m$, $m_2 = m$;

Case 3: upper beam clamped-clamped and lower beam free-free, $e_1 = e$, $e_2 = 0.8e$, $m_1 = m$, $m_2 = 0.2m$.

The dynamic responses of uncontrolled, active controlled and semi-active controlled double-beam system at the midspan of the two beams are shown in Fig. 4-3 to Fig. 4-5. The active control force which is applied at the midspan of both beams, $f_c(0.5L, t)$, is shown in Fig. 4-6. The variation stiffness *K* of the adjustable elastic layer is shown in Fig. 4-7.

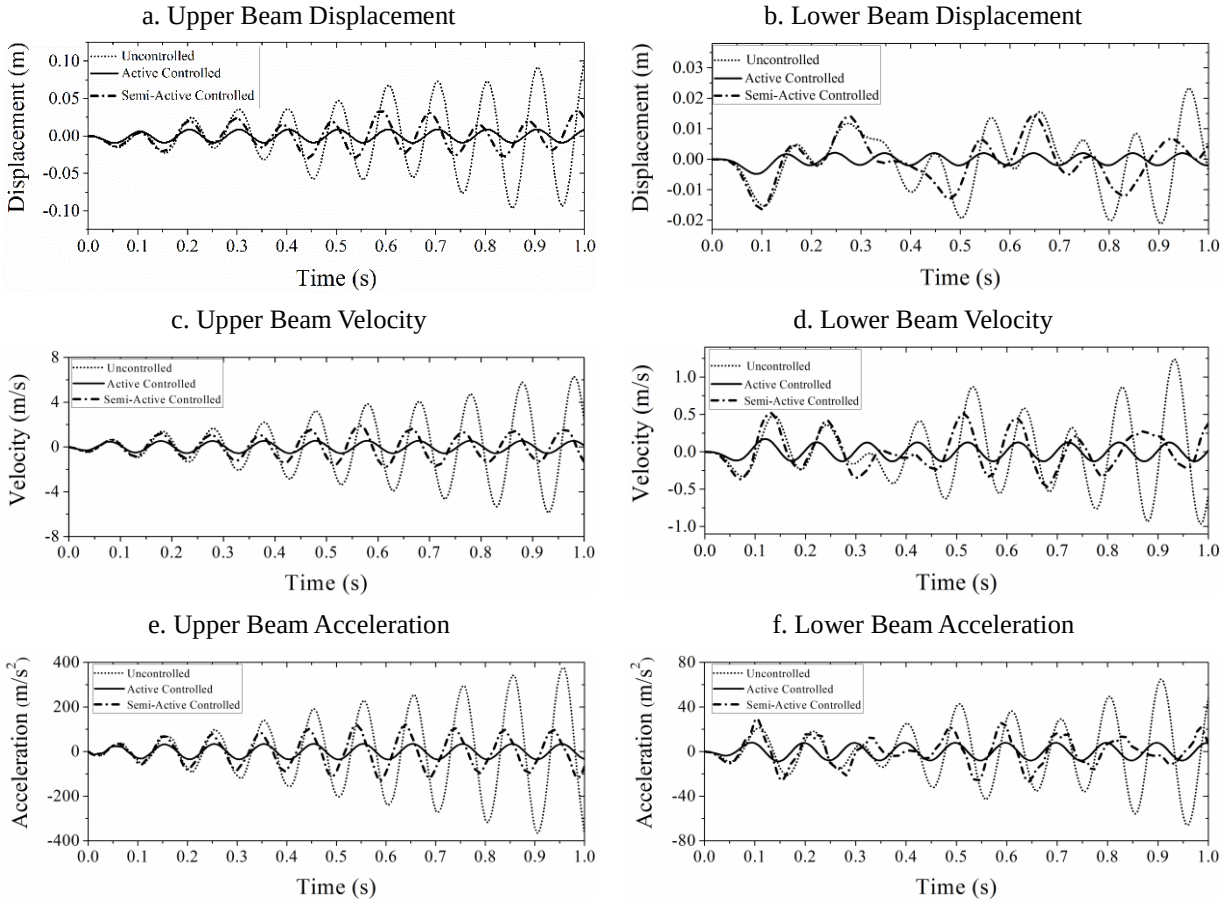

Fig. 4-3. Dynamic responses at midspan point of two beams for Case 1.

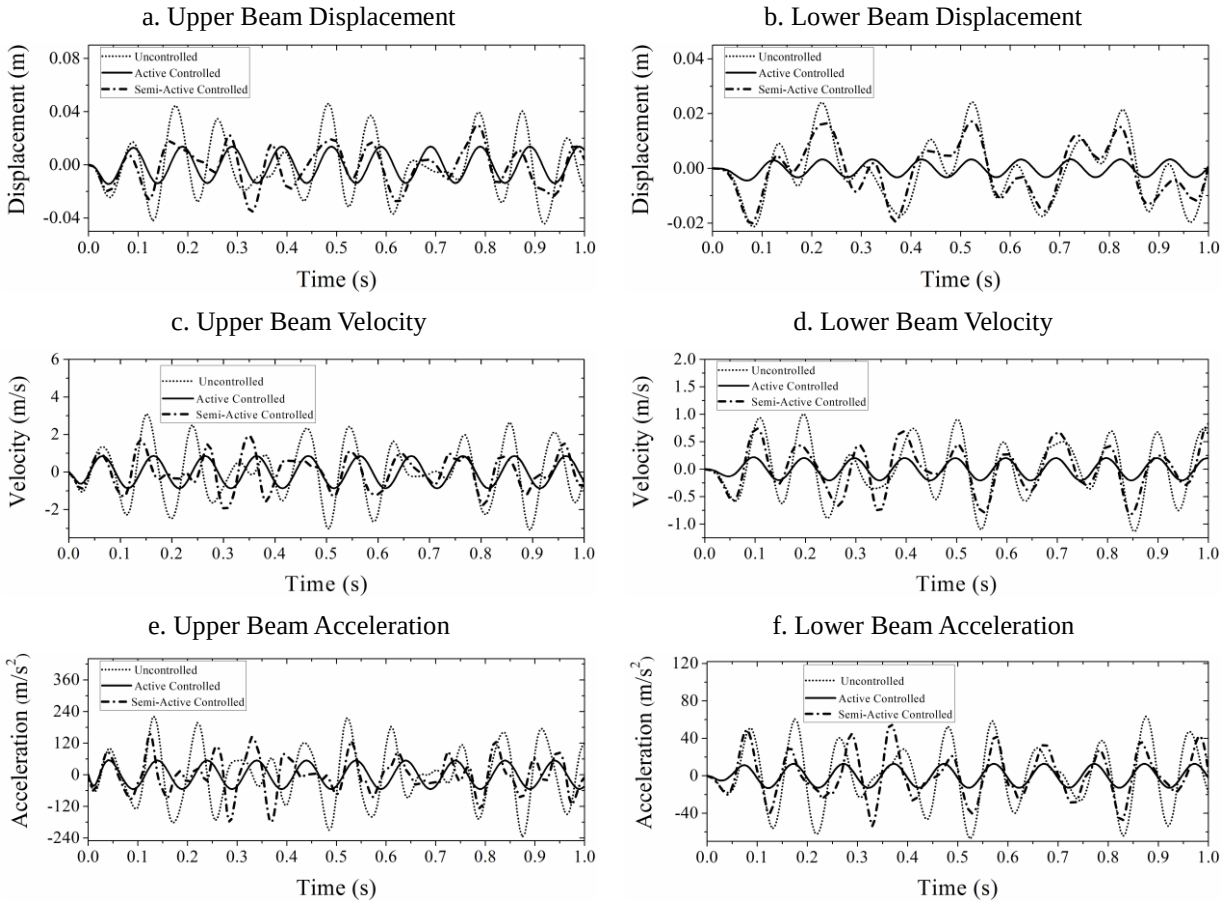

Fig. 4-4. Dynamic responses at midspan point of two beams for Case 2.

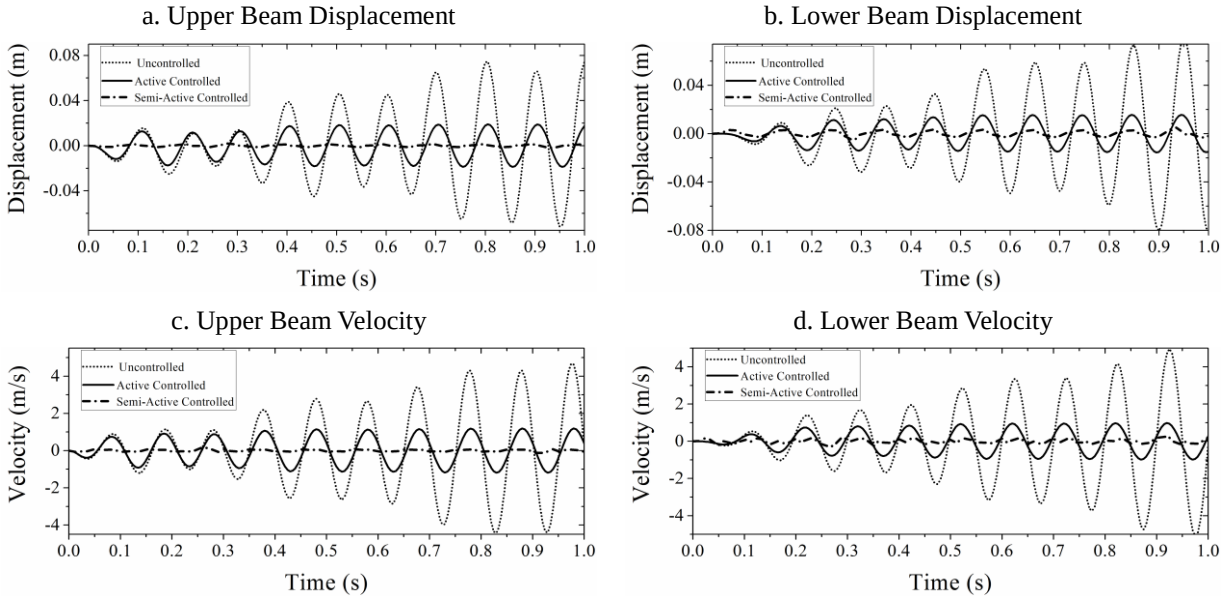

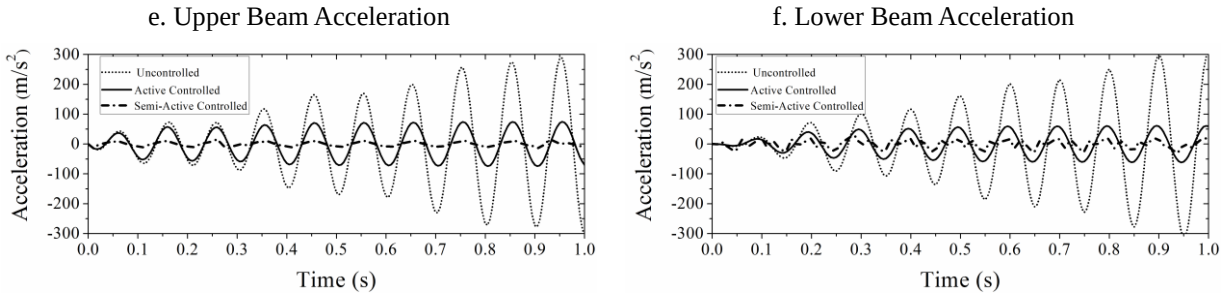

Fig. 4-5. Dynamic responses at midspan point of two beams for Case 3.

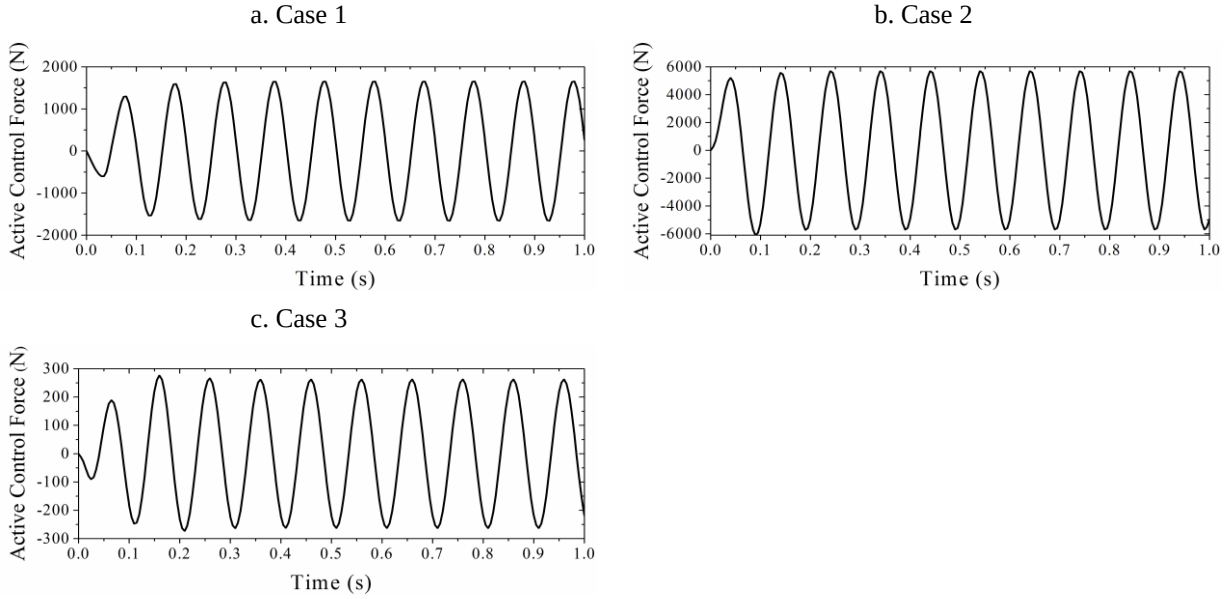

Fig. 4-6. Active control force applied at midspan point of two beams for each case.

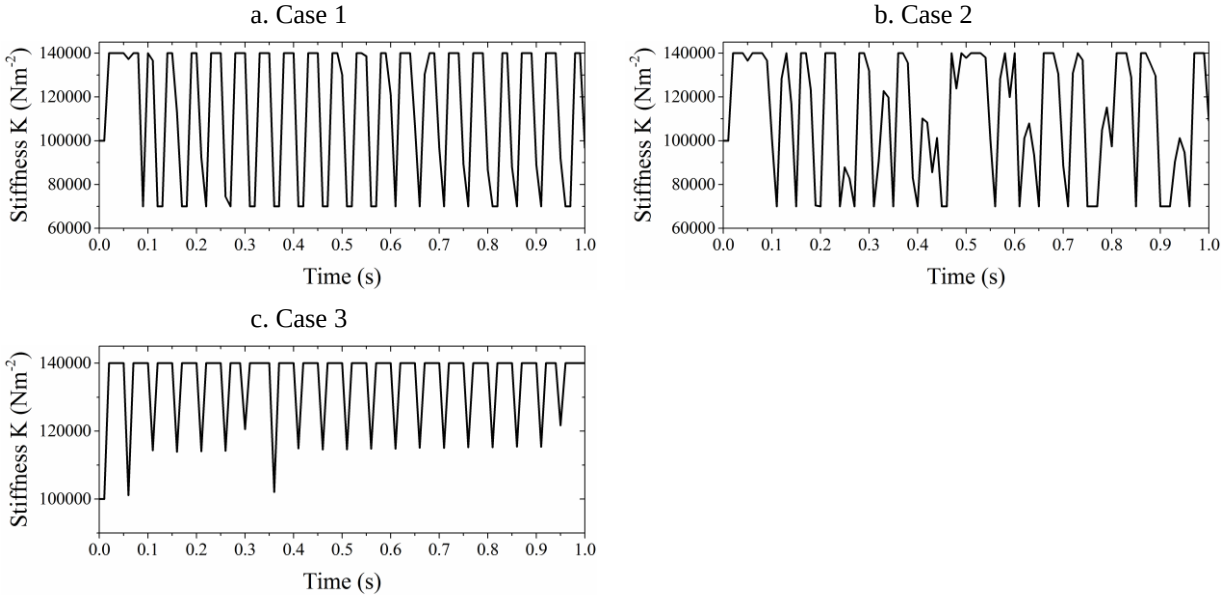

Fig. 4-7. Variation stiffness *K* of the adjustable elastic layer for each case.

As shown in Fig. 4-3 to Fig. 4-5, the active control structure designed for the double-beam system and the corresponding active control algorithm developed in this chapter are effective to suppress the vibrations of both beams, and all the dynamic responses, including displacement, velocity and acceleration, are reduced significantly. Meanwhile, the semi-active control structure and semi-active control algorithm also works well, although it doesn't reduce the dynamic responses of two beams so perfectly as the active control structure in Fig. 4-3 and Fig. 4-4, it also could suppress the vibrations of whole system apparently. Since there are three different boundary conditions in those 3 cases and all the models with them have smaller dynamic responses under the active control or semi-active control, therefore, the active control and semi-active control proposed in this research have the capability to control the double-beam system with arbitrary boundary conditions.

In case 1 (Fig. 4-3), resonance phenomenon is happened in upper beam without active control structure or semi-active control structure, but it is controlled and eliminated when the active control or semi-active control is applied. In case 3 (Fig. 4-5), upper beam and lower beam both meet the resonance conditions and the dynamic responses of them increase gradually, but they are also reduced apparently under the active control or semi-active control. Therefore, the active control and semi-active control proposed in this chapter can effectively avoid the resonance happening in the double-beam system and protect the safety of the whole structure.

From Fig. 4-6, it is shown the value of active control force at midspan of both beams in physical space for 3 cases. Although it is just part of the whole active control force, the existence and presentation of it denote the operability of the proposed active control structure which could control the whole structure by applying that real force and it is very possible for the engineers to apply it in the real engineering practices. Also in Fig. 4-7, the value of variation stiffness *K* of the adjustable elastic layer is shown for all 3 cases, and it is easy to find out that the stiffness *K* has obvious changes under the semi-active control. Comparing with previous classical control algorithms, the change of stiffness K is very close to the ones under switch on – switch off control algorithm, therefore, it proves that the semi-active proposed in this chapter is reasonable and it is practical to apply it in the real structures.

4.7 Conclusions

In this chapter, an active control structure, a semi-active control structure and corresponding control algorithms are proposed to suppress the vibration of the elastically connected double-beam system, which may have arbitrary beam mass, beam flexural rigidity and/or boundary condition. Based on the vibration analysis methods developed in Chapter 2, the calculation methods for double-beam system with that active control and that semi-active control are also developed.

In the active control structure, independent modal space control (IMSC) is applied to decouple the motion equations of double-beam system with the active control, which are coupling partial

differential equations, and transfer them as some decoupled equations in modal space. The vibration control of the infinite freedom system in physical space is also transferred as the vibration control of several modes in modal space by IMSC. linear quadratic regulator is adopted to determine the specific modal active control force for each mode. Then, the active control force in physical space which can be loaded in real structure is obtained by modal active control forces.

In the semi-active control structure, the active control force produced by the active control structure presented above is set up as the objective and the equivalent semi-active control force is assumed to be close to that active force. Based on that principle and with the mode shape filter derived in this chapter, the determination method of stiffness increase is derived.

Various double-beam system with active control structure or semi-active control structure models are calculated to illustrate the efficiency of the proposed active control and semi-active control, and the resonance in the structure is also shown to be avoided by them. Although the semi-active control is not so perfect as the active control, it still can suppress the vibration of the whole double-beam system significantly. Finally, the proposed active control and semi-active control for double-beam system are derived and verified successfully.

Chapter 5 Active and Semi-Active Vibration Control of Double-Beam Systems Interconnected with Viscoelastic Layers

5.1 Introduction

In Chapter 4, the active vibration control for double-beam system interconnected by elastic layer and the semi-active vibration control which changes the stiffness of the elastic layer to reduce the structural vibration, have been derived and introduced specifically. However, as demonstrated in Chapter 3, in real engineering practices, the materials used to connect the upper beam and lower beam in the double-beam system are usually the viscoelastic materials and their damping cannot be ignored. When determining the active control force by the active control algorithm in the double-beam system with viscoelastic layer, the damping effects should be considered. Meanwhile, it will be introduced in the Chapter 7 that the novel adaptive materials applied to complete the semi-active control in this research for vehicle-bridge coupling system of high-speed rail are magnetorheological nanocomposites (MRNs), which are also viscoelastic materials. Under different applied magnetic field, both of their stiffness and damping can be changed and then the structural vibrations could be controlled. In this way, the semi-active control algorithm for MRNs or other adjustable viscoelastic materials cannot just change the stiffness only, but also should change the damping at the same time. In this chapter, based on the research works completed in Chapter 4 and counting the damping of the viscoelastic layer as stated above, the corresponding active control, semi-active control and their control algorithms are introduced and derived to

reduce the dynamic responses of the double-beam system with a viscoelastic layer.

It is totally the same as introduced in Chapter 4, there have been abundant research efforts in the literature about the dynamic behaviors of the double-beam system in recent years. As to the double-beam system with viscoelastic layer in which the damping characteristics must be considered, there are also several important research results (Chen and Sheu 1994, 1995; Li and Hua 2007; Kessel and Raske 1967; Abu 2006; Pavlovic, Kozic and Pavlovic 2012; Vu, Ordonez and Karnopp 2000; Cottle 1990). Meanwhile, great progress in the field of structural vibration control has been achieved over the past few decades as demonstrated specifically in Chapter 4 (Yao 1972; Housner et al. 1997; Soong and Spencer 2002; Soong 1990; Alkhatib and Golnaraghi 2003; Yang, Akbarpour and Ghaemmaghami 1987; Yang, Long and Wong 1988; Yang, Li and Liu 1991; Yang, Li and Liu 1992; Li, Liu, Fang and Tam 2000; Li, Liu, Tang, Zhang and Tam 2004; Soong et al. 1991; Reinhorn et al. 1993; Inman 2001; Meirovitch, Baruh, Montgomery and Williams 1984; Schafer and Holzach 1985; Meirovitch and Silverberg 1983; Meirovitch 1987; Sadek and Esfandiari 1990; Kucuk and Sadek 2005, 2007). However, it is easy to find out that there are very few research papers about the active vibration control or semi-active vibration control on double-beam system with viscoelastic layer and very few scholars or engineers consider to apply an efficient active control structure or semi-active control structure in it.

In this chapter, it proposes an active control structure installed in the viscoelastic layer location of

the double-beam system and a semi-active control structure which adopts the adjustable viscoelastic layer to control the vibration and reduce the dynamic responses of whole system. The double-beam system with an viscoelastic layer is considered in this chapter, and the active control structure is a distributed control structure with many actuators along the viscoelastic layer which can affect both of beams at same time. By synthesizing independent modal space control (IMSC) and linear quadratic regulator (LQR), an active control algorithm is developed for the proposed active control structure. IMSC is used to transfer the coupling motion equations of system in physical space into the decoupled equations in modal space, and the vibration control is also transferred to modal control on each mode. The modal active control force in each mode is determined by LQR, and the final active control force in physical space is finally calculated based on those modal active forces. The semi-active control structure adopts the adjustable viscoelastic layer between two beams and the dynamic mechanical model of that adjustable viscoelastic material is assumed as the linear model based on the experiments results from previous research works. The active control force produced by the active control structure is set up as the objective and the equivalent semi-active control force is assumed to be close to that active force. Based on that principle and with the mode shape filter derived in this chapter, the stiffness increase and the damping increase of the adjustable viscoelastic layer which are used to realize the semi-active control are determined. Various models of uncontrolled, active controlled and semi-active controlled double-beam system, which have a concentrated harmonic force in the midspan of upper beam, are calculated and presented to illustrate the efficiency of the proposed active control and

semi-active control.

5.2 Formulation of the Vibration Control Problem

As shown in Fig. 5-1(a), in this chapter, the physical model of a double-beam system with an active control structure includes an upper beam and a lower beam connected by a uniformly distributed-connecting viscoelastic layer, and is actively controlled by a distributed control structure with many actuators along the viscoelastic layer. Another physical model (as shown in Fig. 5-1(b)) of a double-beam system with a semi-active control structure consists of the same two beams joined by a uniformly distributed adjustable viscoelastic layer. Both beams are homogeneous, prismatic and have the same length L, but they could have different mass, flexural rigidity, and boundary conditions. The motion governing equations for transverse vibrations of the double-beam system with the active control (Fig. 5-1(a)), can be derived by Bernoulli-Euler beam theory as follows:

$$e_1 \frac{\partial^4 W_1}{\partial x^4} + K\left(W_1 - W_2\right) + C\left(\frac{\partial W_1}{\partial t} - \frac{\partial W_2}{\partial t}\right) + \bar{m}_1 \frac{\partial^2 W_1}{\partial t^2} = f_1\left(x,t\right) - f_c\left(x,t\right) \tag{5-1a}$$

$$e_2 \frac{\partial^4 W_2}{\partial x^4} - K\left(W_1 - W_2\right) - C\left(\frac{\partial W_1}{\partial t} - \frac{\partial W_2}{\partial t}\right) + \bar{m}_2 \frac{\partial^2 W_2}{\partial t^2} = f_2\left(x,t\right) + f_c\left(x,t\right) \tag{5-1b}$$

And the motion governing equations for transverse vibrations of the double-beam system with the semi-active control (Fig. 5-1(b)) are as follows:

$$e_1 \frac{\partial^4 W_1}{\partial x^4} + \left(K + \Delta K\right)\left(W_1 - W_2\right) + \left(C + \Delta C\right)\left(\frac{\partial W_1}{\partial t} - \frac{\partial W_2}{\partial t}\right) + \bar{m}_1 \frac{\partial^2 W_1}{\partial t^2} = f_1\left(x,t\right) \tag{5-2a}$$

$$e_2 \frac{\partial^4 W_2}{\partial x^4} - (K + \Delta K)(W_1 - W_2) - (C + \Delta C)\left(\frac{\partial W_1}{\partial t} - \frac{\partial W_2}{\partial t}\right) + \bar{m}_2 \frac{\partial^2 W_2}{\partial t^2} = f_2(x,t) \quad (5\text{-}2b)$$

where $W_i = W_i(x,t)$ is transverse beam deflections, x, t are the spatial co-ordinate and the time, e_i and $\bar{m}_i$ are the beam flexural rigidity and beam mass per unit length, i=1 or 2 represents upper beam or lower beam, *K* and *C* are the stiffness and damping coefficients of the viscoelastic layer, ΔK and ΔC are the stiffness increase and damping increase of the adjustable viscoelastic layer, $f_c(x,t)$ is the active control force produced by the distributed control actuators, and $f_1(x,t)$, $f_2(x,t)$ are the exciting force acting on the upper and lower beams, respectively.

The initial conditions in general form are as follows:

$$W_1(x,0) = W_{10}(x),\ W_2(x,0) = W_{20}(x),\ \dot{W}_1(x,0) = V_{10}(x),\ \dot{W}_2(x,0) = V_{20}(x) \quad (5\text{-}3)$$

Based on the research in Chapter 2 and Chapter 3, it could analyze arbitrary boundary conditions at the ends ($x = 0$, *L*) of the two beams in here, and some common ones can be listed as follows:

Simply supported: $W_i(0,t) = W_i(L,t) = W_i''(0,t) = W_i''(L,t) = 0 \quad (5\text{-}4a)$

Clamped: $W_i(0,t) = W_i(L,t) = W_i'(0,t) = W_i'(L,t) = 0 \quad (5\text{-}4b)$

Free: $W_i''(0,t) = W_i''(L,t) = W_i'''(0,t) = W_i'''(L,t) = 0 \quad (5\text{-}4c)$

Spring supported: $W_i''(0,t) = W_i''(L,t) = 0$, $E_i I_i W_i'''(0,t) = -K W_i(0,t)$,

$E_i I_i W_i'''(L,t) = K W_i(L,t) \quad (5\text{-}4d)$

where i=1 or 2 represents upper beam or lower beam.

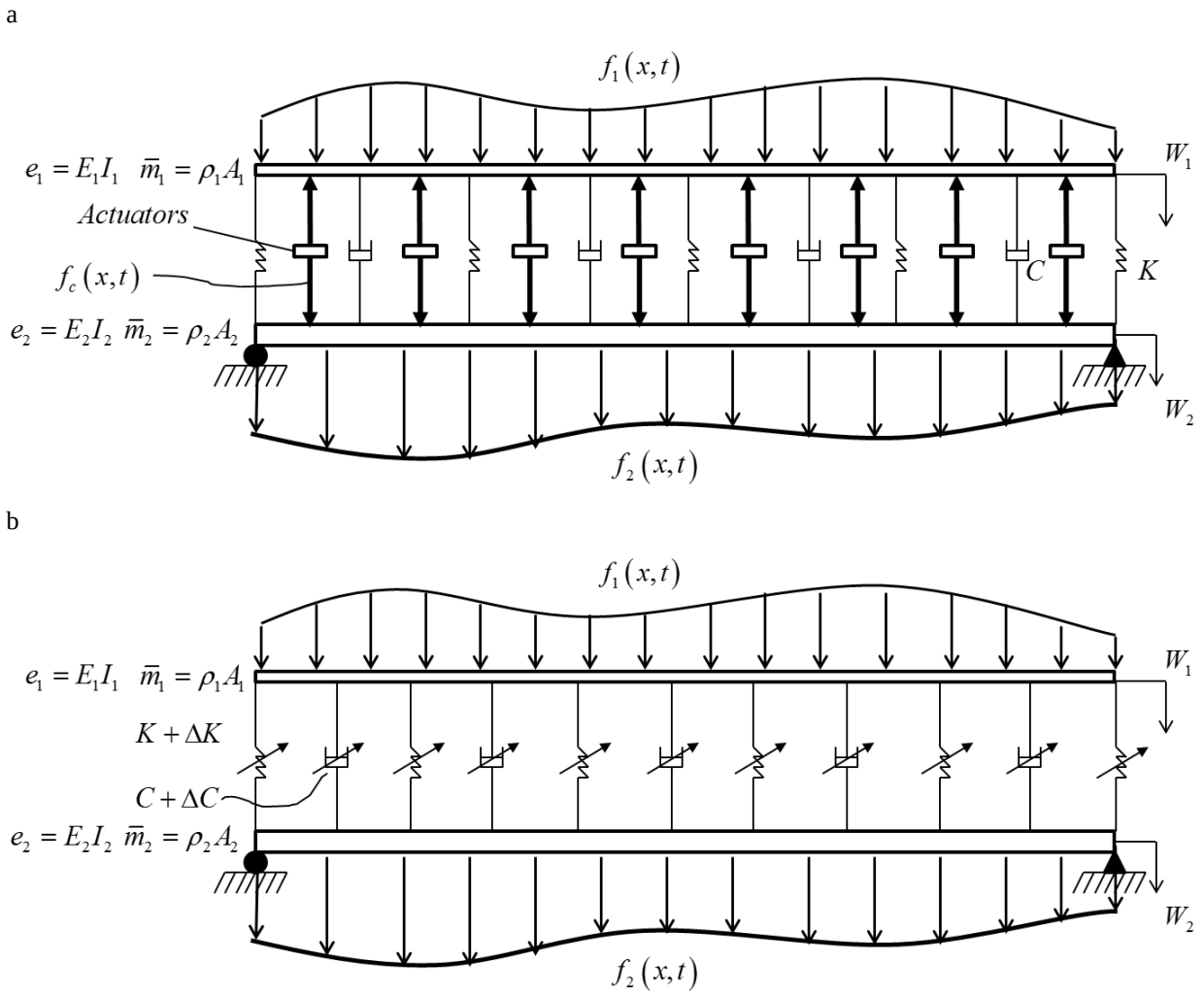

Fig. 5-1. The physical model of a double-beam system: (a) with an active control structure; (b) with a semi-active structure.

5.3 Active Control Algorithm for Actuators in Active Control Structure

It is similar to the discussion about the active control algorithm in Section 4.3, although the double-beam system under a distributed active control structure in this chapter is with viscoelastic layer instead of elastic layer, a similar active control algorithm which also synthesizes independent modal space control and linear quadratic regulator is developed in here.

5.3.1 Independent Modal Space Control Algorithm (IMSC)

The solutions for Eq. (5-1) could be separable in time and space, and can be assumed in a form as:

$$W_1(x,t)=\sum_{n=1}^{\infty}T_n(t)\phi_{n1}(x) \tag{5-5a}$$

$$W_2(x,t)=\sum_{n=1}^{\infty}T_n(t)\phi_{n2}(x) \tag{5-5b}$$

where $\phi_{n1}(x)$, $\phi_{n2}(x)$ are mode shape functions of upper beam and lower beam corresponding to *n*th natural frequency, and $T_n(t)$ is time function corresponding to *n*th natural frequency. It must be noticed that the $\phi_{n1}(x)$ and $\phi_{n2}(x)$ are determined from a free vibration analysis developed in the Chapter 2 which is about the double-beam system with elastic layer instead of viscoelastic layer in Chapter 3, but the elastic layer has same stiffness *K* value as the viscoelastic layer discussed in here. $T_n(t)$ is unknown function which need to be solved.

Substituting the assumed solutions Eq. (5-5) into Eq. (5-1), so they become

$$\begin{aligned}&e_1\sum_{n=1}^{\infty}T_n(t)\frac{d^4\phi_{n1}(x)}{dx^4}+K\sum_{n=1}^{\infty}T_n(t)\left[\phi_{n1}(x)-\phi_{n2}(x)\right]+C\sum_{n=1}^{\infty}\frac{dT_n(t)}{dt}\left[\phi_{n1}(x)-\phi_{n2}(x)\right]\\&+\bar{m}_1\sum_{n=1}^{\infty}\frac{d^2T_n(t)}{dt^2}\phi_{n1}(x)=f_1(x,t)-f_c(x,t)\end{aligned} \tag{5-6a}$$

$$\begin{aligned}&e_2\sum_{n=1}^{\infty}T_n(t)\frac{d^4\phi_{n2}(x)}{dx^4}-K\sum_{n=1}^{\infty}T_n(t)\left[\phi_{n1}(x)-\phi_{n2}(x)\right]-C\sum_{n=1}^{\infty}\frac{dT_n(t)}{dt}\left[\phi_{n1}(x)-\phi_{n2}(x)\right]\\&+\bar{m}_2\sum_{n=1}^{\infty}\frac{d^2T_n(t)}{dt^2}\phi_{n2}(x)=f_2(x,t)+f_c(x,t)\end{aligned} \tag{5-6b}$$

Still considering the free vibration of the double-beam system with elastic layer having same stiffness *K* value as the viscoelastic layer discussed in this chapter, and as shown in Chapter 3 and Eq. (3-29), the solutions for the free vibration can be written as:

$$W_1^*(x,t)=\sum_{n=1}^{\infty}\left(D_{n1}e^{i\omega_{n,Undamped}t}+D_{n2}e^{-i\omega_{n,Undamped}t}\right)\phi_{n1}(x) \tag{5-7a}$$

$$W_2^*(x,t)=\sum_{n=1}^{\infty}\left(D_{n1}e^{i\omega_{n,Undamped}t}+D_{n2}e^{-i\omega_{n,Undamped}t}\right)\phi_{n2}(x) \tag{5-7b}$$

where $\omega_{n,Undamped}$ is the *n*th natural frequency of the double-beam system with elastic layer defined above, $\left(D_{n1}e^{i\omega_{n,Undamped}t}+D_{n2}e^{-i\omega_{n,Undamped}t}\right)$ is the time function for free vibration corresponding to *n*th natural frequency, and $\phi_{n1}(x)$, $\phi_{n2}(x)$ are same mode shape functions as the ones in Eq. (5-5).

Substituting Eq. (5-7) into Eq. (5-1) with free vibration conditions $f_1(x,t)=f_2(x,t)=f_c(x,t)=0$, eliminating the same term $\left(D_{n1}e^{i\omega_{n,Undamped}t}+D_{n2}e^{-i\omega_{n,Undamped}t}\right)$ and multiplying the $T_n(t)$ in each term, the Eq. (5-1) will be in form of:

$$e_1\sum_{n=1}^{\infty}T_n(t)\frac{d^4\phi_{n1}(x)}{dx^4}+K\sum_{n=1}^{\infty}T_n(t)\left[\phi_{n1}(x)-\phi_{n2}(x)\right]=\bar{m}_1\sum_{n=1}^{\infty}\omega_{n,Undamped}^2T_n(t)\phi_{n1}(x) \tag{5-8a}$$

$$e_2\sum_{n=1}^{\infty}T_n(t)\frac{d^4\phi_{n2}(x)}{dx^4}-K\sum_{n=1}^{\infty}T_n(t)\left[\phi_{n1}(x)-\phi_{n2}(x)\right]=\bar{m}_2\sum_{n=1}^{\infty}\omega_{n,Undamped}^2T_n(t)\phi_{n2}(x) \tag{5-8b}$$

Introducing free vibration equations Eq. (5-8) into them, the motion equations of forced vibration with active control, Eq. (5-6), can be simplified as:

$$\sum_{n=1}^{\infty}\left[\bar{m}_1\phi_{n1}(x)\frac{d^2T_n(t)}{dt^2}+\bar{m}_1\omega_{n,Undamped}^2\phi_{n1}(x)T_n(t)\right]=f_1(x,t)-f_c(x,t)-C\left(\frac{\partial W_1}{\partial t}-\frac{\partial W_2}{\partial t}\right) \quad (5\text{-}9a)$$

$$\sum_{n=1}^{\infty}\left[\bar{m}_2\phi_{n2}(x)\frac{d^2T_n(t)}{dt^2}+\bar{m}_2\omega_{n,Undamped}^2\phi_{n2}(x)T_n(t)\right]=f_2(x,t)+f_c(x,t)+C\left(\frac{\partial W_1}{\partial t}-\frac{\partial W_2}{\partial t}\right) \quad (5\text{-}9b)$$

As derived in Chapter 2, the orthogonality condition for different mode shapes of the double-beam system with elastic layer is:

$$\int_0^L\left[\phi_{n1}(x)\bar{m}_1\phi_{m1}(x)+\phi_{n2}(x)\bar{m}_2\phi_{m2}(x)\right]dx=\bar{M}_n\delta_{mn} \quad (5\text{-}10)$$

where $\bar{M}_n$ is the generalized mass in the *n*th mode, and δ_{mn} is the Kronecker delta function.

$Eq.(5-9a)\times\phi_{m1}(x)+Eq.(5-9b)\times\phi_{m2}(x)$, integrate it respect to *x* from 0 to *L*, and apply orthogonality condition Eq. (5-10), so it will be

$$\frac{d^2T_n(t)}{dt^2}+\omega_{n,Undamped}^2T_n(t)=F_n(t)+F_{nc}(t)+F_{nD}(t) \quad (5\text{-}11a)$$

$$F_n(t)=\frac{\int_0^L\left[\phi_{n1}(x)\,f_1(x,t)+\phi_{n2}(x)\,f_2(x,t)\right]dx}{\int_0^L\left[\phi_{n1}(x)\bar{m}_1\phi_{n1}(x)+\phi_{n2}(x)\bar{m}_2\phi_{n2}(x)\right]dx} \quad (5\text{-}11b)$$

$$F_{nc}(t)=\frac{\int_0^L\left\{\left[\phi_{n2}(x)-\phi_{n1}(x)\right]f_c(x,t)\right\}dx}{\int_0^L\left[\phi_{n1}(x)\bar{m}_1\phi_{n1}(x)+\phi_{n2}(x)\bar{m}_2\phi_{n2}(x)\right]dx} \quad (5\text{-}11c)$$

$$F_{nD}(t)=\frac{\int_0^L\left\{\left[\phi_{n2}(x)-\phi_{n1}(x)\right]\left[C\left(\frac{\partial W_1}{\partial t}-\frac{\partial W_2}{\partial t}\right)\right]\right\}dx}{\int_0^L\left[\phi_{n1}(x)\bar{m}_1\phi_{n1}(x)+\phi_{n2}(x)\bar{m}_2\phi_{n2}(x)\right]dx} \quad (5\text{-}11d)$$

Based on the derivations above, the Eq. (5-1), which are the coupling motion equations of double-

beam system with an active control structure in the physical space, are transferred as Eq. (5-11), which are the decoupled motion equations of the same structure in modal space. Therefore, the vibration control of the infinite freedom system in physical space is also transferred as the vibration control of several modes in modal space, and this is called Modal Space Control (MSC). Defining the state vector $Z_n(t)=\left[T_n(t) \quad \dot{T}_n(t)\right]^T$, the state-space form of the decoupled equation of motion, Eq. (5-11a), can be written as

$$\dot{Z}_n(t)=J_n\cdot Z_n(t)+K_n\left[F_n(t)+F_{nD}(t)\right]+L_nF_{nc}(t) \tag{5-12}$$

where $J_n=\begin{bmatrix}0 & 1\\ -\omega_n^2 & 0\end{bmatrix}$, $K_n=L_n=\begin{Bmatrix}0\\1\end{Bmatrix}$, and $Z_n(t)=\begin{Bmatrix}T_n(t)\\ \dot{T}_n(t)\end{Bmatrix}$.

It is like in Section 4.3.1, independent modal space control (IMSC), in which each vibration mode is controlled separately, is applied in here. According to IMSC and to avoid re-coupling the double-beam system with an active control structure descried as Eq. (5-12), each *n*th mode shape is controlled by its own control modal force, and the *n*th control modal force which adopts linear state feedback control law can be calculated as

$$F_{nc}(t)=-G_nZ_n(t)=-g_{n1}T_n(t)-g_{n2}\dot{T}_n(t) \tag{5-13}$$

where $G_n=\left[g_{n1} \quad g_{n2}\right]$ is feedback gain matrix, g_{n1} is displacement gain, g_{n2} is velocity gain, and all of them are control gains needed to be determined.

By means of the linear quadratic regulator control method, the feedback gain matrix

$G_n = [g_{n1} \quad g_{n2}]$ can be determined, therefore, the active control force $F_{nc}(t)$ and $f_c(x,t)$ can be obtained, and the dynamic responses of the double-beam system with an active control structure can be totally calculated eventually.

5.3.2 Linear Quadratic Regulator (LQR)

It is similar to the derivation works in Section 4.3.2, according to LQR and the linear differential equations Eq. (5-12) which represent the whole structure system in state-space form, the quadratic performance index $J(t)$ for the active control on double-beam system is as follows

$$J(t) = \int_0^{t_f} \left[Z_n^T(t) Q Z_n(t) + F_{nc}^T(t) R F_{nc}(t) \right] = \int_0^{t_f} \left[Z_n^T(t) Q Z_n(t) + R F_{nc}^2(t) \right] \tag{5-14}$$

where $Z_n(t)$ is state vector for the structure model, $F_{nc}(t)$ is active control force, Q is a positive definite or a semi-positive definite weight matrix for state vector, and R is a positive definite weight matrix for control force vector.

The mathematic model for the whole double-beam system optimal control can be denoted as:

Find active control force $F_{nc}(t)$,

to satisfy the objective function $J(t) = \int_0^{t_f} \left[Z_n^T(t) Q Z_n(t) + R F_{nc}^2(t) \right] \rightarrow \min$,

with constrained conditions: $\dot{Z}_n(t) = J_n \cdot Z_n(t) + K_n \left[F_n(t) + F_{nD}(t) \right] + L_n F_{nc}(t)$ and $Z_n(0) = Z_{n0}$.

The mathematic model is a functional extremum question with constrained conditions. Applying the Lagrange multiplier method, Hamiltonian function and variation method, a Riccati matrix

equation is finally derived:

$$-PJ_n - J_n^T P + \frac{1}{2} PL_n R^{-1} L_n^T P - Q = 0 \tag{5-15}$$

In this chapter, the weight matrices can be calculated as $Q = \alpha \begin{bmatrix} \omega_n^2 & 0 \\ 0 & 1 \end{bmatrix}$ and $R = \beta$, in where α and β are positive constants. Due to J_n and L_n are also known, the matrix $P = \begin{bmatrix} P_{11} & P_{12} \\ P_{21} & P_{22} \end{bmatrix}$ can be obtained by solving Riccati matrix equation Eq. (5-15). And then, the active control force $F_{nc}(t)$ is determined as:

$$F_{nc}(t) = -\frac{1}{2} R^{-1} L_n^T P Z_n(t) = -\frac{1}{2} R^{-1} \begin{bmatrix} 0 & 1 \end{bmatrix} \begin{bmatrix} P_{11} & P_{12} \\ P_{21} & P_{22} \end{bmatrix} \begin{Bmatrix} T_n(t) \\ \dot{T}_n(t) \end{Bmatrix} = -\frac{1}{2} R^{-1} \left[P_{21} T_n(t) + P_{22} \dot{T}_n(t) \right] \tag{5-16}$$

Comparing Eq. (5-16) with Eq. (5-13), the feedback gain matrix is finally solved by LQR:

$$G_n = \begin{bmatrix} g_{n1} & g_{n2} \end{bmatrix} = \begin{bmatrix} \frac{1}{2} R^{-1} P_{21} & \frac{1}{2} R^{-1} P_{22} \end{bmatrix} \tag{5-17}$$

By applying an active control algorithm which synthesizes IMSC and LQR, the active control force for each mode shape of the double-beam system, $F_{nc}(t)$, is determined successfully. However, $F_{nc}(t)$ is just a kind of modal control force in the modal space, it cannot be used in the real structure to complete the control work. Therefore, the active control force in physical space, $f_c(x,t)$, should be obtained in next step.

5.3.3 Calculation of Active Control Force in Physical Space

Considering Eq. (5-11c) and Eq. (5-16), the active control force in physical space can be assumed in a form as:

$$f_c(x,t)=\sum_{n=1}^{N}\left\{\bar{G}_{n1}\left[\phi_{n1}(x)-\phi_{n2}(x)\right]T_n(t)+\bar{G}_{n2}\left[\phi_{n1}(x)-\phi_{n2}(x)\right]\dot{T}_n(t)\right\} \tag{5-18}$$

where $\bar{G}_{n1}$, $\bar{G}_{n2}$ are the control gains for each mode, $\phi_{n1}(x)-\phi_{n2}(x)$ is used to make the $f_c(x,t)$ is related to the responses of both beams , and *N* is total number of modes which are considered to be controlled.

In IMSC, each modal control force can only control that mode and it doesn't affect other modes. Therefore, when substituting Eq. (5-18) into Eq. (5-11c), only $f_{nc}(x,t)=\bar{G}_{n1}\left[\phi_{n1}(x)-\phi_{n2}(x)\right]T_n(t)+\bar{G}_{n2}\left[\phi_{n1}(x)-\phi_{n2}(x)\right]\dot{T}_n(t)$ is used to calculate the *n*th modal control force $F_{nc}(t)$ as:

$$F_{nc}(t)=\frac{\int_0^L\left\{-\left[\phi_{n1}(x)-\phi_{n2}(x)\right]^2\right\}dx}{\int_0^L\left[\phi_{n1}(x)\bar{m}_1\phi_{n1}(x)+\phi_{n2}(x)\bar{m}_2\phi_{n2}(x)\right]dx}\times\left[\bar{G}_{n1}T_n(t)+\bar{G}_{n2}\dot{T}_n(t)\right] \tag{5-19}$$

Comparing Eq. (5-19) with Eq. (5-16), the control gains $\bar{G}_{n1}$ and $\bar{G}_{n2}$ can be calculated by

$$\bar{G}_{n1}=-\frac{1}{2}R^{-1}P_{21}\frac{\int_0^L\left[\phi_{n1}(x)\bar{m}_1\phi_{n1}(x)+\phi_{n2}(x)\bar{m}_2\phi_{n2}(x)\right]dx}{\int_0^L\left\{-\left[\phi_{n1}(x)-\phi_{n2}(x)\right]^2\right\}dx} \tag{5-20a}$$

$$\bar{G}_{n2} = -\frac{1}{2} R^{-1} P_{22} \frac{\int_0^L \left[\phi_{n1}(x) \bar{m}_1 \phi_{n1}(x) + \phi_{n2}(x) \bar{m}_2 \phi_{n2}(x) \right] dx}{\int_0^L \left\{ -\left[\phi_{n1}(x) - \phi_{n2}(x) \right]^2 \right\} dx} \tag{5-20b}$$

Until here, control gains $\bar{G}_{n1}$ and $\bar{G}_{n2}$ are solved, and by the assumptions as in Eq. (5-18), the active control force in physical space, $f_c(x,t)$, is determined. Then, it is possible to apply that active control force in the real double-beam system and obtain dynamic responses of it with active control structure which uses that active control algorithm.

5.4 Semi-Active Control Algorithm for Adjustable Viscoelastic Layer in Semi-Active Control Structure

The semi-active vibration control problem of a double-beam system with adjustable viscoelastic layer is described as Eq. (5-2), the stiffness increase ΔK and the damping increase ΔC of the adjustable viscoelastic layer in Eq. (5-2) is controlled and determined by the semi-active control structure and algorithm. It is similar to the work in Section 4.4, the active control and active control force presented in Section 5.3 is chosen as the objective, a semi-active control algorithm, which makes the semi-active control to be close to that active control, and a mode shape filter are developed to calculate ΔK and ΔC in here.

5.4.1 The Dynamic Mechanical Model of the Adjustable Viscoelastic Layer

The adjustable viscoelastic layer is applied in this chapter to complete the semi-active control, therefore, its stiffness and damping coefficients should be both changed by the control signal. In order to use the adjustable viscoelastic layer to do the semi-active control effectively, the dynamic mechanical model of itself must be figured out firstly, especially, the calculation model for stiffness and damping coefficients of it must be declared.

According to Eq. (5-2), a simple pseudo linear model (as in Fig. 5-2(a)) is adopted to represent the dynamic mechanical model of the adjustable viscoelastic layer and it can be defines as:

$$f_{ViscoelasticLayer}\left(x,t\right)=\left(K+\Delta K\right)\left(W_1-W_2\right)+\left(C+\Delta C\right)\left(\frac{\partial W_1}{\partial t}-\frac{\partial W_2}{\partial t}\right) \tag{5-21}$$

where $\left(K+\Delta K\right)\left(W_1-W_2\right)$ and $\left(C+\Delta C\right)\left(\frac{\partial W_1}{\partial t}-\frac{\partial W_2}{\partial t}\right)$ is the elastic force and damping force of the viscoelastic layer, respectively, $\left(W_1-W_2\right)$ is the viscoelastic layer deformation displacement, and $\left(\frac{\partial W_1}{\partial t}-\frac{\partial W_2}{\partial t}\right)$ is the viscoelastic layer deformation velocity.

Since this research is discussing the semi-active control on the high speed railway bridge vibrations by applying the magnetorheological nanocomposites (MRNs), therefore, the characters of MRNs material should be considered in here for the study of the adjustable viscoelastic layer dynamic model which is adopted by the semi-active control structure. It is like the traditional MREs material,

the changes of the stiffness and damping coefficients of MRNs depend on the applied magnetic field strength which is produced by the current in the device. Thereupon, the stiffness and damping coefficients of the adjustable viscoelastic layer are assumed to have a linear relation with the applied current, whose calculation models (as shown in Fig. 5-2(b) and Fig. 5-2(c)) are linear model as follows

$$K_T = K_{\min} + \frac{I}{I_m}\left(K_{\max} - K_{\min}\right) \tag{5-22a}$$

$$C_T = C_{\min} + \frac{I}{I_m}\left(C_{\max} - C_{\min}\right) \tag{5-22b}$$

where K_T and C_T are the stiffness and damping coefficients of the adjustable viscoelastic layer under specific current, $K_{\max}$ and $C_{\max}$ is maximum stiffness value and maximum damping value of the adjustable viscoelastic layer, $K_{\min}$ and $C_{\min}$ is minimum stiffness value and damping value of the adjustable viscoelastic layer, I_{m} is the saturation current for the device, and *I* is the inputted current determined by semi-active control.

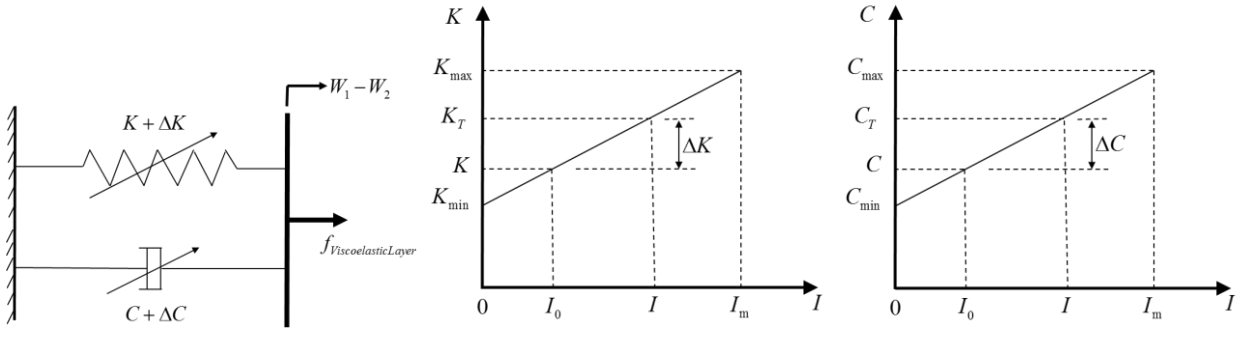

a. Linear Model for Adjustable Viscoelastic Layer Dynamic Mechanical Model

b. Linear Model of Adjustable Viscoelastic Layer Stiffness with Applied Current

c. Linear Model of Adjustable Viscoelastic Layer Damping Coefficient with Applied Current

Fig. 5-2. Linear model for adjustable viscoelastic layer dynamic mechanical model and linear model of adjustable viscoelastic layer stiffness and damping coefficients with applied current.

If the default current inputted is I_0 and the default stiffness and damping coefficients of the adjustable viscoelastic layer are *K* and *C*, respectively, the stiffness increase ΔK and damping increase ΔC (as shown in Fig. 5-2(b) and Fig. 5-2(c)) could be controlled by the current as

$$\Delta K = K_T - K = \frac{I - I_0}{I_m}\left(K_{\max} - K_{\min}\right) \tag{5-23a}$$

$$\Delta C = C_T - C = \frac{I - I_0}{I_m}\left(C_{\max} - C_{\min}\right) \tag{5-23b}$$

Although the simple linear model does not represent the actual behavior of the adjustable viscoelastic layer material or even the MRNs material, it helps us to study the dynamic performance of the controllable viscoelastic layer and a suitable semi-active control algorithm for semi-active control structure in next section, and so, it is proper to adopt it in the discussion in here.

5.4.2 The Determination of Stiffness Increase and Damping Increase in Adjustable Viscoelastic Layer

Based on Eq. (5-2), move the terms, which are related to ΔK and ΔC, to the right side of the equations, then the Eq. (5-2) can be denoted as

$$e_1\frac{\partial^4 W_1}{\partial x^4} + K\left(W_1 - W_2\right) + C\left(\frac{\partial W_1}{\partial t} - \frac{\partial W_2}{\partial t}\right) + \bar{m}_1\frac{\partial^2 W_1}{\partial t^2} = f_1\left(x,t\right) - \Delta K\left(W_1 - W_2\right) - \Delta C\left(\frac{\partial W_1}{\partial t} - \frac{\partial W_2}{\partial t}\right)$$

(5-24a)

$$e_2 \frac{\partial^4 W_2}{\partial x^4} - K\left(W_1 - W_2\right) - C\left(\frac{\partial W_1}{\partial t} - \frac{\partial W_2}{\partial t}\right) + \bar{m}_2 \frac{\partial^2 W_2}{\partial t^2} = f_2\left(x,t\right) + \Delta K\left(W_1 - W_2\right) + \Delta C\left(\frac{\partial W_1}{\partial t} - \frac{\partial W_2}{\partial t}\right)$$

(5-24b)

As shown in Eq. (5-24) and the dynamic mechanical model of the adjustable viscoelastic layer introduced in Eq. (5-21), $\Delta K\left(W_1 - W_2\right) + \Delta C\left(\frac{\partial W_1}{\partial t} - \frac{\partial W_2}{\partial t}\right) = f_{ViscoelasticLayer}\left(x,t\right)$ could be treated as a semi-active control force. Comparing Eq. (5-24) with Eq. (5-1), in order to make the semi-active control being close to the active control, it can assume the semi-active control structure can provide the same control force value as active control structure. However, due to the limit of adjustable viscoelastic layer, the semi-active control force $f_{ViscoelasticLayer}\left(x,t\right)$ cannot reach very value as $f_c\left(x,t\right)$ calculated by active-control algorithm, therefore, the semi-active control force $f_{ViscoelasticLayer}\left(x,t\right)$ is supposed to be defined as follows

(1) If $\Delta K_{\max}\left(W_1 - W_2\right) + \Delta C_{\max}\left(\frac{\partial W_1}{\partial t} - \frac{\partial W_2}{\partial t}\right) < f_c\left(x,t\right)$,

then $f_{ViscoelasticLayer}\left(x,t\right) = \Delta K_{\max}\left(W_1 - W_2\right) + \Delta C_{\max}\left(\frac{\partial W_1}{\partial t} - \frac{\partial W_2}{\partial t}\right)$ (5-25a)

(2) If $\Delta K_{\max}\left(W_1 - W_2\right) + \Delta C_{\max}\left(\frac{\partial W_1}{\partial t} - \frac{\partial W_2}{\partial t}\right) \geq f_c\left(x,t\right) \geq \Delta K_{\min}\left(W_1 - W_2\right) + \Delta C_{\min}\left(\frac{\partial W_1}{\partial t} - \frac{\partial W_2}{\partial t}\right)$,

then $f_{ViscoelasticLayer}\left(x,t\right) = f_c\left(x,t\right)$ (5-25b)

(3) If $\Delta K_{\min}\left(W_1 - W_2\right) + \Delta C_{\min}\left(\frac{\partial W_1}{\partial t} - \frac{\partial W_2}{\partial t}\right) > f_c\left(x,t\right)$,

then $f_{ViscoelasticLayer}(x,t) = \Delta K_{\min}(W_1 - W_2) + \Delta C_{\min}\left(\frac{\partial W_1}{\partial t} - \frac{\partial W_2}{\partial t}\right)$ (5-25c)

where $\Delta K_{\max} = K_{\max} - K$, $\Delta C_{\max} = C_{\max} - C$, $\Delta K_{\min} = K_{\min} - K$, $\Delta C_{\min} = C_{\min} - C$, and K, C are the default stiffness and damping coefficients of the viscoelastic layer.

As to the case (2) shown as Eq. (5-25b), introducing Eq. (5-11c) and substituting Eq. (5-25b) into it, it can be transferred as

$$F_{nc}(t) = H \times \Delta K + J \times \Delta C \tag{5-26a}$$

$$H = \frac{\int_0^L \left\{\left[\phi_{n2}(x) - \phi_{n1}(x)\right]\left[W_1(x,t) - W_2(x,t)\right]\right\} dx}{\int_0^L \left[\phi_{n1}(x)\bar{m}_1\phi_{n1}(x) + \phi_{n2}(x)\bar{m}_2\phi_{n2}(x)\right] dx} \tag{5-26b}$$

$$J = \frac{\int_0^L \left\{\left[\phi_{n2}(x) - \phi_{n1}(x)\right]\left[\frac{\partial W_1(x,t)}{\partial t} - \frac{\partial W_2(x,t)}{\partial t}\right]\right\} dx}{\int_0^L \left[\phi_{n1}(x)\bar{m}_1\phi_{n1}(x) + \phi_{n2}(x)\bar{m}_2\phi_{n2}(x)\right] dx} \tag{5-26c}$$

Considering the calculation model for stiffness and damping coefficients of adjustable viscoelastic layer introduced in Section 5.4.1, and substituting Eq. (5-23) into Eq. (5-26), it will be

$$F_{nc}(t) = H \times \frac{I - I_0}{I_m}(K_{\max} - K_{\min}) + J \times \frac{I - I_0}{I_m}(C_{\max} - C_{\min}) \tag{5-27}$$

In Eq. (5-27), the active control force $F_{nc}(t)$ is calculate by Eq. (5-16) in active control algorithm derived in Section 5.3, therefore, the unknown parameter, current *I*, can be calculated as

$$I = \frac{I_m}{H\left(K_{\max} - K_{\min}\right) + J\left(C_{\max} - C_{\min}\right)} F_{nc}\left(t\right) + I_0 \tag{5-28}$$

Once the current I for the semi-active control is obtained as Eq. (5-28), then, the stiffness increase ΔK and damping increase ΔC can be obtained by Eq. (5-23).

In summary, combing the case (1) and case (3) shown as Eq. (5-25a) and Eq. (5-25c), the stiffness increase and damping increase of the adjustable viscoelastic layer under the semi-active control presented in this chapter can be determined as

(1) If $\Delta K_{\max}\int_0^L \left(W_1 - W_2\right)dx + \Delta C_{\max}\int_0^L \left(\frac{\partial W_1}{\partial t} - \frac{\partial W_2}{\partial t}\right)dx < \int_0^L f_c\left(x,t\right)dx$,

then $\Delta K_d = \Delta K_{\max}$, $\Delta C_d = \Delta C_{\max}$ (5-29a)

(2) If $\Delta K_{\max}\int_0^L \left(W_1 - W_2\right)dx + \Delta C_{\max}\int_0^L \left(\frac{\partial W_1}{\partial t} - \frac{\partial W_2}{\partial t}\right)dx \geq \int_0^L f_c\left(x,t\right)dx$ and

$\Delta K_{\min}\int_0^L \left(W_1 - W_2\right)dx + \Delta C_{\min}\int_0^L \left(\frac{\partial W_1}{\partial t} - \frac{\partial W_2}{\partial t}\right)dx \leq \int_0^L f_c\left(x,t\right)dx$,

then $\Delta K_d = K_T - K = \frac{I - I_0}{I_m}\left(K_{\max} - K_{\min}\right)$, $\Delta C_d = C_T - C = \frac{I - I_0}{I_m}\left(C_{\max} - C_{\min}\right)$, (5-29b)

$$I = \frac{I_m}{H\left(K_{\max} - K_{\min}\right) + J\left(C_{\max} - C_{\min}\right)} F_{nc}\left(t\right) + I_0 \tag{5-28}$$

$$F_{nc}\left(t\right) = -\frac{1}{2} R^{-1}\left[P_{21} T_n\left(t\right) + P_{22}\dot{T}_n\left(t\right)\right] \tag{5-16}$$

(3) If $\Delta K_{\min}\int_0^L \left(W_1 - W_2\right)dx + \Delta C_{\min}\int_0^L \left(\frac{\partial W_1}{\partial t} - \frac{\partial W_2}{\partial t}\right)dx > \int_0^L f_c\left(x,t\right)dx$,

then $\Delta K_d = \Delta K_{\min}$, $\Delta C_d = \Delta C_{\min}$ (5-29c)

where L is the total length of each beam in double-beam system.

Applying Eq. (5-29), Eq. (5-16) and Eq. (5-28), the stiffness increase ΔK_d and damping increase ΔC_d are determined and could be adopted by semi-active control structure. It is the same as the discussion in Section 4.4.1, only one main mode will be chosen to be controlled for the semi-active control structure, ΔK_d and ΔC_d should be determined at each time step and changed during the whole vibration process.

5.4.3 The Mode Shape Filter for the Double-Beam System

The discussion is totally same as the one in Section 4.4.2, therefore, the mode shape filter for the double-beam system is as follows

$$T_n(t) = \frac{\int_0^L \left[\phi_{n1}(x)\bar{m}_1 W_1(x,t) + \phi_{n2}(x)\bar{m}_2 W_2(x,t)\right]dx}{\int_0^L \left[\phi_{n1}(x)\bar{m}_1\phi_{n1}(x) + \phi_{n2}(x)\bar{m}_2\phi_{n2}(x)\right]dx} \quad (5\text{-}30a)$$

$$\dot{T}_n(t) = \frac{\int_0^L \left[\phi_{n1}(x)\bar{m}_1 V_1(x,t) + \phi_{n2}(x)\bar{m}_2 V_2(x,t)\right]dx}{\int_0^L \left[\phi_{n1}(x)\bar{m}_1\phi_{n1}(x) + \phi_{n2}(x)\bar{m}_2\phi_{n2}(x)\right]dx} \quad (5\text{-}30b)$$

where $W_1(x,t)$, $W_2(x,t)$, $V_1(x,t)$ and $V_2(x,t)$ is the displacement and velocity of upper beam and lower beam detected at time *t*, respectively, $\phi_{n1}(x)$ and $\phi_{n2}(x)$ are mode shape functions of upper beam and lower beam corresponding to *n*th natural frequency, which are the same as the ones defined in Eq. (5-5).

Once $\phi_{n1}(x)$ and $\phi_{n2}(x)$ are obtained by free vibration analysis in Chapter 2, and displacement and velocity of the two beam are detected by the sensors in the structure, then, the $T_n(t)$ and $\dot{T}_n(t)$ can be determined by the displacement mode shape filter as Eq. (5-30a) and velocity mode shape filter as Eq. (5-30b), respectively. The mode shape filter for calculating $T_n(t)$ and $\dot{T}_n(t)$ is not only useful in the determination of stiffness increase ΔK and damping increase ΔC as discussing at the beginning of this section, but also is very important for the calculation of the transverse vibration of the whole double-beam system with semi-active control structure, which will be introduced in next section.

5.5 Solution of the Transverse Vibration for Double-Beam System with Vibration Control Structure

Once the active control force or semi-active control parameter is determined by the control algorithm developed in this chapter, the solutions of the transverse vibration for double-beam system with active control structure or semi-active control structure, which is described in Eq. (5-1) or Eq. (5-2), can be solved and the dynamic responses of whole structure system can be obtained.

5.5.1 Solution of the Transverse Vibration for Double-Beam System with Active Control Structure

The active control force is calculated by the active control algorithm as Eq. (5-16), and then,

substituting it into Eq. (5-11), the decoupled motion equations of the double-beam system with active control structure will be

$$\frac{d^2T_n(t)}{dt^2}+\frac{1}{2}R^{-1}P_{22}\frac{dT_n(t)}{dt}+\left(\frac{1}{2}R^{-1}P_{21}+\omega_n^2\right)T_n(t)=F_n(t)+F_{nD}(t) \tag{5-31a}$$

$$F_n(t)=\frac{\int_0^L\left[\phi_{n1}(x)\,f_1(x,t)+\phi_{n2}(x)\,f_2(x,t)\right]dx}{\int_0^L\left[\phi_{n1}(x)\bar{m}_1\phi_{n1}(x)+\phi_{n2}(x)\bar{m}_2\phi_{n2}(x)\right]dx} \tag{5-31b}$$

$$F_{nD}(t)=\frac{\int_0^L\left\{\left[\phi_{n2}(x)-\phi_{n1}(x)\right]\left[C\left(\frac{\partial W_1}{\partial t}-\frac{\partial W_2}{\partial t}\right)\right]\right\}dx}{\int_0^L\left[\phi_{n1}(x)\bar{m}_1\phi_{n1}(x)+\phi_{n2}(x)\bar{m}_2\phi_{n2}(x)\right]dx} \tag{5-31c}$$

Using Duhamel's integral, particular solution of Eq. (5-31a) can be obtained as

$$T_n(t)=\frac{1}{\omega_{nd}}\int_0^t\left[F_n(\tau)+F_{nD}(\tau)\right]e^{-\xi_n\omega_n^*(t-\tau)}\cdot\sin\left[\omega_{nd}(t-\tau)\right]d\tau \tag{5-32}$$

where $\omega_n^*=\sqrt{\omega_n^2+\frac{1}{2}R^{-1}P_{21}}$, $\xi_n=\frac{1}{4}R^{-1}\frac{P_{22}}{\omega_n^*}$, and $\omega_{nd}=\omega_n^*\sqrt{1-\xi_n^2}$ are the calculation parameters.

In Eq. (5-31) and Eq. (5-32), the unknown damping force $C\left(\frac{\partial W_1}{\partial t}-\frac{\partial W_2}{\partial t}\right)$ is included, therefore, they are a kind of implicit equations and it is hard to solve them directly. An iteration method, which could be generally expressed in a flowchart form as in Fig. 5-3, is developed in this chapter to solve that problem. By the iteration method, the transverse vibration equations of a double-beam system with active control structure presented in this chapter are solved successfully.

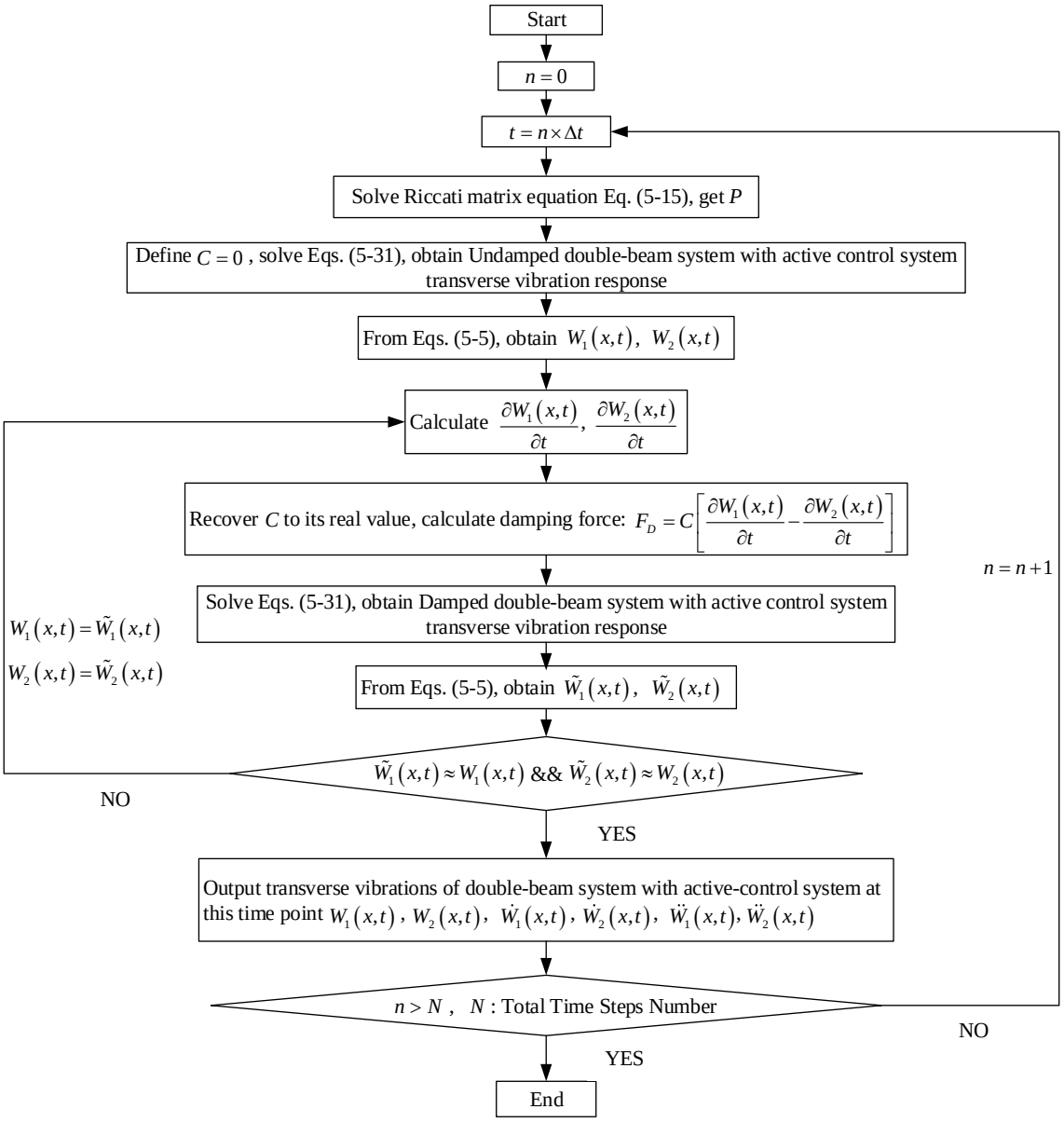

Fig. 5-3. Flowchart of the iteration method to calculate transverse vibration responses of a double-beam system with active control structure.

5.5.2 Solution of the Transverse Vibration for Double-Beam System with Semi-Active Control Structure

It is the same as the discussion in Section 4.5.2, so it also requires that the adjustable viscoelastic layer which is under control should be changed with time during the whole vibration process. The

same three requirements should be satisfied for the vibration calculation of double-beam system with that semi-active control structure:

1. The vibration calculation must be carried out one time step by one time step, because the structure may be different in each time step.

2. In each time step, the analysis of the structure vibration property must be done due to the change of the adjustable viscoelastic layer stiffness and damping coefficients.

3. In each time step, the calculation of the forced vibration of double-beam system with semi-active control is generally same as the method derived in Section 3.4, but the stiffness and damping coefficients of the viscoelastic layer must be $K_L + \Delta K$ and $C_L + \Delta C$ (K_L, C_L are the stiffness and damping coefficients value in last time step, and ΔK, ΔC are calculated by Section 5.4.2 based on the structure and responses from last time step), and the dynamic responses of the two beams in last time step must be applied as the initial condition.

According to the third requirement, the solutions of the forced transverse vibration of double-beam system with semi-active control in time step $T = t_{i-1} \to T = t_i$ can be calculated as follows:

1. Defining the value of viscoelastic layer stiffness as $K_L + \Delta K$ instead of K_L and damping coefficient as $C_L + \Delta C$ instead of C_L (K_L, C_L are the stiffness and damping coefficients values in last time step, and ΔK, ΔC are calculated by Section 5.4.2 based on the structure and responses from last time step), then, the same derivation works as Eq. (3-27) to Eq. (3-32) are completed.

2. Based on the dynamic responses of two beams in last time step: $W_1(x,t_{i-1})$, $W_2(x,t_{i-1})$, $V_1(x,t_{i-1})$ and $V_2(x,t_{i-1})$, and applying the mode shape filter presented as Eq. (5-30), the initial condition $T_n(t_{i-1})$ and $\dot{T}_n(t_{i-1})$ can be obtained.

3. Using Duhamel's integral and considering the initial condition $T_n(t_{i-1})$, $\dot{T}_n(t_{i-1})$, particular solution of Eq. (5-31) in time step $T=t_{i-1}\rightarrow T=t_i$ ($\Delta t=t_i-t_{i-1}$) can be finally obtained as

$$T_n(t_i)=\frac{\dot{T}_n(t_{i-1})}{\omega_n}\sin(\omega_n\Delta t)+T_n(t_{i-1})\cos(\omega_n\Delta t)+\frac{1}{\omega_n}\int_0^{\Delta t}\left[F_n(\tau)+F_{nD}(\tau)\right]\cdot\sin\left[\omega_n(\Delta t-\tau)\right]d\tau \tag{5-33}$$

Based on those three requirements, Eq. (5-33) and the iteration method proposed in Section 3.4, a calculation method which could be generally expressed in a flowchart form as in Fig. 5-4, is developed in this chapter to solve and obtain the dynamic responses of the whole double-beam system with semi-active control structure.

Finally, applying the method shown as flowchart in Fig. 5-4 and doing the calculation one time step by one time step until the end, the dynamic responses of whole double-beam system with semi-active control are solved and obtained successfully.

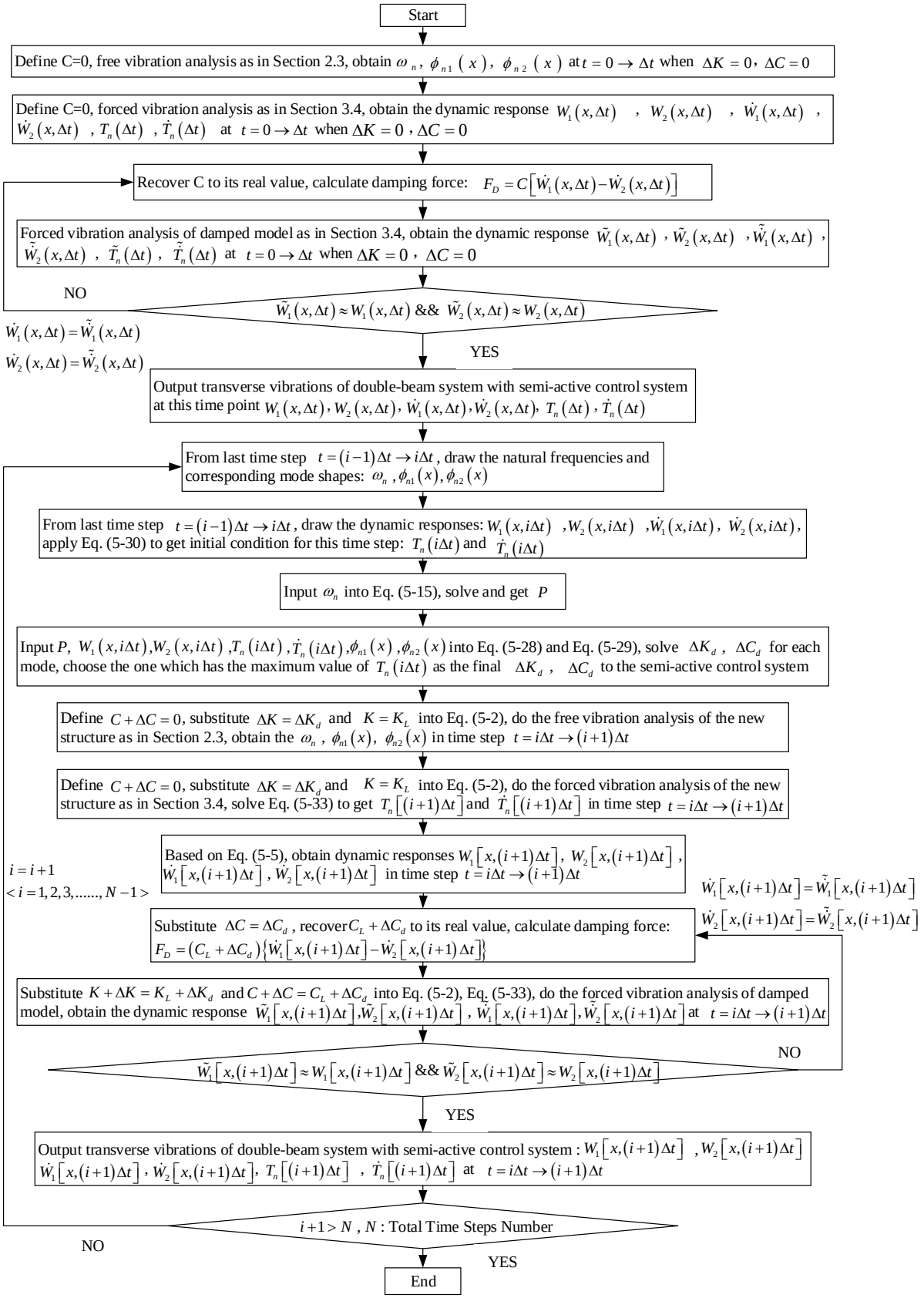
Start
Define C=0, free vibration analysis as in Section 2.3, obtain ω_n, $\phi_{n1}(x)$, $\phi_{n2}(x)$ at $t=0\to\Delta t$ when $\Delta K=0$, $\Delta C=0$
Define C=0, forced vibration analysis as in Section 3.4, obtain the dynamic response $W_1(x,\Delta t)$, $W_2(x,\Delta t)$, $\dot{W}_1(x,\Delta t)$, $\dot{W}_2(x,\Delta t)$, $T_n(\Delta t)$, $\dot{T}_n(\Delta t)$ at $t=0\to\Delta t$ when $\Delta K=0$, $\Delta C=0$
Recover C to its real value, calculate damping force: $F_D=C\left[\dot{W}_1(x,\Delta t)-\dot{W}_2(x,\Delta t)\right]$
Forced vibration analysis of damped model as in Section 3.4, obtain the dynamic response $\tilde{W}_1(x,\Delta t)$, $\tilde{W}_2(x,\Delta t)$, $\dot{\tilde{W}}_1(x,\Delta t)$, $\dot{\tilde{W}}_2(x,\Delta t)$, $\tilde{T}_n(\Delta t)$, $\dot{\tilde{T}}_n(\Delta t)$ at $t=0\to\Delta t$ when $\Delta K=0$, $\Delta C=0$
NO
$\tilde{W}_1(x,\Delta t)\approx W_1(x,\Delta t)$ && $\tilde{W}_2(x,\Delta t)\approx W_2(x,\Delta t)$
$\dot{W}_1(x,\Delta t)=\dot{\tilde{W}}_1(x,\Delta t)$
$\dot{W}_2(x,\Delta t)=\dot{\tilde{W}}_2(x,\Delta t)$
YES
Output transverse vibrations of double-beam system with semi-active control system at this time point $W_1(x,\Delta t)$, $W_2(x,\Delta t)$, $\dot{W}_1(x,\Delta t)$, $\dot{W}_2(x,\Delta t)$, $T_n(\Delta t)$, $\dot{T}_n(\Delta t)$
From last time step $t=(i-1)\Delta t\to i\Delta t$, draw the natural frequencies and corresponding mode shapes: ω_n, $\phi_{n1}(x)$, $\phi_{n2}(x)$
From last time step $t=(i-1)\Delta t\to i\Delta t$, draw the dynamic responses: $W_1(x,i\Delta t)$, $W_2(x,i\Delta t)$, $\dot{W}_1(x,i\Delta t)$, $\dot{W}_2(x,i\Delta t)$, apply Eq. (5-30) to get initial condition for this time step: $T_n(i\Delta t)$ and $\dot{T}_n(i\Delta t)$
Input ω_n into Eq. (5-15), solve and get P
Input P, $W_1(x,i\Delta t)$, $W_2(x,i\Delta t)$, $T_n(i\Delta t)$, $\dot{T}_n(i\Delta t)$, $\phi_{n1}(x)$, $\phi_{n2}(x)$ into Eq. (5-28) and Eq. (5-29), solve ΔK_d, ΔC_d for each mode, choose the one which has the maximum value of $T_n(i\Delta t)$ as the final ΔK_d, ΔC_d to the semi-active control system
Define $C+\Delta C=0$, substitute $\Delta K=\Delta K_d$ and $K=K_L$ into Eq. (5-2), do the free vibration analysis of the new structure as in Section 2.3, obtain the ω_n, $\phi_{n1}(x)$, $\phi_{n2}(x)$ in time step $t=i\Delta t\to(i+1)\Delta t$
Define $C+\Delta C=0$, substitute $\Delta K=\Delta K_d$ and $K=K_L$ into Eq. (5-2), do the forced vibration analysis of the new structure as in Section 3.4, solve Eq. (5-33) to get $T_n[(i+1)\Delta t]$ and $\dot{T}_n[(i+1)\Delta t]$ in time step $t=i\Delta t\to(i+1)\Delta t$
Based on Eq. (5-5), obtain dynamic responses $W_1[x,(i+1)\Delta t]$, $W_2[x,(i+1)\Delta t]$, $\dot{W}_1[x,(i+1)\Delta t]$, $\dot{W}_2[x,(i+1)\Delta t]$ in time step $t=i\Delta t\to(i+1)\Delta t$
$i=i+1$
$<i=1,2,3,.....,N-1>$
$\dot{W}_1[x,(i+1)\Delta t]=\dot{\tilde{W}}_1[x,(i+1)\Delta t]$
$\dot{W}_2[x,(i+1)\Delta t]=\dot{\tilde{W}}_2[x,(i+1)\Delta t]$
Substitute $\Delta C=\Delta C_d$, recover $C_L+\Delta C_d$ to its real value, calculate damping force: $F_D=(C_L+\Delta C_d)\{\dot{W}_1[x,(i+1)\Delta t]-\dot{W}_2[x,(i+1)\Delta t]\}$
Substitute $K+\Delta K=K_L+\Delta K_d$ and $C+\Delta C=C_L+\Delta C_d$ into Eq. (5-2), Eq. (5-33), do the forced vibration analysis of damped model, obtain the dynamic response $\tilde{W}_1[x,(i+1)\Delta t]$, $\tilde{W}_2[x,(i+1)\Delta t]$, $\dot{\tilde{W}}_1[x,(i+1)\Delta t]$, $\dot{\tilde{W}}_2[x,(i+1)\Delta t]$ at $t=i\Delta t\to(i+1)\Delta t$
NO
$\tilde{W}_1[x,(i+1)\Delta t]\approx W_1[x,(i+1)\Delta t]$ && $\tilde{W}_2[x,(i+1)\Delta t]\approx W_2[x,(i+1)\Delta t]$
YES
Output transverse vibrations of double-beam system with semi-active control system : $W_1[x,(i+1)\Delta t]$, $W_2[x,(i+1)\Delta t]$, $\dot{W}_1[x,(i+1)\Delta t]$, $\dot{W}_2[x,(i+1)\Delta t]$, $T_n[(i+1)\Delta t]$, $\dot{T}_n[(i+1)\Delta t]$ at $t=i\Delta t\to(i+1)\Delta t$
$i+1>N$, N : Total Time Steps Number
NO
YES
End

Fig. 5-4. Flowchart of the calculation method to solve and obtain the dynamic responses of double-beam system with semi-active control structure.

5.6 Numerical Examples

In order to illustrate the active control structure, semi-active control structure and the corresponding control algorithms presented in this chapter for double-beam system, some numerical examples of uncontrolled, active controlled and semi-active controlled double-beam system are investigated in detail. The values for the parameters of the double-beam system are as follows

$E = 1\times10^{10}\,Nm^{-2}$, $I = 4\times10^{-4}m^4$, $\rho = 2\times10^{3}\,kgm^{-3}$, $A = 5\times10^{-2}m^2$, $e = EI = 4\times10^{6}\,Nm^2$, $m = \rho A = 1\times10^{2}\,kgm^{-1}$, $L = 10m$, $K = 1\times10^{5}\,Nm^{-2}$, $K_{\max} = 1.4\times10^{5}\,Nm^{-2}$, $K_{\min} = 7\times10^{4}\,Nm^{-2}$

The exciting force of the double-beam system is $f_1(x,t) = f\sin(\omega t)\delta(x-0.5L)$, $f_2(x,t) = 0$, where $f = -10000N$ is amplitude and $\omega = 10Hz$ is frequency of a concentrated harmonic force acted on the midspan of the upper beam, and $\delta(x)$ is Dirac delta function. Three cases are investigated in here for discussion:

Case 1: upper beam spring supported-spring supported and lower beam simply supported-simply supported, $e_1 = e_2 = e$, $m_1 = m_2 = m$, $C = 1\times10^{2}\,Nsm^{-1}$, $C_{\max} = 1.4\times10^{2}\,Nsm^{-1}$, $C_{\min} = 70\,Nsm^{-1}$;

Case 2: upper beam spring supported-spring supported and lower beam simply supported-simply

supported, $e_1 = 0.8e$, $e_2 = e$, $m_1 = 0.2m$, $m_2 = m$, $C = 50Nsm^{-1}$, $C_{\max} = 70Nsm^{-1}$, $C_{\min} = 35Nsm^{-1}$;

Case 3: upper beam clamped-clamped and lower beam free-free, $e_1 = e$, $e_2 = 0.8e$, $m_1 = m$, $m_2 = 0.2m$, $C = 1\times10^2 Nsm^{-1}$, $C_{\max} = 1.4\times10^2 Nsm^{-1}$, $C_{\min} = 70Nsm^{-1}$.

The dynamic responses of uncontrolled, active controlled and semi-active controlled double-beam system at the midspan of the two beams are shown in Fig. 5-5 to Fig. 5-7. The active control force which is applied at the midspan of both beams, $f_c(0.5L,t)$, is shown in Fig. 5-8. The variation *K* and variation *C* of adjustable viscoelastic layer are shown in Fig. 5-9.

a. Upper Beam Displacement

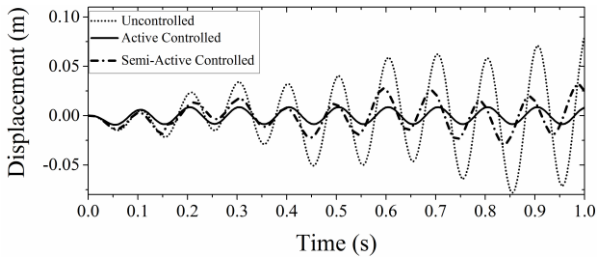

b. Lower Beam Displacement

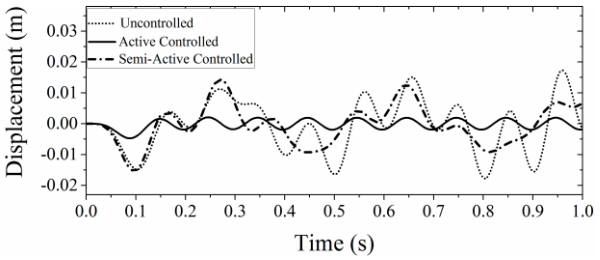

c. Upper Beam Velocity

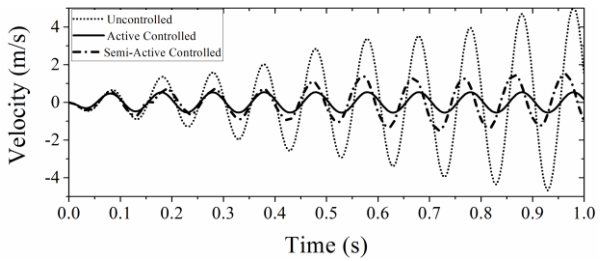

d. Lower Beam Velocity

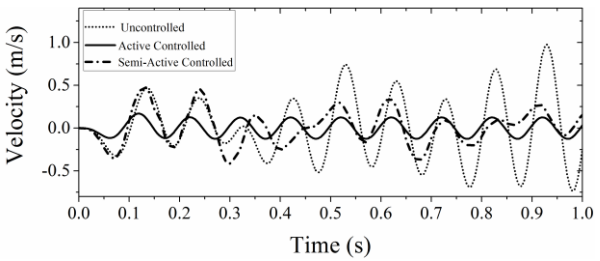

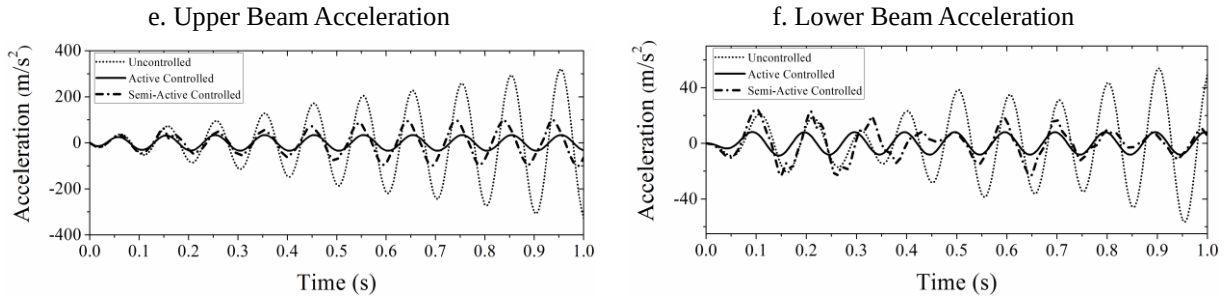

Fig. 5-5. Dynamic responses at midspan point of two beams for Case 1.

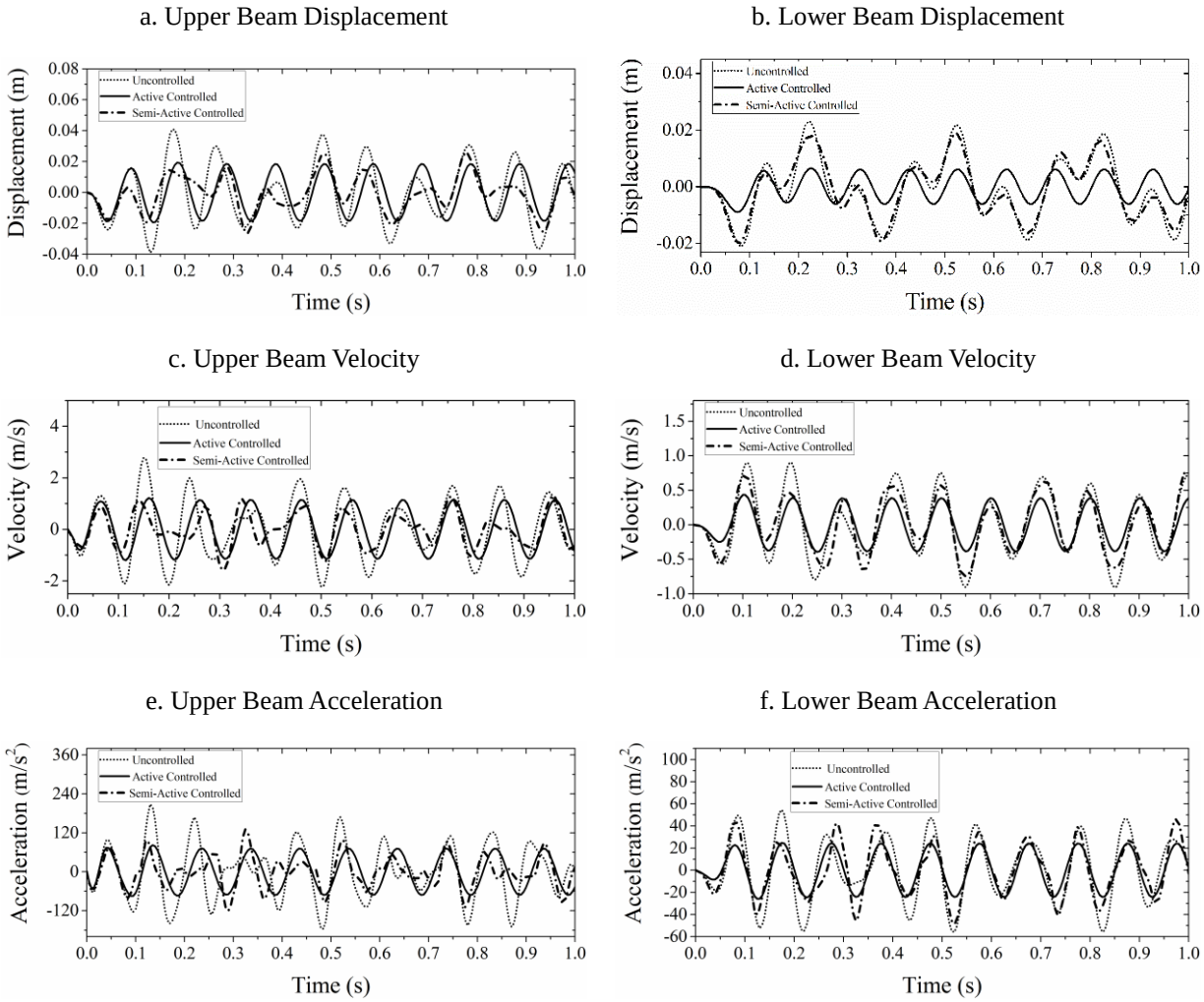

Fig. 5-6. Dynamic responses at midspan point of two beams for Case 2.

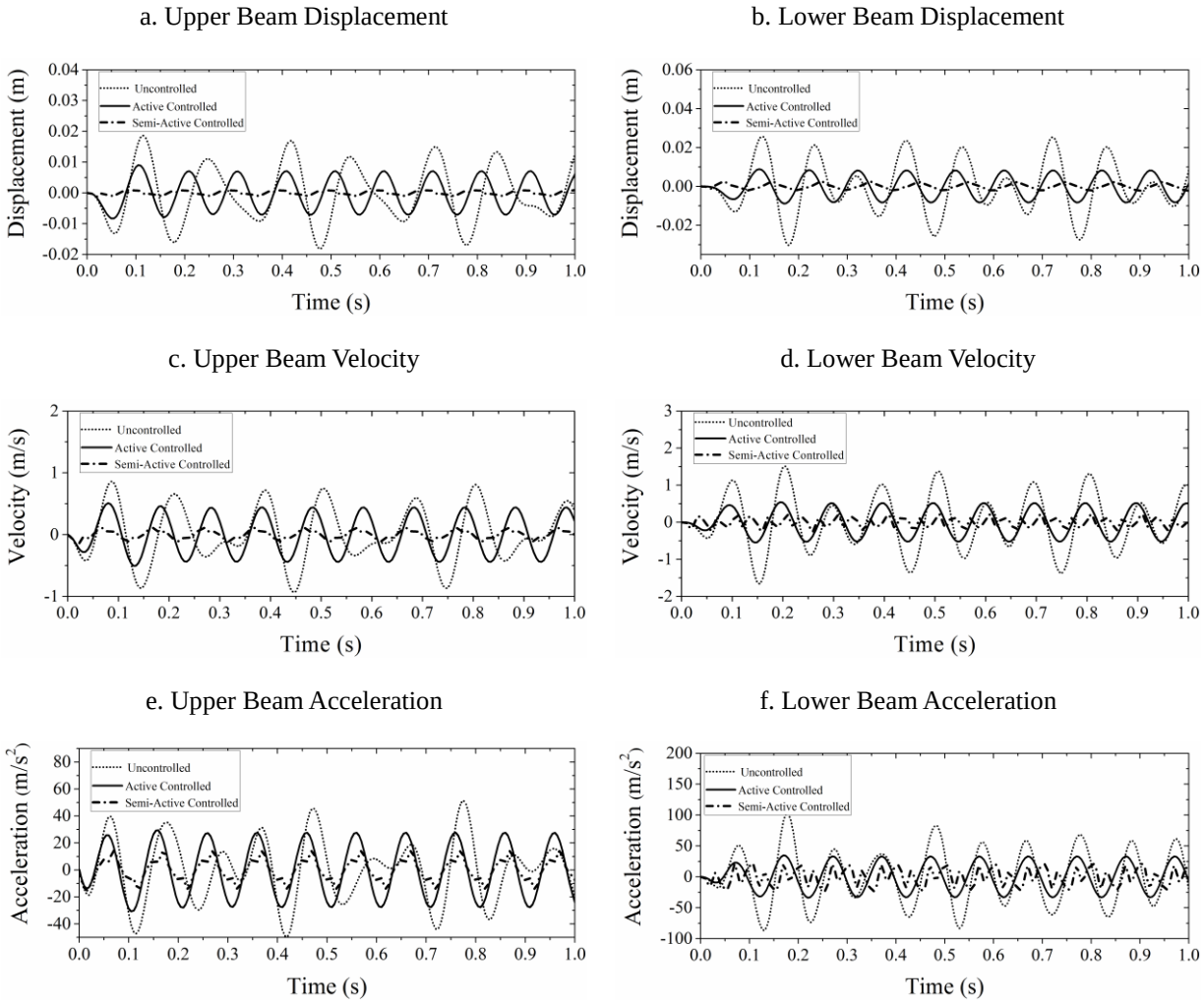

Fig. 5-7. Dynamic responses at midspan point of two beams for Case 3.

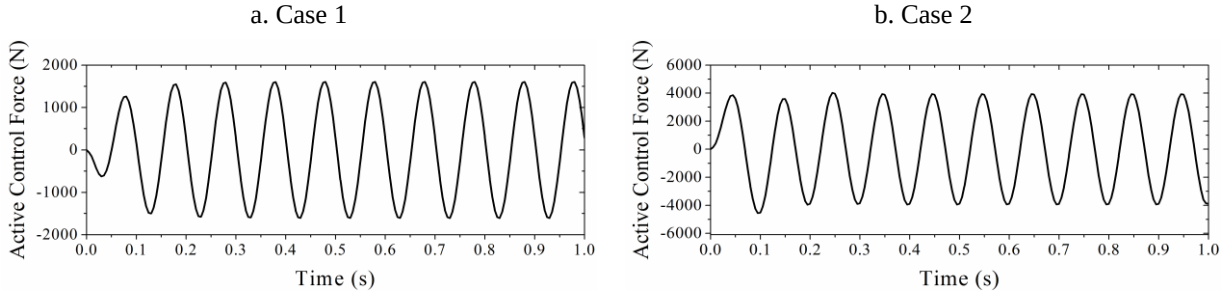

c. Case 3

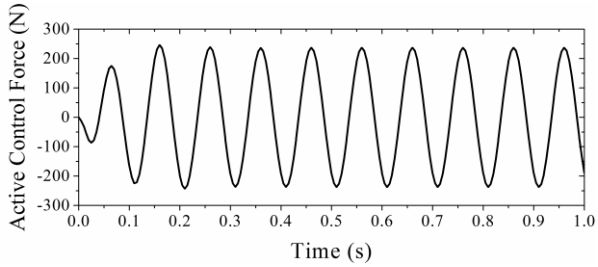

Fig. 5-8. Active control force applied at midspan point of two beams for each case.

a. Case 1 - K

b. Case 2 - K

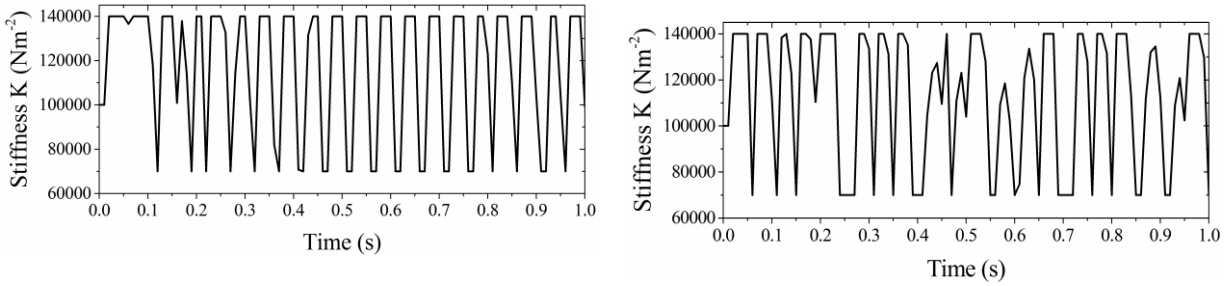

c. Case 3 - K

d. Case 1 - C

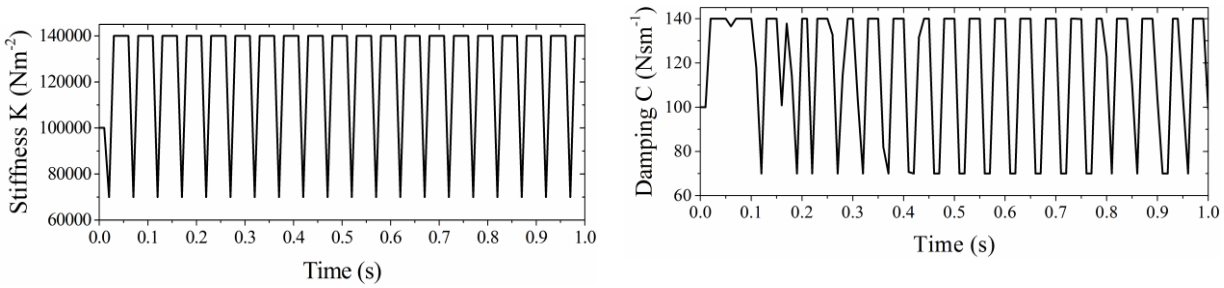

e. Case 2 - C

f. Case 3 - C

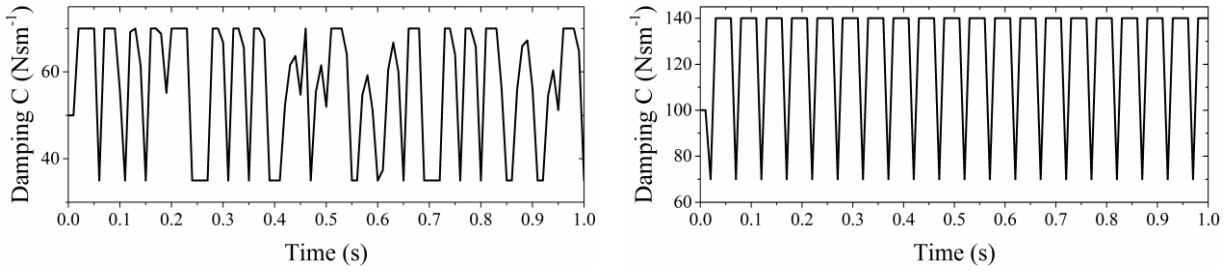

Fig. 5-9. Variation stiffness *K* and variation damping coefficient *C* of adjustable elastic layer for each case.

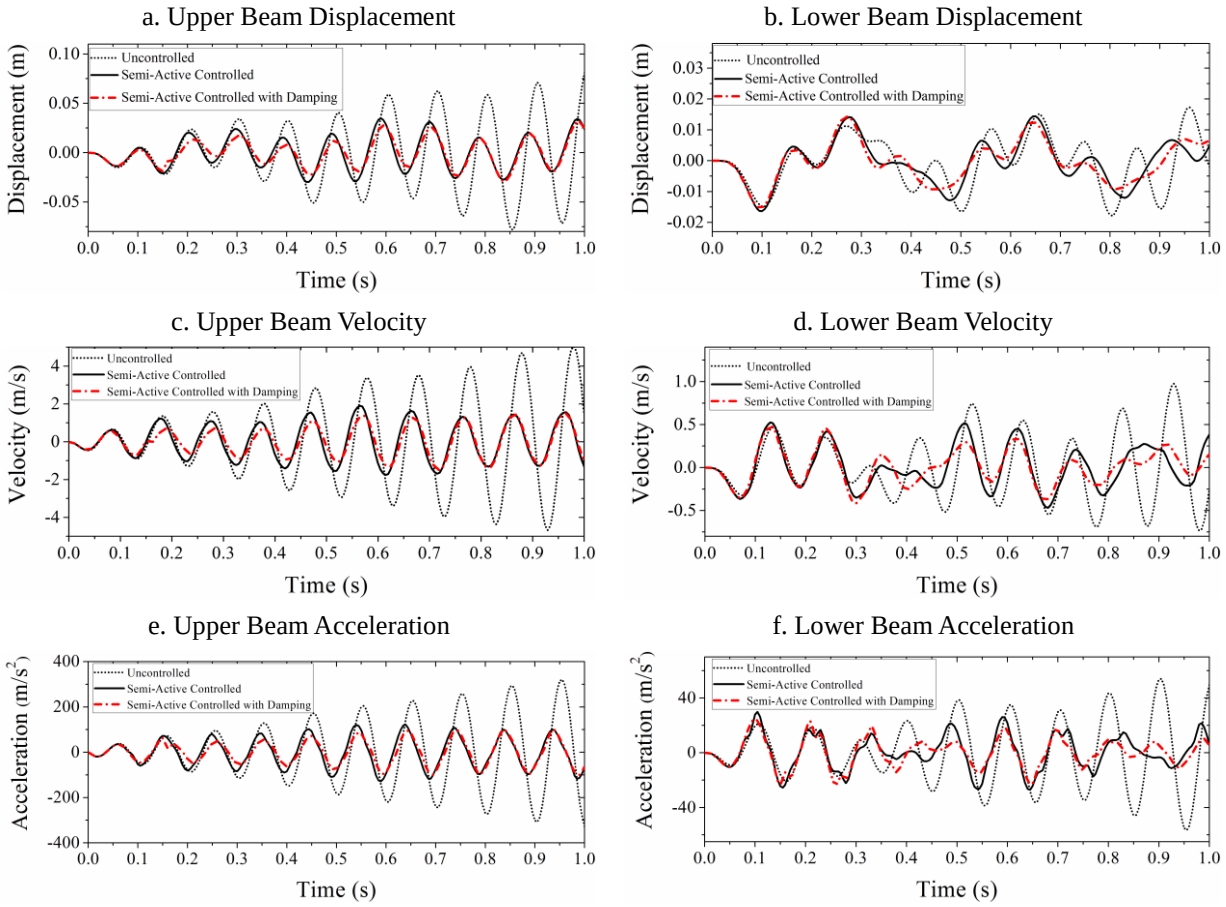

Fig. 5-10. Dynamic responses at midspan point of two beams for Case 1 comparing with Case 1 in Chapter 4.

As shown in Fig. 5-4 to Fig. 5-7, the active control structure designed for the double-beam system and the corresponding active control algorithm developed in this chapter are effective to suppress the vibrations of both beams. The semi-active control structure and semi-active control algorithm also works well, although it doesn't reduce the dynamic responses of two beams so perfectly as the active control structure in Case 1 and Case 2, it also could suppress the vibrations of whole system apparently. Since there are two different boundary conditions in those 3 cases and all the models with them have smaller dynamic responses under the active control or semi-active control, therefore, the active control and semi-active control proposed in this research have the capability

to control the double-beam system with arbitrary boundary conditions.

In case 1 (Fig. 5-5), resonance phenomenon is happened in upper beam without active control structure or semi-active control structure, but it is controlled and eliminated when the active control or semi-active control is applied. Therefore, the active control and semi-active control proposed in this chapter can effectively avoid the resonance happening in the double-beam system and protect the safety of the whole structure.

From Fig. 5-8, it is shown the value of active control force at midspan of both beams in physical space for 3 cases. Although it is just part of the whole active control force, the existence and presentation of it denote the operability of the proposed active control structure which could control the whole structure by applying that real force and it is very possible for the engineers to apply it in the real engineering practices. Also in Fig. 5-9, the value of variation stiffness K and variation damping coefficient C of the adjustable viscoelastic layer are shown for all 3 cases, and it is easy to find out that the stiffness K and damping coefficient C have obvious changes under the semi-active control. Comparing with previous classical control algorithms, the changes of stiffness K and damping coefficient C are very close to the ones under switch on – switch off control algorithm, therefore, it proves that the semi-active proposed in this chapter is reasonable and it is practical to apply it in the real structures.

As shown in Fig. 5-10, the dynamic responses at midspan of two beams for Case 1 are compared with Case 1 in Chapter 4. The two double-beam system models are almost the same except the damping control is considered in this chapter. From Fig. 5-10, the semi-active control with damping reduces the dynamic responses of two beams a little better than the semi-active control which only changes stiffness of elastic layer. Therefore, the damping control can help to do the vibration control in whole system better, and the semi-active control proposed in this chapter which adopts adjustable viscoelastic layer is better to suppress the vibrations of whole system.

5.7 Conclusions

In this chapter, an active control structure, a semi-active control structure and corresponding control algorithms are proposed to suppress the vibration of the double-beam system with viscoelastic layer, which may have arbitrary beam mass, beam flexural rigidity and/or boundary condition. Based on Chapter 3, the calculation methods for double-beam system with that active control and that semi-active control are also developed.

In the active control structure, independent modal space control (IMSC) is applied to decouple the motion equations of double-beam system with the active control, which are coupling partial differential equations, and transfer them as some decoupled equations in modal space. The vibration control of the infinite freedom system in physical space is also transferred as the vibration

control of several modes in modal space by IMSC. Linear quadratic regulator is adopted to determine the specific modal active control force for each mode, then, the active control force in physical space, which can be loaded in real structure, is obtained by modal active control forces.

In the semi-active control structure, the active control force produced by the active control structure presented above is set up as the objective and the equivalent semi-active control force is assumed to be close to that active force. A linear model is assumed as the dynamic mechanical model of the adjustable viscoelastic layer and the relationships between stiffness, damping with inputted currents are also defined as linear models. Based on that calculation principle, the linear model for adjustable viscoelastic layer and with the mode shape filter derived in this chapter, the determination methods of stiffness increase and damping increase are derived.

Various double-beam system with active control or semi-active control models are calculated to illustrate the efficiency of the proposed active control and semi-active control, and the resonance in the structure are also shown to be avoided by them. Although the semi-active control is not so perfect as the active control, it still can suppress the vibration of the whole double-beam system significantly. Finally, the proposed active control and semi-active control for double-beam system are derived and verified successfully.

Chapter 6 Analysis of High-Speed Rail Vehicle - Bridge Coupling Vibration

6.1 Introduction

In Chapter 2 and Chapter 3, the dynamic behaviors of the double-beam system with elastic layer and viscoelastic layer between two beams are calculated and analyzed carefully. And then, the active control and semi-active control for those two kinds of double-beam system are all introduced and derived specifically in Chapter 4 and Chapter 5. The theoretical preparation works of the high-speed rail bridges with floating slab track on them have been completed in those four chapters as stated above. In this chapter, the research works will come back to the real structure: vehicle-bridge coupling system of high-speed rail, and a co-simulation method will be proposed to simulate the whole system. The co-simulation platform built in this chapter will supply a basis for the works in next chapter: applying novel adaptive materials magnetorheological nanocomposites as a semi-active control structure into the vehicle-bridge coupling system of high-speed rail and controlling the vibrations of whole bridge.

The vibration behavior of railway bridges under train loads is a fundamental problem for researchers and engineers to solve in study and design. First, the trains passing the bridge induce dynamic impact to bridge structures, reducing their safety and service life. Second, the vibration of bridges in turn affects the running stability and safety of the trains.

The relative research could date back to the works of Willis (1849) and Stokes (1849) in the mid-19th century in investigating the collapse of Chaster Rail Bridge in England in 1847. In the early works, researchers on bridge dynamics mainly try to get analytical or approximate solutions for some simple problems (Timoshenko 1922; Jeffcott 1929; Inglis 1934). After the computer was invented, researches are able to observe more realistic bridge and vehicle models in analysis. In some structure dynamics texts, people begin to discuss the vibration of structures under moving load (Biggs 1964; Fryba 1972; Fryba 1996). Starting from 1975, Ting and his co-workers update the related researches on vehicle-guideway interactions from time to time (Ting 1975; Genin and Ting 1979; Ting and Genin 1980; Ting and Yener 1983; Taheri 1990). Now, by using powerful numerical methods, the related research has been done more deeply and the models of bridge and vehicle have been more complicated (Yang, Yau and Wu 2004).

Bridge Models (Yang, Yau and Wu 2004)

Almost all the bridges can be simulated as two main methods: finite element method (FEM) and modal expansion method (MEM). MEM can effectively reduce the degree of the bridge and obtain the dynamic response of bridge much faster, but it could only be adopted in linear question and only for simple bridge structure. On contrary, FEM could be widely used in every types of bridge structure and complete the nonlinear analysis on it, but the analysis time will be very long and the process will be difficult (Xia and Zhang 2002).

Until now, various types of bridges can be simulated in vehicle-bridge coupling system, including truss bridges, multispan uniform or nonuniform bridges, girder bridges, continuous beams, curved girder bridges steel plate girder bridges and arch bridges (Wiriyachai 1982; Yang 1995; Kou and DeWolf 1997; Cheung 1999; Huang 193; Cai 1994; Yang 2001; Kawatani and Kim 2001; Ju and Lin 2003; Yang, Yau and Wu 2004). With the development of long span bridge, dynamic response of cable-stayed bridges and suspension bridges to moving vehicles has also been studied (Meisenholder 1974; Wang and Huang 1992; Yang and Fonder 1998; Guo and Xu 2001; Chatterjee 1994; Xia 2000; Xu 2003; Yang, Yau and Wu 2004).

Vehicle Models (Yang, Yau and Wu 2004)

Until now, moving load, moving mass, moving sprung mass and multi degree of freedom models are the main models applied to simulate the vehicles in the majority of literatures.

The moving load model is the simplest model, which is still used in the simple analysis questions or at the beginning of the work. However, the effect of interaction between bridge and moving vehicle is ignored, so this model could be used when the mass of vehicle is much smaller than bridge (Timoshenko 1922; Ayre and Jacobsen 1950; Chen 1978; Wu and Dai 1987; Galdos 1993; Gbadeyan and Oni 1995; Wang 1997; Zheng 1998; Rao 2000; Chen and Li 2000; Dugush and Eisenberger 2002; Yang, Yau and Wu2004). The moving mass model is used to surpass the

limitation of moving load model (Jeffcott 1929; Stanisic and Hardin 1969; Ting 1974; Stanisic 1985; Akin and Mofid 1989; Yang, Yau and Wu 2004). In order to simulate the vehicle better, people consider to add the elastic and damping effects into the models, which then forms a model called sprung mass model (Biggs 1964; Fryba 1972; Pesterev 2001; Pesterev 2003; Yang, Yau and Wu 2004). Later, vehicle models that contain several degrees of freedom (DOFs) have been used to represent the dynamic properties of freight cars or high speed trains. In those models, not only the elastic and damping effect, but also the rotation and vibration inside the vehicle, are all been considered (Chu 1986; Wang 1991; Xia, Xu and Chan 2000; Zhang 2001; Wu 2001; Yang, Yau and Wu 2004).

Vehicle-Bridge Coupling Relationship

The main vehicle-bridge coupling relationship consists of contact displacements and contact forces. As to the contact displacements at the contact area, it is assumed that the bridge ones has the same values as the vehicle ones, and all of the displacements satisfy the specific geometric relationships (Xia, De, Zhang and Zhang 2001; Xu, Zhang and Xia 2004; Guo, Deng and Luo 2009). The contact forces at the contact area are defined as the function of wheel-rail relative motion and they also satisfy the force equivalent conditions (Zhai, Cai and Guo 1996; Zhang, Xia and Guo 2010; Torstensson, Nielson and Baeza 2011; Fayos, Baeza, Denia and Tarancon 2007).

Another coupling relationship between vehicle and bridge is rail irregularities. Since people find

it will produce significantly effect when discussing the interaction between vehicle and bridge, so many people have gotten relative conclusion and model for it, including road profile modeled as a stationary Gaussian random process, power spectral density function, cross level and vertical profile (Gupta 1980; Chu 1986; Wang 1991; Paultre 1992; Wang and Huang 1992; Yang and Lin 1995; Chatterjee 1994; Chang and Lee 1994; Pan and Li 2002; Yang, Yau and Wu 2004).

Railway Bridges and Vehicles (Yang and Yau 2004)

In the research of railway bridges and vehicles, the loading is often a sequence of moving load instead of a single or very small number of loads. The loads produced by a moving train are repetitive in nature, implying that certain frequencies of excitation will be applied on the bridge and the dynamic responses of bridges will be apparently different (Bolotin 1964; Fryba 1972; Kurihara and Shimogo 1978; Chu 1979; Wu and Dai 1987; Savin 2001; Yang, Yau and Wu 2004). As to high-speed rail, scholars try to use other methods to simulate real high-speed train (Matsuura 1976; Chu 1986; Diana and Cheli 1989; Cai 1994; Hsu 1996; Yau 1996; Wu 2000). Researchers also discuss some other issues in high-speed rail, such as: effect of column stiffness (Hsu 1996), effect of elastic bearing (Yau 1996; Yau 2001), influence of sleepers and ballast layers (Museros 2002), and phenomena of resonance and cancellation for elastically supported (Yang 2004).

The previous research works about each aspect of the vehicle-bridge coupling system have been demonstrated specifically as above. Although there have been abundant results in this topic, the

bridge model, vehicle model or vehicle-bridge coupling relationships built in those works have many simplifications and the simulation results are limited in some special cases. In order to simulate the whole vehicle-bridge coupling system precisely and obtain its accurate dynamic responses results, it is necessary to continue to do some further work in that topic.

In this chapter, it proposes a co-simulation method to complete the simulation of vehicle-bridge coupling system in high-speed rail. Bridge structures are the traditional civil engineering structures and they are modeled by finite element method software MSC/NASTRAN to analyze. Vehicle system is a mechanical system, its nature is a multibody system and it is modeled by using dynamics of multibody system software MSC/ADAMS to simulate. The vehicle-bridge coupling relationships including wheel-rail contact geometric parameters, wheel-rail contact forces and track irregularity, are all introduced specifically in this chapter. The Matlab/Simulink is used to build a platform to make MSC/NASTRAN and MSC/ADAMS working together, and the vehicle-bridge coupling relationships are coded as a program block inputted into that platform. A co-simulation by using that Matlab/Simulink platform is realized and the simulation of whole vehicle-bridge coupling system in high-speed rail is completed. Various numerical examples of vehicle-bridge coupling system are calculated to illustrate the practicability and efficiency of the proposed co-simulation method.

6.2 Bridge Model Simulation - Finite Element Method

Bridge structure is an important subsystem in the whole vehicle-bridge coupling system, and it is actually a civil engineering structure. According to abundant simulation and analysis works about the civil engineering structures, especially, the research works about the bridge structures dynamic problems, there are mainly two methods to build the models of bridge structures: finite element method and modal expansion method.

In finite element method (FEM), the bridge structures are divided into finite number elements and the equilibrium equations for each element are established, then, the whole equilibrium equations of the whole structure are assembled by those element equations. With the help of the computer, the equilibrium equations are solved and the force and deformation in each element could be obtained. FEM is very accurate to simulate the civil engineering structures, but the solving difficulty will increase apparently if the elements number is increasing to very large.

In modal expansion method (MEM), the modal orthogonality condition is applied to decouple the structures motion partial differential equations, the responses under each mode are solved then, and the final dynamic responses will be obtained by modal superposition method. MEM could decrease the calculation degrees of freedom significantly, but its disadvantages are also apparent: (1) it can only be applied in linear vibration problems, (2) it cannot calculate the vibration

responses of some small parts in the structures, (3) it doesn't work well to the complex structures since there may be many modes needed to be considered.

In order to analyze large-size and complex bridges, and the deformations in them may be nonlinear, therefore, FEM is chosen in this research to simulate bridges and calculate their dynamic responses. With the fast developments in recent decades, there are many reliable and advanced FEM softwares in engineering areas, such as ANSYS, ABAQUS, and MSC/NASTRAN. Because it is easy and convenient to build models, the calculation is accurate, the analysis speed is fast, and the calculation results are reliable by using those FEM softwares, they are widely accepted and used in engineering areas. In this research, the MSC/NASTRAN is applied to build the bridge models and complete the dynamic responses calculation and analysis works.

6.2.1 FEM for Simulating the Bridge System

The basic process of the FEM for simulating the bridge system could be denoted as following steps:

1. Discretization of the continuous area

In dynamic problems of bridge structure, the questions are 4 dimensional equation since the time coordinate *t* is introduced into the problem. But when the FEM is applied, it only disperse the structure equations in space area whose coordinate is just *x*, *y*, *z*. After dispersing the structure in space, many basic elements are obtained from the original bridge structure.

2. Establishment of the interpolating function in each element

As to each element dispersed from the original bridge structure in step 1, the interpolating function for its displacement could be denoted as

$$u = Nu^e \tag{6-1}$$

where $u = \left[u(x,y,z,t), v(x,y,z,t), w(x,y,z,t)\right]^T$ is the displacement vector in the element, $N = \left[N_1 \quad N_2 \quad \dots \quad N_n\right]$ is the shape function matrix, and u^e is node displacement vector in the same element.

3. Motion equations of the whole bridge system

Base on Eq. (6-1), the strain vector and stress vector of each element can be derived as

$$\varepsilon = \Delta u = \Delta N u^e = B u^e \tag{6-2}$$

$$\sigma = D\varepsilon = DBu^e = Su^e \tag{6-3}$$

where Δ is the differential operator matrix, *B* is element strain matrix, *D* is elastic matrix, and *S* is stain matrix.

The strain energy and kinetic energy of the element can be written as

$$V^e = \frac{1}{2}\int_V \varepsilon^T \sigma dv = \frac{1}{2}\int_V u^{e^T} B^T DBu^e dv = \frac{1}{2} u^{e^T} \left(\int_V B^T DBdv\right) u^e = \frac{1}{2} u^{e^T} K^e u^e \tag{6-4}$$

$$T^e = \frac{1}{2}\int_V \rho \dot{u}^T \dot{u} dv = \frac{1}{2} \dot{u}^{e^T} \left(\int_V \rho N^T N dv\right) \dot{u}^e = \frac{1}{2} \dot{u}^{e^T} m^e \dot{u}^e \tag{6-5}$$

where $K^e = \int_V B^T DBdv$ is element stiffness matrix, and $m^e = \int_V \rho N^T N dv$ is element generalized mass matrix.

The equivalent nodal forces of the element body force and element damping force also can be denoted as

$$R^e = \int_V N^T q^e dv \tag{6-6}$$

$$R_f^e = \int_V N^T q_f^e dv = \int_V N^T \left(-\gamma \dot{u}\right) dv = \int_V N^T \left(-\gamma N \dot{u}^e\right) dv = -\left(\int_V \gamma N^T N dv\right) \dot{u}^e = -C^e \dot{u}^e \tag{6-7}$$

where $C^e = \int_V \gamma N^T N dv$ is the damping matrix.

Using coordinate transformation matrix, the element displacement vector and element force vector are transferred from local coordinate system to global coordinate system, then, total strain energy *V*, kinetic energy *T*, and total virtual work of exciting force and damping force δW can be

$$V = \sum_e V^e = \frac{1}{2} \sum_e u^{e^T} K^e u^e = \frac{1}{2} u^T \left(\sum_e K^e\right) u = \frac{1}{2} u^T K u \tag{6-8}$$

$$T = \sum_e T^e = \frac{1}{2} \sum_e \dot{u}^{e^T} m^e \dot{u}^e = \frac{1}{2} \dot{u}^T \left(\sum_e m^e\right) \dot{u} = \frac{1}{2} \dot{u}^T M \dot{u} \tag{6-9}$$

$$\delta W = \sum_e \delta W^e = \sum_e \delta u^{e^T} \left(R^e + R_f^e\right)^e = \delta u^T \left(\sum_e R^e + \sum_e R_f^e\right) = \delta u^T \left(R + R_f\right) \tag{6-10}$$

where $K = \sum_e K^e$ is the total stiffness matrix of bridge structure, $m = \sum_e m^e$ is the total mass matrix of bridge structure.

The total damping force of the bridge structure can be derived based on Eq. (6-7) as follows

$$R_f = \sum_e R_f^e = -\sum_e C^e \dot{u}^e = -\left(\sum_e C^e\right) \dot{u} = -C\dot{u} \tag{6-11}$$

where $C = \sum_e C^e$ is total damping matrix of bridge structure.

Substituting Eq. (6-8), Eq. (6-9), Eq. (6-10) and Eq. (6-11) into Lagrange equations, it will be

$$M\ddot{u} + Ku = R - C\dot{u} \quad \rightarrow \quad M\ddot{u} + C\dot{u} + Ku = R \tag{6-12}$$

and Eq. (6-12) is the motion equations of the whole bridge structure in global coordinate system.

4. Solution of the bridge system motion equations

With the help of the mathematics, the motion equations of the whole bridge structure are solved by many advanced numerical methods.

5. Strain and stress calculation of the bridge system

After the motion equations of the whole bridge structure are solved in step 4 and the nodal displacements are obtained, they can be transferred from global coordinate system to local coordinate system and the u^e are determined. Based on Eq. (6-2) and Eq. (6-3), the strain and stress of each element in bridge system can be calculated finally.

6.2.2 Modeling and Simulation of Bridge Structures in MSC/NASTRAN

A typical high-speed rail bridge structure is chosen to be simulated in this research, and the sketch of it is as shown in Fig. 6-1.

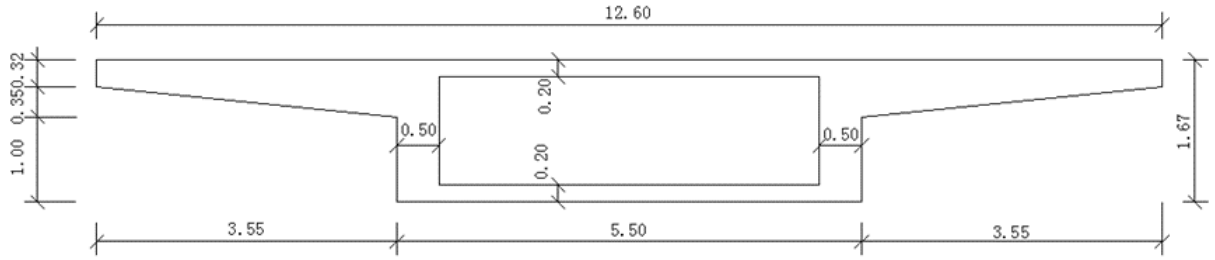

Side View of Bridge Main Beam (Unit: m)

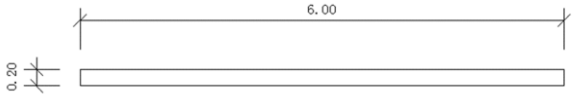

Side View of Floating Slab Track (Unite: m)

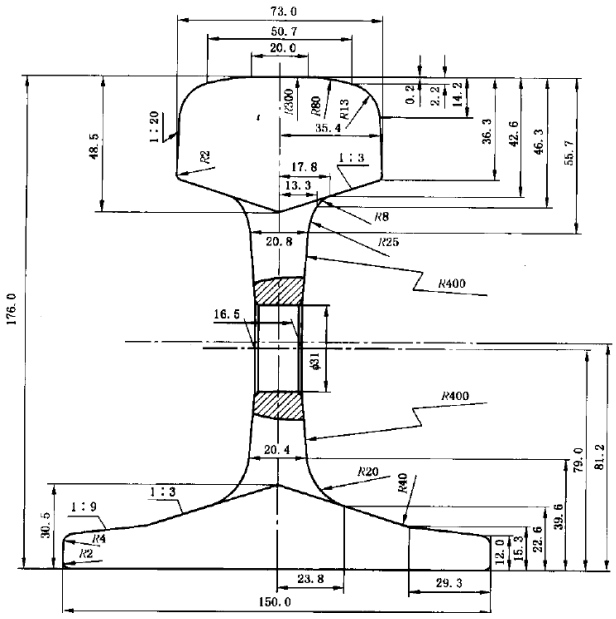

Side View of Rail (by Chinese Standard GB2585, Unit: mm)

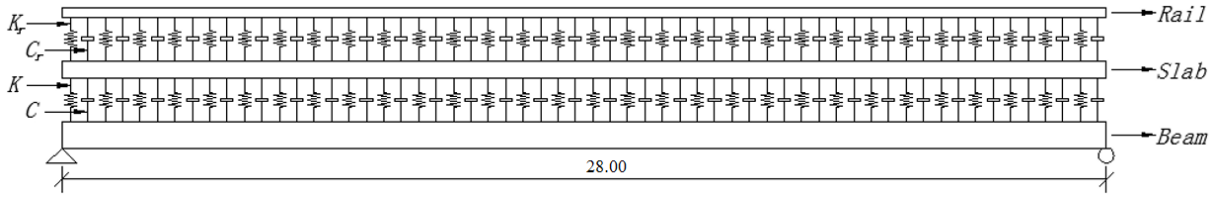

Front View of Bridge Structure (Unit: m)

Fig. 6-1. The sketch of bridge structure.

By using MSC/NASTRAN, that high-speed rail bridge structure shown in Fig. 6-1 is built as a FEM model which is as in Fig. 6-2.

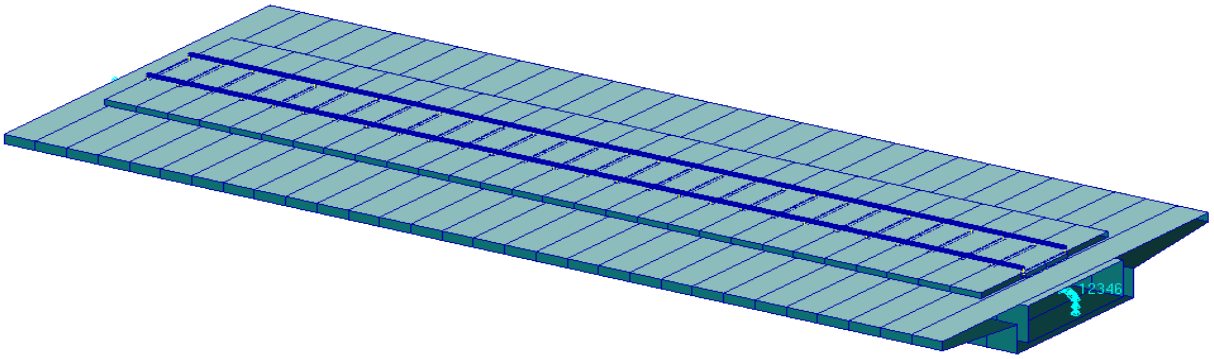

Fig. 6-2. The FEM model of bridge structure.

After the modeling work of bridge structure is completed as above, the bridge structure is transferred as a FEM model and it can be applied into the co-simulation of whole vehicle-bridge coupling system which will be introduced in Section 6.5.

6.3 Vehicle Model Simulation - Dynamics of Multibody System

Vehicle system is actually a mechanical system and it is also another important subsystem in the whole vehicle-bridge coupling system. Due to the limit of the major, in existed research works about the vehicle-bridge coupling system, the civil engineers and scholars make many simplifications on vehicle model and use the simple mechanical models to calculate the vehicle's vibration responses. In general, the development of vehicle model simulation is able to be denoted as several stages as follows

(1) Ignoring the vibrations of vehicle itself, the vehicle is simplified as moving constant forces;

(2) Considering the harmonic vibrations in vehicle but they have no coupling effects with bridge

vibrations, the vehicle is simplified as moving harmonic forces;

(3) Considering the coupling effects of vehicle vibrations and bridge vibrations, the vehicle is modeled as moving mass;

(4) The vibrations in all three dimensions are considered, and the vehicle is modeled as a multiple degrees of freedom system of train body, bogies and wheels interconnected by spring and damper. Until now, the model of mass blocks connected by spring and damper is still widely applied in the research works in civil engineering now. The accuracy of the model is only improved by increase the number of the degree of freedom in the model.

With the development of relative research works, the requirements on the accuracy of vehicle model will be more and more, and the existed method used to simulate the vehicle will be not enough. Based on the nature that the vehicle system is actually a multibody system and it is better to use mechanical engineering view to think about it, therefore, the dynamics of multibody system will be applied to simulate and analyze the vehicle system in this research.

Dynamics of multibody system (DMS), is a subject to study the motion and dynamics of the multibody system which consists of interconnected rigid and deformable bodies. It is based on analytical mechanics and is applied to engineering systems such as a wide variety of machines and all kind of vehicles. In mechanical engineering and automobile engineering, the engineers and scholars just use this theory to simulate and analyze the machines and vehicles and it is much better

and more accuracy than the method used in civil engineering as introduced above.

There are also many reliable and advanced DMS softwares in engineering areas, such as RECURDYN, SIMPACK, and MSC/ADAMS. As the professional software for analyzing the mechanical system, all of those softwares are easy and convenient to build models, the calculation is accurate, the analysis speed is fast, and the calculation results are reliable. In this research, the MSC/ADAMS is applied to build the vehicle models and complete the dynamic responses calculation and analysis works.

6.3.1 DMS for Simulating the Vehicle System

In multibody system, the bodies are rigid or flexible bodies, and the link which is the connection of two or more bodies is defined as certain constraints that restrict the relative motion of those bodies. The motion of the constrained bodies is described by equations that result from Newton's second law, and those equations are usually derived from the Newton-Euler equation or Lagrange's equations. In general, the motion equations of the multibody system can be denoted as

$$M\left(q,t\right)\ddot{q}+\Phi_q^T\left(q,t\right)\lambda-Q\left(q,\dot{q},t\right)=0 \tag{6-13a}$$

$$\Phi\left(q,t\right)=0 \tag{6-13b}$$

where q, $\dot{q}$, $\ddot{q}\in R^n$ are the generalized coordinates and their first order derivatives and second order derivatives, respectively, $\lambda\in R^m$ is the Lagrange multiplier, $M\in R^{n\times n}$ is the mass matrix

which depends on the generalized coordinates, $\Phi_q \in R^{m\times n}$ is constraint Jacobi matrix respect to the coordinates, $Q \in R^n$ is exciting force matrix, $\Phi \in R^m$ is the constraint conditions.

Once those motion equations of the whole vehicle systems are established as Eq. (6-13), abundant advanced numerical solution methods could be applied to solve them and the dynamic responses of the vehicle systems can be obtained finally. This is just the basic theory and process to show how the DMS softwares simulate vehicle systems and solve their vibration problems.

6.3.2 Modeling and Simulation of Vehicle Structures in MSC/ADAMS

Since this research is about the high-speed rail engineering, a typical high-speed rail train, CRH5, is chosen to be simulated in here and the simple sketch of it is as shown in Fig. 6-3.

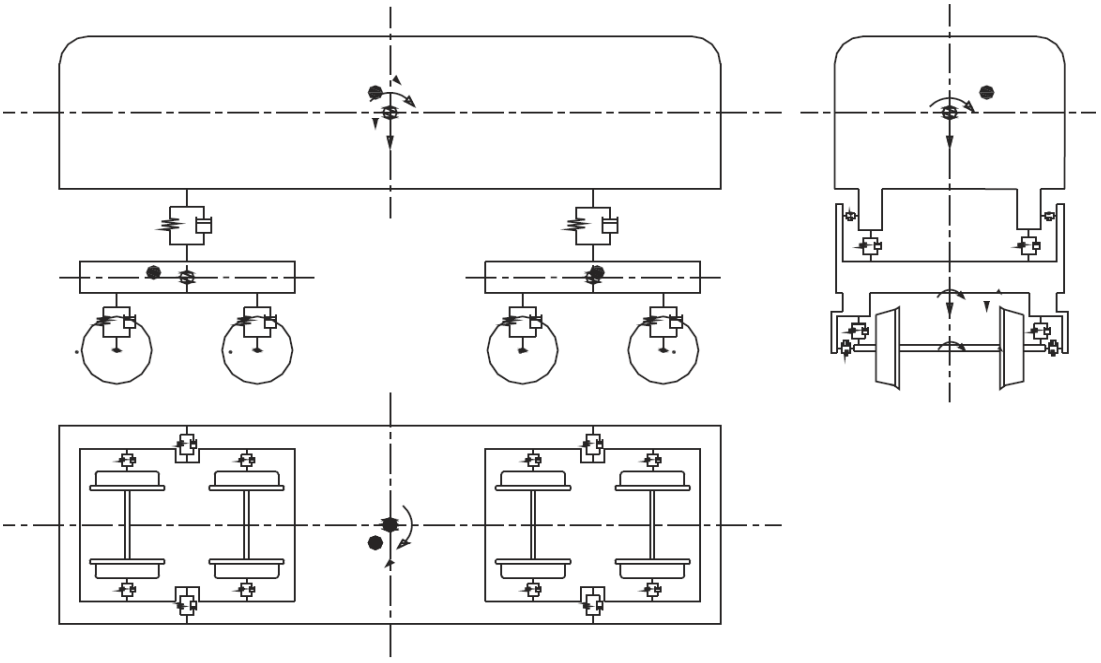

Fig. 6-3. The sketch of CRH5 high-speed rail train system (by Xin and Gao 2011).

By using MSC/ADAMS, that high-speed rail train system shown in Fig. 6-3 is built as a DMS model which is as in Fig. 6-4 and Fig. 6-5.

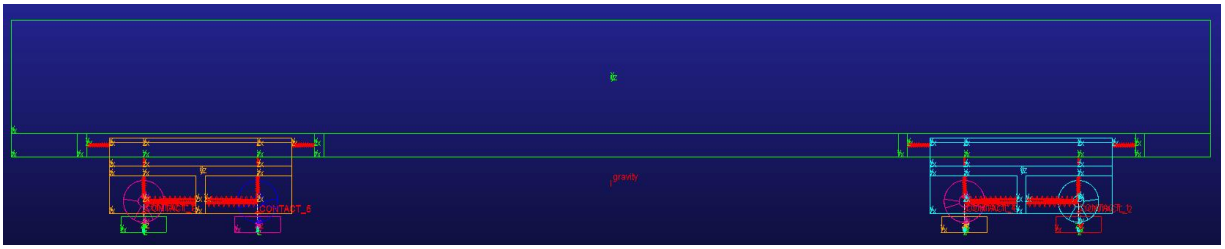

Front View

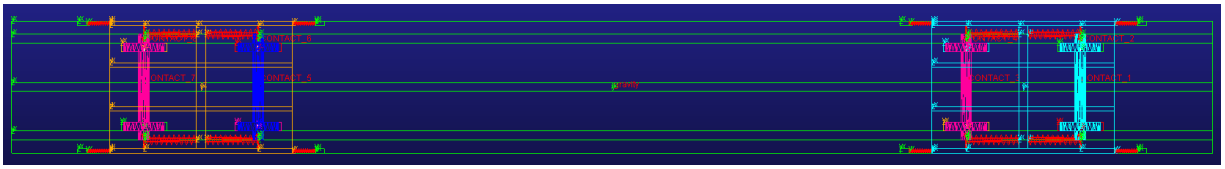

Plan View

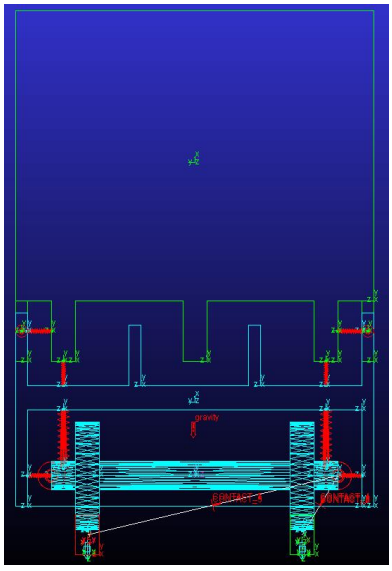

Side View

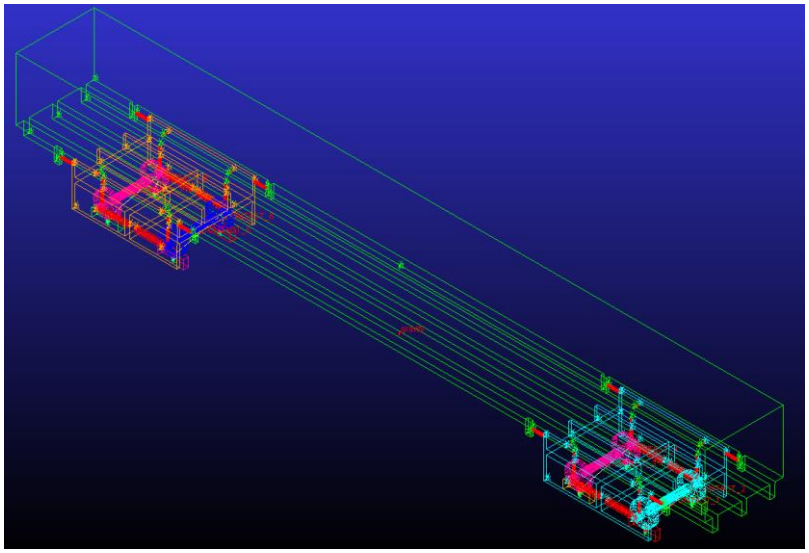

Isometric View

Fig. 6-4. The DMS model of CRH5 high-speed rail train system.

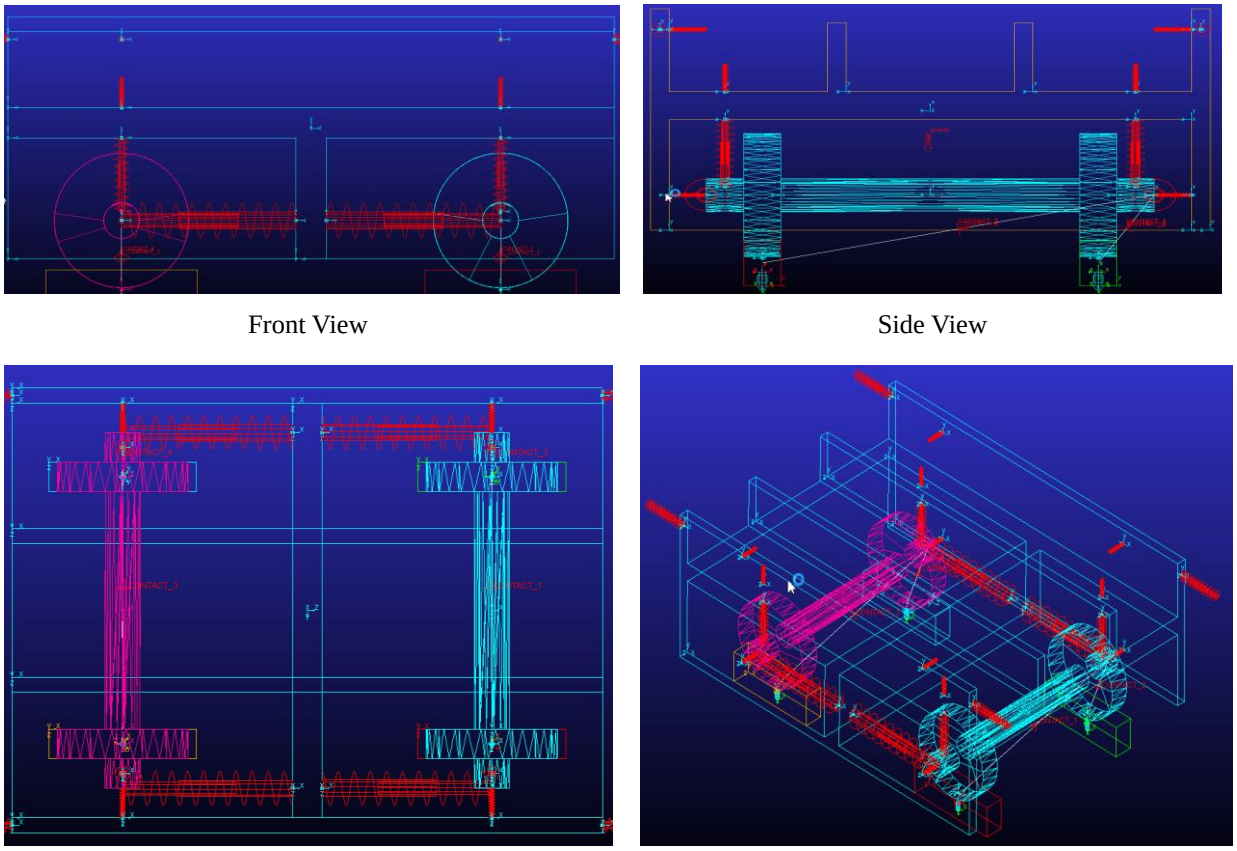

Front View Side View

Plan View Isometric View

Fig. 6-5. The DMS model of CRH5 high-speed rail train suspension system.

The modeling work of vehicle system can be completed by MSC/ADAMS as introduced above. In this way, the train system is transferred as a DMS model and it can be applied into the co-simulation of whole vehicle-bridge coupling system which is introduced in Section 6.5.

6.4 Vehicle-Bridge Coupling Relationship

As shown in Section 6.2 and Section 6.3, the bridge subsystem and vehicle subsystem are simulated and analyzed, respectively. In this section, the vehicle-bridge coupling relationship will

be introduced and link those two subsystems together to form the final vehicle-bridge coupling system.

In fact, the main vehicle-bridge coupling relationship is the coordinative relationship of the displacement and force between vehicle and bridge, and it can be denoted as follows

1. At the wheel and rail contact area, the displacement of vehicle and the displacement of bridge are coordinative;

2. At the wheel and rail contact area, the force and reacting force between wheel and rail are equivalent.

The vehicle-bridge coupling system just uses those two coordinative relationships to combine the vehicle subsystem and bridge subsystem together, and complete the vibration analysis of the whole system.

Except those two coordinative relationships, the track irregularity is another important issue in the vehicle-bridge coupling relationship and it must be considered in whole system vibration analysis.

6.4.1 Wheel-Rail Contact Geometric Parameters

When the train is running on rails, the wheels will do horizontal motion and sidewinder motion relative to rails and the wheel-rail contact point location will be changed with the time. If the contact point location is different, the wheel-rail contact geometric parameters are also changed

since they depends on the specific contact point location. The main wheel-rail contact geometric parameters are shown in Fig. 6-6 and they include:

1. Contact angle of left wheel and right wheel: δ_L, δ_R;

2. Real rolling radius of left wheel and right wheel: r_L, r_R;

3. Wheel radius of curvature for left wheel and right wheel at wheel-rail contact point: ρ_{wL}, ρ_{wR};

4. Rail radius of curvature for left rail and right rail at wheel-rail contact point: ρ_{tL}, ρ_{tR}.

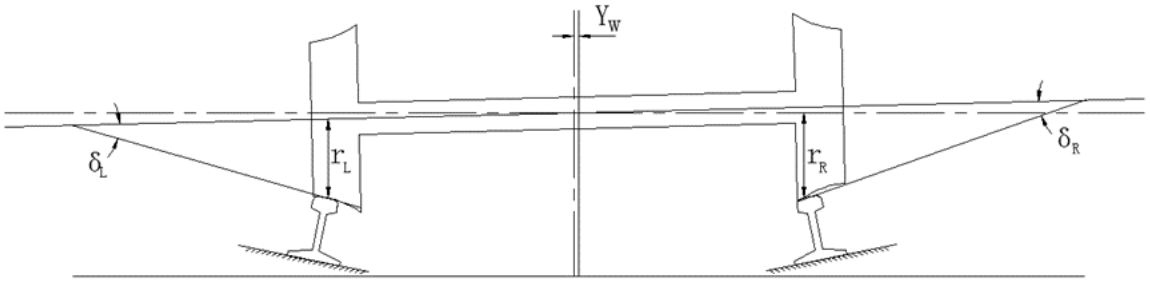

Fig. 6-6. The diagrammatic sketch of wheel-rail contact geometric relationship.

In this section, the profiles for both wheel and rail tread are introduced firstly, then, a left-right wheel-rail equidistant iteration method is applied to determine the specific location of wheel-rail contact point and the wheel-rail contact geometric parameters at that location can be obtained.

6.4.1.1 Profile of Wheel Tread

All wheels in trains follow the national standards and their tread profiles are made as the same. The profile of the train wheel tread consists of several arcs and straight lines, and one typical wheel tread profile which is adopted in this research can be shown as in Fig. 6-7.

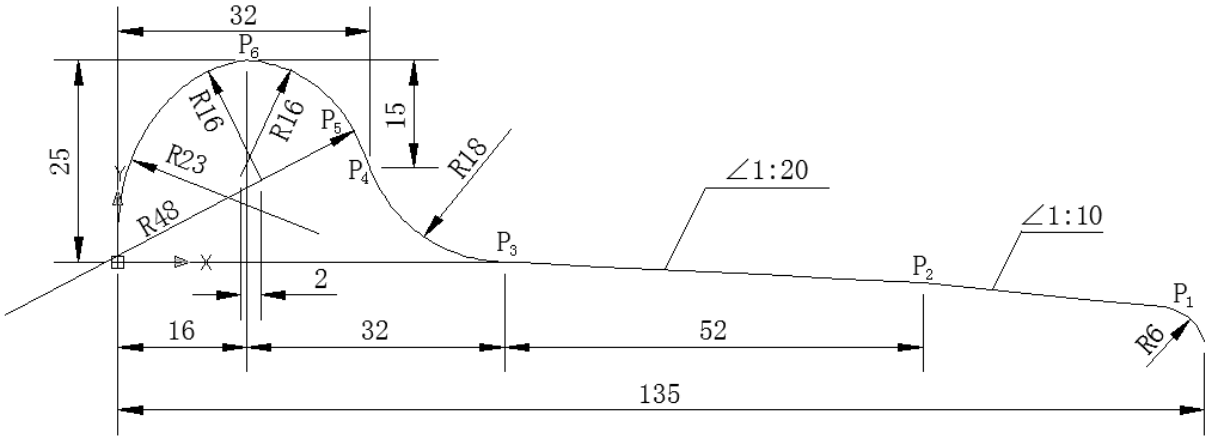

Fig. 6-7. The profile of LM train wheel tread.

The specific details about the wheel tread profile are described as the following formulations:

$$f_1(x) = 4.2265 + \left[529 - (x-23)^2\right]^{1/2}, \quad x \in [0.0000, 6.5714] \tag{6-14a}$$

$$f_2(x) = 9.1255 + \left[256 - (x-18)^2\right]^{1/2}, \quad x \in [6.5714, 16.0000] \tag{6-14b}$$

$$f_3(x) = 9.0313 + \left[256 - (x-15)^2\right]^{1/2}, \quad x \in [16.0000, 29.3351] \tag{6-14c}$$

$$f_4(x) = -5.1822 + \left[2304 - (x+13.6701)^2\right]^{1/2}, \quad x \in [29.3351, 31.2716] \tag{6-14d}$$

$$f_5(x) = 17.9996 - \left[324 - (x-48.1247)^2\right]^{1/2}, \quad x \in [31.2716, 48.0000] \tag{6-14e}$$

$$f_6(x) = -0.05(x-48), \quad x \in [48.0000, 100.0000] \tag{6-14f}$$

$$f_7(x) = -0.1(x-100) - 2.6, \quad x \in [100.0000, 129.8623] \tag{6-14g}$$

$$f_8(x) = -11.5565 + \left[36 - (x-129.2653)^2\right]^{1/2}, \quad x \in [129.8623, 135] \tag{6-14h}$$

Significantly, the wheel-rail contact point can be only located between point P_1 and point P_6.

6.4.1.2 Profile of Rail Tread

It is the same as the train wheel tread profile introduced in Section 6.4.1.1, the profiles of rail tread are also the same according to the national standards. One typical rail tread profile is chosen in this research and it is shown as in Fig. 6-8.

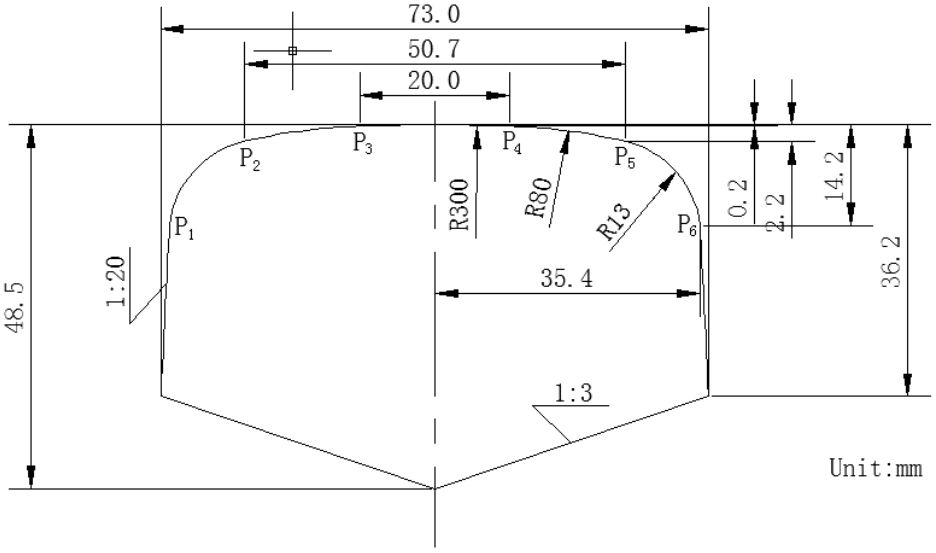

Fig. 6-8. The profile of standard rail tread.

The specific details about the rail tread profile are also described as the following formulations:

$$f_1(x) = -250 + \left[250^2 - x^2\right]^{1/2}, \quad x \in [0.0000, 10.0000] \tag{6-15a}$$

$$f_2(x) = -80.1573 + \left[80^2 - (x - 7.3874)^2\right]^{1/2}, \quad x \in [10.0000, 25.3500] \tag{6-15b}$$

$$f_3(x) = -14.8648 + \left[13^2 - (x - 22.4795)^2\right]^{1/2}, \quad x \in [25.3500, 35.4000] \tag{6-15c}$$

$$f_4(x) = -20(x - 35.4) - 14.2, \quad x \in [35.4000, 36.5000] \tag{6-15d}$$

and the profile in $x \in [-36.5000, 0]$ is just the symmetry comparing with the one above.

From Fig. 6-8, the wheel-rail contact point can be only located between point P_1 and point P_6.

6.4.1.3 Determination of Wheel-Rail Contact Geometric Parameters

The details about the wheel tread and rail tread are shown in Section 6.4.1.1 and Section 6.4.1.2, and all geometric parameters of those profiles are already given. In order to determine the wheel-rail contact geometric parameters at each time, the key problem is how to confirm the exact location of the wheel-rail contact point. In this research, a left-right wheel-rail equidistant iteration method is adopted to solve that problem and determine the wheel-rail contact geometric parameters.

The theoretical principle for that left-right wheel-rail equidistant iteration method is: the vertical distance between wheel and rail must be zero at the location of wheel-rail contact point, otherwise, it must be nonzero at other locations. Based on that principle, if the wheels are moved up a certain distance, the condition for wheel-rail contact point location will be changed as that the vertical distance between wheel and rail must be the minimum one, which is as shown in Fig. 6-9.

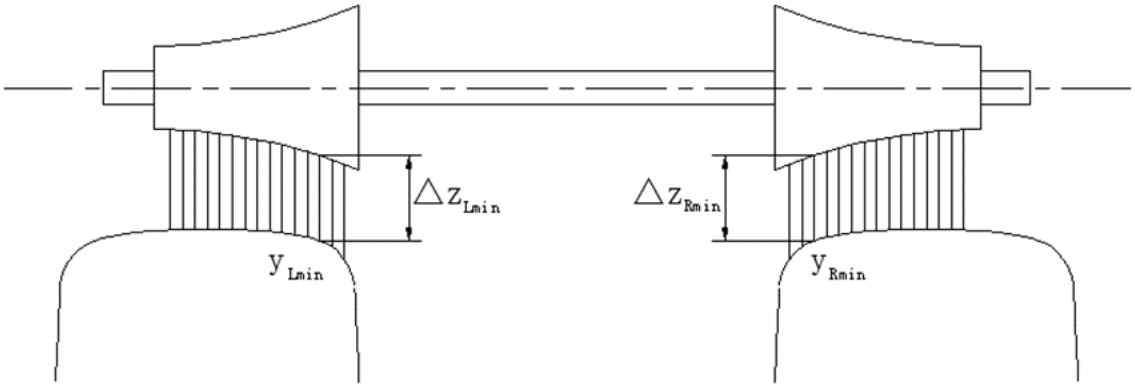

Fig. 6-9. The calculation principle of left-right wheel-rail equidistant iteration method.

According to Fig. 6-9 and assuming the wheels are in one horizontal location, the horizontal coordinate y can be divided into several small distances and the vertical distances Δz_L and Δz_R between wheel and rail corresponding to each horizontal distance y_L and y_R can be calculated. Checking the values of all Δz_L and Δz_R, and the minimum values Δz_{Lmin} and Δz_{Rmin} can be found and their corresponding y coordinate can be obtained as y_{Lmin} and y_{Rmin}.

If $\Delta z_{L\min} = \Delta z_{R\min}$, then, the left wheel and right wheel can both touch the rail at the same time, and y_{Lmin}, y_{Rmin} are the exact wheel-rail contact point locations.

If $\Delta z_{L\min} \neq \Delta z_{R\min}$, the left wheel and right wheel cannot touch the rail at the same time and y_{Lmin}, y_{Rmin} are not the real wheel-rail contact point locations. In this case, a rotation of the wheels according to longitudinal axis must be done to modify the sidewinder angle. When $\Delta z_{L\min} > \Delta z_{R\min}$, the counterclockwise rotation angle γ can be chosen as

$$\gamma = \frac{\Delta z_{R\min} - \Delta z_{L\min}}{y_{R\min} - y_{L\min}} \tag{6-16}$$

After rotating the wheels as the rotation angle γ, the process introduced above need to be repeated and it needs to check if the minimum values Δz_{Lmin} and Δz_{Rmin} are equal. But due to the numerical error, it is impossible to achieve the absolute equivalent condition and it usually can be accepted once the condition $\left|\Delta z_{R\min} - \Delta z_{L\min}\right| < \varepsilon$ (ε is providing error) is satisfied.

The iteration process as shown above should be done several times, and it can be stopped once $\left|\Delta z_{R\min} - \Delta z_{L\min}\right| < \varepsilon$ is satisfied. In this way, the exact location of the wheel-rail contact point y_{Lmin} and y_{Rmin} can be determined, and the final sidewinder angle can be calculated by

$$\varphi_W = \varphi_{W0} + \sum_{i=1}^{k} \gamma_i \tag{6-17}$$

When the exact location of the wheel-rail contact point y_{Lmin} and y_{Rmin} are obtained, according to the specific geometric parameters given in Section 6.4.1.1 and Section 6.4.1.2, the wheel-rail contact geometric parameters can be determined finally and they will be applied to calculate the wheel-rail contact forces introduced in next section.

6.4.2 Determination of Wheel-Rail Contact Forces

The wheel-rail contact forces are the acting and reacting forces between wheel and rail when they contact each other, and they are just located at the wheel-rail contact area. The wheel-rail contact forces which act on wheels are equivalent as the ones acting on rails but their directions are opposite. There are two kinds of contact forces in wheel-rail contact forces: wheel-rail normal contact force and wheel-rail tangential contact force. The Hertz contact theory will be applied to calculate the wheel-rail normal contact force and the wheel-rail tangential contact force will be determined by Kalker linear theory and Shen's theory in this research.

6.4.2.1 Determination of Wheel-Rail Normal Contact Force

The wheel-rail normal contact force depends on the normal compression displacement between wheel and rail, therefore, according to Hertz nonlinear contact theory, it can be calculated as

$$p(t)=\left[\frac{1}{G}\delta Z(t)\right]^{2/3} \tag{6-18}$$

where G is the wheel-rail contact constant, $G=3.86R^{-0.115}\times10^{-8}\left(m/N\right)^{2/3}$, R is radius of the wheel, $\delta Z(t)$ is the compression displacement between wheel and rail.

Once the compression displacement between wheel and rail is obtained by the analysis as shown in Section 6.4.1, the wheel-rail normal contact force can be calculated as Eq. (6-18) directly. If $\delta Z(t)<0$, it means that the wheel breaks away from the rail and $p(t)=0$ in this case.

6.4.2.2 Determination of Wheel-Rail Tangential Contact Force

When two rigid bodies repress each other and a trundle between them is allowed, the creep phenomenon will be existed and a contact area, whose shape is an oval according to Hertz theory, will be produced around their contact point. The wheel-rail tangential contact force is located in that oval contact area and can be calculated by Kalker linear theory and Shen's theory in here.

Before calculating the major semiaxis a and minor semiaxis b of the oval contact area, the

parameters ρ and β are introduced and defined as

$$\frac{1}{\rho}=\frac{1}{4}\left[\frac{1}{r}+\left(\frac{1}{\rho_w}+\frac{1}{\rho_t}\right)\right] \tag{6-19}$$

$$\beta=\arccos\left[\frac{\rho}{4}\left|\frac{1}{r}-\frac{1}{\rho_w}-\frac{1}{\rho_t}\right|\right] \tag{6-20}$$

where r is rolling radius of the wheel, ρ_w is the wheel radius of curvature at wheel-rail contact point, ρ_t is rail radius of curvature at wheel-rail contact point.

With the β obtained by Eq. (6-20) and checking the Table. (6-1), the values of the parameters m, n can be determined.

Table 6-1. The relationship of β and the values of m, n

β	0°	10°	20°	30°	35°	40°	45°	50°
m	∞	6.612	3.778	2.731	2.397	2.130	1.926	1.754
n	0	0.319	0.408	0.493	0.530	0.567	0.604	0.641
β	55°	60°	65°	70°	75°	80°	85°	90°
m	1.611	1.486	1.378	1.284	1.202	1.128	1.061	1.000
n	0.678	0.717	0.759	0.802	0.846	0.893	0.944	1.000

When the wheel and rail contact each other, and both of them are made of steel which have Poisson ratio $\upsilon=0.3$ and Young's modulus $E=200Gpa$, the intermediate variable a_e, b_e are defined:

If $\rho/r\le 2$: $a_e=0.1506m\left(\frac{\rho}{r}\right)^{1/3}\times10^{-3}$, $b_e=0.1506n\left(\frac{\rho}{r}\right)^{1/3}\times10^{-3}$ (6-21a)

If $\rho/r>2$: $a_e=0.1506n\left(\frac{\rho}{r}\right)^{1/3}\times10^{-3}$, $b_e=0.1506m\left(\frac{\rho}{r}\right)^{1/3}\times10^{-3}$ (6-21b)

and the multiplying constant is always existed as $a_e b_e = 22.68mn\left(\frac{\rho}{r}\right)^{2/3} \times 10^{-9}$ (6-21c)

The major semiaxis *a* and minor semiaxis *b* of the oval contact area are determined as follows

$$a = a_e \left(Nr\right)^{1/3},\ \ b = b_e \left(Nr\right)^{1/3},\ \ ab = a_e b_e \left(Nr\right)^{2/3},\ \ a/b = a_e / b_e \tag{6-22}$$

where *N* is the wheel-rail normal contact force calculated in Section 6.4.2.1 as Eq. (6-18).

The creep parameters f_{ij} are calculate as follows

$$f_{11} = C_{11} Eab,\ \ f_{22} = C_{22} Eab,\ \ f_{23} = C_{23} E\left(ab\right)^{3/2},\ \ f_{33} = C_{33} E\left(ab\right)^{2} \tag{6-23}$$

where the constants C_{ij} are Kalker parameters and they can be checked out from Table. (6-2).

Table 6-2. The calculation table for Kalker parameters C_{ij} $(\upsilon = 0.3)$

a/b	C_{11}	C_{22}	C_{23}	C_{33}	a/b	C_{11}	C_{22}	C_{23}	C_{33}
0.1	1.35	0.98	0.195	3.34	0.9	1.70	1.49	0.628	0.425
0.2	1.37	1.01	0.242	1.74	0.8	1.75	1.56	0.689	0.396
0.3	1.40	1.06	0.288	1.18	0.7	1.81	1.65	0.768	0.366
0.4	1.44	1.11	0.328	0.925	0.6	1.90	1.76	0.875	0.336
0.5	1.47	1.18	0.368	0.766	0.5	2.03	1.93	1.04	0.304
0.6	1.50	1.22	0.410	0.661	0.4	2.21	2.15	1.27	0.275
0.7	1.54	1.28	0.451	0.588	0.3	2.51	2.54	1.71	0.246
0.8	1.57	1.32	0.493	0.533	0.2	3.08	3.26	2.64	0.215
0.9	1.60	1.39	0.535	0.492	0.1	4.60	5.15	5.81	0.183
1.0	1.60	1.43	0.579	0.458	-	-	-	-	-

The nominal velocity of the wheel on the rail is calculated as

$$V' = \frac{1}{2}\left(V + \frac{r}{R_W} V \cos R_{ZW} \right) \tag{6-24}$$

where V is the velocity of the vehicle, r is rolling radius of the wheel, R_W is real rolling radius of wheel at contact point, and R_{ZW} is panning angle of the wheels.

Since the velocities of wheel and rail at their contact surface are different, the creep ratio in the local coordinate is existed and is calculated by

$$\varepsilon_x = \frac{\dot{X}_W - \dot{X}_t}{V'}, \quad \varepsilon_y = \frac{\dot{Y}_W - \dot{Y}_t}{V'}, \quad \varepsilon_{sp} = \frac{\dot{R}_{ZW} - \dot{R}_{Zt}}{V'} \tag{6-25}$$

where $\dot{X}_W$, $\dot{Y}_W$, $\dot{R}_{ZW}$ are the local velocities of wheel in x, y and panning angle direction, and $\dot{X}_t$, $\dot{Y}_t$, $\dot{R}_{Zt}$ are the local velocities of rail deformation in x, y and panning angle direction.

Finally, according to Kalker linear creep theory, the wheel-rail tangential contact force in linear range can be determined by the equations as follows

$$F_X = -f_{11}\varepsilon_x \tag{6-26a}$$

$$F_Y = -f_{22}\varepsilon_y - f_{23}\varepsilon_{sp} \tag{6-26b}$$

$$M_Z = f_{23}\varepsilon_y - f_{33}\varepsilon_{sp} \tag{6-26c}$$

Kalker linear creep theory as shown above is only applied in small creep ratio case, but it cannot calculate the creep force accurately when there is large creep happened in the wheel-rail contact area. In this research, Shen's theory is applied to modify the Kalker linear creep theory to determine

the wheel-rail tangential contact force in nonlinear range. Based on Eq. (6-26), the total creep force is combined the longitudinal creep force F_X and horizontal creep force F_Y as

$$F = \sqrt{F_X^2 + F_Y^2} \tag{6-27}$$

A creep force parameter F' is defined as

If $F \le 3fN$, then $F' = fN\left[\frac{F}{fN} - \frac{1}{3}\left(\frac{F}{fN}\right)^2 + \frac{1}{27}\left(\frac{F}{fN}\right)^3\right]$ (6-28a)

If $F > 3fN$, then $F' = fN$ (6-28b)

where $f = 0.25$ is friction factor between wheel and rail.

Introducing compensation factor $\varepsilon = F'/F$, the modified wheel-rail tangential contact force in nonlinear range are calculated as follows

$$F_X' = \varepsilon F_X, \quad F_Y' = \varepsilon F_Y, \quad M_Z' = \varepsilon M_Z \tag{6-29}$$

6.4.3 Track Irregularity

Track irregularity is the geometric dimension error of the two rail tracks, on which trains are running, comparing with their ideal locations. Based on abundant real engineering projects, there are mainly four types of the track irregularity and they can be shown as in Fig. 6-10. Due to the limit of the construction precision and the effects of the railway operation, it is impossible to eliminate the track irregularity totally and it is existed in all rail tracks objectively.

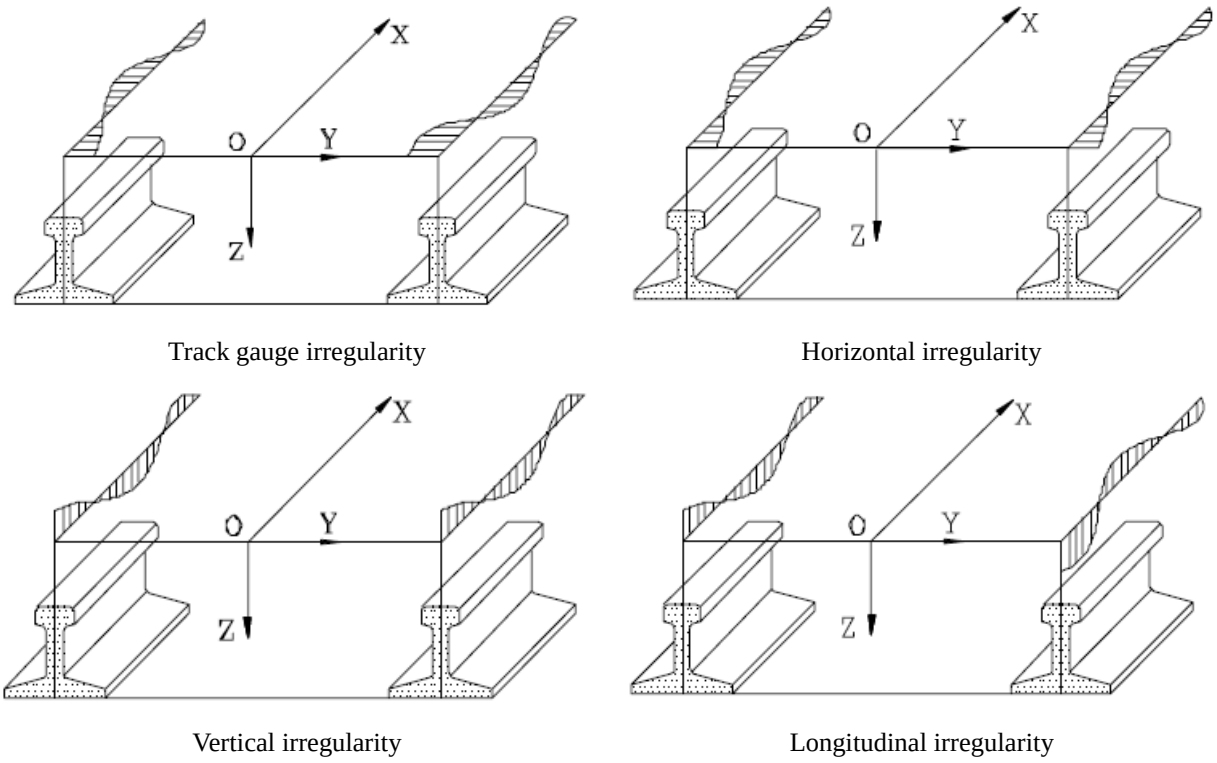

Fig. 6-10. The four types of track irregularity (by Li 2000).

Track irregularity brings the vibrations to vehicles which are running on the track and it is the main excitation for the vehicle vertical vibration. Track irregularity is also the main reason to produce the track structure vibrations and failures. Specifically speaking, track irregularity changes the wheel-rail contact relationships and affects the dynamic properties of wheel-rail system. The vibrations produced by track irregularity will be transferred to both vehicle system and bridge system at the wheel-rail contact point, and the whole vehicle-bridge coupling system will be affected significantly. Therefore, it is very necessary and important to analyze and calculate track irregularity, and input it into the whole vehicle-bridge coupling system in here.

According to previous research works, all kinds of the track irregularity existed in real rail tracks are the superposition of several random rough waves which have different wavelength, phase and amplitude, and it is just a complicated random process relative to rail line. In this way, only the statistical parameters in random process theory can be applied to describe the track irregularity. In this research, a track irregularity power spectrum which is formulated by U.S. Department of Transportation – Federal Railroad Administration (FRA) is adopted as follows

Longitudinal irregularity: $S_a(\Omega) = \dfrac{k \cdot A_a \cdot \Omega_c^2}{\Omega^2\left(\Omega^2 + \Omega_c^2\right)}$ (6-30a)

Vertical irregularity: $S_v(\Omega) = \dfrac{k \cdot A_v \cdot \Omega_c^2}{\Omega^2\left(\Omega^2 + \Omega_c^2\right)}$ (6-30b)

Horizontal and track gauge irregularity: $S_c(\Omega) = S_g(\Omega) = \dfrac{4k \cdot A_v \cdot \Omega_c^2}{\left(\Omega^2 + \Omega_c^2\right)\left(\Omega^2 + \Omega_s^2\right)}$ (6-30c)

where $S(\Omega)$ is track power spectrum ($cm^2/(rad/m)$), Ω is the space angular frequency of track irregularity (rad/m), k is safety factor (0.25-1.0, usually choose 0.25), Ω_c, Ω_s are cut frequency (rad/m), A_v, A_a are roughness constant ($cm^2 \cdot rad/m$). The values for those parameters are divided as six grades and they are shown as in Table. (6-3).

Based on track irregularity power spectrum shown in Eq. (6-30), a numerical method can be used to calculate the track irregularity analog quantity. Since the track irregularity random function is a stable Gauss random process, the triangle series superposition method can be applied in here as

$$\omega(x) = \sqrt{2}\sum_{k=1}^{N}\sqrt{S(\omega_k)\Delta\omega}\cos(\omega_k x + \phi_k) \quad (6\text{-}31)$$

where $\omega(x)$ is track irregularity produced by power spectrum, $S(\omega_k)$ is the track irregularity power spectrum, ω_k ($k=1,2,\cdots,N$) is the considered frequency, $\Delta\omega$ is the frequency bandwidth, ϕ_k is the phase corresponding to *k*th frequency.

Table 6-3. The parameters for U.S. track irregularity power spectrum.

Parameters		Line grade					
		1	2	3	4	5	6
A_v $(cm^2 \cdot rad/m)$		1.2107	1.0181	0.6816	0.5376	0.2095	0.0339
A_a $(cm^2 \cdot rad/m)$		3.3634	1.2107	0.4128	0.3027	0.0762	0.0339
Ω_s (rad/m)		0.6046	0.9308	0.8520	1.1312	0.829	0.4380
Ω_c (rad/m)		0.8245	0.8245	0.8245	0.8245	0.8245	0.8245
Maximum velocity (km/h)	Freight train	16	40	64	96	128	176
	Passenger train	24	48	96	128	144	176

Until here, according to the track irregularity power spectrum formulated by national standard, the track irregularity in different directions can be calculated by using the triangle series superposition method, and they can be inputted into the vehicle-bridge coupling system now.

6.4.4 Vehicle-Bridge Coupling Relationship for Whole System Analysis

As introduced at the beginning of this Section 6.4, the main vehicle-bridge coupling relationship is the coordinative relationship of the displacement and force between vehicle and bridge. The introductions about the wheel-rail contact geometric parameters, wheel-rail contact forces, and track irregularity are shown in the sections above, hence, the vehicle-bridge coupling relationship

for the final calculation works in the whole system can be denoted as follows.

1. In one time step, the wheel-rail contact forces calculated from Section 6.4.2 will act and react on both vehicle system and bridge structure at the same time. As the exciting forces to each subsystem, it will produce the corresponding dynamic responses in those two subsystems. The force equivalent condition can be denoted as a general equations as follows

$$F_{bv}^{i} = -F_{vb}^{i} \tag{6-32}$$

where F_{bv}^{i} are the wheel-rail contact forces acted on vehicle system at wheel-rail contact point *i*, and F_{vb}^{i} are the wheel-rail contact forces acted on bridge structure at wheel-rail contact point *i*.

2. In one time step, the bridge structure deformation obtained from Section 6.2, vehicle wheel deformation calculated from Section 6.3 and the track irregularity obtained from Section 6.4.3 satisfy displacement coordinative condition at wheel-rail contact point.

$$u_{v}^{i} = u_{b}^{i} + y_{s} \tag{6-33}$$

where u_{v}^{i} is vehicle wheel deformation at wheel-rail contact point *i*, u_{b}^{i} is bridge deformation at wheel-rail contact point *i*, and y_{s} is the track irregularity at wheel-rail contact point *i*.

Based on those two specific coupling relationships introduced above and synthesizing the calculation methods in Section 6.4.1 to Section 6.4.2, the simulation and calculation of vehicle system in Section 6.3 and bridge system in Section 6.2 can be linked together and the unified

simulation for the whole vehicle-bridge coupling system can be completed. That whole system simulation will be done by co-simulation method which is introduced in next section.

6.5 Co-Simulation of Vehicle-Bridge Coupling System

This section will introduce how to use co-simulation method to complete the simulation and calculation works of the whole vehicle-bridge coupling system.

As shown in Section 6.2 to Section 6.4, the bridge structures are molded by FEM software MSC/NASTAN, the vehicle systems are simulated by DMS software MSC/ADAMS, and the coupling relationships between those two subsystems are also introduced already. Then, the main problems are how to link those two different softwares together, make them work with each other at the same time and how to input and consider the coupling relationships of them in the whole simulation system. In this research, a co-simulation method is adopted to solve those problems and realize the simulation and operation of the whole vehicle-bridge coupling system.

Co-simulation, is a method to make multiple different softwares working together and exchanging the needed data with each other, and finally output the response results of each subsystem from its own software under the constraint conditions. The core problem of the co-simulation is just how to make multiple different softwares working together at the same time. Based on those

requirements, since Matlab/Simulink platform is able to control the operation of both MSC/NASTRAN and MSC/ADAMS, the co-simulation is achieved by coding the program in Matlab/Simulink platform and the coupling relationships of those two subsystems are also inputted in Matlab/Simulink platform to ensure the data from each software could be output, processed and exchanged with another software. In this way, the simulation of the whole vehicle-bridge coupling system can be realized and the general process is as the flowchart in Fig. 6-11.

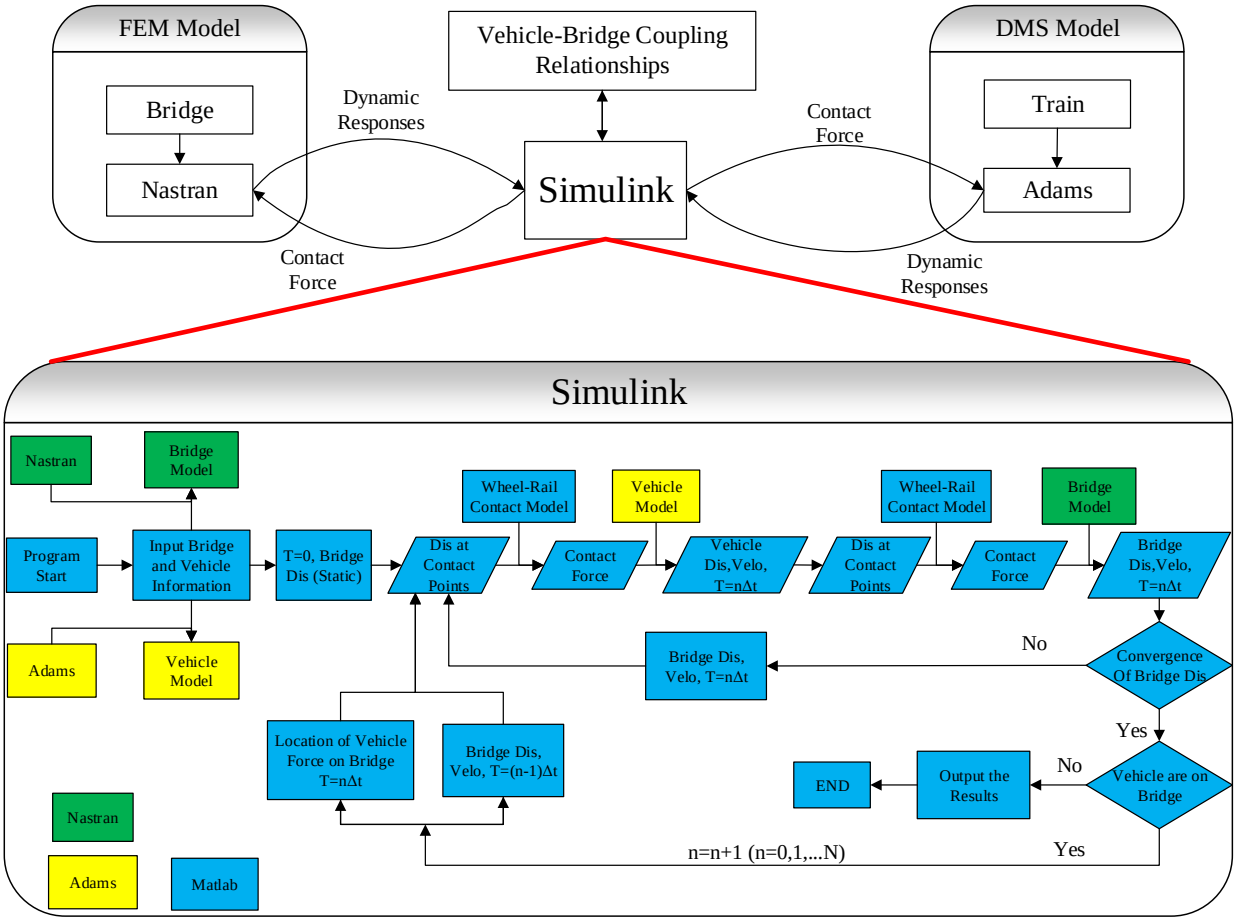

Fig. 6-11. Flowchart of the whole vehicle-bridge coupling system simulation.

As shown in Fig. 6-11, the bridge model built by MSC/NASTRAN is sealed as a M file module, and the vehicle model simulated by MSC/ADAMS is saved as a mechanic module in Matlab/Simulink platform. The vehicle-bridge coupling relationships are coded as M files and inputted into Matlab/Simulink platform. Therefore, those two subsystems and their coupling relationships are all realized on Matlab/Simulink platform, and the simulation of whole vehicle-bridge coupling system can be completed by that platform now.

6.6 Numerical Examples

In order to illustrate the co-simulation method presented in this chapter for simulating the vehicle-bridge coupling system, some numerical examples are investigated in detail. The values for the parameters of the vehicle-bridge coupling system are as follows.

1. The parameters for bridge structure.

The specific size details about the bridge structure are as shown in Fig. (6-1), and the FEM model built by MSC/NASTRAN is totally based on those sizes. In addition, the bridge main beam and floating slab track are made of concrete which has $E_c = 3.45\times10^{10}\,Nm^{-2}$, $\rho_c = 2500 kgm^{-3}$, $\upsilon_c = 0.2$, the rail track is made of steel which has $E_s = 2\times10^{11}\,Nm^{-2}$, $\rho_s = 7850 kgm^{-3}$, $\upsilon_s = 0.2$, and the rubber for connecting rail and floating slab track has $K_r = 1\times10^{8}\,Nm^{-2}$, $C_r = 3\times10^{4}\,Nsm^{-1}$. The stiffness and damping of the viscoelastic layer between bridge main beam and floating slab track are variables and their effects on the dynamic behavior of bridge structure

will be discussed in this section.

2. The parameters for train system.

A high-speed rail train, CRH5, is adopted in this research for the simulation of train system, and the specific details about CRH5 size and other parameters are as shown in Table. (6-4).

Table 6-4. The parameters for CRH5 train system.

Parameters	Notation	Unit	Value
Mass of car body	m_c	kg	6.2904×10^4
Mass of bogie frame	m_b	kg	2.929×10^3
Mass of wheel-set	m_w	kg	1.95×10^3
Moment of inertia of car body frame about the x-axis	I_{cx}	$kg\cdot m^2$	7.55×10^4
Moment of inertia of car body frame about the y-axis	I_{cy}	$kg\cdot m^2$	3.1598×10^6
Moment of inertia of car body frame about the z-axis	I_{cz}	$kg\cdot m^2$	3.1598×10^6
Moment of inertia of bogie frame about the x-axis	I_{bx}	$kg\cdot m^2$	2.247×10^3
Moment of inertia of bogie frame about the y-axis	I_{by}	$kg\cdot m^2$	5.045×10^3
Moment of inertia of bogie frame about the z-axis	I_{bz}	$kg\cdot m^2$	2.806×10^3
Moment of inertia of wheel-set about the x-axis	I_{wx}	$kg\cdot m^2$	900
Moment of inertia of wheel-set about the y-axis	I_{wy}	$kg\cdot m^2$	96
Moment of inertia of wheel-set about the z-axis	I_{wz}	$kg\cdot m^2$	900
Vertical stiffness of primary suspension	K_{1z}	N/m	2.1216×10^6
Vertical damping of primary suspension	C_{1z}	$N\cdot s/m$	1.77×10^4
Horizontal stiffness of primary suspension	K_{1y}	N/m	1.2944×10^6

Horizontal damping of primary suspension	C_{1y}	$N \cdot s / m$	1.77×10^4
Longitudinal stiffness of primary suspension	K_{1x}	N / m	1.2944×10^6
Longitudinal damping of primary suspension	C_{1x}	$N \cdot s / m$	1.77×10^4
Vertical stiffness of secondary suspension	K_{2z}	N / m	1.86×10^6
Vertical damping of secondary suspension	C_{2z}	$N \cdot s / m$	1.00×10^4
Horizontal stiffness of secondary suspension	K_{2y}	N / m	7.00×10^6
Horizontal damping of secondary suspension	C_{2y}	$N \cdot s / m$	1.00×10^4
Horizontal stiffness of secondary suspension	K_{2x}	N / m	7.00×10^6
Horizontal damping of secondary suspension	C_{2z}	$N \cdot s / m$	1.00×10^4
Radius of wheel	R_w	m	0.445
Full length	l	m	10
Half-distance between two bogies	d_b	m	4
Half-distance between wheel-sets	d_w	m	0.5
Half-distance between rolling circularity	d_r	m	0.748
Half-distance between first suspension system	d_1	m	1.10
Half-distance between second suspension system	d_2	m	1.10
Distance between car body and second suspension system	h_1	m	1.80
Distance between second suspension system and bogie	h_2	m	0.20
Distance between bogie and wheel-set	h_3	m	0.645

6.6.1 Effect of Viscoelastic Layer Stiffness K

Viscoelastic layer is the connection between floating slab track and bridge main beam in high-speed rail bridge structures, therefore, its properties will affect the dynamic responses of bridge structures apparently. Some discussions about the effect of viscoelastic layer stiffness K on dynamic responses of floating slab track and bridge main beam are shown in here. Three cases are investigated in here: $V = 40m/s$, $C = 35000N \cdot s/m$, Case 1: $K = 1\times10^6 N/m$, $K = 2\times10^6 N/m$, $K = 3\times10^6 N/m$. Only one train is simulated to pass the bridge. The dynamic responses at the midspan of the floating slab track and bridge main beam are shown in Fig. 6-12.

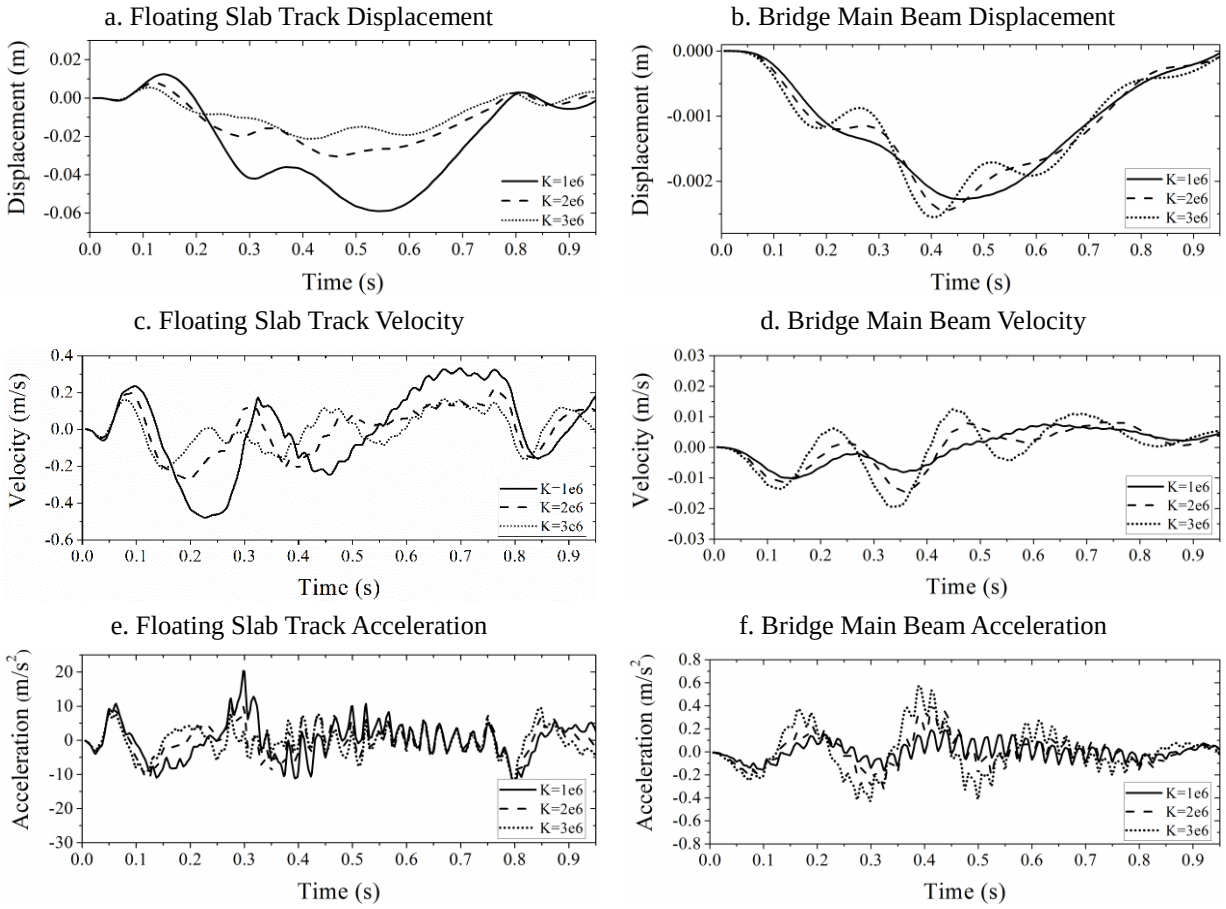

Fig. 6-12. Dynamic responses at midspan point of floating slab track and bridge main beam.

The dynamic responses of floating slab track is apparently decreased with the increase of viscoelastic layer stiffness *K* (as shown in Fig. 6-12). It is the same as the analysis in Section 3.5.2.2, floating slab track in here is a kind of a beam on viscoelastic foundation, when the viscoelastic layer becomes stiffer, the restrict to it gets stronger, therefore the it vibrates smaller and smaller. From Fig. 6-12, the dynamic responses of bridge main beam is generally increased with the increase of layer stiffness *K*. The energy which let bridge main beam vibrate is all from viscoelastic layer. Once the viscoelastic layer gets stiffer, its deformation will be smaller and less

energy will be absorbed by floating slab track, therefore, more exciting energy will be obtained by bridge main beam and makes its dynamic responses increased.

6.6.2 Effect of Viscoelastic Layer Damping C

Another parameter of the viscoelastic layer is the damping coefficient, *C*, which is an important issue to reduce the vibrations of both floating slab track and bridge main beam. Three cases are investigated in here for discussion of the damping effects on bridge dynamic responses: $V = 40m/s$, $K = 1\times10^6 N/m$, Case 1: $C = 10000N\cdot s/m$, Case 2: $C = 20000N\cdot s/m$, Case 3: $C = 35000N\cdot s/m$. Only one train is simulated to pass the bridge. The dynamic responses at the midspan of the floating slab track and bridge main beam are shown in Fig. 6-13.

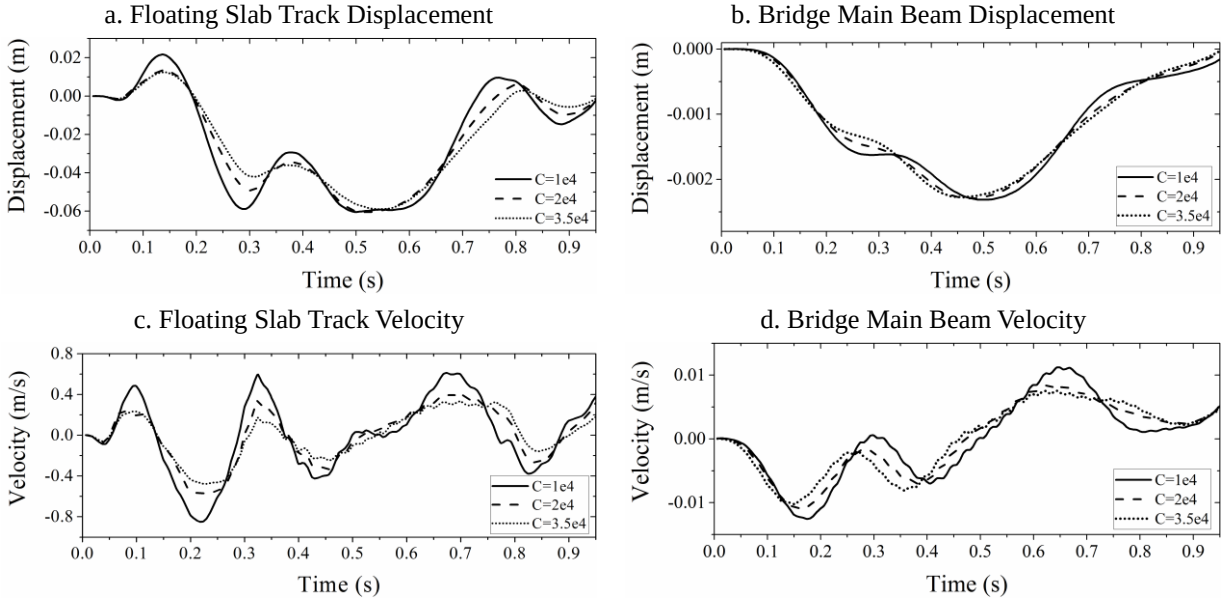

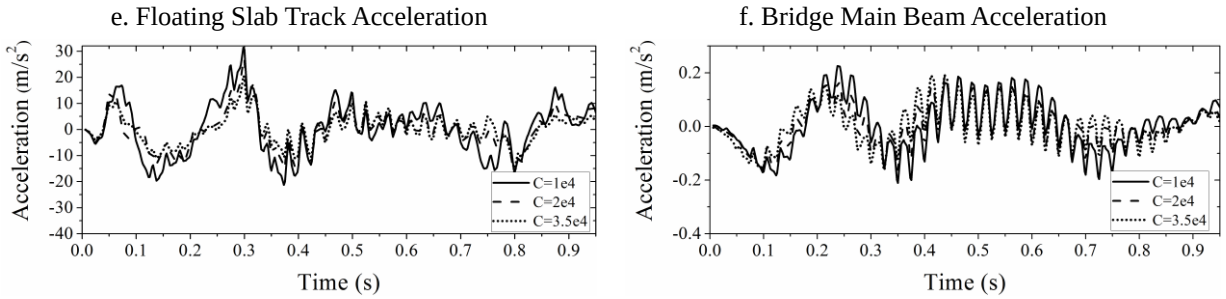

Fig. 6-13. Dynamic responses at midspan point of floating slab track and bridge main beam.

As shown in Fig. 6-13, for both floating slab track and bridge main beam, the dynamic responses are generally reduced with the increase of damping *C*. It is the same as the explanation in Section 3.5.2.3, damping is a kind of vibration energy absorber, when increase the damping value, more energy will be absorbed and less energy will be applied to make structure vibrations. The viscoelastic layer is just between floating slab track and bridge main beam, its damping can effectively absorb the energy when the trains are passing the bridge. Therefore, with the increase of viscoelastic layer damping, more exciting energy could be absorbed and less of them will be applied floating slab track and bridge main beam, that's why both of them have a reduction on dynamic responses.

6.7 Conclusions

In this chapter, a co-simulation method is proposed to complete the dynamic simulation of vehicle-bridge coupling system. Bridge structures are the traditional civil engineering structures which are better to use finite element method (FEM) to analyze, and the FEM software MSC/NASTRAN is

applied in here to build the bridge model. Vehicle system is actually a mechanical system, its nature is a multibody system which is better to use dynamics of multibody system (DMS) to analyze, and the professional DMS software MSC/ADAMS is used in this research to simulate the vibration of vehicle system. The vehicle-bridge coupling relationships are introduced specifically in this chapter and the classical theories about them are adopted in this research, including wheel-rail contact geometric parameters, wheel-rail contact forces and track irregularity. The Matlab/Simulink is used to build a platform to ensure MSC/NASTRAN and MSC/ADAMS working together, and the vehicle-bridge coupling relationships are coded as a program block and inputted into that platform. In this way, a co-simulation by using that Matlab/Simulink platform is realized and the simulation of whole vehicle-bridge coupling system is completed.

Various numerical examples of vehicle-bridge coupling system are calculated to illustrate the practicability and efficiency of the proposed co-simulation method. Parametric studies about the effects of stiffness and damping of viscoelastic layer, which is between floating slab track and bridge main beam, on the dynamic responses of bridge are completed. The results not only are helpful to engineers to design, but also show the potentiality of the semi-active control based on novel adaptive materials which will be introduced in Chapter 7.

Finally, the proposed co-simulation method is derived, and the corresponding platform by using Matlab/Simulink is built and verified successfully.

Chapter 7 Semi-Active Control in High-Speed Rail Vehicle-Bridge Coupling System with Magnetorheological Nanocomposites

7.1 Introduction

The main topic of the research in this dissertation is using novel adaptive materials magnetorheological nanocomposites (MRNs) to build a semi-active control structure, and further apply it into the vehicle-bridge coupling system of high-speed rail so that the vibration of the whole system could be controlled effectively and the dynamic responses of bridge can be reduced significantly. In Chapter 4 and Chapter 5, the semi-active controls of the double-beam system with elastic layer and viscoelastic layer have been introduced and derived. In Chapter 6, a co-simulation platform based on Matlab/Simulink for the whole vehicle-bridge coupling system has been built successfully. In this chapter, the semi-active control algorithm is needed to be inputted and applied in the co-simulation platform, and the semi-active control for vehicle-bridge coupling system should be completed to reduce the bridge dynamic responses and protect the whole system safety.

As introduced in Chapter 4 and Chapter 5, from that Yao (1972) firstly introduced the modern control theory into civil engineering in 1972, great progress in the field of structural vibration control has been achieved over the past few decades (Yao 1972; Housner et al. 1997; Soong and Spencer 2002; Soong 1990; Alkhatib and Golnaraghi 2003; Yang, Akbarpour and Ghaemmaghami 1987; Yang, Long and Wong 1988; Yang, Li and Liu 1991; Yang, Li and Liu 1992; Li, Liu, Fang

and Tam 2000; Li, Liu, Tang, Zhang and Tam 2004; Soong et al. 1991; Reinhorn et al. 1993; Inman 2001; Meirovitch, Baruh, Montgomery and Williams 1984; Schafer and Holzach 1985; Meirovitch and Silverberg 1983; Meirovitch 1987; Sadek and Esfandiari 1990; Kucuk and Sadek 2005, 2007).

In those research works about the structural vibration control, applying smart materials to build control structure to reduce the structural dynamic responses is just one popular and valuable research topic. Among plenty of existed smart materials, magnetorheological fluids (MRFs) and magnetorheological elastomers (MREs) have been studied for a long time and there have been many valuable research results (Ginder, Nichols, Elie and Tardiff 1999; Ginder, Nichols, Elie and Clark 2000; Ramallo, Johnson and Spencer 2002; Yoshioka, Ramallo and Spencer 2002; Koo, Sung, Lee and Jung 2008; Deng and Gong 2007; Koo, Jang, Usman and Jung 2009; Hoang, Zhang and Du 2009; Opie and Yim 2009; Dong, Yu, Liao and Chen 2009; Jung, Park and Koo 2010; Du, Li and Zhang 2011; Behrooz, Wang and Gordaninejad 2014).

Many research works about the vehicle-bridge coupling system have been stated specifically in Chapter 6, however, in most of those previous studies, the effects of the track structures on the bridges have been completely neglected or only partially accounted. Several researchers take into consider the elastic properties of the track structures by computing the combined stiffness of track and bridge (Wiriyachai, Chu and Garg 1982; Chu, Garg and Wang 1986; Wang, Garg and Chu 1991). Yang and Yau (1997) study the ballast stiffness of the track by continuously distributed

springs while implicitly neglecting the stiffness of the rail, and the similar work is done by Yau et al. (1999). Le et al. (1999) make some numerical work and field measurements on ballast mats on high-speed bridges, the track and bridge are modelled by conventional Timoshenko beam finite elements, and sleepers and ballast are modelled as spring-damper system. Cheng, Au and Cheung (2001) develop a new finite element called bridge-track-vehicle element to investigate the interactions among a moving train, supporting railway track and bridge, and the effect of track structure on the dynamic responses of bridge structure is shown.

As to the real bridge structures in railway engineering, several researchers also make some efforts to control and reduce their vibration when the trains are passing on the bridge. Minsili, Zhong and Xia (2002) suggest to install supplemental diagonal elements in truss bridges connected to original braces by Slotted Friction Connections, in order to reduce the vibrations induced by traffic or earthquake. Martinez-Rodrigo, Lavado and Museros (2010a) propose and evaluate a solution, which is based on retrofitting the bridge with fluid viscous dampers connected to the slab and to an auxiliary structure, to reduce inadmissible levels of deck vertical acceleration. Another similar work is also completed by the same researchers (Martinez-Rodrigo, Lavado and Museros 2010b).

As shown above, although the structural vibration control and the control by using smart materials have been studied for a long time, there are few research works on the vibration control of bridge structures in vehicle-bridge coupling system. The effect of track structure on the dynamic

responses of bridge is not considered in many works, so there is not any research considering to use track structure to realize the bridge vibration control. In this way, installing the vibration control structure on track structure and using the vibration of track to control and reduce the dynamic responses of the bridges in bridge-vehicle coupling system is really a new topic.

In this chapter, considering the ballastless track structure, which chooses floating slab track as the main constituent part, is widely existed in modern high-speed rail engineering, MRNs with corresponding electromagnetic field devices are applied as the viscoelastic layer between floating slab track and bridge main beam to realize the semi-active control on vehicle-bridge coupling system of high-speed rail. Simplifying the connection between rail and floating slab track, the simply supported bridge with floating slab track in real high-speed rail project is actually a double-beam system. It means that the semi-active control developed in Chapter 4 and Chapter 5 based on double-beam system can be used in here. After introducing the MRNs and their dynamic mechanical model, the specific semi-active control algorithm for MRNs applied in high-speed rail bridge is derived according to the works in Chapter 5. That semi-active control algorithm is coded as a program block and inputted into the co-simulation platform which is built in Chapter 6. Finally, the simulation of the whole vehicle-bridge coupling system with semi-active control in high-speed rail can be completed. Numerical examples are demonstrated and discussed in details to verify the efficiency of the semi-active control structure proposed in this research by MRNs, which may be applied in real engineering practices in future.

7.2 Introduction of Ballastless Track and Floating Slab Track

In modern railway engineering, especially in high-speed rail engineering, the ballastless track structure is widely used in railway constructions and gradually becomes the main current structural style. Comparing with traditional railway track structure ballast track (as shown in Fig. 7-1(a)), the most obvious difference of the ballastless track is that it adopts the overall concrete bed structure to take the place of the ballast bed (as shown in Fig. 7-1(b)). The biggest advantages of using ballastless track consist of : (1) Stability, precision, and ride comfort; (2) Flexibility and end-to-end effectiveness in application; (3) Long life cycles and practically no maintenance. That is why it is so popular in high-speed rail engineering and is constructed over the world now.

a. Ballast Track (by Lechner 2011) b. Ballastless Track (by Wang 2011)

Fig. 7-1. The railway track structure: ballast track and ballastless track.

In ballastless track, the floating slab track is the most important part and it is used in almost all ballastless tracks to reduce the vibrations produced by trains and transferred to ground or bridge

under it. As shown in Fig. 7-2, floating slab track is usually a overall concrete slab with rails installed on it, and it is connected with ground or bridge main beam under it by viscoelastic layer. Considering the floating slab track on bridge main beam is basically a long concrete slab, they can form a mechanical model as shown in Fig. 7-3.

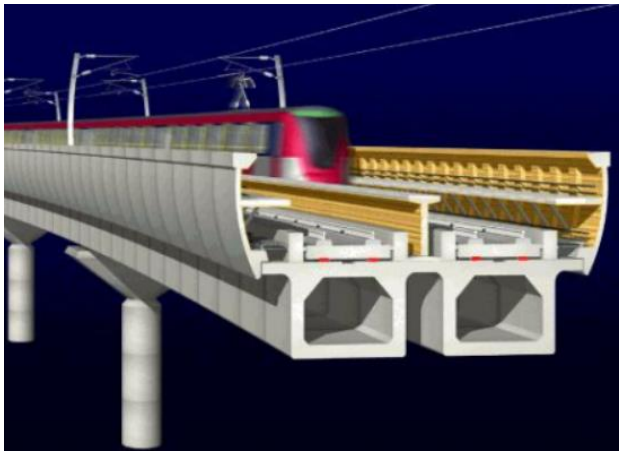

a. Floating Slab Track on Bridge (by Wilson 2004)

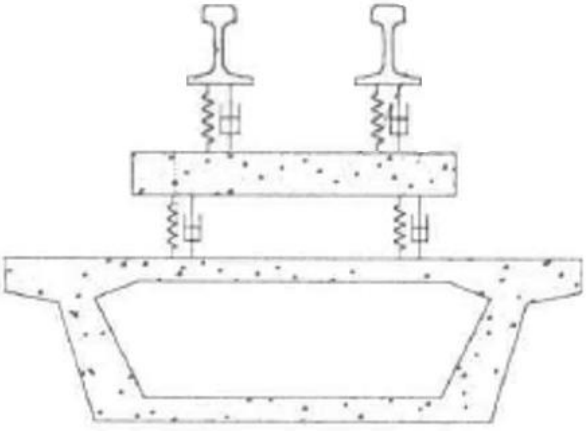

b. Floating Slab Track on Bridge

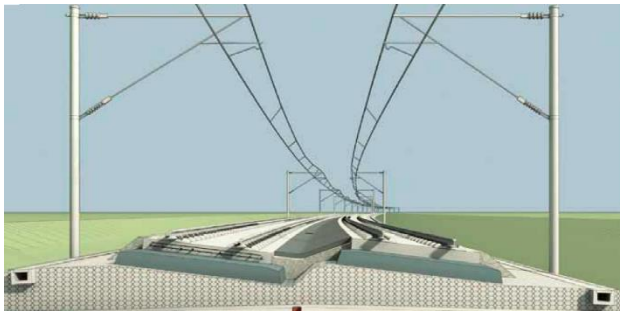

c. Floating Slab Track on Ground (by SSF Ingenieure)

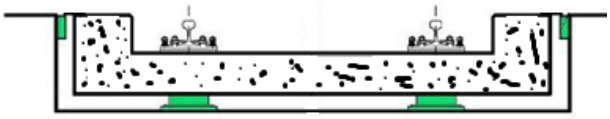

d. Floating Slab Track on Ground

Fig. 7-2. Floating slab track.

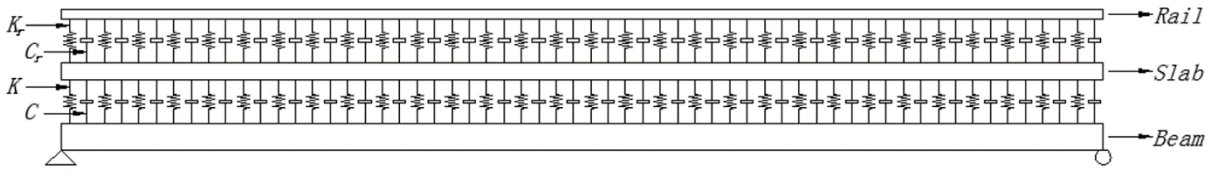

Fig. 7-3. Mechanical model of bridge main beam with floating slab track.

If we simplify the connections between rails and floating slab track, assume that they are joined by rigid connections and they can be treated as just one substructure, in fact, the floating slab track and bridge main beam will form a typical double-beam system as shown in Fig. 7-4. In this way, the analysis on the vibrations and dynamic responses of double-beam system in Chapter 2 and Chapter 3, the active control and semi-active control for double-beam system in Chapter 4 and Chapter 5, all of them, can be applied in the real structure in here.

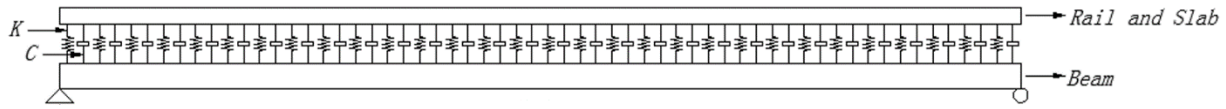

Fig. 7-4. Mechanical model of bridge main beam with simplified floating slab track: a double-beam system.

In this research, the simplified double-beam system formed by bridge main beam and floating slab track as introduced above and shown in Fig. 7-4 will be used to study the semi-active control in vehicle-bridge coupling system of high-speed rail by novel adaptive materials MRNs. The specific derivations about the semi-active control algorithm will be introduced in Section 7.4.

7.3 The Introduction and Dynamic Mechanical Model of the Magnetorheological Nanocomposites

It is well known that the magnetorheological elastomers (MREs) are smart materials whose mechanical behavior can be controlled by external magnetic fields rapidly and reversibly, showing

abilities for wide use in structural control applications. However, due to matrix materials, MREs have comparatively inferior mechanical properties. In order to make up those limits of MREs, some other smart materials are developed by many scholars, and magnetorheological nanocomposites (MRNs) are just one kind of those new smart materials. In this section, the microstructure and dynamic mechanical model of MRNs will be introduced and derived.

7.3.1 Introduction of Magnetorheological Nanocomposites

A research group led by Professor Lizhi Sun at University of California, Irvine (UCI) developed the novel adaptive materials MRNs, which use carbon nanotubes (CNT) to enhance and increase stiffness, strength and damping performances of the elastomers. In another word, MRNs are a kind of improved MREs by adding CNT to enhance the matrix materials. It is similar to MREs, for MRNs, magnetic particles are aligned in chains in nonmagnetic matrix along the direction of curing magnetic fields (as shown in Fig. 7-5(a)), and when it is exposed to external magnetic fields, the bulk mechanical properties of MRNs can be changed by controlling the magnetic field strength due to the interaction between the magnetic particles. The microstructures of MREs and MRNs by scanning electron microscope are shown in Fig. 7-5 (b, c).

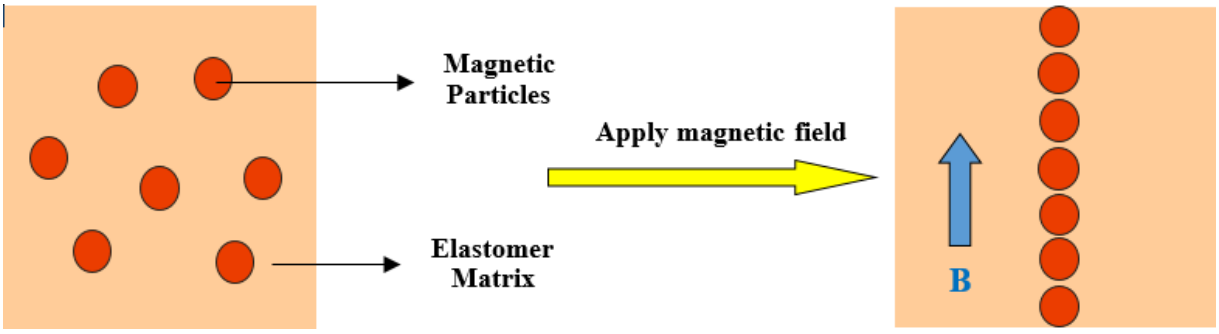

a. The formation of chain structure in MREs and MRNs by curing magnetic field.

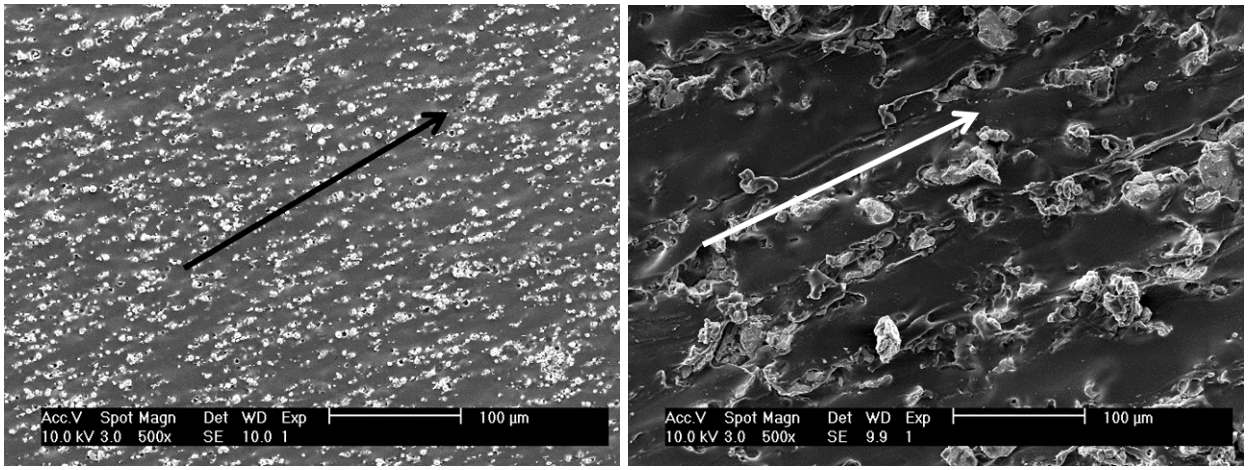

b. Microstructure of MREs by scanning electron microscope, the direction of iron particle chains are shown by arrow in the figure.

c. Microstructure of MRNs by scanning electron microscope, the direction of iron particle chains are shown by arrow in the figure.

Fig. 7-5. Microstructure of MREs and MRNs (by Li 2011).

Dr. Rui Li in Professor Sun's group at UCI completed plenty of experiment works on MRNs and discovered several very important results about the dynamic properties of those novel adaptive materials (Li 2011). Some of those experiment works can be shown as in Fig. 7-6 and Fig. 7-7.

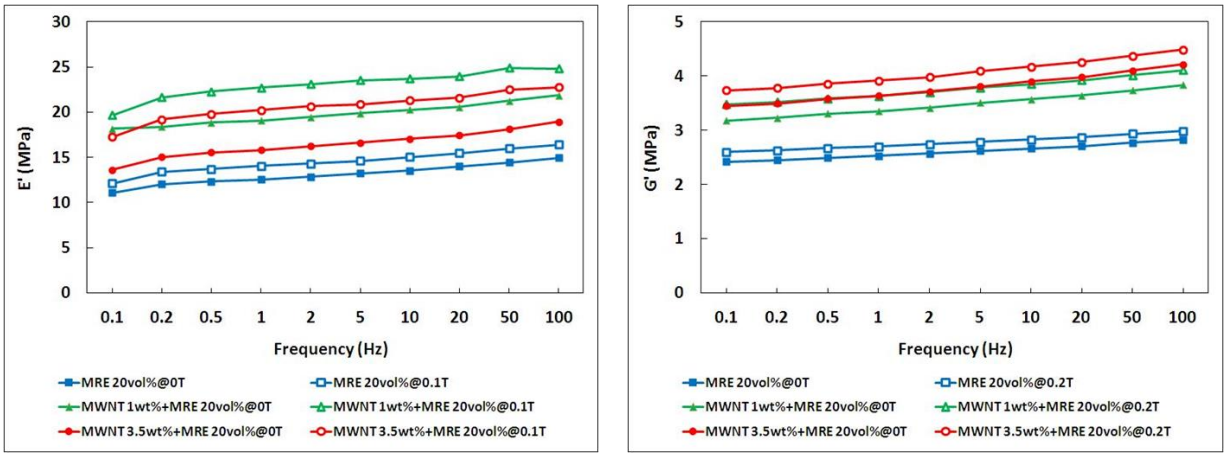

Compression Test

Shear Test

Fig. 7-6. Dynamic stiffness of MRNs with and without magnetic field (by Li 2011).

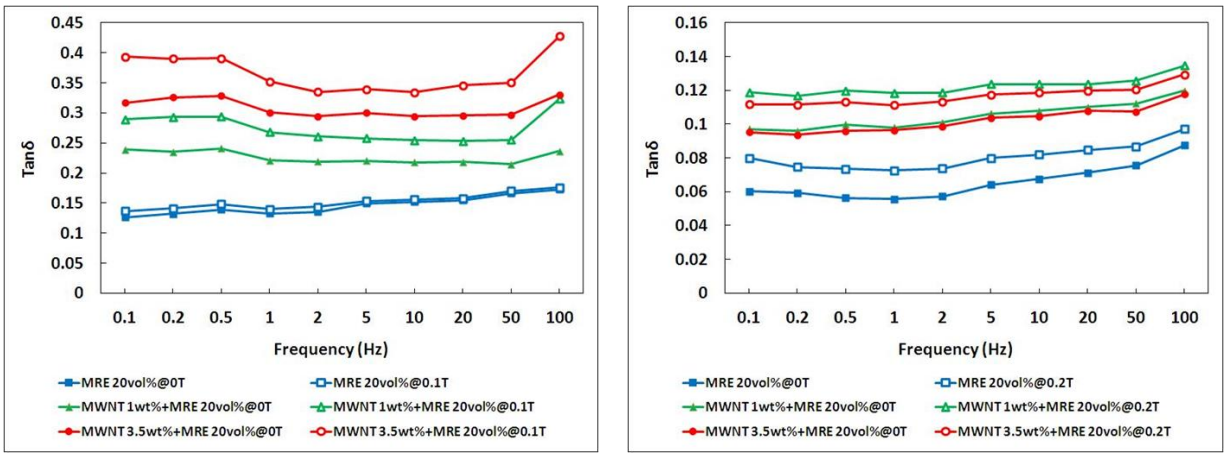

Compression Test Shear Test

Fig. 7-7. Dynamic damping of MRNs with and without magnetic field (by Li 2011).

From those experiment works, one most important result about the dynamic properties of MRNs can be concluded as: adding CNTs significantly increase the dynamic stiffness and damping of the conventional MREs and clearly enhances the MR effect in both compression and shear mode. Because of that result, the MRNs has larger dynamic stiffness and damping, and the MR effect in it is stronger, therefore, MRNs has more potentialities than MREs to be applied in structural control.

7.3.2 Dynamic Mechanical Model of Magnetorheological Nanocomposites

It is the same as the discussion in Section 5.4.1, the dynamic mechanical model of MRNs is the basis for its corresponding semi-active control algorithm, and it is very important to identify it firstly in order to apply MRNs in structural vibration control.

In plenty of existed research works about the dynamic mechanical model of traditional MREs, the

linear model is just an easy but still practical one for the MREs' application in structural vibration control (Jung, Park and Koo 2010; Behrooz, Wang and Grodaninejad 2014; Usman, Jang, Kim, Jung and Koo 2009; Yang, Du, Li, Li, Li, Sun and Deng 2013). Based on the research results of MRNs obtained by Dr. Rui Li (Li 2011) and comparing them with MREs, a simple pseudo linear model (as shown in Fig. 7-8(a)) is adopted to represent the dynamic mechanical model of MRNs and it can be defined as introduced in Section 5.4.1 as:

$$f_{MRNs} = \left(K + \Delta K\right)\Delta W + \left(C + \Delta C\right)\Delta \dot{W} \tag{7-1}$$

where $\left(K + \Delta K\right)\Delta W$ and $\left(C + \Delta C\right)\Delta \dot{W}$ is the elastic force and damping force of the MRNs, respectively, K and C are the stiffness and damping coefficients of MRNs, ΔK and ΔC is the stiffness increase and damping increase of MRNs, ΔW is the MRNs deformation displacement, and $\Delta \dot{W}$ is the MRNs deformation velocity.

The stiffness and damping coefficients of the MRNs are assumed to have a linear relation with the applied current, whose calculation model is a linear model (as shown in Fig. 7-8(b) and Fig. 7-8(c)) as follows

$$K_T = K_{\min} + \frac{I}{I_m}\left(K_{\max} - K_{\min}\right) \tag{7-2a}$$

$$C_T = C_{\min} + \frac{I}{I_m}\left(C_{\max} - C_{\min}\right) \tag{7-2b}$$

where K_T and C_T are the stiffness and damping coefficients of the MRNs under specific current, $K_{\max}$ and $C_{\max}$ is maximum stiffness value and maximum damping value of the MRNs,

$K_{\min}$ and $C_{\min}$ is minimum stiffness value and damping value of the MRNs, I_{m} is the saturation current for the device, and *I* is the inputted current determined by semi-active control.

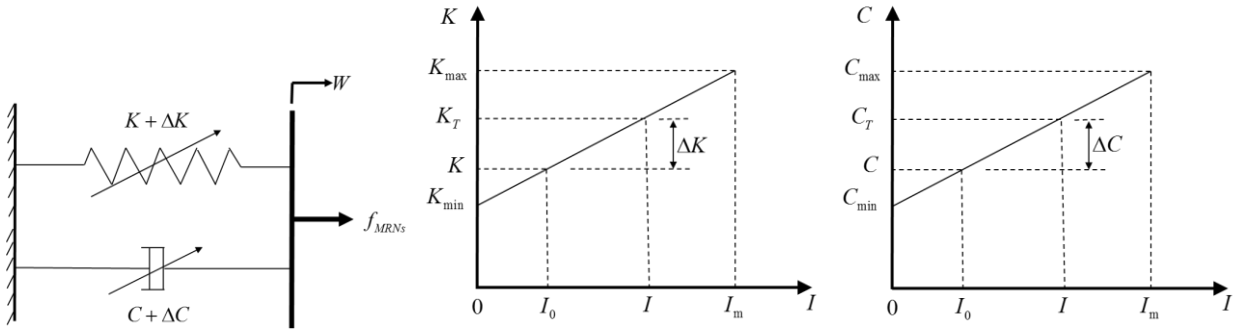

a. Linear Model for MRNs Dynamic Mechanical Model

b. Linear Model of MRNs Stiffness with Applied Current

c. Linear Model of MRNs Damping Coefficient with Applied Current

Fig. 7-8. Linear model for MRNs dynamic mechanical model and linear model of MRNs stiffness and damping coefficients with applied current.

If the default current inputted is I_0 and the default stiffness and damping coefficients of the MRNs are *K* and *C*, respectively, the stiffness increase ΔK and damping increase ΔC (as shown in Fig. 7-8(b) and Fig. 7-8(c)) could be controlled by the current as

$$\Delta K = K_T - K = \frac{I - I_0}{I_m}\left(K_{\max} - K_{\min}\right) \tag{7-3a}$$

$$\Delta C = C_T - C = \frac{I - I_0}{I_m}\left(C_{\max} - C_{\min}\right) \tag{7-3b}$$

Although the simple linear model does not represent the actual behavior of MRNs, it helps us to study a suitable semi-active control algorithm for the semi-active control structure in next section, and so, it is proper to adopt it in the discussion in here.

7.4 Semi-Active Control Algorithm based on MRNs for High-Speed Rail Vehicle-Bridge Coupling System

As introduced in Section 7.2, with the simplification of the connections between rails and floating slab track, the floating slab track with rails on it and the bridge main beam will form a double-beam system. Considering the semi-active control of double-beam system with viscoelastic layer studied in Chapter 5, in this research, the semi-active control in vehicle-bridge coupling system of high-speed rail is proposed by applying the controllable MRNs in the viscoelastic layer between bridge main beam and floating slab track (as shown in Fig. 7-9). In this section, the specific semi-active control algorithm based on MRNs applied in vehicle-bridge coupling system of high-speed rail will be studied.

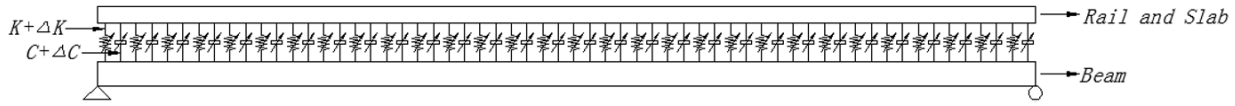

Fig. 7-9. Double-beam system of floating slab track and bridge main beam with controllable MRNs as viscoelastic layer between them.

From Fig. 7-9, the floating slab track with rails on it and the bridge main beam form a double-beam system. It means that the semi-active control algorithm derived in Chapter 5, which is for the double-beam system with viscoelastic layer, can be applied in here. Meanwhile, the dynamic mechanical model of MRNs defined in Section 7.3 is also the same linear model as the one in Section 5.4.1. Therefore, based on the research works in Chapter 5, the semi-active control

algorithm based on MRNs in vehicle- bridge coupling system can be:

(1) If $\Delta K_{\max}\int_0^L (W_1 - W_2)\,dx + \Delta C_{\max}\int_0^L \left(\frac{\partial W_1}{\partial t} - \frac{\partial W_2}{\partial t}\right)dx < \int_0^L f_c(x,t)\,dx$,

then $\Delta K_d = \Delta K_{\max}$, $\Delta C_d = \Delta C_{\max}$ (7-4a)

(2) If $\Delta K_{\max}\int_0^L (W_1 - W_2)\,dx + \Delta C_{\max}\int_0^L \left(\frac{\partial W_1}{\partial t} - \frac{\partial W_2}{\partial t}\right)dx \geq \int_0^L f_c(x,t)\,dx$ and

$\Delta K_{\min}\int_0^L (W_1 - W_2)\,dx + \Delta C_{\min}\int_0^L \left(\frac{\partial W_1}{\partial t} - \frac{\partial W_2}{\partial t}\right)dx \leq \int_0^L f_c(x,t)\,dx$

then $\Delta K_d = K_T - K = \frac{I - I_0}{I_m}(K_{\max} - K_{\min})$, $\Delta C_d = C_T - C = \frac{I - I_0}{I_m}(C_{\max} - C_{\min})$, (7-4b)

(3) If $\Delta K_{\min}\int_0^L (W_1 - W_2)\,dx + \Delta C_{\min}\int_0^L \left(\frac{\partial W_1}{\partial t} - \frac{\partial W_2}{\partial t}\right)dx > \int_0^L f_c(x,t)\,dx$,

then $\Delta K_d = \Delta K_{\min}$, $\Delta C_d = \Delta C_{\min}$ (7-4c)

where $\Delta K_{\max} = K_{\max} - K$, $\Delta C_{\max} = C_{\max} - C$, $\Delta K_{\min} = K_{\min} - K$, $\Delta C_{\min} = C_{\min} - C$, K, C are the default stiffness and damping coefficients of the MRNs, respectively, $f_c(x,t)$ is the active control forced determined as in Section 5.3.3, $W_i = W_i(x,t)$ is transverse displacements, $\frac{\partial W_i}{\partial t} = \frac{\partial W_i(x,t)}{\partial t}$ is transverse velocities, i=1 or 2 represents floating slab track or bridge main beam, and L is the length of bridge main beam or floating slab track.

The parameters in Eq. (7-4b) are calculated as in Section 5.4.2 as follows

$$I = \frac{I_m}{H(K_{\max} - K_{\min}) + J(C_{\max} - C_{\min})} F_{nc}(t) + I_0 \quad (7\text{-}5a)$$

$$F_{nc}(t) = -\frac{1}{2} R^{-1}\left[P_{21} T_n(t) + P_{22}\dot{T}_n(t)\right] \tag{7-5b}$$

$$H = \frac{\int_0^L \left\{\left[\phi_{n2}(x) - \phi_{n1}(x)\right]\left[W_1(x,t) - W_2(x,t)\right]\right\} dx}{\int_0^L \left[\phi_{n1}(x)\bar{m}_1\phi_{n1}(x) + \phi_{n2}(x)\bar{m}_2\phi_{n2}(x)\right] dx} \tag{7-5c}$$

$$J = \frac{\int_0^L \left\{\left[\phi_{n2}(x) - \phi_{n1}(x)\right]\left[\frac{\partial W_1(x,t)}{\partial t} - \frac{\partial W_2(x,t)}{\partial t}\right]\right\} dx}{\int_0^L \left[\phi_{n1}(x)\bar{m}_1\phi_{n1}(x) + \phi_{n2}(x)\bar{m}_2\phi_{n2}(x)\right] dx} \tag{7-5d}$$

where $F_{nc}(t)$ is modal active control force in the modal space which is determined as in Section 5.3.2, $\bar{m}_1$, $\bar{m}_2$ are the beam mass per unit length of floating slab track and bridge main beam, and $\phi_{n1}(x)$, $\phi_{n2}(x)$ are mode shape functions of floating slab track and bridge main beam corresponding to *n*th natural frequency.

The specific derivation works of the semi-active control algorithm based on MRNs in vehicle-bridge coupling system, which are shown as Eq. (7-4) and Eq. (7-5) above, can be referred to the derivation works in Chapter 5.

Until here, based on the semi-active control algorithm introduced in this section, the stiffness increase ΔK_d and damping increase ΔC_d of MRNs are determined and could be adopted by semi-active control structure. It is the same as the discussion in Section 5.4.2, only one main mode will be chosen to be controlled for the semi-active control structure, ΔK_d and ΔC_d should be determined at each time step and changed during the whole vibration process when the trains are

passing the bridge.

7.5 Co-Simulation Platform for Vehicle-Bridge Coupling System with Semi-Active Control

The semi-active control algorithm based on MRNs for semi-active control in vehicle-bridge coupling system has been introduced and determined in Section 7.4, in this section, that semi-active control structure and corresponding semi-active control algorithm will be inputted into the co-simulation platform of vehicle-bridge coupling system and the final simulation of whole system with semi-active control will be completed.

In Section 6.5, the co-simulation platform has been built successfully by Matlab/Simulink, MSC/NASTRAN and MSC/ADAMS. The semi-active control algorithm derived in Section 7.4 can be coded as a program block and inputted into the Matlab/Simulink platform, and then, it could work in the co-simulation platform. In this way, the simulation of the whole vehicle-bridge coupling system with semi-active control based on MRNs can be realized and the general process is as the flowchart in Fig. 7-10. And the simulation of the semi-active control structure based on MRNs in the co-simulation platform can be denoted as the flowchart in Fig. 7-11.

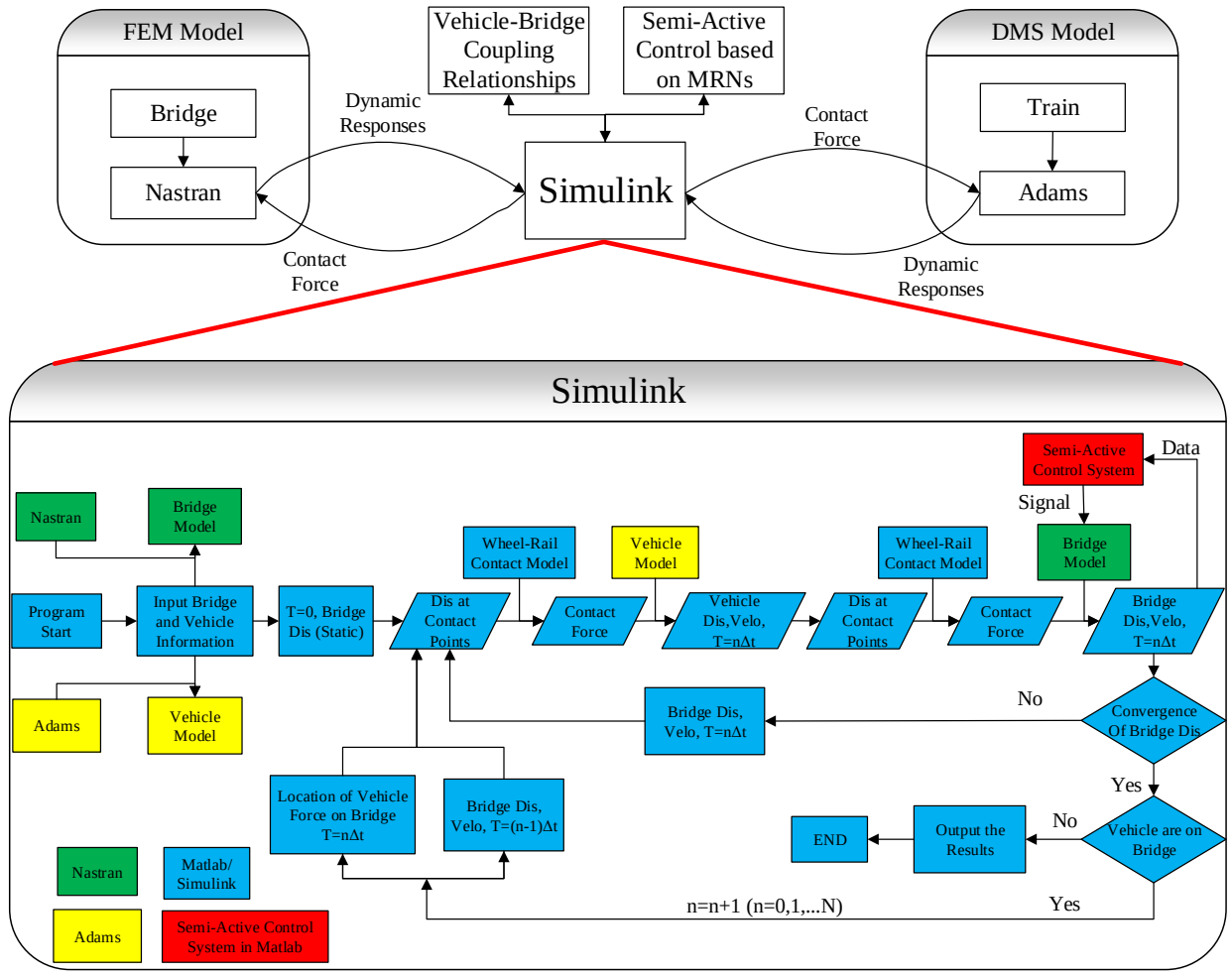

Fig. 7-10. Flowchart of the simulation for whole vehicle-bridge coupling system with semi-active control based on MRNs.

In the real high-speed rail engineering projects, during each time step when the trains are passing the bridge, the displacements and velocities of the bridge main beam and floating slab track can be detected by the sensors installed on bridge structure, and then inputted into the central control computer. The central computer will calculate and determine the semi-active control signals ΔK_d, ΔC_d and applied current I following the calculation procedure as shown in the flowchart in Fig. 7-11. Those semi-active control signals will be outputted to the electromagnetic field devices

designed for MRNs. According to those control signals, the stiffness and damping coefficients of MRNs can be changed to complete the semi-active control in this time step. Repeating that control process one time step by one time step until the train passes the whole bridge, the semi-active vibration control for whole vehicle-bridge coupling system of high-speed rail is just completed.

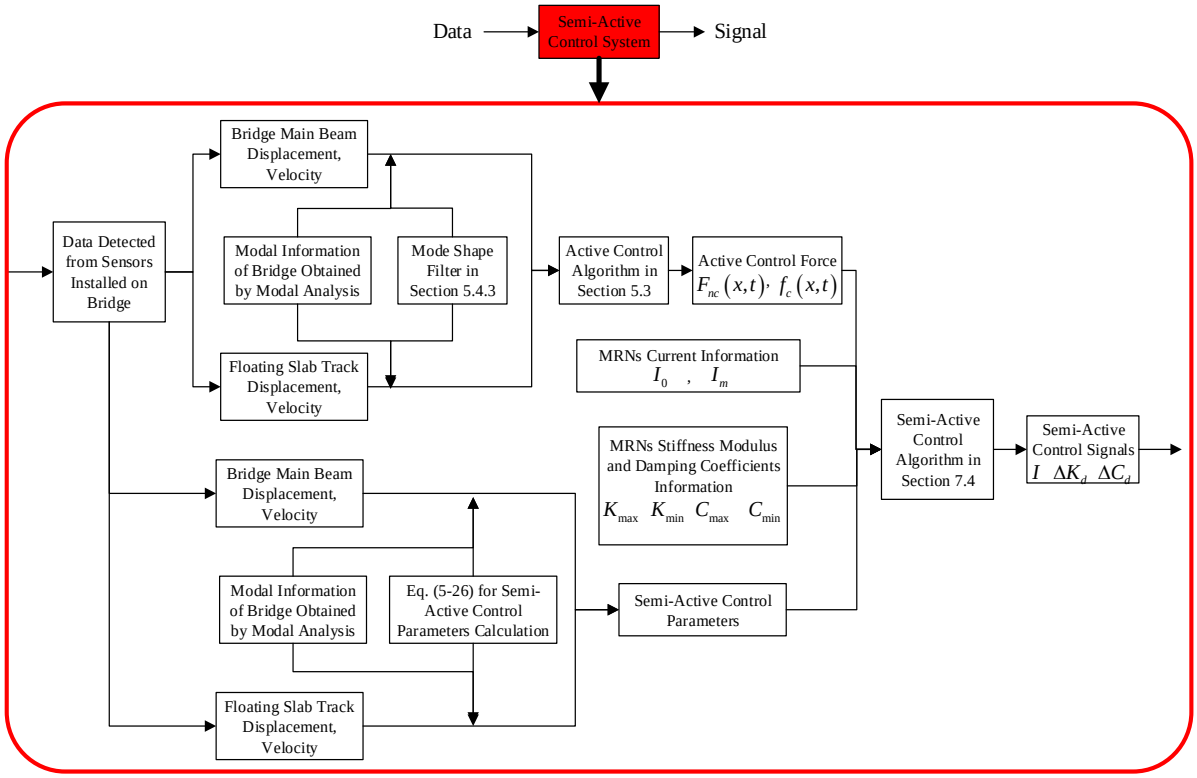

Fig. 7-11. Flowchart of the semi-active control structure based on MRNs in co-simulation platform for vehicle-bridge coupling system of high-speed rail.

7.6 Numerical Examples

In order to illustrate the effectiveness of the semi-active control based on MRNs in vehicle-bridge coupling system of high-speed rail, which is proposed in this chapter and is also the main objective

of this research, some numerical examples are investigated in detail. The values for parameters of the vehicle-bridge coupling system with semi-active control are as follows.

1. The parameters for bridge structure.

The specific size details about the bridge structure are the same as shown in Fig. 6-1. In addition, the bridge main beam and floating slab track are made of concrete which has $E_c = 3.45\times10^{10}\,Nm^{-2}$, $\rho_c = 2500 kgm^{-3}$, $\upsilon_c = 0.2$, the rail track is made of steel which has $E_s = 2\times10^{11}\,Nm^{-2}$, $\rho_s = 7850 kgm^{-3}$, $\upsilon_s = 0.2$, and the rubber for connecting rail and floating slab track has $K_r = 1\times10^{8}\,Nm^{-2}$, $C_r = 3\times10^{4}\,Nsm^{-1}$. The stiffness and damping of the viscoelastic layer which is made of MRNs and between bridge main beam and floating slab track are controlled and changed by semi-active control structure. The specific value of MRNs layer stiffness and damping will be shown in Fig. 7-14.

2. The parameters for train system.

A high-speed rail train, CRH5, is adopted in this research for the simulation of train system, and the specific details about CRH5 size and other parameters are as shown in Table. (7-1).

Table 7-1. The parameters for CRH5 train system.

Parameters	Notation	Unit	Value
Mass of car body	m_c	kg	6.2904×10^4
Mass of bogie frame	m_b	kg	2.929×10^3
Mass of wheel-set	m_w	kg	1.95×10^3

Moment of inertia of car body frame about the x-axis	I_{cx}	$kg \cdot m^2$	7.55×10^4
Moment of inertia of car body frame about the y-axis	I_{cy}	$kg \cdot m^2$	3.1598×10^6
Moment of inertia of car body frame about the z-axis	I_{cz}	$kg \cdot m^2$	3.1598×10^6
Moment of inertia of bogie frame about the x-axis	I_{bx}	$kg \cdot m^2$	2.247×10^3
Moment of inertia of bogie frame about the y-axis	I_{by}	$kg \cdot m^2$	5.045×10^3
Moment of inertia of bogie frame about the z-axis	I_{bz}	$kg \cdot m^2$	2.806×10^3
Moment of inertia of wheel-set about the x-axis	I_{wx}	$kg \cdot m^2$	900
Moment of inertia of wheel-set about the y-axis	I_{wy}	$kg \cdot m^2$	96
Moment of inertia of wheel-set about the z-axis	I_{wz}	$kg \cdot m^2$	900
Vertical stiffness of primary suspension	K_{1z}	N/m	2.1216×10^6
Vertical damping of primary suspension	C_{1z}	$N \cdot s/m$	1.77×10^4
Horizontal stiffness of primary suspension	K_{1y}	N/m	1.2944×10^6
Horizontal damping of primary suspension	C_{1y}	$N \cdot s/m$	1.77×10^4
Longitudinal stiffness of primary suspension	K_{1x}	N/m	1.2944×10^6
Longitudinal damping of primary suspension	C_{1x}	$N \cdot s/m$	1.77×10^4
Vertical stiffness of secondary suspension	K_{2z}	N/m	1.86×10^6
Vertical damping of secondary suspension	C_{2z}	$N \cdot s/m$	1.00×10^4
Horizontal stiffness of secondary suspension	K_{2y}	N/m	7.00×10^6
Horizontal damping of secondary suspension	C_{2y}	$N \cdot s/m$	1.00×10^4
Horizontal stiffness of secondary suspension	K_{2x}	N/m	7.00×10^6
Horizontal damping of secondary suspension	C_{2z}	$N \cdot s/m$	1.00×10^4
Radius of wheel	R_w	m	0.445
Full length	l	m	10
Half-distance between two bogies	d_b	m	4
Half-distance between wheel-sets	d_w	m	0.5
Half-distance between rolling circularity	d_r	m	0.748

Half-distance between first suspension system	d_1	m	1.10
Half-distance between second suspension system	d_2	m	1.10
Distance between car body and second suspension system	h_1	m	1.80
Distance between second suspension system and bogie	h_2	m	0.20
Distance between bogie and wheel-set	h_3	m	0.645

In this chapter, three trains are simulated to pass the bridge one by one, and the velocities of them are all the same as $V=80m/s$ for Case 1 and $V=100m/s$ for Case 2. The dynamic responses at the midspan of the floating slab track and bridge main beam with passive control and semi-active control are shown in Fig. 7-12 and Fig. 7-13. The variation stiffness *K* and variation damping coefficient *C* of MRNs layer controlled by semi-active control structure are shown in Fig. 7-14, and the current applied to control MRNs are also shown in Fig. 7-14.

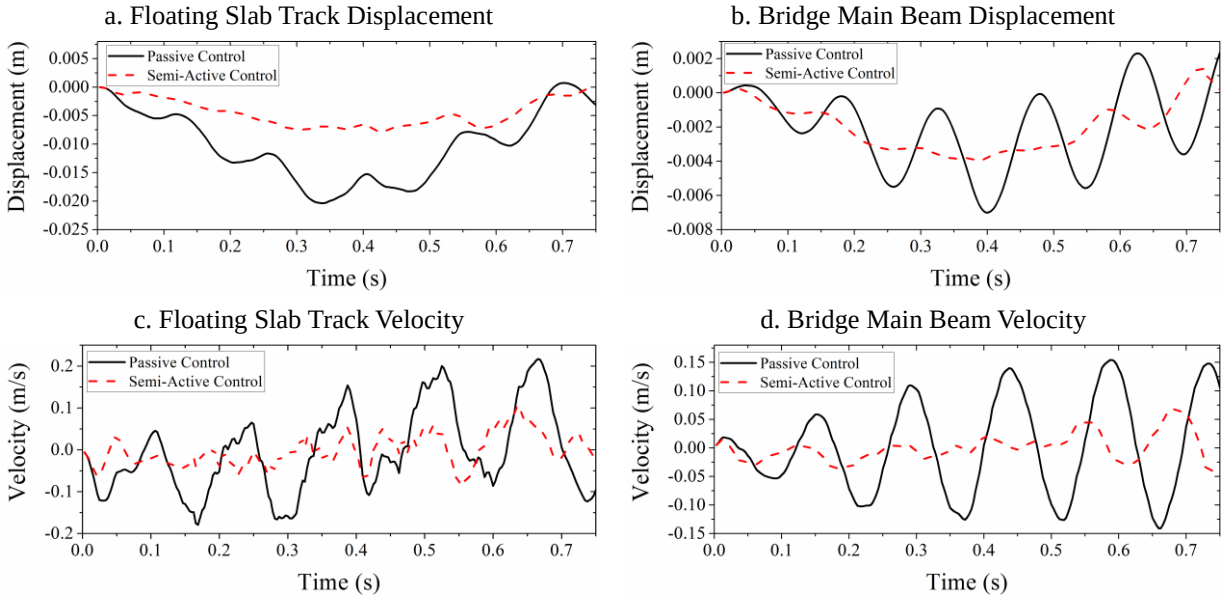

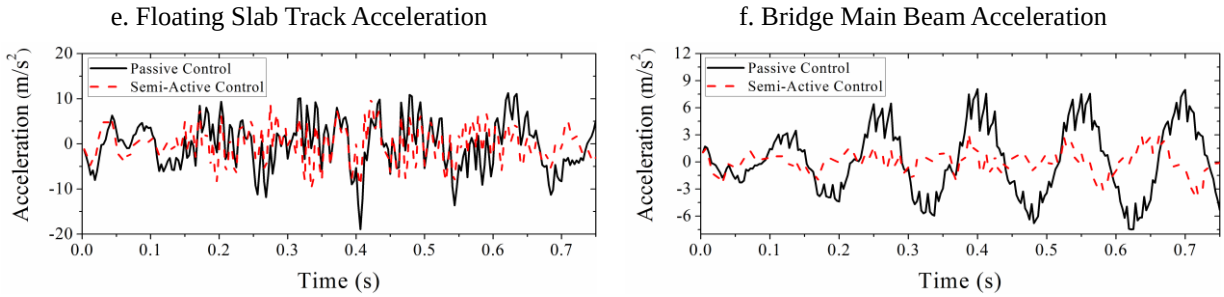

Fig. 7-12. Dynamic responses at midspan point of floating slab track and bridge main beam for Case 1: V=80m/s.

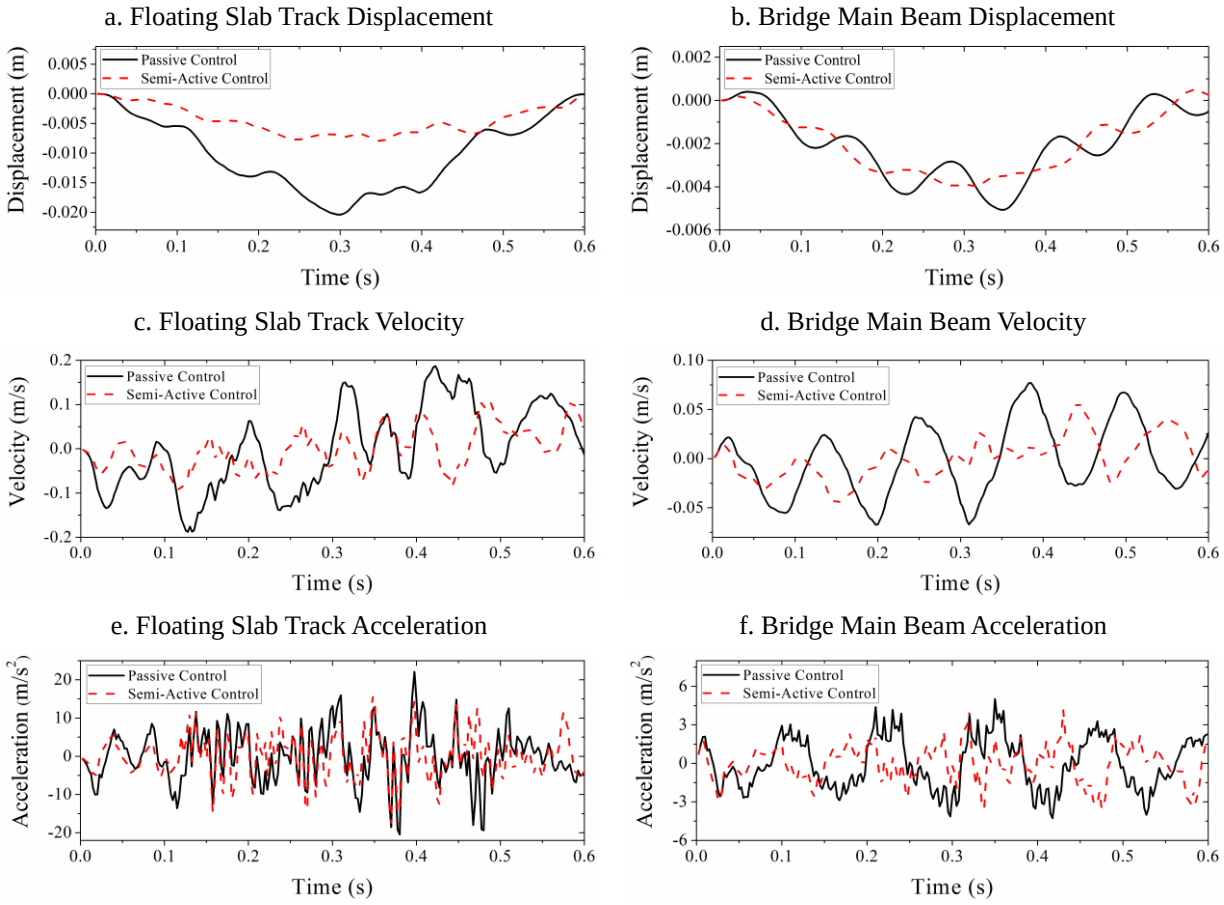

Fig. 7-13. Dynamic responses at midspan point of floating slab track and bridge main beam for Case 2: V=100m/s.

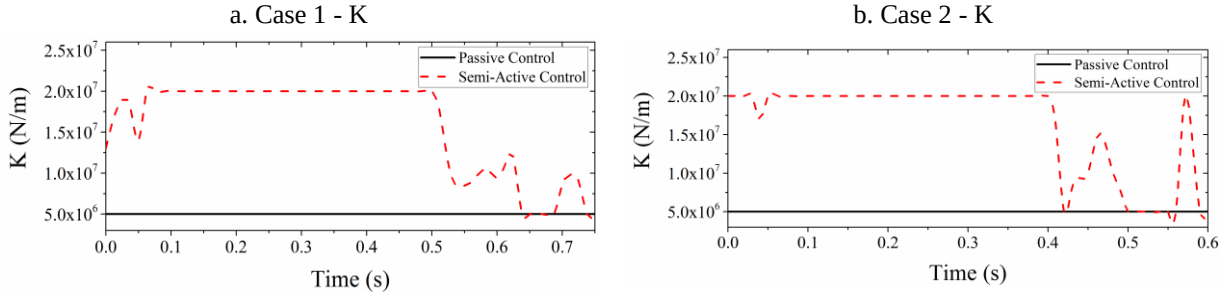

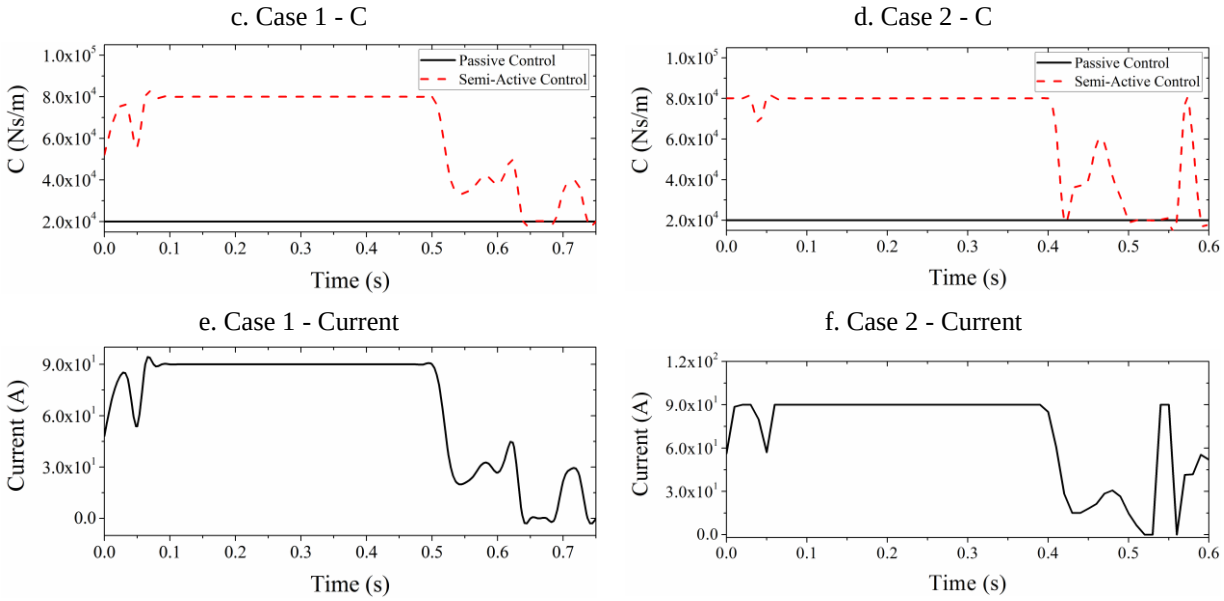

Fig. 7-14. Variation stiffness *K* and variation damping coefficient *C* of MRNs layer controlled by semi-active control structure, and current applied to MRNs for each case.

As shown in Fig. 7-12 and Fig. 7-13, comparing with the viscoelastic layer with constant stiffness and damping called passive control in here, the semi-active control structure based on MRNs and the corresponding semi-active control algorithm developed in this research are more effective to suppress the vibrations and reduce the dynamic responses of both floating slab track and bridge main beam. Although the acceleration is not controlled so well as displacement and velocity, the reduction effects of it on both floating slab track and bridge main beam are still apparent.

In case 1 (Fig. 7-12), resonance phenomenon is happened in bridge main beam with passive control, but it is controlled and eliminated when the semi-active control is applied. Therefore, the semi-active control proposed in this research can effectively avoid the resonance happening in the bridge structure when the trains are passing and protect the safety of the whole structure.

In Fig. 7-14, the value of variation stiffness K and variation damping coefficient C of the MRNs layer are shown for all cases, and it is easy to find out that both of them have obvious changes under the semi-active control. The range of those two parameters are $K = 5\times10^6 \sim 2\times10^7 N/m$ and $C = 2\times10^4 \sim 8\times10^4 N\cdot s/m$. The maximum value of each parameter is just 4 times of the minimum value, which could be reached by existed MRNs material. The current applied to MRNs and determined by semi-active control algorithm is also shown in Fig. 7-14, and the existence and presentation of it denote the operability of the proposed semi-active control. In summary, from Fig. 7-14, it proves that the semi-active based on MRNs proposed in this research is reasonable and it is practical to apply it in the real bridge structures in high-speed rail engineering.

7.7 Conclusions

The main objective of the research in this dissertation is applying the novel adaptive materials magnetorheological nanocomposites (MRNs) to build a semi-active control structure in vehicle-bridge coupling system of high-speed rail, controlling the vibration and reducing the dynamic responses of the bridge by that semi-active control. In this chapter, that main objective is completed and the semi-active control based on MRNs for vehicle-bridge coupling system of high-speed rail is presented.

Considering the ballastless track structure, which chooses floating slab track as the main constituent part, is widely existed in high-speed rail engineering, the MRNs are applied as the viscoelastic layer between floating slab track and bridge main beam to build the semi-active control structure. The dynamic mechanical model of MRNs is derived by their properties from experiments. Simplifying the connection between rail and floating slab track, the simply supported bridge with floating slab track is actually a double-beam system. Combining the linear model of MRNs dynamic mechanical model which is the same as the viscoelastic layer in Chapter 5, the semi-active control developed in Chapter 5 can be used in here. That semi-active control algorithm is inputted into the co-simulation platform of whole vehicle-bridge coupling system, and the simulation of that coupling system with semi-active control based on MRNs is completed finally.

Numerical examples are demonstrated and discussed in details to verify the efficiency of the MRNs semi-active control structure proposed in this research for the vehicle-bridge coupling system of high-speed rail. Comparing with the passive control that the viscoelastic layer has constant stiffness and damping, the semi-active control based on MRNs can suppress the vibrations of both floating slab track and bridge main beam more effectively. That semi-active control can also eliminate the resonance happened in bridge structure when the trains are passing, and protect the safety of the whole structure. The acceptable changes of stiffness and damping of MRNs layer prove that the semi-active structure is reasonable and it is practical to apply it in the real bridge in high-speed rail. In the end, the main objective of this research is accomplished successfully.

Chapter 8 Conclusions and Future Work

8.1 Conclusions

In the present dissertation, a novel adaptive materials magnetorheological nanocomposites (MRNs) are used to build a semi-active control structure, which is applied into the vehicle-bridge coupling system of high-speed rail so that the vibration of the whole system could be controlled effectively and the dynamic responses of bridge can be reduced significantly. Both theoretical and numerical experimental efforts have been made to analyze the dynamic behavior of the basic mechanical model, design and derive the control algorithms for the structure system, and simulate the whole structure system with vibration control. As a final remark, some achievements in this dissertation are summarized as follows.

As the first major contribution, the dynamic behavior of an undamped double-beam system interconnected by elastic layer is investigated. A semi-analytical method is developed to analyze the natural frequencies and corresponding mode shapes of that undamped double-beam system, which may have arbitrary beam mass, beam flexural rigidity and/or boundary condition. The initial conditions are considered to find the free vibration final form, which are the exact solutions of the motion differential equations formulated by the classical Bernoulli-Fourier method. The dynamic responses of forced system vibration are determined by the modal-expansion method using the natural frequencies and mode shapes obtained from the free vibration analysis. The specific

orthogonality condition for a double-beam system is derived, and then applied to decouple the motion differential equations. Various double-beam system models are studied to verify the semi-analytical method and conduct the systematic parametric analysis of the structural resonance condition and dynamic responses.

Second, considering the viscoelastic layer damping existed in real engineering practices, the double-beam system interconnected by viscoelastic layer is analyzed and the damping effects of the viscoelastic layer on the dynamic behavior of whole system are studied. A similar semi-analytical method is developed to analyze the natural frequencies and corresponding mode shapes of the general double-beam system, which may have arbitrary viscoelastic layer damping, arbitrary beam mass, beam flexural rigidity and/or boundary condition. The free vibration final forms, which are the exact solutions of the motion differential equations formulated by the classical Bernoulli-Fourier method, are solved based on the initial conditions. An iteration algorithm with the modal-expansion method is applied to find the dynamic responses of forced system vibration using the natural frequencies and mode shapes obtained from the free vibration analysis. Various double-beam system with viscoelastic layer models are studied to verify the semi-analytical method and the iteration method, and conduct the systematic parametric analysis of the structural resonance condition and dynamic responses.

Third, an active control structure, a semi-active control structure and corresponding control

algorithms are proposed to suppress the vibration of the elastically connected double-beam system. In the active control structure, independent modal space control is applied to decouple the motion equations of double-beam system with the active control, and transfer the vibration control of the infinite freedom system in physical space into the vibration control of several modes in modal space. Linear quadratic regulator is adopted to determine the specific modal active control force for each mode and the active control force in physical space. In the semi-active control structure, the active control force produced by the active control structure presented above is set up as the objective and the equivalent semi-active control force is assumed to be close to that active force. Based on that principle and with the mode shape filter derived, the determination method of stiffness increase is derived. Various double-beam system with active control structure or semi-active control structure models are calculated to illustrate the efficiency of the proposed active control and semi-active control.

Fourth, an active control structure, a semi-active control structure and corresponding control algorithms are proposed to suppress the vibration of the double-beam system with viscoelastic layer, since the materials used to connect the upper beam and lower beam in the double-beam system are usually the viscoelastic materials and their damping cannot be ignored in real engineering practices. In the active control structure, independent modal space control and linear quadratic regulator are also applied to decouple motion equations with active control and determine the active control force in physical space. In the semi-active control structure, the active

control force produced by the active control structure presented above is still set up as the objective and the equivalent semi-active control force is assumed to be close to that active force. A linear model is assumed as the dynamic mechanical model of the adjustable viscoelastic layer and the relationships between stiffness, damping with inputted currents are also defined as linear models. Based on that calculation principle, the linear model for adjustable viscoelastic layer and the mode shape filter, the determination methods of stiffness increase and damping increase are derived. The calculation methods for double-beam system with that active control and that semi-active control are also developed. The efficiency of the proposed active control and semi-active control for double-beam system with viscoelastic layer is illustrated by various numerical models.

Fifth, a co-simulation method is proposed to complete the dynamic simulation of vehicle-bridge coupling system of high-speed rail. Bridge structures are modelled by finite element method software MSC/NASTRAN, and dynamics of multibody system software MSC/ADAMS is used to simulate the vibration of vehicle system. The vehicle-bridge coupling relationships are all introduced and the classical theories about them are adopted, including wheel-rail contact geometric parameters, wheel-rail contact forces and track irregularity. The Matlab/Simulink is used to build a platform to ensure MSC/NASTRAN and MSC/ADAMS working together, and the vehicle-bridge coupling relationships are coded as a program block and inputted into that platform. In this way, the co-simulation by using that Matlab/Simulink platform is realized and the simulation of whole vehicle-bridge coupling system is completed. Various numerical examples of

vehicle-bridge coupling system are calculated to illustrate the practicability and efficiency of the proposed co-simulation method.

Finally, the semi-active control structure based on MRNs is developed and applied into the vehicle-bridge coupling system of high-speed rail so that the vibration of the whole system could be controlled effectively and the dynamic responses of bridge can be reduced significantly. MRNs are applied as the viscoelastic layer between floating slab track and bridge main beam to build the semi-active control structure for high-speed rail bridges. The dynamic mechanical model of MRNs is derived based on their properties obtained from experiments. Simplifying the connection between rail and floating slab track, the simply supported bridge with floating slab track is actually a double-beam system. The semi-active control algorithms developed for double-beam system with viscoelastic layer is used to derive the semi-active control algorithm for MRNs. That semi-active control is inputted into the co-simulation platform of vehicle-bridge coupling system, and the simulation of the whole system with semi-active control is completed. Numerical examples are demonstrated to prove the efficiency of the MRNs semi-active control structure proposed in this research for the vehicle-bridge coupling system of high-speed rail.

8.2 Suggestions for Future Work

In the future research on MRNs and its application for semi-active control in vehicle-bridge

coupling system of high-speed rail, there are several suggestions summarized as follows.

First, the fabrication techniques of MRNs should be improved, and the better MRNs materials with wider adjustable range in stiffness and damping should be developed to make better control effects for their application in civil engineering structural vibration control.

Second, the specific electromagnetic devices for MRNs should be invented so that the semi-active control devices based on MRNs could be installed and used in real structures.

Third, the theoretical research on the dynamic behavior of double-beam system should be continued. The double-beam system with non-uniformly distributed elastic layer or viscoelastic layer should be studied carefully, since it will be the basis for the decentralized control in future.

Fourth, the semi-active control algorithms based on MRNs for vehicle-bridge coupling system of high-speed rail should be improved. Several specific semi-active control algorithms should be developed based on the properties of MRNs and the bridge structure with floating slab track. And a decentralized control method and correspond algorithm should be observed.

Fifth, the co-simulation platform should be improved so that the calculation and simulation will be faster and more accurate, especially when simulating some complex bridges and vehicles.

Finally, the semi-active control based on MRNs and developed in this research is needed to be applied on real bridge structures and do some field tests, and their control effects should be proved by those field tests so that they can be used in real engineering projects in future.

References

1. Abu-Hilal, M., (2006), "Dynamic response of a double Euler-Bernoulli beam due to a moving constant load." *Journal of Sound and Vibration*, 297(3-5), 477-491.

2. Aida, T., Toda, S., Ogawa, N., and Imada, Y., (1992), "Vibration control of beams by beam-type dynamic vibration absorbers." *Journal of Engineering Mechanics*, 118(2), 248-258.

3. Akin, J.E., and Mofid, M., (1989), "Numerical solution for response of beams with moving mass." *Journal of Structural Engineering*, 115(1), 120–131.

4. Alkhatib, R., and Golnaraghi, M. F., (2003), "Active structural vibration control: a review." *The Shock and Vibration Digest*, 35(5), 367-383.

5. Ayre, R.S., and Jacobsen, L.S., (1950), "Transverse vibration of a two-span beam under the action of a moving alternating force." *Journal of Applied Mechanics*, 17(3), 283–290.

6. Behrooz, M., Wang, X.J., and Gordaninejad, F., (2014), "Modeling of a new semi-active/passive magnetorheological elastomer isolator." *Smart Materials and Structures*, 23(1), 045013.

7. Biggs, J.M., (1964), "Introduction to Structural Dynamics." *McGraw-Hill*, New York, U.S.A.

8. Bolotin, V.V., (1964), "The Dynamic Stability of Elastic Systems." *HoldenDay, Inc.*, San Francisco, California, U.S.A.

9. Cai, Y., Chen, S.S., Rote, D.M., and Coffey, H.T., (1994), "Vehicle/guideway interaction for high speed vehicles on a flexible guide way." *Journal of Sound and Vibration*, 175(5), 625–646.

10. Chang, D., and Lee, H., (1994), "Impact factors for simple-span highway girder bridges."

Journal of Structural Engineering, 120(3), 704–715.

11. Chatterjee, P.K., Datta, T.K., and Surana, C.S., (1994), "Vibration of suspension bridges under vehicular movement." *Journal of Structural Engineering*, 120(3), 681–703.

12. Chen, Y.H., (1978), "Dynamic analysis of continuous beams subjected to moving loads." *Journal of the Chinese Institute of Civil and Hydraulic Engineering*, 5(2), 1–7 (in Chinese).

13. Chen, Y.H., and Sheu, J.T., (1993), "Axially-loaded damped Timoshenko beam on viscoelastic foundation." *International Journal for Numerical Methods in Engineering*, 36(6), 1013-1027.

14. Chen, Y.H., and Sheu, J.T., (1994), "Dynamic characteristics of layered beam with flexible core." *Journal of Vibration and Acoustics*, 116(3), 350-356.

15. Chen, Y.H., and Sheu, J.T., (1995), "Beam on viscoelastic foundation and layered beam." *Journal of Engineering Mechanics*, 121(2), 340-344.

16. Chen, Y.H., and Lin, C.Y., (1998), "Structural analysis and optimal design of a dynamic absorbing beam." *Journal of Sound and Vibration*, 212(5), 759-769.

17. Chen, Y.H., and Li, C.Y., (2000), "Dynamic response of elevated high-speed railway." *Journal of Bridge Engineering*, 5(2), 124–130.

18. Cheng, Y.S., Au, F.T.K., and Cheung, Y.K., (2001), "Vibration of railway bridges under a moving train by using bridge-track-vehicle element." *Engineering Structures*, 23(1), 1597-1606.

19. Cheung, Y.K., Au, F.T.K., Zheng, D.Y., and Cheng, Y.S., (1999), "Vibration of multi-span non-uniform bridges under moving vehicles and trains by using modified beam vibration functions." *Journal of Sound and Vibration*, 228(3), 611–628.

20. Chonan, S., (1976), "Dynamical behaviors of elastically connected double-beam systems subjected to an impulsive load." *Bull. JSME*, 19, 595-603.

21. Cottle, E.T., (1990), "Damping of layered beams with mixed boundary conditions." *Master thesis, Air Force Institute of Technology,* Wright-Patterson Air Force Base, OH, U.S.A..

22. Chu, K.H., Garg, V.K., and Dhar, C.L., (1979), "Railway–bridge impact: Simplified train and bridge model." *Journal of the Structural Division*, 105(9), 1823–1844.

23. Chu, K.H., Garg, V.K., and Wang, T.L., (1986), "Impact in railway prestressed concrete bridges." *Journal of Structural Engineering*, 112(5), 1036–1051.

24. Deng, H.X., and Gong, X.L., (2007), "Adaptive tuned vibration absorber based on magnetorheological elastomer." *Journal of Intelligent Material Systems and Structures*, 18(12), 1205-1210.

25. Diana, G., and Cheli, F., (1989), "Dynamic interaction of railway systems with large bridges." *Vehicle System Dynamics*, 18, 71–106.

26. Dong, X., Yu, M., Liao, C., and Chen, W., (2009), "A new variable stiffness absorber based on magnetorheological elastomer." *Transactions of Nonferrous Metals Society of China*, 19, 611–615.

27. Douglas, B.E., and Yang, J.C.S., (1978), "Transverse compressional damping in the vibratory response of elastic-viscoelastic-elastic beams." *AIAA Journal*, 16(9), 925-930.

28. Du, H., Li, W., and Zhang, N., (2011), "Semi-active variable stiffness vibration control of vehicle seat suspension using an MR elastomer isolator." *Smart Structures and Materials*, 20, 105003.

29. Dublin, M., Friedrich, H.R., (1956), "Forced responses of two elastic beams interconnected by spring-damper systems." *Journal of the Aeronautical Sciences (Institute of the Aeronautical Sciences)*, 23(9), 824-829.

30. Dugush, Y.A., and Eisenberger, M., (2002), "Vibrations of non-uniform continuous beams under moving loads." *Journal of Sound and Vibration*, 254(5), 911–926.

31. Fayos, J., Baeza, L., Denia, F.D., and Tarancon, J.E., (2007), "An Eulerian coordinate-based method for analyzing the structural vibrations for a solid of revolution rotating about its main axis." *Journal of Sound and Vibration*, 306(3-5), 618-635.

32. Frostig, Y., and Baruch, M., (1993), "High-order buckling analysis of sandwich beams with transversely flexible core." *Journal of Engineering Mechanics*, 119(3), 476-495.

33. Frostig, Y., and Baruch, M., (1994), "Free vibrations of sandwich beams with a transversely flexible core: a high order approach." *Journal of Sound and Vibration*, 176(2), 195-208.

34. Fryba, L., (1972), "Vibration of Solids and Structures under Moving Loads." *Noordhoff international Publishing*, Groningen, The Netherlands.

35. Fryba, L., (1996), "Dynamics of Railway Bridges." *Thomas Telford*, London, England.

36. Galdos, N.H., Schelling, D.R., and Sahin, M.A., (1993), "Methodology for impact factor of horizontally curved box bridges." *Journal of Structural Engineering*, 119(6), 1917–1934.

37. Gbadeyan, J.A. and Oni, S.T., (1995), "Dynamic behavior of beams and rectangular plates under moving loads." *Journal of Sound and Vibration*, 182(5), 677–695.

38. Genin, J., and Ting, E.C., (1979), "Vehicle–guide way interaction problems." *The Shock and*

Vibration Digest, 11(12), 3–9.

39. Ginder, J.M., Nichols, M.E., Elie, L.D., and Tardiff, J.L., (1999), "Magnetorheological elastomers: properties and applications." *Smart Structures and Materials 1999*: *Smart Materials Technologies,* Proc. SPIE 3675, 131-138.

40. Ginder, J.M., Nichols, M.E., Elie, L.D., and Clark, S.M., (2000), "Controllable stiffness components based on magnetorheological elastomers." *Smart Structures and Materials 1999*: *Smart Materials Technologies,* Proc. SPIE 3985, 418–425.

41. Guo, W.H., and Xu, Y.L., (2001), "Fully computerized approach to study cable-stayed bridge–vehicle interaction." *Journal of Sound and Vibration*, 248(4), 745–761.

42. Guo, X.R., Deng, Z.M., Luo, H., (2009), "Dynamic responses of time-dependent system of Tianxingzhou bridge and train under wind load." *Proceedings of environmental vibrations: prediction, monitoring, mitigation and evaluation*, Beijing, China, 1208-1213.

43. Gupta, R.K., (1980), "Dynamic loading of highway bridges." *Journal of the Engineering Mechanics Division*, 106(2), 337–393.

44. Hamada, T.R., Nakayama, H., and Hayashi, K., (1983), "Free and forced vibrations of elastically connected double beam systems." *Bull. JSME,* 26, 1936-1942.

45. Hoang, N., Zhang, N., and Du, H., (2009), "A dynamic absorber with a soft magnetorheological elastomer for powertrain vibration suppression." *Smart Materials and Structures,* 18, 074009.

46. Housner, G. W., Bergman, L.A., Caughey, T. K., Chassiakos, A. G., Claus, R. O., Masri, S. F., Skelton, R. E., Soong, T. T., Spencer, B. F., Yao, T. P., (1997), "Structural control: past, present,

and future." *Journal of Engineering Mechanics*, 123(9), 897-971.

47. Hsu, L.C., (1996), "Impact responses of bridges traveled by high speed trains." *Master's thesis*, *National Taiwan University*, Taipei, Taiwan, R.O.C. (in Chinese).

48. Huang, D., Wang, T.L., and Shahawy, M., (1993), "Impact studies on multigirder concrete bridges." *Journal of Structural Engineering*, 119(8), 2387–2402.

49. Inglis, C.E., (1934), "A Mathematical Treatise on Vibration in Railway Bridges." *The University Press*, Cambridge, England.

50. Inman, D.J., (2001), "Active modal control for smart structures." *Philosophical Transactions of the Royal Society*, Series A, 359(1778), 205-219.

51. Irie, T., Yamada, G., and Kobayashi, Y., (1982), "The steady-state response of an internally damped double-beam system interconnected by several springs." *The Journal of the Acoustical Society of America*, 71(5), 1155-1162.

52. Jeffcott, H.H., (1929), "On the vibrations of beams under the action of moving loads." *Philosophical Magazine*, Ser. 7, 8(48), 66–97.

53. Ju, S.H. and Lin, H.T., (2003), "Numerical investigation of a steel arch bridge and interaction with high speed trains." *Engineering Structures*, 25, 241–250.

54. Jung, H.J., Park, J.S., and Koo, J.H., (2010), "Dynamic analysis of a smart base-isolation system based on MR elastomers." *ASME 2010 conference on smart materials, SMASIS2010,* Philadelphia, Pennsylvania, U.S.A..

55. Kawazoe, K., Kono, I., Aida, T., Aso, T., and Ebisuda, K., (1998), "Beam-type dynamic

vibration absorber comprised of free-free beam." *Journal of Engineering Mechanics*, 124(4), 476-479.

56. Kawatani, M., and Kim, C.W., (2001), "Computer simulation for dynamic wheel loads of heavy vehicles." *Structural Engineering and Mechanics*, 12(4), 409–428.

57. Kessel, P.G., (1966), "Resonances excited in an elastically connected double-beam system by a cyclic moving load." *The Journal of the Acoustical Society of America*, 40(3), 684-687.

58. Kessel, P.G., and Raske, T.F., (1967), "Damped response of an elastically connected double-beam system due to a cyclic moving load." *The Journal of the Acoustical Society of America*, 42(4), 873-881.

59. Koo, J. H., Sung, S. H., Lee, H. J., and Jung, H. J., (2008), "Seismic protection of structures using smart base isolation systems based on MR elastomers." *Proceedings of the 4th International Conference on Advances in Structural Engineering and Mechanics (ASEM08)*, Jeju, Korea.

60. Kou, J.W., and DeWolf, J. T., (1997), "Vibrational behavior of continuous span highway bridge — Influencing variables." *Journal of Structural Engineering*, 123(3), 333–344.

61. Kucuk, I., and Sadek, I., (2005), "Optimal control of an elastically connected rectangular plate-membrane system." *Journal of Computational and Applied Mathematics*, 180(2), 345-363.

62. Kucuk, I., and Sadek, I., (2007), "Active vibration control of an elastically connected double-string continuous system." *Journal of Franklin Institute*, 344(5), 684-697.

63. Kukla, S., and Skalmierski, B., (1994), "Free vibration of a system composed of two beams separated by an elastic layer." *Journal of Theoretical and Applied Mechanics*, 32(3), 581-590.

64. Kurihara, M., and Shimogo, T., (1978a), "Stability of a simply-supported beam subjected to random spaced moving loads." *Journal of Mechanical Design*, 100(7), 507–513.

65. Kurihara, M., and Shimogo, T., (1978b), "Vibration of an elastic beam subjected to discrete moving loads." *Journal of Mechanical Design*, 100(7), 514–519.

66. Le, R., Ripke, B., and Zacher, M., (1999), "Ballast mats on high speed bridges." *Proceedings of The Fourth European Conference on Structural Dynamics*, EURODYN, Prague (Czech Republic), 70, 699-703.

67. Lechner, I.B., (2011), "Railway concrete pavements." *2nd International Conference on Best Practices for Concrete Pavements*, Florianopolis, Brazil.

68. Li, J., and Hua, H. X., (2007), "Spectral finite element analysis of elastically connected double-beam systems." *Finite Elements in Analysis and Design*, 43(15), 1155-1168.

69. Li, Q.S., Liu, D.K., Fang, J.Q., and Tam, C.M., (2000), "Multi-level optimal design of buildings with active control under winds using genetic algorithms." *Journal of Wind Engineering and Industrial Aerodynamics*, 86(1), 65-86.

70. Li, Q.S., Liu, D.K., Tang, J., Zhang, N., and Tam, C.M., (2004), "Combinatorial optimal design of number and positions of actuators in actively controlled structures using genetic algorithms." *Journal of Sound and Vibration*, 270(4-5), 611-624.

71. Li, R., (2011), "Dynamic Mechanical Behavior of Magnetorheological Nanocomposites." *Ph.D. thesis, University of California, Irvine,* CA, USA.

72. Li, Y.X., and Sun, L.Z., (2015), "Transverse vibration of undamped elastically connected

double-beam system with arbitrary conditions." *Journal of Engineering Mechanics*, vol. 141, 04015070.

73. Lu, Y. P., and Douglas, B. E., (1974), "On the forced vibrations of three-layer damped sandwich beams." *Journal of Sound and Vibration*, 32(4), 513-516.

74. Li, X.Z., (2000), "Studies on theory and application of train-bridge system coupling vibration in high-speed railway." *Ph.D. thesis, Southwest Jiaotong University,* Chengdu, Sichuan, P.R.China.

75. Macé, M., (1994), "Damping of beam vibrations by means of a thin constrained viscoelastic layer: evaluation of a new theory." *Journal of Sound and Vibration*, 172(5), 577-591.

76. Mao, Q., and Wattanasakulpong, N., (2015), "Vibration and stability of a double-beam system interconnected by an elastic foundation under conservative and nonconservative axial forces." *International Journal of Mechanical Sciences*, 93, 1-7.

77. Martinez-Rodrigo, M.D., Lavado, J., and Museros, P., (2010a), "Transverse vibrations in existing railway bridges under resonant conditions: single-track versus double-track configurations." *Engineering Structures*, 32(1), 1861-1875.

78. Martinez-Rodrigo, M.D., Lavado, J., and Museros, P., (2010b), "Dynamic performance of existing high-speed railway bridges under resonant conditions retrofitted with fluid viscous dampers." *Engineering Structures*, 32(1), 808-828.

79. Matsuura, A., (1976), "A study of dynamic behavior of bridge girder for high speed railway." *Proc. JSCE*, 256, 35–47 (in Japanese).

80. Meirovitch, L., Baruh, H., Montgomery, R.C., and Williams, J.P., (1984), "Nonlinear natural

control of an experimental beam." *Journal of Guidance, Control, and Dynamics*, 7(4), 437-442.

81. Meirovitch, L., and Silverberg, L.M., (1983), "Globally optimal control of self-adjoint distributed systems." *Optimal Control Applications and Methods*, 4(1), 365-386.

82. Meirovitch, L., (1987), "Some problems associated with the control of distributed structures." *Journal of Optimization Theory and Applications*, 54(1), 1-21.

83. Meisenholder, S.G. and Weidlinger, P., (1974), "Dynamic interaction aspects of cable-stayed guideways for high speed ground transportation." *Journal of Dynamic Systems, Measurement, and Control*, 96(2), 180–192.

84. Minsili L.S., Zhong T., Xia H., Manguelle D.E., (2002), "Design and vibration control by friction dampers in truss bridges." *Proc. of the second international conference on construction in developing countries: Challenges facing the construction industry in developing countries*, Gaborone, Botswana.

85. Museros, P., Romero, M.L., Poy, A., and Alarcon, E., (2002), "Advances in the analysis of short span railway bridges for high-speed lines." *Computers & Structures*, 80, 2121–2132.

86. Oniszczuk, Z., (1999), "Transverse vibrations of the elastically connected rectangular double-membrane compound system." *Journal of Sound and Vibration*, 221(2), 235-250.

87. Oniszczuk, Z., (2000), "Free transverse vibrations of elastically connected simply supported double-beam complex system." *Journal of Sound and Vibration*, 232(2), 387-403.

88. Oniszczuk, Z., (2000a), "Transverse vibrations of elastically connected double-string complex system, Part I: Free vibrations." *Journal of Sound and Vibration*, 232(2), 355-366.

89. Oniszczuk, Z., (2000b), "Transverse vibrations of elastically connected double-string complex system, Part II: Forced vibrations." *Journal of Sound and Vibration*, 232(2), 367-386.

90. Oniszczuk, Z., (2000c), "Free transverse vibrations of elastically connected simply supported double-beam complex system." *Journal of Sound and Vibration*, 232(2), 387-403.

91. Oniszczuk, Z., (2000d), "Free transverse vibrations of an elastically connected rectangular simply supported double-plate complex system." *Journal of Sound and Vibration*, 236(4), 595-608.

92. Oniszczuk, Z., (2002a), "Free transverse vibrations of an elastically connected complex beam-string system." *Journal of Sound and Vibration*, 254(4), 703-715.

93. Oniszczuk, Z., (2002b), "Damped vibration analysis of a two-degree-of-freedom discrete system." *Journal of Sound and Vibration*, 257(2), 391-403.

94. Oniszczuk, Z., (2003), "Forced transverse vibrations of an elastically connected complex simply supported double-beam system." *Journal of Sound and Vibration*, 264(2), 273-286.

95. Oniszczuk, Z., (2003), "Damped vibration analysis of an elastically connected complex double-string system." *Journal of Sound and Vibration*, 264(2), 253-271.

96. Oniszczuk, Z., (2003a), "Free transverse vibrations of an elastically connected rectangular plate–membrane complex system." *Journal of Sound and Vibration*, 264(1), 37-47.

97. Oniszczuk, Z., (2003b), "Damped vibration analysis of an elastically connected complex double-string system." *Journal of Sound and Vibration*, 264(2), 253-271.

98. Oniszczuk, Z., (2003c), "Forced transverse vibrations of an elastically connected complex simply supported double-beam system." *Journal of Sound and Vibration*, 264(2), 273-286.

99. Oniszczuk, Z., (2004), "Forced transverse vibrations of an elastically connected complex rectangular simply supported double-plate system." *Journal of Sound and Vibration*, 270(4–5), 997-1011.

100. Opie, S., and Yim, W., (2009), "Design and control of a real-time variable stiffness vibration isolator." *Proceedings of 2009 IEEE/ASME International Conference on Advanced Intelligent Mechatronics*, Singapore.

101. Pan, T.C. and Li, J., (2002), "Dynamic vehicle element method for transient response of coupled vehicle–structure systems." *Journal of Structural Engineering*, 128(2), 214–223.

102. Pavlovic, R., Kozic, P., and Pavlovic, I., (2012), "Dynamic stability and instability of a double-beam system subjected to random forces." *International Journal of Mechanical Sciences*, 62(1), 111-119.

103. Paultre, P., Chaallal, O., and Proulx, J., (1992), "Bridge dynamics and dynamic amplification factors — A review of analytical experimental findings." *Canadian Journal of Civil Engineering*, 19, 260–278.

104. Pesterev, A.V., Yang, B., Bergman, L.A., and Tan, C.A., (2001), "Response of elastic continuum carrying multiple moving oscillators." *Journal of Engineering Mechanics*, 127(3), 260–265.

105. Pesterev, A.V., Bergman, L.A., Tan, C.A., Tsao, T.C., and Yang, B., (2003), "On asymptotics of the solution of the moving oscillator problem." *Journal of Structural Engineering*, 260, 519–536.

106. Rao, S.S., (1974), "Natural vibrations of systems of elastically connected Timoshenko beams." *The Journal of the Acoustical Society of America*, 55(6), 1232-1237.

107. Ramallo, J. C., Johnson, E.A., and Spencer, B. F., Jr., (2002), "'Smart' base isolation systems." *Journal of Engineering Mechanics*, 128(10), 1088-1099.

108. Rao, G.V., (2000), "Linear dynamics of an elastic beam under moving loads." *Journal of Vibration and Acoustics*, 122(7), 281–289.

109. Reinhorn, A.M., Soong, T.T., Riley, M.A., Lin, R.C., and Higashino, M., (1993), "Full-scale implementation of active control. II: installation and performance." *Journal of Structural Engineering*, 119(6), 1935-1960.

110. Sadek, I.S., and Esfandiari, R.S., (1990), "Optimal active control of distributed-parameter systems with applications to a Rayleigh beam." *IMA Journal of Mathematical Control and Information*, 7(1), 59-76.

111. Savin, E., (2001), "Dynamic amplification factor and response spectrum for the evaluation of vibrations of beams under successive moving loads." *Journal of Sound and Vibration*, 248, 267–288.

112. Schafer, B.E., and Holzach, H., (1985), "Experimental research on flexible beam modal control." *Journal of Guidance, Control, and Dynamics*, 8(5), 597-604.

113. Seelig, J.M., and Hoppmann, W.H., (1964a), "Normal mode vibrations of systems of elastically connected parallel bars." *The Journal of the Acoustical Society of America*, 36(1), 93-99.

114. Seelig, J.M., and Hoppmann, W.H., (1964b), "Impact on an elastically connected double-beam system." *Journal of Applied Mechanics*, 31(4), 621-626.

115. Soong, T.T., (1990), "Active structural control: theory and practice." *Wiley*, New York.

116. Soong, T.T., Reinhorn, A.M., Wang, Y.P., and Lin, R.C., (1991), "Full-scale implementation of active control. I: design and simulation." *Journal of Structural Engineering*, 117(11), 3516-3536.

117. Soong, T.T., and Spencer, B.F., (2002), "Supplemental energy dissipation: state-of-the-art and state-of-the-practice." *Engineering Structures*, 24(3), 243-259.

118. SSF Ingenieure, "Ballastless track on high-speed lines: a guarantee for travel safety and comfort." *SSF Ingenieure AG Consulting Engineers*.

119. Standardization Administration of the P.R.China, (2007), "Hot-rolled steel rails for railway. " *National Standard of P.R.China*, GB2585-2007.

120. Stanisic, M.M., (1985), "On a new theory of the dynamic behavior of the structures carrying moving masses." *Ingenieur-Archiv*, 55, 176–185.

121. Stanisic, M.M. and Hardin, J.C., (1969), "On the response of beams to an arbitrary number of concentrated moving masses." *Journal of The Franklin Institute*, 287, 115–123.

122. Stojanovic, V., and Kozic, P., (2012), "Forced transverse vibration of Rayleigh and Timoshenko double-beam system with effect of compressive axial load." *International Journal of Mechanical Sciences*, 60(1), 59-71.

123. Stokes, G.G., (1849), "Discussion of a differential equation relating to the breaking of railway

bridges." *Transactions of the Cambridge Philosophical Society*, 8(5), 707–735.

124. Taheri, M.R., Ting, E.C., and Kukreti, A.R., (1990), "Vehicle–guideway interactions: A literature review." *The Shock and Vibration Digest*, 22(6), 3–9.

125. Timoshenko, S.P., (1922), "On the forced vibrations of bridges." *Philosophical Magazine*, Ser. 6, 43, 1018–1019.

126. Ting, E.C., Genin, J., and Ginsberg, J.H., (1974), "A general algorithm for the moving mass problem." *Journal of Sound and Vibration*, 33(1), 49–58.

127. Ting, E.C., Genin, J., and Ginsberg, J.H., (1975), "Dynamic interaction of bridge structures and vehicles." *The Shock and Vibration Digest*, 7(11), 21–29.

128. Ting, E.C. and Genin, J., (1980), "Dynamics of bridge structures." *SM Archives*, 5(3), 217–252.

129. Ting, E.C. and Yener, M., (1983), "Vehicle–structure interactions in bridge dynamics." *The Shock and Vibration Digest*, 15(12), 3–9.

130. Torstensson P.T., Nielson J.C.O., Baeza L., (2011), "Dynamic train-track interaction at high vehicle speeds-modeling of wheelset dynamics and wheel rotation." *Journal of Sound and Vibration*, 330(22), 5309-5321.

131. Usman, M., Jang, D.D., Kim, I.H., Jung, H.J., and Koo, J.H., (2009), "Dynamic testing and modeling of Magneto-rheological elastomers." *ASME 2009 Conference on Smart Materials*, Oxnard, California, USA.

132. Vu, H.V., (1987), "Distributed dynamic vibration absorber." *Ph.D. Thesis, University of*

Michigan, Ann Arbor, MI, U.S.A..

133. Vu, H.V., OrdÓÑez, A.M., and Karnopp, B.H., (2000), "Vibration of a double-beam system." *Journal of Sound and Vibration,* 229(4), 807-822.

134. Wang, T.L., Garg, V.K., and Chu, K.H., (1991), "Railway bridge/vehicle interaction studies with new vehicle model." *Journal of Structural Engineering*, 117(7), 2099–2116.

135. Wang, T.L. and Huang, D., (1992), "Cable-stayed bridge vibration due to road surface roughness." *Journal of Structural Engineering,* 118(5), 1354–1374.

136. Wang, R.T., (1997), "Vibration of multi-span Timoshenko beams to a moving force." *Journal of Sound and Vibration*, 207(5), 731–742.

137. Wang, J.J., (2011), "The ballastless track technology for China high-speed line." Seminar, *China Academy of Railway Sciences*.

138. Willis, R., (1849), "Appendix to the report of the commissioners appointed to inquire into the application of iron to railway structures." *H. M. Stationary Office,* London, England.

139. Wilson, G.P., (2004), "Rail system noise and vibration control." *AAS ACOUSTICS 2004*, Gold Coast, Australia.

140. Wiriyachai, A., Chu, K.H., and Garg, V.K., (1982), "Bridge impact due to wheel and track irregularities." *Journal of Engineering Mechanics,* 108(4), 648–666.

141. Wu, J.S. and Dai, C.W., (1987), "Dynamic responses of multispan nonuniform beam due to moving loads." *Journal of Structural Engineering*, 113(3), 458–474.

142. Wu, Y.S., (2000), "Dynamic interaction of train–rail–bridge system under normal and seismic

conditions." *Ph.D. thesis, National Taiwan University,* Taipei, Taiwan, R.O.C.

143. Wu, Y.S., Yang, Y.B., and Yau, J.D., (2001), "Three-dimensional analysis of train–rail–bridge interaction problems." *Vehicle System Dynamics*, 36(1), 1–35.

144. Wu, Y., and Gao, Y., (2015), "Analytical solutions for simply supported viscously damped double-beam system under moving harmonic loads." *Journal of Engineering Mechanics*, 141(7), 04015004.

145. Xia, H., Xu, Y.L., and Chan, T.H.T., (2000), "Dynamic interaction of long suspension bridges with running trains." *Journal of Sound and Vibration*, 237(2), 263–280.

146. Xia, H., De Roeck, G., Zhang, H.R., and Zhang, N., (2001), "Dynamic of train-bridge system and its application in steel girder reinforcement." *Computers & Structures*, 79(21-22), 1851-1860.

147. Xia, H., and Zhang, N., (2002), "Dynamic interaction of vehicles and structures." *Science Press, Beijing, P.R.China.*

148. Xin, T., and Gao, L., (2011), "Reducing slab track vibration into bridge using elastic materials in high speed railway." *Journal of Sound and Vibration*, 330(10), 2237-2248.

149. Xu, Y.L., Xia, H., and Yan, Q.S., (2003), "Dynamic response of suspension bridge to high wind and running train." *Journal of Bridge Engineering*, 8(1), 46–55.

150. Xu, Y.L., Zhang, N., Xia, H., (2004), "Vibration of coupled train and cable-stayed bridge systems in cross winds." *Engineering Structures*, 26(10), 1389-1406.

151. Yamaguchi, H., (1985), "Vibrations of a beam with an absorber consisting of a viscoelastic beam and a spring-viscous damper." *Journal of Sound and Vibration*, 103(3), 417-425.

152. Yankelevsky, D.Z., (1991), "Analysis of a composite layered elastic foundation." *International Journal of Mechanical Sciences*, 33(3), 169-177.

153. Yang, F. and Fonder, G.A., (1998), "Dynamic response of cable-stayed bridges under moving loads." *Journal of Engineering Mechanics*, 214(7), 741–747.

154. Yang, J., Du, H.P., Li, W.H., Li, Y.C., Li, J.C., Sun, S.S., and Deng H.X., (2013), "Experimental study and modeling of a novel magnetorheological elastomer isolator." *Smart Materials and Structures*, 22(1), 1-14.

155. Yang, J.N., Akbarpour, A., and Ghaemmaghami, P., (1987), "New optimal control algorithms for structural control." *Journal of Engineering Mechanics*, 113(9), 1364-1386.

156. Yang, J.N., Long, F.X., and Wong, D., (1988), "Optimal control of nonlinear structures." *Journal of Applied Mechanics*, 55(4), 931-938.

157. Yang, J.N., Li, Z., and Liu, S.C., (1991), "Instantaneous optimal control with acceleration and velocity feedback." *Probabilistic Engineering Mechanics*, 6(3-4), 204-211.

158. Yang, J.N., Li, Z., and Liu, S.C., (1992), "Stable controllers for instantaneous optimal control." *Journal of Engineering Mechanics*, 118(8), 1621-1630.

159. Yang, Y.B., Liao, S.S., and Lin B.H., (1995), "Impact formulas for vehicles moving over simple and continuous beams." *Journal of Structural Engineering*, 121(11), 1644–1650.

160. Yang, Y.B. and Lin, B.H., (1995), "Vehicle–bridge interaction analysis by dynamic condensation method." *Journal of Structural Engineering*, 121(11), 1636–1643.

161. Yang Y.B., Yau J.D., (1997), "Vehicle-bridge interaction element for dynamic analysis."

Journal of Structural Engineering, 123(11), 1512-1518.

162. Yang Y.B., Yau, J.D., and Wu Y.S., (2004), "Vehicle-bridge interaction dynamics: with applications to high-speed railways." *World Scientific Publishing Co. Pte. Ltd.,* Singapore.

163. Yang, Y.B., Wu, C.M., and Yau, J.D., (2001), "Dynamic response of a horizontally curved beam subjected to vertical and horizontal moving loads." *Journal of Sound and Vibration*, 242(3), 519–537.

164. Yang, Y.B. and Wu, Y.S., (2001), "A versatile element for analyzing vehicle–bridge interaction response." *Engineering Structures*, 23, 452–469.

165. Yang, Y.B., Lin, C.L., Yau, J.D., and Chang, D.W., (2004), "Mechanism of resonance and cancellation for train-induced vibrations on bridges with elastic bearings." *Journal of Sound and Vibration*, 269(1–2), 345–360.

166. Yao, T.P., (1972), "Concept of structural control." *Journal of the Structural Division*, 98(7), 1567-1574.

167. Yau, J.D., (1996), "Dynamic response of bridges travelled by trains — Analytical and numerical approaches." *Ph.D. thesis, National Taiwan University,* Taipei, Taiwan, R.O.C.

168. Yau, J.D., Yang Y.B., and Kuo S.R., (1999), "Impact response of high speed rail bridges and riding comfort of rail cars." *Engineering Structures*, 21, 836-844.

169. Yau, J.D., Wu, Y.S., and Yang, Y.B., (2001), "Impact response of bridges with elastic bearings to moving loads." *Journal of Sound and Vibration*, 248(1), 9–30.

170. Yoshioka, H., Ramallo, J., and Spencer, B., Jr., (2002), "“Smart” Base Isolation Strategies

Employing Magnetorheological Dampers." *Journal of Engineering Mechanics*, 128(5), 540–551.

171. Zhai, W.M., Cai, C.B., and Guo, S.Z., (1996), "Coupling model of vertical and lateral vehicle/rack interactions." *Vehicle System Dynamics*, 26(1), 61-79.

172. Zhang, N., Xia, H., Guo, W.W., and De Roeck, G., (2010), "A vehicle-bridge linear interacted model and its validation." *International Journal of Structural Stability and Dynamics*, 10(2), 335-361.

173. Zhang, Q. L., Vrouwenvelder, A., and Wardenier, J., (2001a), "Numerical simulation of train-bridge interactive dynamics." *Computers & Structures*, 79, 1059–1075.

174. Zhang, Q. L., Vrouwenvelder, A., and Wardenier, J., (2001b), "Dynamic amplification factors and EUDL of bridges under random traffic flows." *Engineering Structures*, 23, 663–672.

175. Zhang, Y.Q., Lu, Y., and Ma, G.W., (2008), "Effect of compressive axial load on forced transverse vibrations of a double-beam system." *International Journal of Mechanical Sciences*, 50(2), 299-305.

176. Zhang, Z., Huang, X., Zhang, Z., and Hua, H., (2014), "On the transverse vibration of Timoshenko double-beam systems coupled with various discontinuities." *International Journal of Mechanical Sciences*, 89, 222-241.

177. Zheng, D.Y., Cheung, Y.K., Au, F.T.K., and Cheng, Y.S., (1998), "Vibration of multi-span non-uniform bridges under moving loads by using modified beam vibration functions." *Journal of Sound and Vibration*, 212, 455–467.